**Extending the frontiers of mass spectrometric instrumentation and methods**

By

**Gregg Martin Schieffer**

A dissertation submitted to the graduate faculty
in partial fulfillment of the requirements for the degree of
DOCTOR OF PHILOSOPHY

Major: Analytical Chemistry

Program of Study Committee:
R. S. Houk, Major Professor
Joseph Burnett
George Kraus
Young-Jin Lee
Klaus Schmidt-Rohr

Iowa State University
Ames, IA

2010

# Table of Contents

# CHAPTER 1

# INTRODUCTION TO MASS SPECTROMETRIC INSTRUMENTATION AND METHODS

## BACKGROUND

Analytical chemistry is the discipline that identifies and quantifies matter. One method to identify and measure matter is through the use of instrumentation. The instrument used for this research is the mass spectrometer (MS). A MS measures the mass-to-charge ratio (m/z) of anything that is a charged particle or ion. The key is to take a sample and convert some of it into ions. These processes are described in this introduction.

The application of MS has grown tremendously in the past 100 years. At least six Nobel Prizes in either physics or chemistry have been awarded for research that has become integral to the development of MS. Several Nobel Prize winners integral to mass spectrometry have been discussed.[1, 2] One Nobel Prize in chemistry, awarded to Fenn and Tanaka in 2002, honored the development of electrospray [3-5] and matrix-assisted laser-desorption [6, 7] as novel "soft" ionization methods. As Fenn remarked, we've made elephants fly. These "elephants" are large molecules that prefer decomposition to volatilization. The "soft" ionization methods used in the papers presented in this dissertation are direct analysis in real time (DART) [8, 9], laser desorption ionization (LDI) [10] using non-traditional matrices such as graphite [11, 12], and electrospray ionization (ESI). These ionization methods were applied to the analysis of coal, plant metabolites, and proteins

### Ionization Methods

#### DART MS

Direct analysis in real time (DART) ionization utilizes an electrical discharge in the presence of helium atoms and a heated gas stream (> 200 °C). The discharge forms [$He^{+\bullet}$] ions, which are accelerated due to voltages on grids and collide with other helium ions

to form metastable, neutral He ($2^3S$) atoms. Most of the free electrons and charged helium atoms are kept within the DART apparatus. The heated gas stream that exits the DART source contains some electronically excited neutral He ($2^3S$), the balance composed of ground state helium gas. The electronically excited, neutral He ($2^3S$) atoms react with ambient water molecules to form charged water clusters.[8] A proposed mechanism is shown below.

$$He\ (2^3S) + nH_2O \rightarrow [(H_2O_{n-1})H]^+ + OH^- + He\ (1^1S) \qquad (1)$$

Negatively charged water cluster ions can be simultaneously created as well. Analyte molecules, either as a gas or desorbing off a sample holder in the heated gas stream, undergo proton transfer with the charged water clusters. This is one of the primary methods analyte becomes ionized via the DART source. Analyte with a greater proton affinity than a positively charged water cluster will abstract the proton from the water cluster to become $[Analyte + H]^+$. For negative ion mode, negatively charged water clusters with a greater proton affinity than the analyte will pull off a proton, forming $[Analyte - H]^-$. The external ion source of the MS then guides the charged analyte ion into the MS vacuum system for mass analysis. The addition of atmospheric gases nitrogen and oxygen, in addition to certain DART parameters, to the helium gas stream or the presence of ambient ammonia gas expands the range of analyte ionized by the DART to non-polar compounds, such as branched alkanes.[9] DART is amenable to analyze any gas, liquid, and solid. Its use has exploded since its introduction in 2005. Eighty six papers, of which at least 39 have come in the past year and a half, use the DART ionization method for applications that vary from determining counterfit drugs [13] to analyzing compounds from well-behaved (i.e. stationary) fruit flies.[14] One more paper, featured in this dissertation, will be added to the list with the identification of coal degradation products by DART MS (Chapter 2).

**LDI MS**

Karas and Tanaka developed the laser desorption ionization method using a matrix (MALDI) in the early 1980s.[15, 16] In MALDI, another material that strongly absorbs the laser light coats or co-crystallizes with the analyte of interest. Organic molecules, such as 2,5-dihydroxy benzoic acid or sinapinic acid, that strongly absorb the laser light are mixed

with analyte in a ~1000:1 ratio and allowed to dry.[17] Once the laser fires at the sample, some of the material rapidly heats and ejects into space. Only the top few molecular layers in the crystal absorb the laser light, but a much greater portion of the sample sublimates. The volatized analyte that did not absorb the laser light remains intact. The analyte interacts with the matrix to become either positively or negatively charged ions, via the primary ionization mechanism of proton transfer. Some analyte becomes ionized through other mechanisms as cation (e.g. positively charged $Na^+$) and anion adducts (e.g. negatively charged $Cl^-$) can be formed. Voltages within the mass spectrometer direct the ions for mass analysis. It is well suited for analyzing large biomolecules such as proteins.[18] Some MALDI reviews are available.[19-21]

While MALDI works great for the analysis of large biomolecules, it is not as well suited for metabolite analysis and imaging. Many metabolites are hydrophobic and do not associate with the hydrophilic organic acid matrix. The matrix crystals formed by the organic acids have dimensions on the order of >10 µm. These crystal sizes yield "sweet spots" during imaging. Thus not all laser shots yield signal. Another downside to traditional MALDI for metabolite analysis is the mass-to-charge overlap. Ion signal originating from the MALDI matrix can overwhelm the signal from analyte. Finally, MALDI MS instruments do the analysis in an intermediate (200 mbar) or high vacuum (100 µbar) environment. Volatile metabolites quickly evaporate away (within a few minutes) before analysis is complete.

One solution to some of these problems with using traditional MALDI matrices with metabolite imaging is to use colloidal graphite [11, 12] with laser desorption ionization at atmospheric pressure [22, 23]. Some researchers call the graphite LDI method GALDI (graphite assisted LDI). A paper showing the analysis of metabolite standards and plant samples by atmospheric pressure GALDI is shown in Appendix III.[24] Atmospheric pressure LDI analysis was a logical next step to enable the imaging of metabolites because one can do *in situ* plant imaging and retain volatile metabolites.

**ESI MS**

The electrospray ionization (ESI) method interfaces with nearly every commercial mass spectrometer produced today. The first ESI papers [3, 25-27] describe an ion source

that produced multiply charged ions. Incidentally, the multiple charges per analyte ion produced mass-to-charge ratios within the mass range of most mass spectrometers of the late 1980s. This ionization method is commonly coupled to liquid chromatography [28, 29] as well. The ESI process became miniaturized with the introduction of nano-ESI.[4, 30, 31]

Electrospray ionization [5] can work over a wide range of flow rates (20 nL/min to 1 mL/min) and solvents (100% water to 100% organic solvent such as chloroform). Detection limits can be as low as parts per trillion. Both positive and negative charged ions can form.[32] Nano-ESI was used primarily for the work in this dissertation. A voltage is applied via a thin stainless steel wire to solution inside a pulled glass capillary tip. The electric field and the solution at the tip form a Taylor cone [33, 34], which emits a spray of fine water droplets (Figure 1). The droplets, which contain charged analyte, dry. Upon reaching the Rayleigh limit, which is the point where the potential energy of like charges repelling each other equals the surface tension of the solvent holding the droplet together, the droplet deforms and explodes into smaller charged droplets. The excess charge quickly is expelled via the formation of these smaller droplets. This process repeats until the analyte is desolvated.[35] Proteins and other large biomolecules most likely follow this ionization mechanism, which is known as the charged residue model.

Nano-ESI is the primary ionization method for making the ions measured in this dissertation on the three ion source – ion trap – ion mobility – TOF MS as described in chapters 3 and 4 and Appendix I and II.

**ION MOBILITY – MASS SPECTROMETRY**

The mobility of a gas-phase ion is a measurement of how quickly it moves through a buffer gas under the influence of an electric field.[36] The mathematical relationship to describe this effect is as follows:

$$v_d = KE = L/t_d \qquad (2)$$

The mobility, K, is an intrinsic property of an ion; $v_d$ denotes the velocity of the ion under a certain electric field, E. By definition, the velocity, $v_d$, equals the displacement or length of the mobility cell, L, divided by the time, $t_d$, that it took to travel through the cell. The $t_d$ value is called the drift time.[37] An ion with the same charge but more compact shape will

have fewer collisions with the buffer gas and thus a higher mobility than the same ion with a more elongated shape. In this manner, ion mobility separates ions based on their size-to-charge ratio. Under certain conditions, one can determine the average collision cross section of the measured gas phase ions. The specific condition regime is described next.

Mobility measurements are dependent on the properties of the buffer gas system, as well as the length and electric field applied to the drift tube. A reduced mobility, $K_o$, factors in the pressure and temperature of the buffer gas within the drift tube. Rearranged to solve for the reduced mobility, $K_o$, and account for STP conditions, the relationship is:

$$K_o = \frac{L}{t_d E} \frac{273.2}{T} \frac{p}{760} \qquad (3)$$

The pressure, *p*, is in Torr, and the temperature, *T*, is in Kelvin. The electric field, E, is Volts per centimeter.[36]

The measured cross section values depend on the ratio of the electric field (E) to gas number density (N).[36, 38] All experiments and measurements employed in this dissertation occur in the low field regime. For the pressure used in our drift tube, the gas phase protein ions undergo at least $10^5$ collisions per centimeter. The ion velocity increases proportionally to an increase in electric field; therefore the collisions with the buffer gas become more energetic. Above the low field limit, the energy gained by the ion due to the collisions with the drift tube buffer gas is greater than the energy dissipated by the collisions.[36] Some of the excess energy converts to heat, changing the shape of the ion. High-field asymmetric waveform ion mobility spectrometry (FAIMS) uses this principle under the high field regime to separate ions.[39, 40] Also, the dipole of the gas phase ion under the high field limit may align to some extent with the electric field in the drift tube.[41] The low field limit, on the other hand, is the E / N regime where the collision energy gained by the ion is dissipated by the same collisions with the buffer gas. The protein ions thermalize to the buffer gas temperature, freely rotate, and 'tumble' through the drift tube. Thus, the drift time accounts for the collision cross section averaged across all orientations.

In the low field limit, the ion mobility is independent of the electric field, but dependent on the cross section, Ω, of the ion. The mobility of the ion is expressed by the relationship [36, 42]:

$$K = \frac{(18\pi)^{1/2}}{16}\left[\frac{1}{m} + \frac{1}{m_b}\right]^{1/2}\frac{ze}{(k_B T)^{1/2}\Omega_{avg}^{(1,1)}}\frac{1}{n} \qquad (4)$$

Solving the relationship (4) for Ω, simplifying the terms, and using the corrected nested drift time, $t_d$, the equation becomes:

$$\Omega = \frac{3}{16}\sqrt{\frac{2\pi}{\mu k_B T}}\frac{Q}{n}\frac{t_d U}{L^2} \qquad (5)$$

Equation (5) was used to calculate all rotationally averaged collision cross sections. The reduced mass is μ using the mass of the ion [kg] and mass of a buffer gas molecule [kg], $k_B$ is the Boltzmann constant, Q [coulombs] equals the charge, *n* is the number gas density, U [volts] is the voltage drop across the drift tube, and L [cm] is the length of the drift tube.

The initial ion and buffer gas collisions experienced by the ion entering the drift tube are quite energetic. Once the ion enters the drift tube, it collisionally cools by the subsequent collisions with the buffer gas. In general Clemmer found that ions in some charge states unfold as they're injected into the drift tube. One exception was reported by Shelimov and Jarrold.[43] Upon injecting the apomyoglobin 6+ ion with increasing energy (300 to 1800 eV), the ion folded to a compact conformer using the higher injection energy.

**Measurement of Non-Covalent Protein Interactions**

Ion mobility mass spectrometry (IM MS) measures the absolute collision cross section of gas phase ions, which is a low resolution, bulk shape measurement compared to NMR and X-ray crystallography structure measurements. A strength of IM MS lies in its ability to measure large biological systems, including those as large as viruses.[44, 45] Few IM MS instruments have investigated protein / protein complexes because no commercial counterpart existed until recently, other than home-built instruments. Counterman and Clemmer [46, 47] were among the first to measure non-covalent complexes; they investigated peptide multimers using their pulsed ion injection – IM – MS. Bowers followed suit with his own home-built IM – MS instrument.[38] Bernstein and Bowers used that instrument to report that α-synuclein, a monomer in a solution with a pH near pI = 2, forms a dimer when it is electrosprayed out of a denaturing buffer at pH = 7.[48] Loo's group uses

their own version of IM – MS [49, 50] to measure the size of protein complexes based on the gas-phase electrophoretic mobility molecular analyzer (GEMMA).[51] Last, Wright and Douglas used their own version of an IM – MS based on a triple quadrupole to measure the collision cross section of hemoglobin monomer, dimer, and tetramer.[52]

The recently introduced commercial Synapt instrument by Waters uses an ion mobility process called traveling wave ion mobility.[53, 54] The traveling wave method, also known as the t-wave ion mobility, does not give an absolute collision cross section like traditional ion mobility does. Rather, one can calibrate the t-wave ion mobility using proteins with known collision cross sections.[55] The t-wave works with either electrospray ionization or MALDI.[56] Scarff and Scrivens have measured the collision cross sections of well-characterized proteins [57] and protein complexes like hemoglobin [58] using the t-wave ion mobility Synapt instrument. The ion mobility measured cross sections are comparable to those deduced from x-ray crystal structures of the same proteins. Other non-covalent protein complexes have been studied using the Synapt.[59-61] The only other commercial traditional ion mobility mass spectrometer instrument is sold by Ionwerks, and it is used primarily for lipid and peptide imaging using a MALDI source.[62]

The home-built three ion source – ion trap – ion mobility – TOF MS instrument [63] built by Badman et al. was used to analyze the protein / protein interactions in the YbhB protein from *Escherichia coli* and the YbhB protein homolog from the *Arabidopsis thaliana* plant. The extent of dimer formation and collision cross section for the YbhB proteins are discussed (Chapter 3). Dimer ions are dissociated to monomers and adducts are removed due to more energetic injection conditions. Ion mobility cross section measurements were also used for the time-resolved protein ion heating study (Chapter 4).

**Pulsed Injection – Ion Mobility – Mass Spectrometers**

The designs of other similar ion mobility mass spectrometry instruments, which utilize a short pulse of ions (referred to as an ion packet), are of interest to the time-resolved protein ion heating paper (Chapter 4). Since the early 1990s, ion mobility mass spectrometer instruments evolved to measure the shape of biomolecules.[64-70] Early reduced pressure ion mobility instruments injected a 30 to 50 µs pulse of ions into the mobility cell through an 80 µm i.d. aperture, containing 2.5 to 6.5 mbar helium gas.[37, 71-75] A quadrupole

performed mass analysis for these injected ion mobility instruments. The next iteration of ion mobility mass spectrometry instruments added a 3D quadrupole ion trap [76-79] or 2D linear ion trap [80-82] to collect and cool the ions before injecting them into the mobility cell. Ions in the 3D trap were stored and cooled for tens of milliseconds. A 40 to 400 V square wave DC pulse, applied for 0.2 to 4 µs on the exit lens, extracted the ions out of the ion trap. The mobility cell had either 80 or 160 µm i.d. entrance apertures, containing 2.5 to 6.5 mbar helium gas. One variation of the 3D ion trap ion mobility instrument by Creaser [83] extracted ions out of the trap using a fast, 0.2 to 1 µs attractive DC pulse (3 to 95 V). The 3D ion trap – IM MS instruments built by Clemmer and Creaser are similar to the one featured in this dissertation.[63] The 2D linear traps needed a long (100 µs) extraction pulse because the ions spread out along the entire z-axis of the ion trap. In subsequent 2D IT – IM – qTOF MS instruments the entrance aperture of the mobility cell was enlarged to 1000 µm i.d. [80-82, 84].

Subsequent designs of trapping – IMS – qTOF MS instruments led to tandem IMS-IMS [85, 86] and the traveling wave (T-wave) instrument [87]. The IMS / IMS instrument continued to use the 1000 µm and 2500 µm i.d. entrance and exit aperture for the mobility cell, respectively [84] and a long (50 to 100 µs) extraction pulse. The pressure remained 2.6 to 6.5 mbar in the mobility cell. The T-wave instrument uses 2000 µm i.d. for the entrance and exit aperture, containing 1.3 mbar of helium gas [87]. To handle the extra gas leaking out of the larger apertures on the mobility cell, the IMS cell was placed into a separate chamber that is pumped out using an additional roughing vacuum pump or turbomolecular and roughing vacuum pump combination.

Our instrument design follows the 3D ion trap – IM – TOF MS built in Clemmer's group [37, 77, 78, 88], but to our knowledge they did not notice the effect concerning the extraction duration and voltage magnitude, nor has any other research group. It may be that i) they did not use long (> 9 µs) extraction pulses for the 3D ion trap instruments, and ii) they used large injection voltages (≥ 50 V) that would suppress compact conformers. They stated investigating the ion trap extraction conditions did not appreciably broaden the width of the measured ion packets.[76, 77] Their ion mobility experiments involving the 3D ion traps used a short pulse (0.2 to 4 µs) to extract a short, sharp ion packet. A dense ion packet would

not diffuse as much in the drift tube as a broad ion packet. Once the instrument designs started using the longer 2D ion traps, much longer (50 to 100 μs) extraction pulses were needed to extract the trapped ions. This result was confirmed with our home built 2D linear ion trap.[89] Further discussion about the protein ion heating due to specific instrument parameters follows in the paper "Time-Resolved Heating and Unfolding of Protein Ions Due to Ion Injection Conditions in an Ion Trap – Ion Mobility – Time-of-Flight Mass Spectrometer" (Chapter 4).

**DISSERTATION OVERVIEW**

The focus of this dissertation is two-fold: developing novel analysis methods using mass spectrometry and the implementation and characterization of a novel ion mobility mass spectrometry instrumentation. The novel mass spectrometry combines ion trap for ion / ion reactions coupled to an ion mobility cell. The long term goal of this instrumentation is to use ion / ion reactions to probe the structure of gas phase biomolecule ions.

The analysis of the degradation products in coal (Chapter 2) and the imaging plant metabolites (Appendix III) fall under the methods development category. These projects use existing commercial instrumentation (JEOL AccuTOF MS and Thermo Finnigan LCQ IT, respectively) for the mass analysis of the degraded coal products and the plant metabolites, respectively. The coal degradation paper discusses the use of the DART ion source for fast and easy sample analysis. The sample preparation consisted of a simple 50 fold dilution of the soluble coal products in water and placing the liquid in front of the heated gas stream. This is the first time the DART ion source has been used for analysis of coal. Steven Raders under the guidance of John Verkade came up with the coal degradation projects. Raders performed the coal degradation reactions, worked up the products, and sent them to me. I, Gregg Schieffer, developed the method and wrote the paper demonstrating the use of the DART ion source for the fast and easy sample analysis.

The plant metabolite imaging project extends the use of colloidal graphite as a sample coating for atmospheric pressure LDI. DC Perdian and I closely worked together to make this project work. Perdian focused on building the LDI setup whereas Schieffer focused

on the $MS^n$ analysis of the metabolites. Both Perdian and I took the data featured in the paper. Perdian was the primary writer of the paper and used it as a chapter in his dissertation (Chapter 5, page 100). Perdian and Schieffer worked together to address the revisions and publish it in Rapid Communications in Mass Spectrometry Journal.[24]

The IT – IM – TOF MS instrument and ubiquitin paper (Appendix I), cytochrome *c* paper (Appendix II), YAP and YBHB protein complexes paper (Chapter 3), and the time resolved protein ion heating paper (Chapter 4) fall under the characterization and use of novel ion mobility mass spectrometry instrumentation to probe the structure of biomolecules. The ubiquitin and cytochrome *c* protein ions were chosen to characterize the IT – IM – TOF MS instrument because the gas phase ions of those two proteins are well-characterized and understood. Matt Soyk, Qin Zhao, and I closely worked together under the guidance of Ethan Badman, and then Sam Houk to build and make the IT – IM – TOF MS instrument to work. Soyk, Zhao, and Schieffer performed experiments on the instrument. Most of the mass spectra featured in the ubiquitin and instrument paper were taken by Zhao. Soyk, Zhao, and Houk were the primary writers of the paper. Matt used the instrument paper as chapter 3 (page 71) in his dissertation. Qin used this paper as Chapter 2 (page 38). I helped finish the revisions with Dr. Houk and get it published in the Journal for the American Society for Mass Spectrometry.[63]

Most of the experiments discussed in the cytochrome c paper were done by Zhao. Zhao, Soyk, and Houk wrote the paper. Zhao used this paper as Chapter 3 (page 79) in her dissertation. Soyk used this paper as chapter 4 (page 100) in his dissertation. Schieffer worked up the data listed in the tables, acquired the cytochrome *c* data shown in figure 5, and addressed the revisions with Houk to publish it in the Journal for the American Society for Mass Spectrometry.[90]

The YbhB protein paper applies the analysis and characterization of protein complexes by the IT – IM – TOF MS. Libuse Brachova works for Basil Nikolau. Brachova expressed and purified all the YbhB and YbhB homolog protein. Schieffer took all the nESI mass spectra on the IT – IM – TOF MS. Joel Nott acquired the MALDI data. Schieffer wrote the paper with Houk's help. Brachova wrote portions of the introduction

and experimental sections concerning the YbhB and YbhB homolog proteins. We plan to publish the YbhB protein paper in a mass spectrometry journal.

Last, the time-resolved protein ion heating paper further explores the unexpected heating effect due to the duration and magnitude of the extraction pulse on the exit endcap of the ion trap through a series of experiments. Ubiquitin, as well as other proteins, were used to investigate this heating effect. Zhao, Soyk, and Schieffer first noticed this effect in 2005. It wasn't until 2007 or 2008 that Zhao noticed the ions "refolded" due to a long extraction pulse. In 2008 and 2009 Houk and Schieffer sought to explain and characterize the heating effect due to the extraction and injection conditions. Derrick Morast investigated the heating using carbonic anhydrase and lysozyme. Morast and Schieffer also worked together to keep the instrument working well. Houk and Schieffer wrote the time-resolved protein ion heating paper together. We plan to submit it to the International Journal of Mass Spectrometry.

**REFERENCES (International Journal of Mass Spectrometry formatting)**

[1] J. Hughes, Making Isotopes Matter: Francis Aston and the Mass-Spectrograph, Dynamis, 29 (2009) 131-165.
[2] I.W. Griffiths, J. J. Thomson - the Centenary of His Discovery of the Electron and of His Invention of Mass Spectrometry, Rapid Commun. Mass Spectrom., 11 (1997) 2-16.
[3] J.B. Fenn, M. Mann, C.K. Meng, S.F. Wong, C.M. Whitehouse, Electrospray Ionization-Principles and Practice, Mass Spectrom. Rev., 9 (1990) 37-70.
[4] M. Wilm, M. Mann, Analytical Properties of the Nanoelectrospray Ion Source, Anal. Chem., 68 (1996) 1-8.
[5] N.B. Cech, C.G. Enke, Practical Implications of Some Recent Studies in Electrospray Ionization Fundamentals, Mass Spectrom. Rev., 20 (2001) 362-387.
[6] F. Hillenkamp, M. Karas, R.C. Beavis, B.T. Chait, Matrix-Assisted Laser Desorption Ionization Mass-Spectrometry of Biopolymers, Anal. Chem., 63 (1991) A1193-A1202.
[7] U. Bahr, M. Karas, F. Hillenkamp, Analysis of Biopolymers by Matrix-Assited Laser-Desorption Ionization (MALDI) Mass-Spectrometry, Fresenius J. Anal. Chem., 348 (1994) 783-791.
[8] R.B. Cody, J.A. Laramee, H.D. Durst, Versatile New Ion Source for the Analysis of Materials in Open Air under Ambient Conditions, Anal. Chem., 77 (2005) 2297-2302.
[9] R.B. Cody, Observation of Molecular Ions and Analysis of Nonpolar Compounds with the Direct Analysis in Real Time Ion Source, Anal. Chem., 81 (2009) 1101-1107.
[10] S.N. Jackson, A.S. Woods, Direct Profiling of Tissue Lipids by MALDI-TOFMS, J. Chromatogr. B, 877 (2009) 2822-2829.
[11] S.W. Cha, E.S. Yeung, Colloidal Graphite-Assisted Laser Desorption/Ionization Mass Spectrometry and $MS^n$ of Small Molecules. 1. Imaging of Cerebrosides Directly from Rat Brain Tissue, Anal. Chem., 79 (2007) 2373-2385.
[12] H. Zhang, S.W. Cha, E.S. Yeung, Colloidal Graphite-Assisted Laser Desorption/Ionization MS and $MS^n$ of Small Molecules. 2. Direct Profiling and Ms Imaging of Small Metabolites from Fruits, Anal. Chem., 79 (2007) 6575-6584.
[13] F.M. Fernandez, R.B. Cody, M.D. Green, C.Y. Hampton, R. McGready, S. Sengaloundeth, N.J. White, P.N. Newton, Characterization of Solid Counterfeit Drug Samples by Desorption Electrospray Ionization and Direct-Analysis-in-Real-Time Coupled to Time-of-Flight Mass Spectrometry, ChemMedChem, 1 (2006) 702-+.
[14] J.Y. Yew, R.B. Cody, E.A. Kravitz, Cuticular Hydrocarbon Analysis of an Awake Behaving Fly Using Direct Analysis in Real-Time Time-of-Flight Mass Spectrometry, Proc. Natl. Acad. Sci. U. S. A., 105 (2008) 7135-7140.
[15] M. Karas, D. Bachmann, F. Hillenkamp, Influence of the Wavelength in High-Irradiance Ultraviolet-Laser Desorption Mass-Spectrometry of Organic-Molecules, Anal. Chem., 57 (1985) 2935-2939.

[16] K. Tanaka, H. Waki, Y. Ido, S. Akita, Y. Yoshida, T. Yoshida, T. Matsuo, Protein and Polymer Analyses up to m/z 100000 by Laser Ionization Time-of-Flight Mass Spectrometry, Rapid Commun. Mass Spectrom., 2 (1988) 151-153.
[17] M. Karas, M. Gluckmann, J. Schafer, Ionization in Matrix-Assisted Laser Desorption/Ionization: Singly Charged Molecular Ions Are the Lucky Survivors, J. Mass Spectrom., 35 (2000) 1-12.
[18] M. Karas, D. Bachmann, U. Bahr, F. Hillenkamp, Matrix-Assisted Ultraviolet-Laser Desorption of Nonvolatile Compounds, Int. J. Mass Spectrom. Ion Process., 78 (1987) 53-68.
[19] R. Zenobi, R. Knochenmuss, Ion Formation in MALDI Mass Spectrometry, Mass Spectrom. Rev., 17 (1998) 337-366.
[20] M. Karas, R. Kruger, Ion Formation in MALDI: The Cluster Ionization Mechanism, Chem. Rev., 103 (2003) 427-439.
[21] R. Knochenmuss, Ion Formation Mechanisms in UV-MALDI, Analyst, 131 (2006) 966-986.
[22] V.V. Laiko, S.C. Moyer, R.J. Cotter, Atmospheric Pressure MALDI/Ion Trap Mass Spectrometry, Anal. Chem., 72 (2000) 5239-5243.
[23] S.G. Moyer, R.J. Cotter, Atmospheric Pressure MALDI, Anal. Chem., 74 (2002) 468A-476A.
[24] D.C. Perdian, G.M. Schieffer, R.S. Houk, Atmospheric Pressure Laser Desorption/Ionization of Plant Metabolites and Plant Tissue Using Colloidal Graphite, Rapid Commun. Mass Spectrom., 24 (2010) 397-402.
[25] M. Yamashita, J.B. Fenn, Electrospray Ion-Source - Another Variation on the Free-Jet Theme, J. Phys. Chem., 88 (1984) 4451-4459.
[26] M. Yamashita, J.B. Fenn, Negative-Ion Production with the Electrospray Ion-Source, J. Phys. Chem., 88 (1984) 4671-4675.
[27] J.B. Fenn, M. Mann, C.K. Meng, S.F. Wong, C.M. Whitehouse, Electrospray Ionization for Mass-Spectrometry of Large Biomolecules, Science, 246 (1989) 64-71.
[28] C.M. Whitehouse, R.N. Dreyer, M. Yamashita, J.B. Fenn, Electrospray Interface for Liquid Chromatographs and Mass Spectrometers, Anal. Chem., 57 (1985) 675-679.
[29] B. Mehlis, U. Kertscher, Liquid Chromatography Mass Spectrometry of Peptides of Biological Samples, Anal. Chim. Acta, 352 (1997) 71-83.
[30] R. Juraschek, T. Dulcks, M. Karas, Nanoelectrospray - More Than Just a Minimized-Flow Electrospray Ionization Source, J. Am. Soc. Mass Spectrom., 10 (1999) 300-308.
[31] M. Karas, U. Bahr, T. Dulcks, Nano-Electrospray Ionization Mass Spectrometry: Addressing Analytical Problems Beyond Routine, Fresenius J. Anal. Chem., 366 (2000) 669-676.
[32] M.H. Amad, N.B. Cech, G.S. Jackson, C.G. Enke, Importance of Gas-Phase Proton Affinities in Determining the Electrospray Ionization Response for Analytes and Solvents, J. Mass Spectrom., 35 (2000) 784-789.

[33] P. Nemes, I. Marginean, A. Vertes, Spraying Mode Effect on Droplet Formation and Ion Chemistry in Electrosprays, Anal. Chem., 79 (2007) 3105-3116.
[34] A. Gomez, K.Q. Tang, Charge and Fission of Droplets in Electrostatic Sprays, Phys. Fluids, 6 (1994) 404-414.
[35] M. Dole, L.L. Mack, R.L. Hines, Molecular Beams of Macroions, J. Chem. Phys., 49 (1968) 2240-&.
[36] D.E. Clemmer, M.F. Jarrold, Ion Mobility Measurements and Their Applications to Clusters and Biomolecules, J. Mass Spectrom., 32 (1997) 577-592.
[37] C.S. Hoaglund, S.J. Valentine, C.R. Sporleder, J.P. Reilly, D.E. Clemmer, Three-Dimensional Ion Mobility TOFMS Analysis of Electrosprayed Biomolecules, Anal. Chem., 70 (1998) 2236-2242.
[38] T. Wyttenbach, P.R. Kemper, M.T. Bowers, Design of a New Electrospray Ion Mobility Mass Spectrometer, Int. J. Mass Spectrom., 212 (2001) 13-23.
[39] R. Guevremont, R.W. Purves, Atmospheric Pressure Ion Focusing in a High-Field Asymmetric Waveform Ion Mobility Spectrometer, Rev. Sci. Instrum., 70 (1999) 1370-1383.
[40] A.A. Shvartsburg, F.M. Li, K.Q. Tang, R.D. Smith, Distortion of Ion Structures by Field Asymmetric Waveform Ion Mobility Spectrometry, Anal. Chem., 79 (2007) 1523-1528.
[41] R.A. Dressler, H. Meyer, S.R. Leone, Laser Probing of the Rotational Alignment of $N_2^+$ Drifted in Helium, J. Chem. Phys., 87 (1987) 6029-6039.
[42] H.E. Revercomb, E.A. Mason, Theory of Plasma Chromatography Gaseous Electrophoresis - Review, Anal. Chem., 47 (1975) 970-983.
[43] K.B. Shelimov, M.F. Jarrold, Conformations, Unfolding, and Refolding of Apomyoglobin in Vacuum: An Activation Barrier for Gas-Phase Protein Folding, J. Am. Chem. Soc., 119 (1997) 2987-2994.
[44] J.J. Thomas, B. Bothner, J. Traina, W.H. Benner, G. Siuzdak, Electrospray Ion Mobility Spectrometry of Intact Viruses, Spectr.-Int. J., 18 (2004) 31-36.
[45] M. Sharon, C.V. Robinson, The Role of Mass Spectrometry in Structure Elucidation of Dynamic Protein Complexes, Annu. Rev. Biochem., 76 (2007) 167-193.
[46] A.E. Counterman, S.J. Valentine, C.A. Srebalus, S.C. Henderson, C.S. Hoaglund, D.E. Clemmer, High-Order Structure and Dissociation of Gaseous Peptide Aggregates That Are Hidden in Mass Spectra, J. Am. Soc. Mass Spectrom., 9 (1998) 743-759.
[47] A.E. Counterman, A.E. Hilderbrand, C.A.S. Barnes, D.E. Clemmer, Formation of Peptide Aggregates During ESI: Size, Charge, Composition, and Contributions to Noise, J. Am. Soc. Mass Spectrom., 12 (2001) 1020-1035.
[48] S.L. Bernstein, D.F. Liu, T. Wyttenbach, M.T. Bowers, J.C. Lee, H.B. Gray, J.R. Winkler, α-Synuclein: Stable Compact and Extended Monomeric Structures and Ph Dependence of Dimer Formation, J. Am. Soc. Mass Spectrom., 15 (2004) 1435-1443.

[49] J.A. Loo, B. Berhane, C.S. Kaddis, K.M. Wooding, Y.M. Xie, S.L. Kaufman, I.V. Chernushevich, Electrospray Ionization Mass Spectrometry and Ion Mobility Analysis of the 20S Proteasome Complex, J. Am. Soc. Mass Spectrom., 16 (2005) 998-1008.
[50] C.S. Kaddis, S.H. Lomeli, S. Yin, B. Berhane, M.I. Apostol, V.A. Kickhoefer, L.H. Rome, J.A. Loo, Sizing Large Proteins and Protein Complexes by Electrospray Ionization Mass Spectrometry and Ion Mobility, J. Am. Soc. Mass Spectrom., 18 (2007) 1206-1216.
[51] S.L. Kaufman, Analysis of Biomolecules Using Electrospray and Nanoparticle Methods: The Gas-Phase Electrophoretic Mobility Molecular Analyzer (GEMMA), J. Aerosol. Sci., 29 (1998) 537-552.
[52] P.J. Wright, D.J. Douglas, Gas-Phase H/D Exchange and Collision Cross Sections of Hemoglobin Monomers, Dimers, and Tetramers, J. Am. Soc. Mass Spectrom., 20 (2009) 484-495.
[53] K. Giles, S.D. Pringle, K.R. Worthington, D. Little, J.L. Wildgoose, R.H. Bateman, Applications of a Travelling Wave-Based Radio-Frequencyonly Stacked Ring Ion Guide, Rapid Commun. Mass Spectrom., 18 (2004) 2401-2414.
[54] S.D. Pringle, K. Giles, J.L. Wildgoose, J.P. Williams, S.E. Slade, K. Thalassinos, R.H. Bateman, M.T. Bowers, J.H. Scrivens, An Investigation of the Mobility Separation of Some Peptide and Protein Ions Using a New Hybrid Quadrupole/Travelling Wave IMS/OA-TOF Instrument, Int. J. Mass Spectrom., 261 (2007) 1-12.
[55] B.T. Ruotolo, J.L.P. Benesch, A.M. Sandercock, S.J. Hyung, C.V. Robinson, Ion Mobility-Mass Spectrometry Analysis of Large Protein Complexes, Nat. Protoc., 3 (2008) 1139-1152.
[56] W.B. Ridenour, M. Kliman, J.A. McLean, R.M. Caprioli, Structural Characterization of Phospholipids and Peptides Directly from Tissue Sections by MALDI Traveling-Wave Ion Mobility-Mass Spectrometry, Anal. Chem., 82 (2010) 1881-1889.
[57] C.A. Scarff, K. Thalassinos, G.R. Hilton, J.H. Scrivens, Travelling Wave Ion Mobility Mass Spectrometry Studies of Protein Structure: Biological Significance and Comparison with X-Ray Crystallography and Nuclear Magnetic Resonance Spectroscopy Measurements, Rapid Commun. Mass Spectrom., 22 (2008) 3297-3304.
[58] C.A. Scarff, V.J. Patel, K. Thalassinos, J.H. Scrivens, Probing Hemoglobin Structure by Means of Travelling-Wave Ion Mobility Mass Spectrometry, J. Am. Soc. Mass Spectrom., 20 (2009) 625-631.
[59] S.J. Hyung, C.V. Robinson, B.T. Ruotolo, Gas-Phase Unfolding and Disassembly Reveals Stability Differences in Ligand-Bound Multiprotein Complexes, Chem. Biol., 16 (2009) 382-390.
[60] J.A. Leary, M.R. Schenauer, R. Stefanescu, A. Andaya, B.T. Ruotolo, C.V. Robinson, K. Thalassinos, J.H. Scrivens, M. Sokabe, J.W.B. Hershey, Methodology for Measuring Conformation of Solvent-Disrupted Protein Subunits Using T-Wave Ion Mobility Ms: An

Investigation into Eukaryotic Initiation Factors, J. Am. Soc. Mass Spectrom., 20 (2009) 1699-1706.
[61] T. Wyttenbach, M. Grabenauer, K. Thalassinos, J.H. Scrivens, M.T. Bowers, The Effect of Calcium Ions and Peptide Ligands on the Relative Stabilities of the Calmodulin Dumbbell and Compact Structures, J. Phys. Chem. B, 114 (2010) 437-447.
[62] S.N. Jackson, M. Ugarov, T. Egan, J.D. Post, D. Langlais, J.A. Schultz, A.S. Woods, MALDI-Ion Mobility-TOF MS Imaging of Lipids in Rat Brain Tissue, J. Mass Spectrom., 42 (2007) 1093-1098.
[63] Q. Zhao, M.W. Soyk, G.M. Schieffer, K. Fuhrer, M.M. Gonin, R.S. Houk, E.R. Badman, An Ion Trap-Ion Mobility-Time of Flight Mass Spectrometer with Three Ion Sources for Ion/Ion Reactions, J. Am. Soc. Mass Spectrom., 20 (2009) 1549-1561.
[64] T. Covey, D.J. Douglas, Collision Cross-Sections for Protein Ions, J. Am. Soc. Mass Spectrom., 4 (1993) 616-623.
[65] P.D. Schnier, D.S. Gross, E.R. Williams, Electrostatic Forces and Dielectric Polarizability of Multiply Protonated Gas-Phase Cytochrome *c* Ions Probed by Ion/Molecule Chemistry, J. Am. Chem. Soc., 117 (1995) 6747-6757.
[66] D.S. Gross, P.D. Schnier, S.E. RodriguezCruz, C.K. Fagerquist, E.R. Williams, Conformations and Folding of Lysozyme Ions in Vacuo, Proc. Natl. Acad. Sci. U. S. A., 93 (1996) 3143-3148.
[67] B.A. Collings, D.J. Douglas, Conformation of Gas-Phase Myoglobin Ions, J. Am. Chem. Soc., 118 (1996) 4488-4489.
[68] M.F. Jarrold, Peptides and Proteins in the Vapor Phase, Annu. Rev. Phys. Chem., 51 (2000) 179-207.
[69] C.S. Creaser, J.R. Griffiths, C.J. Bramwell, S. Noreen, C.A. Hill, C.L.P. Thomas, Ion Mobility Spectrometry: A Review. Part 1. Structural Analysis by Mobility Measurement, Analyst, 129 (2004) 984-994.
[70] B.C. Bohrer, S.I. Merenbloom, S.L. Koeniger, A.E. Hilderbrand, D.E. Clemmer, Biomolecule Analysis by Ion Mobility Spectrometry, Annu. Rev. Anal. Chem., 1 (2008) 293-327.
[71] Y.S. Liu, D.E. Clemmer, Characterizing Oligosaccharides Using Injected-Ion Mobility Mass Spectrometry, Anal. Chem., 69 (1997) 2504-2509.
[72] Y.S. Liu, S.J. Valentine, A.E. Counterman, C.S. Hoaglund, D.E. Clemmer, Injected-Ion Mobility Analysis of Biomolecules, Anal. Chem., 69 (1997) A728-A735.
[73] S.J. Valentine, J.G. Anderson, A.D. Ellington, D.E. Clemmer, Disulfide-Intact and -Reduced Lysozyme in the Gas Phase: Conformations and Pathways of Folding and Unfolding, J. Phys. Chem. B, 101 (1997) 3891-3900.
[74] S.J. Valentine, D.E. Clemmer, H/D Exchange Levels of Shape-Resolved Cytochrome *c* Conformers in the Gas Phase, J. Am. Chem. Soc., 119 (1997) 3558-3566.

[75] S.J. Valentine, A.E. Counterman, D.E. Clemmer, Conformer-Dependent Proton-Transfer Reactions of Ubiquitin Ions, J. Am. Soc. Mass Spectrom., 8 (1997) 954-961.
[76] C.S. Hoaglund, S.J. Valentine, D.E. Clemmer, An Ion Trap Interface for ESI-Ion Mobility Experiments, Anal. Chem., 69 (1997) 4156-4161.
[77] S.C. Henderson, S.J. Valentine, A.E. Counterman, D.E. Clemmer, ESI/Ion Trap/Ion Mobility/Time-of-Flight Mass Spectrometry for Rapid and Sensitive Analysis of Biomolecular Mixtures, Anal. Chem., 71 (1999) 291-301.
[78] C.S. Hoaglund-Hyzer, D.E. Clemmer, Ion Trap/Ion Mobility/Quadrupole/Time of Flight Mass Spectrometry for Peptide Mixture Analysis, Anal. Chem., 73 (2001) 177-184.
[79] C.S. Hoaglund-Hyzer, Y.J. Lee, A.E. Counterman, D.E. Clemmer, Coupling Ion Mobility Separations, Collisional Activation Techniques, and Multiple Stages of MS for Analysis of Complex Peptide Mixtures, Anal. Chem., 74 (2002) 992-1006.
[80] Y.J. Lee, C.S. Hoaglund-Hyzer, C.A.S. Barnes, A.E. Hilderbrand, S.J. Valentine, D.E. Clemmer, Development of High-Throughput Liquid Chromatography Injected Ion Mobility Quadrupole Time-of-Flight Techniques for Analysis of Complex Peptide Mixtures, J. Chromatogr. B, 782 (2002) 343-351.
[81] S. Myung, Y.J. Lee, M.H. Moon, J. Taraszka, R. Sowell, S. Koeniger, A.E. Hilderbrand, S.J. Valentine, L. Cherbas, P. Cherbas, T.C. Kaufmann, D.F. Miller, Y. Mechref, M.V. Novotny, M.A. Ewing, C.R. Sporleder, D.E. Clemmer, Development of High-Sensitivity Ion Trap Ion Mobility Spectrometry Time-of-Flight Techniques: A High-Throughput Nano-LC-IMS-TOF Separation of Peptides Arising from a *Drosophila* Protein Extract, Anal. Chem., 75 (2003) 5137-5145.
[82] R.A. Sowell, S.L. Koeniger, S.J. Valentine, M.H. Moon, D.E. Clemmer, Nanoflow LCMS-MS and LCMS-CID/MS of Protein Mixtures, J. Am. Soc. Mass Spectrom., 15 (2004) 1341-1353.
[83] C.S. Creaser, M. Benyezzar, J.R. Griffiths, J.W. Stygall, A Tandem Ion Trap/Ion Mobility Spectrometer, Anal. Chem., 72 (2000) 2724-2729.
[84] S.J. Valentine, S.L. Koeniger, D.E. Clemmer, A Split-Field Drift Tube for Separation and Efficient Fragmentation of Biomolecular Ions, Anal. Chem., 75 (2003) 6202-6208.
[85] S.L. Koeniger, S.I. Merenbloom, S.J. Valentine, M.F. Jarrold, H.R. Udseth, R.D. Smith, D.E. Clemmer, An IMS-IMS Analogue of MS-MS, Anal. Chem., 78 (2006) 4161-4174.
[86] S.I. Merenbloom, S.L. Koeniger, S.J. Valentine, M.D. Plasencia, D.E. Clemmer, IMS-IMS and IMS-IMS-IMS/MS for Separating Peptide and Protein Fragment Ions, Anal. Chem., 78 (2006) 2802-2809.
[87] D.P. Smith, K. Giles, R.H. Bateman, S.E. Radford, A.E. Ashcroft, Monitoring Copopulated Conformational States During Protein Folding Events Using Electrospray Ionization-Ion Mobility Spectrometry-Mass Spectrometry, J. Am. Soc. Mass Spectrom., 18 (2007) 2180-2190.

[88] E.R. Badman, S. Myung, D.E. Clemmer, Gas-Phase Separations of Protein and Peptide Ion Fragments Generated by Collision-Induced Dissociation in an Ion Trap, Anal. Chem., 74 (2002) 4889-4894.
[89] M.W. Soyk, Q. Zhao, R.S. Houk, E.R. Badman, A Linear Ion Trap Mass Spectrometer with Versatile Control and Data Acquisition for Ion/Ion Reactions, J. Am. Soc. Mass Spectrom., 19 (2008) 1821-1831.
[90] Q. Zhao, G.M. Schieffer, M.W. Soyk, T.J. Anderson, R.S. Houk, E.R. Badman, Effects of Ion/Ion Proton Transfer Reactions on Conformation of Gas-Phase Cytochrome *c* Ions, J. Am. Soc. Mass Spectrom., (2010) *in press*.

**FIGURE**

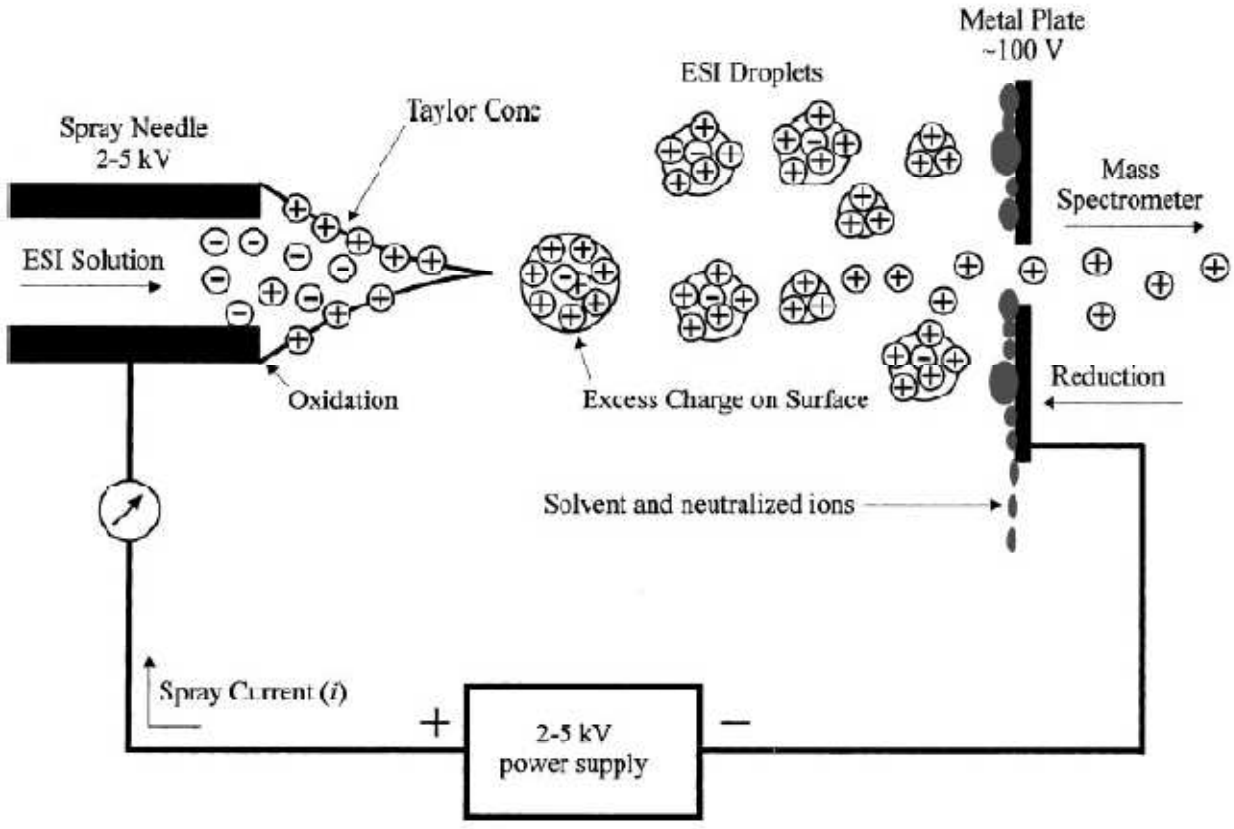


Figure 1) Adapted from Cech and Enke's paper.[5] The electrospray ionization (ESI) process forms an aerosol containing charged analyte. The droplets dry and fission into smaller droplets, repeating until naked analyte ions remain. Some of the naked analyte ions are focused into the mass spectrometer.
The ESI process makes a closed power circuit.

# CHAPTER 2

# IDENTIFICATION OF DEGRADATION PRODUCTS FROM LIGNITE COAL BY DIRECT ANALYSIS IN REAL TIME TIME-OF-FLIGHT MASS SPECTROMETRY

Gregg M. Schieffer, Steven M. Raders,[a] John G. Verkade, and R. S. Houk*

Department of Chemistry, Iowa State University, Ames, IA 50011 USA
*Ames Laboratory U. S. Department of Energy, Ames, IA 50011 USA

[a]Present Address: Department of Chemistry, University of Alabama, Tuscaloosa, AL 35487

*Corresponding Author. Tel (515) 294-9462 Fax-0050 rshouk@iastate.edu

For submission to Rapid Communications in Mass Spectrometry

**ABSTRACT**

Direct Analysis in Real Time (DART) mass spectrometry (MS) is used for the first time for the rapid identification of coal degradation products. DART ionizes the water-soluble, liquid and water-insoluble, solid coal degraded samples without additional sample preparation. The high mass accuracy of the time-of-flight MS enabled tentative elemental composition assignments of the product ions from the coal degradation reactions. The method described herein is a fast way to ascertain the products from coal degradation reactions without additional sample preparation. The DART MS analysis revealed that the i) 150 °C coal degradation reaction using trimethylolpropane phosphite compared to the 37 °C reaction and ii) higher pressure coal degradation reaction using pyrocatechol compared to the atmospheric pressure reaction liberated larger and more abundant compounds from the coal.

Keywords: direct analysis in real time (DART), mass spectrometry, coal degradation, trimethylolpropane phosphite, pyrocatechol

**INTRODUCTION**

Lignin is a complex, heterogeneous [1] substance that provides structure and protection to plant cells. Lignite coal is the first stage in the metamorphic conversion of degradation resistant lignin in peat into coal.[2] Roughly half of the world's coal reserves are lignite coal.[3] However, its high water and ash content, poor energy value, and storage instability make lignite coal an undesirable option for use in power plants.[4]

Since the beginning of the 20th century, researchers have sought to extract compounds from coal to determine the different components or to convert the lignite into a better fuel source. For example, pyridine is one of the best solvents and dissolves 10 to 20 % (w/w) coal. Other solvents (e.g., acetonitrile) only dissolve two to four percent (w/w) coal.[5] Further work on extracting compounds involve: a) oxidation reactions [6] to degrade

coal via nitric acid, dichromate, or other oxidizing agents, b) halogenation, [6] or c) reacting the coal with ampholytic solvents above 100 °C.[5] A more recent oxidative hydrolysis method uses cupric oxide and steam at 170 °C in steel bombs to hydrolyze lignite coal.[7, 8] An advantage of this process is that the original building blocks of the coal are retained. Analysis by gas chromatography electron impact MS and capillary electrophoresis yielded details concerning the amount, quality, and stage of degradation of the lignin in the coal.[9]

Mass spectrometry (MS) is a recent entrant for coal analysis. Early work in the 1950s identified the volatile thermal degradation products of coal via electron impact MS.[10, 11] Newer ionization methods such as fast atom bombardment,[12] electrospray ionization,[13] and laser desorption ionization [14] experiments paved the way to liberate and ionize non-volatile molecules from coal. Marshall et al. used electrospray ionization with Fourier transform ion cyclotron resonance mass spectrometry (FTICR MS) to resolve 10,000 distinct polar components in pyridine soluble coal extracts.[15] Recently Linford et al. [16] analyzed the organic and inorganic ions in coal samples by time-of-flight secondary ion mass spectrometry (TOF SIMS) using a 69Ga+ ion beam.

The use of Direct Analysis in Real Time (DART) with MS has grown quickly since its introduction in 2005.[17] Samples analyzed using DART range from drug tablets,[17, 18] drug discovery,[19] chemical warfare agents [20] to monitoring pheromones from well behaved (i.e., stationary) fruit flies.[21] Sample preparation for analysis is minimal so long as the sample encounters the DART gas stream and the analyte readily accepts or loses a proton. Another competing ionization mechanism involves a reactive DART specie removing an electron from the analyte.[22] Volatile, liquid, or solid samples are all amenable to analysis. The DART ion source couples to any MS that accepts an external ion source such as single and triple quadrupoles,[23-25] the Orbitrap,[26] FTICR,[27] and a field portable ion trap.[28] High spectral resolution is particularly valuable with DART because the samples are mixtures and the resulting mass spectra can be complex.

In the present work, aqueous solutions of trimethylolpropane phosphite (EtCage, Drawing 1)[29] and pyrocatechol [5] were used to degrade lignite coal. The cost and disposal expenses of organic solvent wastes are thus avoided. The products were divided into two portions, water-soluble or insoluble, for rapid characterization by MS. This report

mainly emphasizes the use of the DART ion source for quick analysis and qualitative characterization of the degradation products from both the water-soluble and the insoluble coal samples. The high mass accuracy and elemental composition software of the time-of-flight MS (JEOL AccuTOF) facilitate tentative assignments of the primary components from the degraded coal. The overall degradation efficiency of the various reagents and different conditions can be assessed quickly by DART MS.

## EXPERIMENTAL

### Sample Preparation

All samples were prepared in house by grinding chunks of a particular piece of Louisiana lignite coal to 106 to 125 mesh.

### Coal Degradation Using EtCage

To a 15 mL pressure tube was added 1.7 grams of ground coal, 7.14 grams (44.06 mmol) of the solid EtCage and 1 mL of water. The pressure tube was sealed and placed in a 37 °C oil bath for one month. The result was an amber colored oil with solid coal residue particles. The vessel was then allowed to cool to room temperature, methanol was added to mobilize the soluble compounds and make it easier to separate the oil from the insoluble residue. The sample was filtered, and the remaining insoluble particles were removed by centrifugation. The method using the methanol to segregate the soluble and insoluble portions was repeated until the amber color disappeared in the solution. All solutions containing the soluble portion of the degraded coal were combined. The methanol used to segregate the soluble coal supernatant was then removed by evaporation, resulting in a viscous liquid. This liquid was diluted 50 fold (w/w) with water for analysis. The remaining insoluble solids after the segregation were dried in an oven and weighed. This reaction scheme was also used on additional chunks of coal at 80 and 150 °C in an oil bath.

### Soluble Coal Using Pyrocatechol

To a 15 mL pressure tube was added 1.7 grams of ground coal and 11.28 mL of a stock solution (43 g pyrocatechol / 100 mL water) of pyrocatechol (44.06 mmol). The pressure tube was sealed and placed in a 37 °C oil bath for one month. The vessel was allowed to cool, solids were filtered, methanol was added, and solid residue removed

by centrifugation and weighed, as described above. The water-soluble portion formed a solid after the methanol was evaporated. This procedure was repeated at elevated pressure (83 bar) using a Parr bomb reactor.

**Sample Analysis**

The methanol derived water-soluble coal degraded solutions from the above procedures were diluted 50 fold (w/w) with water as necessary. A clean glass melting point tube from Fisher Scientific (Pittsburgh, PA) was then dipped into the solution containing the soluble coal and held within the heated DART source gas stream about 5 mm from the AccuTOF orifice. The DART gas stream evaporated the residual liquid off the glass melting point tube. Solid samples were held in the DART source gas stream at the same position using clean stainless steel tweezers. Data were acquired at a rate of two mass spectra per second for at least 90 seconds for every sample. The mass range was m/z 60 to 800.

**Ion Source / Mass Spectrometer**

The DART 100 ion source[17] (IonSense, Saugus, MA) and orthogonal acceleration single reflectron TOFMS (AccuTOF, JEOL USA, Inc., Peabody, MA) in positive ion mode were used for all the experiments. The AccuTOF MS is an orthogonal acceleration single-reflectron time-of-flight mass spectrometer. The instrument was tuned using the [(H2O)2H]+ dimer from ambient air to determine the voltage settings for the best ion signal. Table 1 lists the conditions used for the coal analyses.

**Analysis by Elemental Composition Software**

Mass calibration was performed before each set of coal analysis runs. Each mass calibration spectrum was averaged and the m/z scale calibrated using protonated ions from liquid PEG1000 as external standards. The measured m/z values for the PEG1000 ions always agreed within 2 ppm or better with the calculated PEG1000 mass values. The typical resolution of the TOF was ~ 6000 (m /Δm).

The elemental composition software associated with the AccuTOF MS software generated the best elemental compositions using the defined parameters for all ions with signal above the set threshold, typically 2% of the most intense peak. All the elemental composition parameters included carbon, hydrogen, oxygen, and nitrogen atoms. For the EtCage samples, phosphorous was also included. The mass difference tolerance was

10 mTh. Many tentative elemental composition assignments agreed within 20 ppm. Some tentative elemental compositions from the insoluble portions only agreed within 110 ppm, making their assignments quite uncertain. The suggested elemental compositions reported below were verified manually using the appropriate 13C isotope peaks. Generally, the more intense the peak (i.e. more counts) and the greater the mass-to-charge ratio, the closer the tentative elemental composition compared to the calculated mass.

Only qualitative information was determined from the mass spectra as no internal standards were added to the coal before the degradation reactions. The AccuTOF lacks an additional mass spectrometer stage, excluding the use of collision induced dissociation to further confirm the identity of the measured coal degradation products.

## RESULTS AND DISCUSSION

### Analysis of Unreacted Coal

The unreacted coal proved amenable to analysis by DART mass spectrometry (Figure 1). All the ions from unreacted coal are below m/z 650. Note that the abundant ions continue above m/z 300. These high mass ions are some of the compounds degraded by the reagents in experiments described below. The inset shows an expanded view of one region to illustrate the peak shape and resolution. The FWHM for the m/z 377 peak is 75 mTh, for a resolution (m /Δm) of ~ 5000.

### DART MS Analysis of the Water-Soluble Fraction from Degraded Coal.

Aqueous solutions of pyrocatechol and EtCage (Drawing 1) are effective reagents for degradation of coal; they dissolve 60 % or more of the lignite coal sample used. The results of a few such experiments are shown below mainly to illustrate the value of DART MS for this analysis. The discussion is not meant to be a complete evaluation of different reagents.

In one such experiment, the effect of reaction temperature was assessed. Sections of the same coal lot were treated with aqueous EtCage at 37, 80, and 150 °C for one month. The resulting DART mass spectra for the soluble fractions are shown in Figure 2. The reagent ([M+H]+, m/z 163) reacts with itself in water to form various condensation products, which account for the most abundant peaks. The coal-derived ions are at lower abundance.

In general, these coal-derived ions indicate more extensive degradation (i.e., heavy, water-soluble compounds are generally more abundant) at 150 °C (Figure 2d) than at either 37 °C (Figure 2b) or 80 °C (Figure 2c). A few of the coal product ions contain phosphorous, such as $C_{13}H_{14}OP$ (15 ppm error, nominal m/z 217) and $C_{22}H_{18}O_{11}P$ (3 ppm error, nominal m/z 489), meaning the phosphite group from the EtCage attacks the coal. A detailed evaluation of the use of phosphite esters as degradation reagents on lignin is found in a paper by Oshel.[29]

Coal was degraded with the other reagent (pyrocatechol, Drawing 1) at two pressure values (1 bar and 83 bar) for one month at 37 °C. The degradation reaction via pyrocatechol at 1 bar dissolved 41% of the coal; 61% of the coal dissolved at 83 bar. The mass spectra from the resulting water-soluble fractions are shown in Figures 3 and 4. For the reaction done at 1 bar, most of the water-soluble ions are below m/z 350. For the high-pressure reaction, there are more ions up to m/z ~ 450. The high-pressure reaction also contains more ion peaks than the reaction done at 1 bar. Thus, larger and more numerous compounds are solubilized from coal when the reaction is done at higher pressure. The * and ** designations refer to the protonated pyrocatechol monomer ions (C6H7O2) and protonated pyrocatechol dimer (C12H13O4), respectively. The accurate masses listed for the reagent ions are within 10.8 and 9.1 ppm, respectively. The *** denotes an interference ion from protonated dioctyladipate (nominal protonated mass 371), which is a plasticizer from the melting point tube packaging.

Nearly all of the ions are singly protonated, $[M + H]^+$, confirmed by tentative elemental compositions (Tables 2 through 5). No multiply charged ions were made by DART. The tentative elemental compositions often contain oxygen atoms, suggesting that the species generated by our DART source preferentially ionize polar molecules through proton transfer reactions.[17, 22] To verify this hypothesis, a solid sample of pure naphthalene (eg. non-polar) was analyzed under the same DART conditions (Table 1) used for all the featured experiments; no signal was observed (data not shown). Recently Domin et al. measured large, insoluble polycyclic aromatic compounds (five rings and greater) by DART MS in positive ion mode.[30] The polycyclic aromatic compounds preferentially formed protonated species with a small amount of radical cation present. This suggests that

either polycyclic aromatic compounds need to have many rings to readily accept a proton or that the DART conditions used for this paper did not generate appreciable amounts of proper reactive species, such as $O_2^{+\bullet}$, to ionize a non-polar compound like naphthalene. Cody reported specific DART source conditions for a certain atmospheric pressure interface that generated abundant, odd-electron ions from saturated alkanes and other non-polar species.[22] These alternate experimental conditions [22] were not employed for the experiments featured in this paper.

Suggested elemental formulas for the more abundant product ions from the water-soluble pyrocatechol degraded coal are shown in Tables 2 and 3, respectively. All the ions are protonated and most contain oxygen. The m/z values for the indicated elemental compositions for the water-soluble portions are all within 30 ppm of the measured m/z values.

For the ions identified in Table 2, the double bond equivalence[31] (DBE) increases as the mass increases. For the reaction done at 1 bar, compounds two through fifteen are mostly aromatic because the DBE is greater than four (Table 2). Many of the higher mass compounds liberated from this coal sample at the high pressure lack aromaticity and may be fatty acids (Table 3), which are thought to be components of this coal in general.

**DART MS Analysis of the Insoluble Fraction from Degraded Coal.**

The dried, solid insoluble portion of the degraded coal was also amenable to DART analysis. The coal solids from the pyrocatechol reagents were brittle; some grains crumbled in the DART gas stream during analysis. In general, the coal residues were more fragile the more extensive the degradation reaction.

Mass spectra from coal residue after treatment with pyrocatechol solutions are shown in Figures 5 and 6; elemental assignments are given in Tables 4 and 5, respectively. Again, coal-derived ions from the solid residue stop at m/z ~ 460 when the reaction is done at 1 bar; these ions progress to higher m/z values (~ 550) when the reaction is done at higher pressure. Comparison of Figures 5 and 6 indicates that the residue from the high-pressure degradation reaction yields fewer peaks than that from the low pressure reaction. Mass spectra from the insoluble residues (Figures 5 and 6) generally have more peaks than those from the

water-soluble fractions (Figures 3 and 4). Also, the ions seen from the residues (Tables 4 and 5) are less likely to contain oxygen than their soluble counterparts (Tables 2 and 3). It seems that the presence of oxygen in the coal degradation products enhances their solubility in water and methanol. The proposed insoluble compounds in Tables 4 and 5 range from small fatty acids to large polyaromatic hydrocarbons. The presence of fatty acids in this coal was determined using another mass spectrometer (data not shown).

## CONCLUSION

DART MS is a fast and easy method, needing only a few minutes per sample, to characterize both the water-soluble and insoluble portions of degraded coal. The use of liquid chromatography MS, may take one hour to complete a run and is limited to analyzing the water-soluble portion. The high resolution and mass accuracy of the TOF MS and the instrument software enables tentative determination of the elemental compositions from the complex spectra. The DART MS shows that reactions using EtCage at a higher temperature degrade more of the coal and yields more abundant larger compounds than the lower temperature reaction. The coal degradation reaction at high pressure using pyrocatechol also yields higher mass ions in both the water-soluble and insoluble portions than the same reaction at atmospheric pressure.

## ACKNOWLEDGEMENTS

We thank Roger Jones, Tonu Reinot, and John McClelland for the use of the JEOL DART AccuTOF MS. The grant award, 2006-DN-BK-K017, from the National Institute of Justice, Office of Justice Program, and the U.S. Department of Justice purchased the DART AccuTOF MS. This present work was supported by a grant from Ciris Energy.

**REFERENCES (International Journal of Mass Spectrometry formatting)**

[1] N. Berkowitz, Coal Science and Technology; Vol. 7: The Chemistry of Coal, Elsevier Science, New York, NY, 1985.
[2] P.G. Hatcher, D.J. Clifford, The Organic Geochemistry of Coal: From Plant Materials to Coal, Org. Geochem., 27 (1997) 251-+.
[3] O.C. Kopp, Lignite (Coal), in: I. Encyclopaedia Britannica (Ed.) The New Encyclopaedia Brittannica, Chicago, Illinois, 2007.
[4] L. Zavodska, J. Lesny, Recent Development in Lignite Investigation, in, Slovakia, pp. 15. *manuscript.*
[5] N. Berkowitz, Coal Science and Technology; Vol. 7: The Chemistry of Coal, in: Coal, Elsevier Science, New York, NY, 1985, pp. Chapter 8.
[6] N. Berkowitz, Coal Science and Technology; Vol. 7: The Chemistry of Coal, in: Coal, Elsevier Science, New York, NY, 1985, pp. Chapter 5.
[7] R. Hayatsu, R.E. Botto, R.G. Scott, R.L. McBeth, R.E. Winans, Evaluation of Lignin and Cellulose Contributions to Low-Rank Coal Formation by Alkaline Cupric Oxide Oxidation, Fuel, 65 (1986) 821-826.
[8] J.I. Hedges, D.C. Mann, Characterization of Plant-Tissues by Their Lignin Oxidation-Products, Geochim. Cosmochim. Acta, 43 (1979) 1803-1807.
[9] M. Stefanova, O. Maman, B. Guillet, J.R. Disnar, Preserved Lignin Structures in Miocene-Aged Lignite Lithotypes, Bulgaria, Fuel, 83 (2004) 123-128.
[10] H.W. Holden, J.C. Robb, Mass Spectrometry of Substances of Low Volatility, Nature, 182 (1958) 340-340.
[11] H.W. Holden, J.C. Robb, A Study of Coal by Mass Spectrometry-Ii - Extracts and Extractable Pyrolysis Products, Fuel, 39 (1960) 485-494.
[12] G. Ricca, L. Federico, C. Astori, R. Gallo, Structural Investigations of Humic-Acid from Leonardite by Spectroscopic Methods and Thermal-Analysis, Geoderma, 57 (1993) 263-274.
[13] D.L. Zhan, J.B. Fenn, Electrospray Mass Spectrometry of Fossil Fuels, Int. J. Mass Spectrom., 194 (2000) 197-208.
[14] P. John, C.A.F. Johnson, J.E. Parker, G.P. Smith, A.A. Herod, A.F. Gaines, C.Z. Li, R. Kandiyoti, High Mass Material (Greater-Than-10(4) Daltons) in a Coal-Liquefaction Extract, by Laser-Desorption Mass-Spectrometry, Rapid Commun. Mass Spectrom., 5 (1991) 364-367.
[15] Z.G. Wu, S. Jernstrom, C.A. Hughey, R.P. Rodgers, A.G. Marshall, Resolution of 10,000 Compositionally Distinct Components in Polar Coal Extracts by Negative-Ion Electrospray Ionization Fourier Transform Ion Cyclotron Resonance Mass Spectrometry, Energy Fuels, 17 (2003) 946-953.
[16] L. Pei, G. Jiang, B.J. Tyler, L.L. Baxter, M.R. Linford, Time-of-Flight Secondary Ion Mass Spectrometry of a Range of Coal Samples: A Chemometrics (PCA, Cluster, and PLS) Analysis, Energy Fuels, 22 (2008) 1059-1072.
[17] R.B. Cody, J.A. Laramee, H.D. Durst, Versatile New Ion Source for the Analysis of Materials in Open Air under Ambient Conditions, Anal. Chem., 77 (2005) 2297-2302.
[18] F.M. Fernandez, R.B. Cody, M.D. Green, C.Y. Hampton, R. McGready, S. Sengaloundeth, N.J. White, P.N. Newton, Characterization of Solid Counterfeit Drug Samples by Desorption Electrospray Ionization and Direct-Analysis-in-Real-Time Coupled to Time-of-Flight Mass Spectrometry, ChemMedChem, 1 (2006) 702-+.

[19] C. Petucci, J. Diffendal, D. Kaufman, B. Mekonnen, G. Terefenko, B. Musselman, Direct Analysis in Real Time for Reaction Monitoring in Drug Discovery, Anal. Chem., 79 (2007) 5064-5070.
[20] J.M. Nilles, T.R. Connell, H.D. Durst, Quantitation of Chemical Warfare Agents Using the Direct Analysis in Real Time (DART) Technique, Anal. Chem., 81 (2009) 6744-6749.
[21] J.Y. Yew, R.B. Cody, E.A. Kravitz, Cuticular Hydrocarbon Analysis of an Awake Behaving Fly Using Direct Analysis in Real-Time Time-of-Flight Mass Spectrometry, Proc. Natl. Acad. Sci. U. S. A., 105 (2008) 7135-7140.
[22] R.B. Cody, Observation of Molecular Ions and Analysis of Nonpolar Compounds with the Direct Analysis in Real Time Ion Source, Anal. Chem., 81 (2009) 1101-1107.
[23] Y.P. Zhao, M. Lam, D.L. Wu, R. Mak, Quantification of Small Molecules in Plasma with Direct Analysis in Real Time Tandem Mass Spectrometry, without Sample Preparation and Liquid Chromatographic Separation, Rapid Commun. Mass Spectrom., 22 (2008) 3217-3224.
[24] O.P. Haefliger, N. Jeckelmann, Direct Mass Spectrometric Analysis of Flavors and Fragrances in Real Applications Using DART, Rapid Commun. Mass Spectrom., 21 (2007) 1361-1366.
[25] T. Rothenbacher, W. Schwack, Rapid and Nondestructive Analysis of Phthalic Acid Esters in Toys Made of Poly(Vinyl Chloride) by Direct Analysis in Real Time Single-Quadrupole Mass Spectrometry, Rapid Commun. Mass Spectrom., 23 (2009) 2829-2835.
[26] T. Rothenbacher, W. Schwack, Rapid Identification of Additives in Poly(Vinyl Chloride) Lid Gaskets by Direct Analysis in Real Time Ionisation and Single-Quadrupole Mass Spectrometry, Rapid Commun. Mass Spectrom., 24 (2010) 21-29.
[27] J.L. Rummel, A.M. McKenna, A.G. Marshall, J.R. Eyler, D.H. Powell, The Coupling of Direct Analysis in Real Time Ionization to Fourier Transform Ion Cyclotron Resonance Mass Spectrometry for Ultrahigh-Resolution Mass Analysis, Rapid Commun. Mass Spectrom., 24 (2010) 784-790.
[28] J.M. Wells, M.J. Roth, A.D. Keil, J.W. Grossenbacher, D.R. Justes, G.E. Patterson, D.J. Barket, Implementation of DART and DESI Ionization on a Fieldable Mass Spectrometer, J. Am. Soc. Mass Spectrom., 19 (2008) 1419-1424.
[29] R.E. Oshel, M.V. Nandakumar, S. Urgaonkar, D.G. Hendricker, J.G. Verkade, Water Solubilization of DDGS Via Derivatization with Phosphite Esters, Bioresour. Technol., 99 (2008) 5193-5205.
[30] M.A. Domin, B.D. Steinberg, J.M. Quimby, N.J. Smith, A.K. Greene, L.T. Scott, Routin Analysis and Characterization of Highly Insoluble Polycyclic Aromatic Compounds by Direct Analysis in Real Time Mass Spectrometry (DART), Analyst, 135 (2010) 700-704.
[31] E. Pretsch, P. Buehlmann, C. Affolter, Structure Determination of Organic Compounds, 3 ed., Springer-Verlag, New York, 2000.

**REAGENTS**

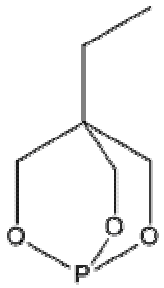


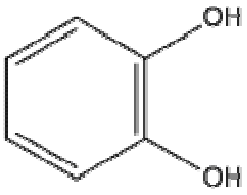


pyrocatechol

trimethylolpropane phosphite / EtCage

Drawing 1) These are the chemical structures of the two reagents, EtCage and pyrocatechol, used to degrade and water-solubilize coal.

**TABLES**

Table 1) Instrumental Operating Conditions

DART

| Parameter | Value |
|---|---|
| 99.999% pure He gas | 3.25 L / min (measured with an external flow meter) |
| He gas | 250° C |
| Needle | 3500 V |
| Discharge | 650 V |
| Grid | 150 V |

TOF MS Conditions

| Parameter | Value |
|---|---|
| Ring lens | 3 V |
| Orifice 1 | 80° C, 20 V |
| Orifice 2 | 3 V |
| Bias | 27 V |
| Pusher bias | -0.75 V |
| Focus | -90 V |
| Focus lens | 10 V |
| Quadrupole lens | 20 V |
| Right / Left lenses | 8.0 V |
| Top/Bottom lenses | 0.2 V |
| Reflectron | 990 V |
| Detector | 2500 V |

Table 2) Suggested elemental compositions for product ions identified in Figure 3. The coal was degraded by pyrocatechol at 37 °C and 1 bar for one month.

| Peak Number | m/z | Elemental Composition | Error, ppm |
|---|---|---|---|
| 1 | 83.0860 | $C_6H_{11}$ | 16.8 |
| 2 | 93.0313 | $C_6H_5O$ | 28.5 |
| 3 | 127.0412 | $C_6H_7O_3$ | 9.4 |
| 4 | 155.0370 | $C_7H_7O_4$ | 16.7 |
| 5 | 161.0646 | $C_{10}H_9O_2$ | 4.4 |
| 6 | 169.0500 | $C_8H_9O_4$ | 0.1 |
| 7 | 179.1056 | $C_{11}H_{15}O_2$ | 1.6 |
| 8 | 221.0697 | $C_{15}H_9O_2$ | 9.5 |
| 9 | 223.0697 | $C_{15}H_{11}O_2$ | 6.2 |
| 10 | 233.0587 | $C_{16}H_9O_2$ | 1.5 |
| 11 | 249.0580 | $C_{16}H_9O_3$ | 2.8 |
| 12 | 263.0579 | $C_{13}H_{11}O_6$ | 2.4 |
| 13 | 267.0548 | $C_{12}H_{11}O_7$ | 4.3 |
| 14 | 293.0669 | $C_{14}H_{13}O_7$ | 0.8 |
| 15 | 327.2110 | $C_{18}H_{31}O_5$ | 6.1 |

Table 3) Suggested elemental compositions for product ions identified in Figure 4. The coal was degraded by pyrocatechol at 37 °C and 83 bar for one month.

| Peak Number | m/z | Elemental Composition | Error, ppm |
|---|---|---|---|
| 1 | 83.0861 | $C_6H_{11}$ | 12.5 |
| 2 | 93.0352 | $C_6H_5O$ | 12.4 |
| 3 | 127.0420 | $C_6H_7O_3$ | 21.0 |
| 4 | 135.1020 | $C_6H_{15}O_3$ | 1.9 |
| 5 | 137.0600 | $C_8H_9O_2$ | 1.8 |
| 6 | 169.0510 | $C_8H_9O_4$ | 3.8 |
| 7 | 179.1080 | $C_{11}H_{15}O_2$ | 2.2 |
| 8 | 255.2370 | $C_{16}H_{31}O_2$ | 17.0 |
| 9 | 257.2440 | $C_{16}H_{33}O_2$ | 17.3 |
| 10 | 283.2680 | $C_{18}H_{35}O_2$ | 13.6 |
| 11 | 391.3010 | $C_{28}H_{39}O$ | 3.3 |
| 12 | 425.4040 | $C_{27}H_{53}O_3$ | 11.3 |
| 13 | 439.3750 | $C_{27}H_{51}O_4$ | 8.4 |

Table 4) Suggested elemental compositions for the insoluble coal residue product ions identified in Figure 5. The coal was degraded by pyrocatechol at 37 °C and 1 bar for one month.

| Peak Number | m/z | Elemental Composition | Error, ppm |
|---|---|---|---|
| 1 | 75.0368 | $C_3H_7O_2$ | 103.8 |
| 2 | 75.0714 | $C_4H_{11}O$ | 127.2 |
| 3 | 85.0592 | $C_5H_9O$ | 71.5 |
| 4 | 87.0397 | $C_4H_7O_2$ | 55.8 |
| 5 | 87.0756 | $C_5H_{11}O$ | 61.6 |
| 6 | 89.0552 | $C_4H_9O_2$ | 56.9 |
| 7 | 97.0664 | $C_6H_9O$ | 10.9 |
| 8 | 99.0436 | $C_5H_7O_2$ | 9.9 |
| 9 | 101.0720 | $C_5H_9O_2$ | 116.2 |
| 10 | 115.0790 | $C_6H_{11}O_2$ | 26.9 |
| 11 | 117.0906 | $C_6H_{13}O_2$ | 8.0 |
| 12 | 123.0497 | $C_7H_7O_2$ | 41.7 |
| 13 | 125.0998 | $C_8H_{13}O$ | 20.7 |
| 14 | 127.0975 | $C_8H_{15}O$ | 115.9 |
| 15 | 129.1264 | $C_8H_{17}O$ | 11.4 |
| 16 | 131.0827 | $C_6H_{11}O_3$ | 90.8 |
| 17 | 147.1024 | $C_7H_{15}O_3$ | 2.1 |
| 18 | 161.1101 | $C_8H_{17}O_3$ | 47.1 |
| 19 | 163.1298 | $C_8H_{19}O_3$ | 21.9 |
| 20 | 169.1217 | $C_{10}H_{17}O_2$ | 6.8 |
| 21 | 177.1145 | $C_8H_{17}O_4$ | 10.8 |
| 22 | 199.2010 | $C_{13}H_{27}O$ | 25.8 |
| 23 | 269.2714 | $C_{18}H_{37}O$ | 48.3 |
| 24 | 271.2373 | $C_{16}H_{31}O_3$ | 37.0 |
| 25 | 273.2560 | $C_{16}H_{33}O_3$ | 47.7 |
| 26 | 325.2836 | $C_{20}H_{37}O_3$ | 29.0 |
| 27 | 327.2891 | $C_{20}H_{39}O_3$ | 2.4 |
| 28 | 329.2976 | $C_{20}H_{41}O_3$ | 24.2 |
| 29 | 339.2814 | $C_{21}H_{39}O_3$ | 24.9 |
| 30 | 341.2767 | $C_{20}H_{37}O_4$ | 22.2 |
| 31 | 343.2825 | $C_{20}H_{39}O_4$ | 6.5 |
| 32 | 345.2933 | $C_{20}H_{41}O_4$ | 20.6 |
| 33 | 375.2972 | $C_{24}H_{39}O_3$ | 19.4 |

| Peak Number | m/z | Elemental Composition | Error, ppm |
|---|---|---|---|
| 34 | 377.3200 | $C_{24}H_{41}O_3$ | 38.3 |
| 35 | 379.3233 | $C_{24}H_{43}O_3$ | 5.5 |
| 36 | 381.3453 | $C_{24}H_{45}O_3$ | 22.2 |
| 37 | 383.3482 | $C_{24}H_{47}O_3$ | 11.0 |
| 38 | 407.3392 | $C_{22}H_{47}O_6$ | 5.0 |
| 39 | 409.3631 | $C_{26}H_{49}O_3$ | 12.1 |
| 40 | 411.3785 | $C_{26}H_{51}O_3$ | 12.7 |
| 41 | 423.3733 | $C_{30}H_{47}O$ | 25.1 |
| 42 | 425.3819 | $C_{30}H_{49}O$ | 8.4 |

Table 5) Suggested elemental compositions for insoluble coal residue product ions identified in Figure 6. The coal was degraded by pyrocatechol at 37 °C and 83 bar for one month.

| Peak Number | m/z | Elemental Composition | Error, ppm |
|---|---|---|---|
| 1 | 83.0869 | $C_6H_{11}$ | 10.4 |
| 2 | 85.0751 | $C_5H_9O$ | 115.7 |
| 3 | 89.0610 | $C_4H_9O_2$ | 8.5 |
| 4 | 91.0397 | $C_3H_7O_3$ | 2.3 |
| 5 | 117.0913 | $C_6H_{13}O_2$ | 1.7 |
| 6 | 135.1017 | $C_6H_{15}O_3$ | 2.6 |
| 7 | 143.1367 | $C_9H_{19}O$ | 48.1 |
| 8 | 157.1545 | $C_{10}H_{21}O$ | 29.7 |
| 9 | 173.1540 | $C_{10}H_{21}O_2$ | 0.5 |
| 10 | 185.1618 | $C_{11}H_{21}O_2$ | 41.6 |
| 11 | 201.1850 | $C_{12}H_{25}O_2$ | 2.3 |
| 12 | 211.2049 | $C_{14}H_{27}O$ | 6.1 |
| 13 | 225.2347 | $C_{15}H_{29}O$ | 57.0 |
| 14 | 229.2176 | $C_{14}H_{29}O_2$ | 3.7 |
| 15 | 239.2408 | $C_{16}H_{31}O$ | 13.9 |
| 16 | 243.2345 | $C_{15}H_{31}O_2$ | 8.8 |
| 17 | 255.2361 | $C_{16}H_{31}O_2$ | 14.8 |
| 18 | 257.2471 | $C_{16}H_{33}O_2$ | 3.6 |
| 19 | 275.2635 | $C_{16}H_{35}O_3$ | 17.8 |
| 20 | 283.2668 | $C_{18}H_{35}O_2$ | 10.9 |
| 21 | 285.2813 | $C_{18}H_{37}O_2$ | 6.9 |
| 22 | 299.2787 | $C_{22}H_{35}$ | 16.3 |
| 23 | 369.3543 | $C_{27}H_{45}$ | 6.1 |
| 24 | 391.2903 | $C_{24}H_{39}O_4$ | 14.1 |
| 25 | 411.4044 | $C_{30}H_{51}$ | 12.9 |
| 26 | 481.4963 | $C_{32}H_{65}O_2$ | 4.5 |

**FIGURES**

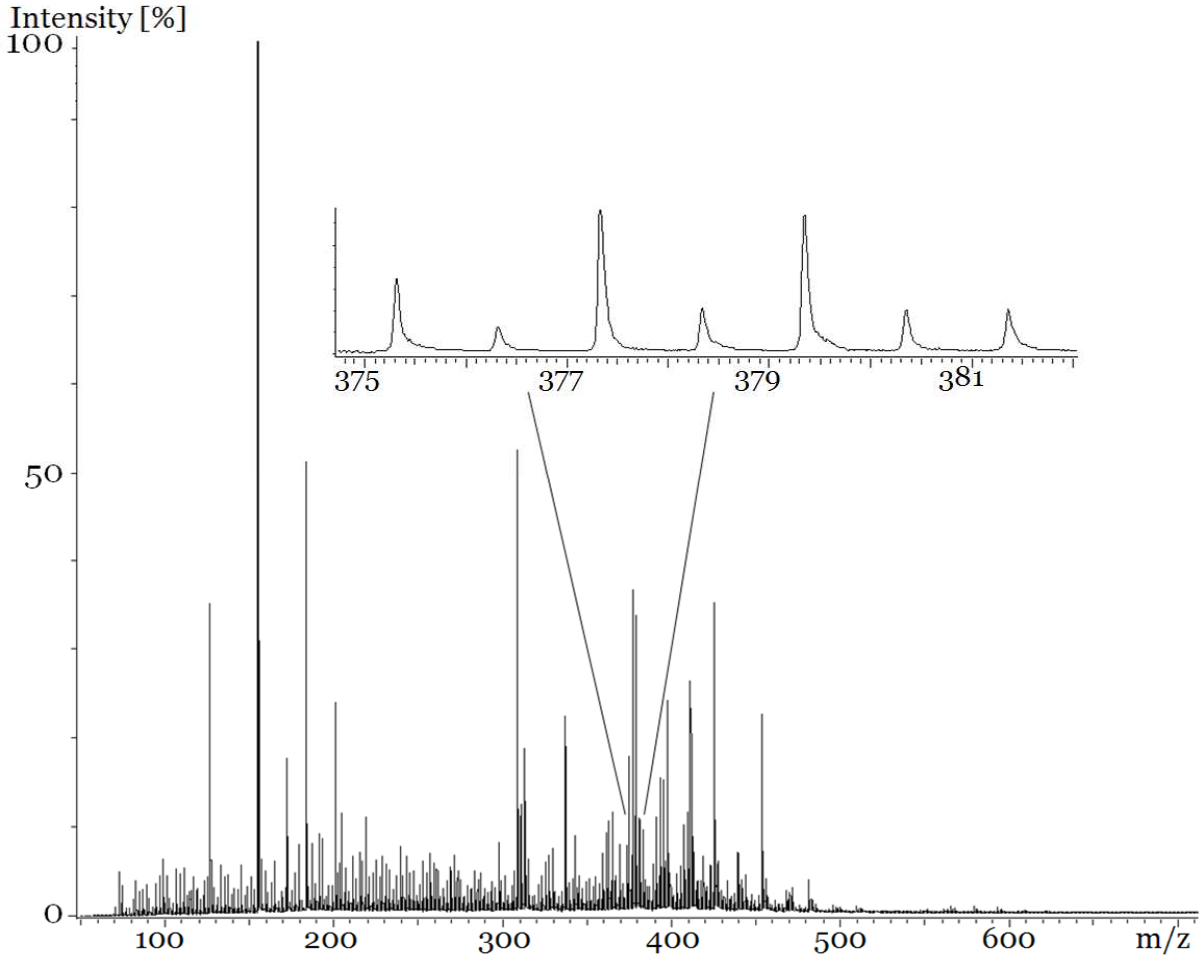


Figure 1) Mass spectrum of unreacted, solid coal. The vertical scale for the inset is magnified 2X.

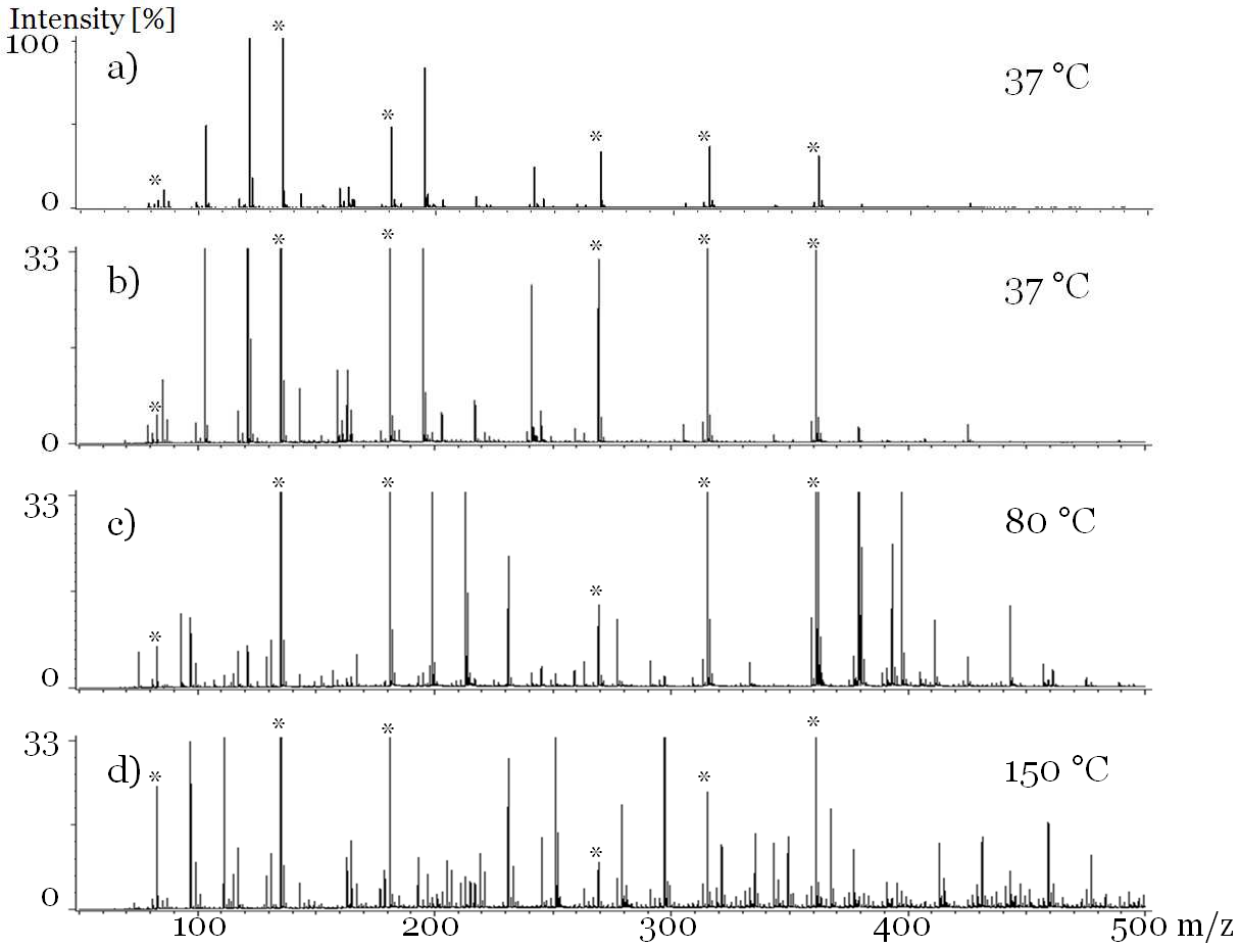


Figure 2) Mass spectra from water-soluble products of caged phosphite reacted with coal for one month at 37 °C (a and b), c) 80 °C and d) 150 °C. The spectrum in b) is the same as that in a) with the vertical scale magnified 3X to show the less-abundant ions derived from coal. Asterisks * designate ions from the reagent and products of condensation reactions between reagent molecules.

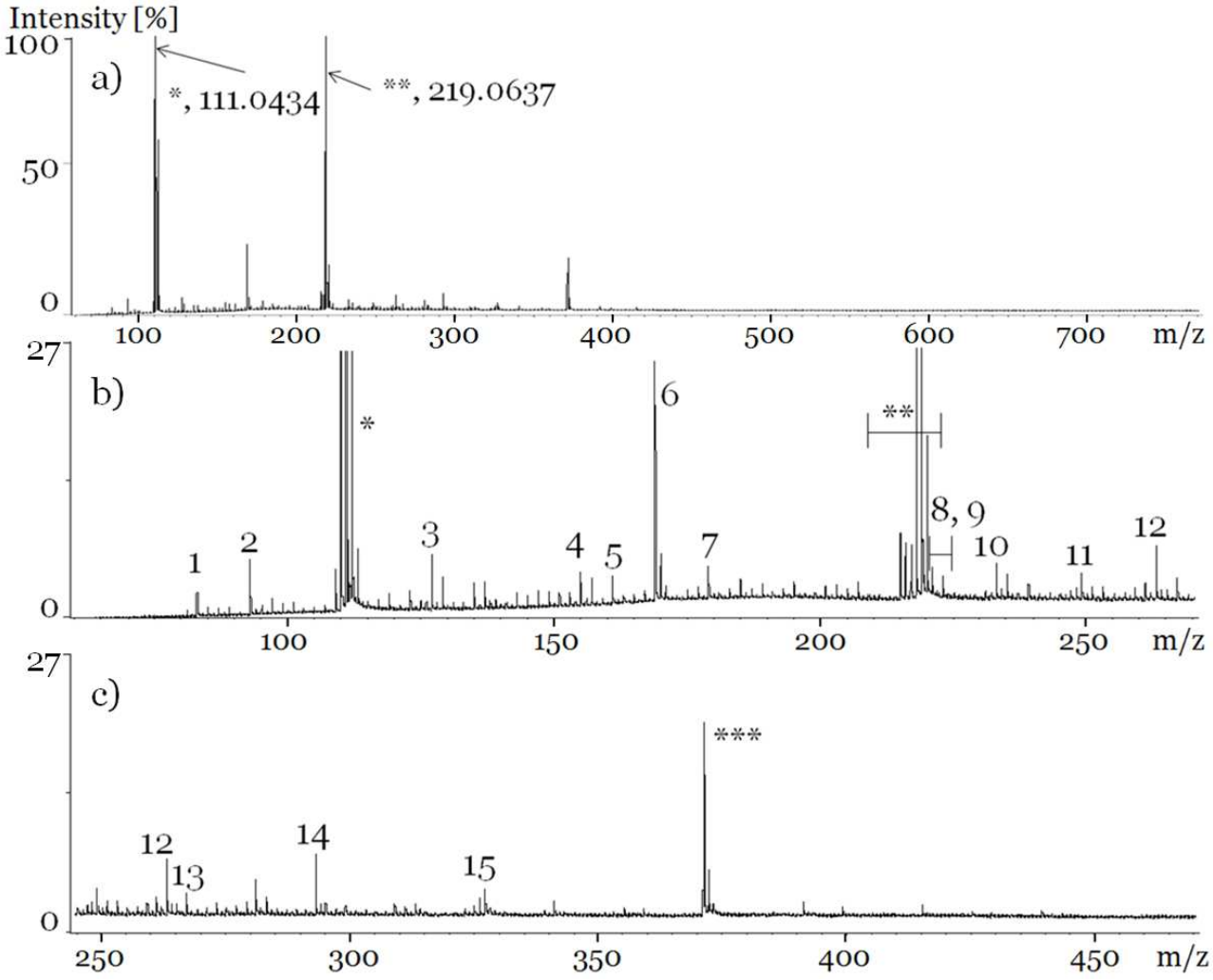


Figure 3) Mass spectra from water-soluble products of coal reacted with aqueous pyrocatechol at 37 $^{o}$C and 1 bar for one month. The two primary peaks labelled * and ** are due to protonated pyrocatechol and a protonated derivative of pyrocatechol. The spectra are plotted with different vertical scales to facilitate observation of the less-abundant ions from coal. The numbered peaks are identified in Table 2. a) m/z range to ~ 270; b) m/z range 245 to ~ 470.

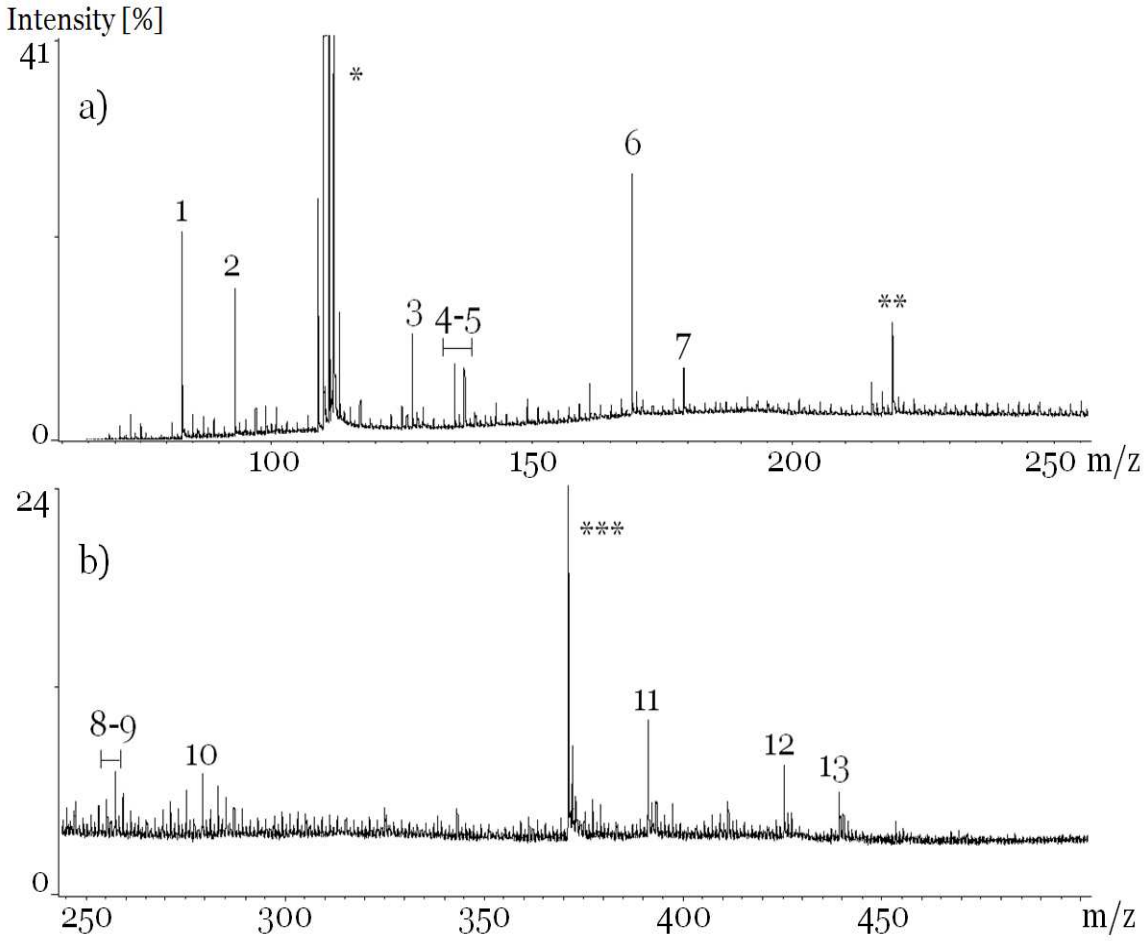


Figure 4) Mass spectra from water-soluble products of coal reacted with aqueous pyrocatechol at 37 $^{o}$C and 83 bar for one month. Same notation as Figure 3. The spectra are plotted on different scales to assist the observation of the low abundance ions. The numbered peaks are identified in Table 3. a) m/z range to ~ 260; b) m/z range 245 to ~ 500.

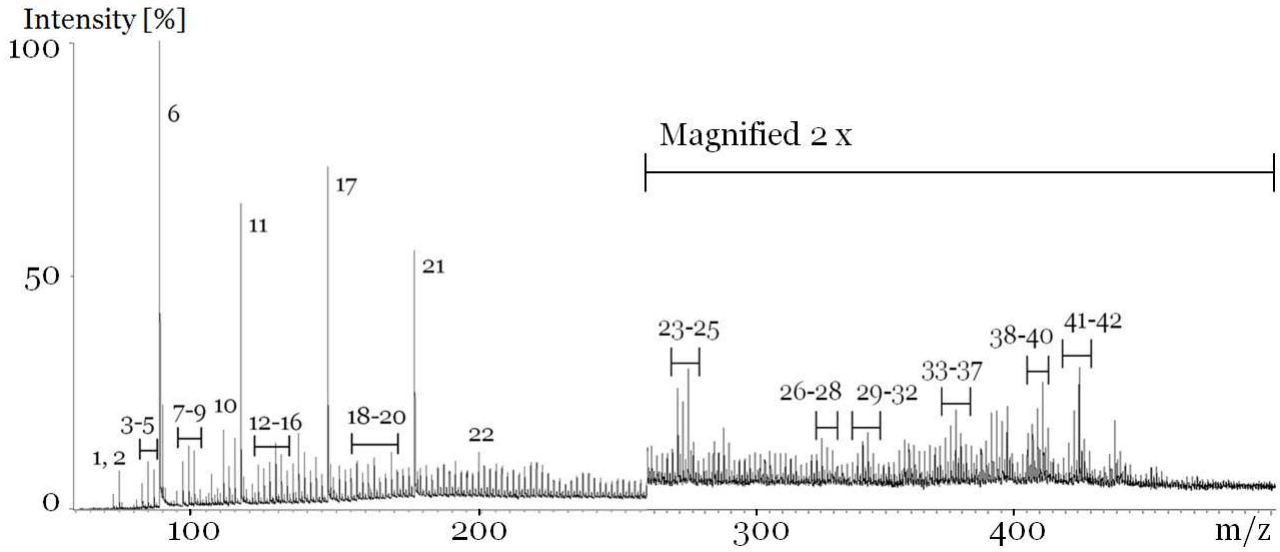


Figure 5) Mass spectra from insoluble coal residue after reaction with aqueous pyrocatechol at 37 °C and 1 bar for one month. Numbered peaks are identified in Table 4.

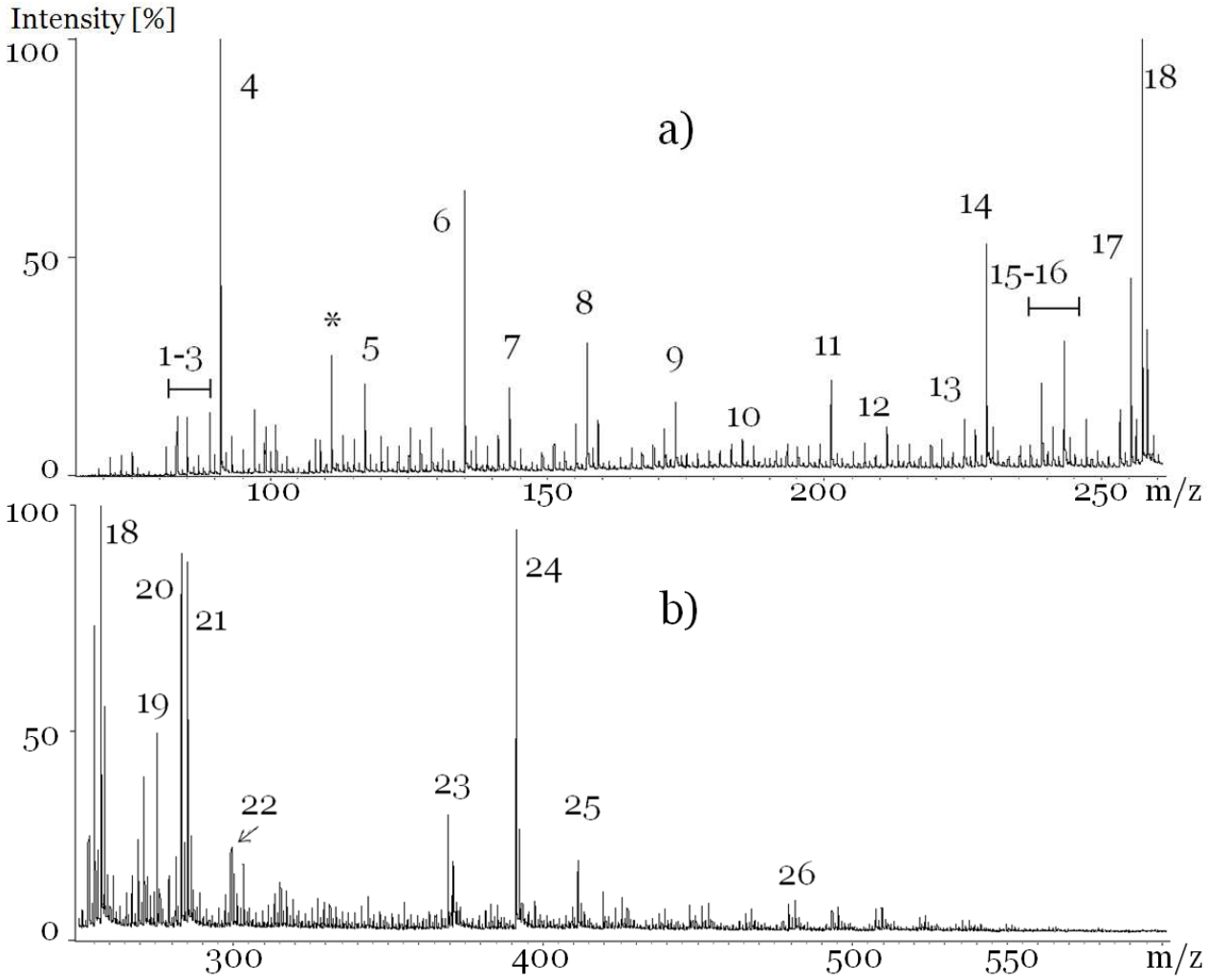


Figure 6) Mass spectra from insoluble coal residue after reaction with aqueous pyrocatechol at 37 °C and 83 bar for one month. Numbered peaks are identified in Table 5. a) m/z range to ~ 260; b) m/z range to ~ 600.

# CHAPTER 3

# THE YBHB PROTEIN FROM *ESCHERICHIA COLI* AND *ARABIDOPSIS THALIANA* HOMOLOG OF YBHB CHARACTERIZATED BY MASS SPECTROMETRY AND ION MOBILITY MASS SPECTROMETRY

Gregg M. Schieffer[a], Libuse Brachova[b,c,d], Basil J. Nikolau[b,c,d,e], Ethan R. Badman[f], and R. S. Houk[a]*

Ames Laboratory U. S. Department of Energy

[a]Department of Chemistry, and [b]Department of Biochemistry, Biophysics and Molecular Biology, [c]Center for Metabolic Biology, [d]Plant Sciences Institute, and [e]Center for Biorenewable Chemicals
Iowa State University, Ames, IA 50011 USA

[f]Hoffman-La Roche Inc., Non-Clinical Safety, Nutley, NJ 07110 USA

*Corresponding Author. Tel (515) 294-9462 Fax-0050 rshouk@iastate.edu

**ABSTRACT**

The YbhB protein from *E. coli* and the *Arabidopsis thaliana* homolog of the YbhB protein were analyzed by ion mobility mass spectrometry and matrix assisted laser desorption ionization mass spectrometry to determine the extent of multimer formation. Collision cross sections were measured for each protein charge state using native electrospray ionization (ESI) conditions in ammonium acetate buffer. For the native ESI mass spectral experiments, the YbhB protein from *E. coli* preferentially formed dimer compared to the *Arabidopsis thaliana* homolog. Native gel electrophoresis confirmed the presence of YbhB dimer and monomer. The cross section for the dimer 12+ *E. coli* and *Arabidopsis* homolog of the YbhB protein YbhB protein was 2480 $Å^2$ and 2560, respectively. The *Arabidopsis* homolog of the YbhB protein was analyzed under acid denatured conditions. The *Arabidopsis* homolog of the YbhB protein formed more dimer and the cross sections for each charge state under the denatured conditions were greater than under native ESI.

**INTRODUCTION**

Understanding protein structure and non-covalent binding is critical to determining protein function. Many reviews have been published in the past fifteen years describing the utility of mass spectrometry (MS) to characterize non-covalent biomolecular complexes.[1-11] Combining MS with ion mobility (IM) provides low resolution structure details for non-covalent biomolecule complexes.[10, 12-15] Ion mobility mass spectrometry, which measures the collision cross section for each charge state, is complementary to other methods that analyze proteins and protein complexes, such as nuclear magnetic resonance (NMR), X-ray crystallography and circular dichroism.[16] Many studies show good agreement between the collision cross section deduced from ion mobility and those calculated from X-ray and NMR structures.[14, 15, 17-22] NMR [23-27] and X-ray crystallography have atomic resolution and are considered the best standard for determining protein structure.[1, 28] However, these other techniques i) require relatively high quantities (milligrams) of homogeneous and pure protein sample and ii) take time (hours) and thus are not easily amenable to high throughput analysis. X-ray crystallography is a technique that only allows

a static view of proteins and some proteins are difficult to crystallize. Solution state NMR is currently limited to proteins weighing less than 30 kDa,[4, 27] although this is improving.

Analyzing protein complexes by mass spectrometry, on the other hand, has the four "S" advantages: speed, sensitivity, specificity, and stoichiometry. Mass spectrometry is amenable to high throughput analysis and commercial instruments have femtomole detection limits. The mass spectrum yields stoichiometry of the non-covalent protein complex and provides an estimate of the extent of substrate binding. Time-of-flight mass spectrometers (TOF MS) can theoretically measure protein and macromolecular ions of any size.[12, 29-31] In some cases the mass spectrometric method, including the vacuum and desolvation process, does not irreversibly destroy biomolecules because proteins [32] and viruses [30] convert back to viable forms after mass analysis.

Electrospray ionization (ESI) is the accepted ionization method to probe protein complexes under native solution conditions. For proteins with a neutral pI (pI = 7), the solvent consists of an aqueous, buffered solution with a neutral pH (between pH 6 to 8). Ammonium acetate at 5 to 50 mM is the buffer of choice. The introduction of nanoelectrospray ionization [33] (nESI) expanded the application of mass spectrometry to studying the structure of non-covalent protein complexes under native solution conditions. The initial droplets via nESI are smaller, it can tolerate a moderately high level of contaminants, salts, and less sample is consumed relative to conventional electrospray.[34] The low flow rate for nESI generates smaller droplets, which are more likely to contain only one protein or biomolecule complex.[8] This reduces the chance to artificially form oligomers during solvent evaporation; a protein concentration less than 30 μM is recommended. Under certain conditions, nESI can also be more gentle in preserving protein complex ions than conventional ESI.[35] Common MALDI conditions often denature complexes or yield artificial, non-physiological oligomers.[36]

This work studies two related proteins, the YbhB protein of *Escherichia coli* [37] and its *Arabidopsis thaliana* homolog, the protein encoded by the *Arabidopsis* gene locus, At5g01300. Amino acid alignment of these two proteins (NCBI database BLASTp) revealed that they belong to a highly conserved family of bacterial/archial phosphatidylethanolamine-binding proteins and also to its eukaryotic homolog Raf Kinase Inhibitor Protein (RKIP).

*E. coli ybhB* gene is located within the biotin biosynthesis operon, but its exact biochemical function is unclear. The *Arabidopsis* gene encoding the YbhB homolog is located on the fifth chromosome; its function is also unknown.

Here we report and discuss the results from our home-built ion mobility TOF MS [38, 39] and a MALDI TOF MS to characterize the *E. coli* YbhB protein and its *Arabidopsis* homolog. This is the first publication detailing the characteristics of this particular plant protein. The focus of the discussion covers a) protein masses, b) extent of multimer formation under different solution conditions, c) the collision cross sections for each charge state, and d) comparison of the gas-phase results to analogous data derived from the published crystal structure of the *E. coli* YbhB protein dimer.[37]

## EXPERIMENTAL

### Sample Preparation

#### *Arabidopsis* YbhB homolog

BLASTP analysis of the *Arabidopsis* genome database, using the YbhB amino acid sequence as the query, detected a single gene (At5g01300) encoding a protein that shares 31% identity and 49% similarity in amino acid sequence (E value 3e-14) with the query. An EST cDNA clone derived from the gene locus At5g01300 (YAP157T7, ABRC, Columbus, OH) was PCR-amplified with Taq polymerase and cloned into the expression vector (Invitrogen, Carlsbad, CA). The resulting construct was transformed into *E. coli* TOP10 One Shot competent cells (Invitrogen, Carlsbad, CA) and expression was induced during growth in Laura Broth medium by the addition of 1 mM isopropyl β-thiogalactoside (IPTG). Cells were collected by centrifugation after 5 hours of induction and lysed with BugBuster Protein Extraction Reagent (Novagen/EMD Chemicals, San Diego, CA). The *Arabidopsis* recombinant protein was purified by standard nickel-affinity chromatography, using the His.Bind kit (Novagen, EMD Chemicals, San Diego, CA).

Briefly, 20 ml of solubilized and cleared cell extract was loaded onto 500 µl of His.Bind resin. The column was washed with 10 column-volumes of binding buffer and 6 column-volumes of wash buffer. The bound protein was eluted with a buffer containing

0.3 M imidazole. The purified protein solution was dialyzed against 10 mM Tris-HCl buffer or 1 mM ammonium acetate buffer, both with pH 7.2. The average yield of affinity purified protein was 5 mg / 500 mL of culture.

***E. coli* YbhB**

The E. coli genomic DNA fragment encoding the YbhB protein was PCR-amplified using two genomic primers (5'-CACCATGAAACTCATCAGTAAC-3' and 5'-TCACTCTGCCAGATGGCGCA-3'). The PCR product was cloned into the pTrcHis TOPO TA expression vector, and transformed into E. coli TOP10 One Shot competent cells (Invitrogen, Carlsbad, CA). Protein was over-expressed by induction with 1 mM IPTG, and purified as described above for the Arabidopsis homolog.

**Native gel electrophoresis**

Monomeric/dimeric states of the purified YbhB proteins were analyzed by native gel electrophoresis. Electrophoresis was conducted in 4-20% polyacrylamide gradient gels, buffered with Tris-HCl, pH 6.8 (Hercules, CA). Each sample, containing 50 µg of purified protein was subjected to electrophoresis in Tris-glycine buffer, (pH 6.8) for 40 hours at 4C. Proteins were visualized by staining the gels with Coommassie Brilliant Blue.

**Mass Spectrometers**

**MALDI-MS**

Two mass spectrometers were used to characterize the two YbhB proteins. A Perseptive Biosystems Voyager DE-PRO (Framington, MA) MALDI TOF MS used a 337 nm $N_2$ laser. A 0.5 µL portion of solution containing the analyte was mixed with 0.5 µL of sinapinic acid solution and dried on a stainless steel plate. The sinapinic acid was at a concentration of 10 mg/mL in 70% acetonitrile/water, 0.1% TFA. Three amounts of protein, 2.5, 1, and 0.2 µg of the YbhB protein was spotted. The mass range was m/z 70,000, calibrated using bovine serum albumin.

**nESI-IM-MS**

The ESI experiments used our home-built ESI-IM-MS. The three ion source - ion trap - ion mobility - qTOF mass spectrometer (IT – IM – TOF MS) instrument is described

elsewhere.[38] The instrument parameters used for these experiments are listed in Table 1. Briefly a 1 mM ammonium acetate buffer containing the protein was ionized by nESI. The buffer needs to be kept at the lowest concentration possible or too many buffer ion adducts are seen. The ion source is unheated and has a pressure of about 1.1 mbar. The ions were trapped for a short time (20 ms) to avoid extensive ion conformation rearrangement [21, 40, 41] and then injected by an extraction pulse (7 to 12 µs) into the stacked ring DC drift tube (DT). The separated ion packets were extracted and mass analyzed by a quadrupole time-of-flight mass spectrometer (Tofwerk, Thun, Switzerland). The data acquisition and processing software (Ionwerks, Houston, TX) measured the ion mobility data. Each mass spectrum was collected for a minimum of ten minutes. Positive ion mode was used by all instruments to analyze these protein samples.

**Collision cross section calculation**

Each protein collision cross section was manually calculated using the ion measurements and instrument parameters, subtracting the corrected flight time from the nested drift time, $t_d$. The following equation is used to calculate the collision cross section ($\Omega$):

$$\Omega = \frac{3}{16}\sqrt{\frac{2\pi}{\mu k_B T}}\frac{Q}{n}\frac{t_d U}{L^2} \qquad (1)$$

The mobility equation variables are listed in Table 1. The number gas density, *n*, is calculated using the pressure and temperature of the gas in the drift tube. The mobility drift time, $t_d$, for the protein ions is between 1800 and 4500 µs. The correction to the drift time is calculated using TOF equations, accounting for the time the ion spends outside the mobility cell between the ion trap and mass analysis. The correction to the total flight time ranges from 100 to 200 µs.

## RESULTS AND DISCUSSION

### Recombinant YbhB proteins

The *Arabidopsis* and *E. coli* YbhB proteins were recombinantly produced and purified using the identical production system for both proteins. For convenience in purification, we used the expression vector pTrcHis, which introduced the identical N-terminal His-tag sequence (MSYYHHHHHHLESTSLYKKAGSAAAPFT) to each protein. This provided a simple means of achieving purification with nickel-ligand affinity matrix. The resulting preparations were over 98% pure, as judged by SDS-PAGE, in which the recombinant proteins were overloaded (>150 µg protein per lane; data not shown). The resulting *E. coli* YbhB "tagged"-protein contained 186 amino acids with the calculated molecular weight of 20276.65 g/mole (predicted pI = 6.00). The recombinant *Arabidopsis* YbhB homolog contained 190 amino acids with the calculated molecular weight of 21014.94 g/mole (predicted pI = 6.10). The quaternary organization of these two homologous proteins were analyzed and compared under a variety of solution conditions. The amino acid sequence for the *E. coli* YbhB is listed below. The HIS tag amino acid sequence is in bold type.

**MSYYHHHHHHLESTSLYKKAGSAAAPFT**MKLISNDLRDGDKLPHRHVFNGMGY
DGDNISPHLAWDDVPAGTKSFVVTCYDPDAPTGSGWWHWVVVNLPADTRVLPQG
FGSGLVAMPDGVLQTRTDFGKTGYDGAAPPKGETHRYIFTVHALDIERIDVDEGASG
AMVGFNVHFHSLASASITAMFS (2)

The *Arabidopsis* homolog of YbhB protein amino acid sequence is listed below. The HIS tag amino acid sequence is in bold type.

**MSYYHHHHHHLESTSLYKKAGSAAAPFT**MSSEELRLVSPTIDNDGKLPRKYTMA
GQGVKKDISPPLEWYNVPEGTKTLALVVEDIDAPDPSGPLVPWTVWVVVDIPPEMK
GLPEGYSGNEDQTTGIREGNNDHKIPGWRGPLLPSHGHRFQFKLFALDDKPKIGHTV
TKERLLIAIEGHVLGEAILTCLA (3)

### Native Gel Electrophoresis

The native gel electrophorogram of the two protein preparations is shown in Figure 1. This figure shows a typical result, and identical results were obtained upon analyses

of triplicate preparations of these proteins. The most intense band for these two proteins is the YbhB monomer. However, in both cases a small portion of dimers also occurs; no evidence of trimeric quaternary organization was detected. Based upon the intensity of these two bands, we estimate that 85% of both the *E. coli* and *Arabidopsis* homolog occur as monomeric units during the conditions used for electrophoresis (Table 2 and 3).

**Analysis of the *E. coli* YbhB Protein by nESI – IM – MS Instrument**

The IM-MS of the *E. coli* YbhB protein, at 100 µM concentration, at pH 7.2 native solution conditions shows a molecular mass of 20200 ± 60 Da and 40400 ± 400 Da for the monomer and dimer, respectively (Figure 2). The mass average and error is the standard deviation calculated from deconvoluting each protein charge state to the 1+ charge. The protein molecular mass also includes the 28 amino acid His tag. The charge states adopted by the *E. coli* YbhB protein from solution are 15+ to 5+ for monomer and 25+ to 10+ for the dimer. The dimer is estimated to be 80 % of the total detected protein ion signal, the 20 % balance being monomer (Table 2). The mass spectrum was smoothed by our mobility and mass spectra acquisition software (Ionwerks, Houston, TX) to distinguish charge states. The non-covalent protein complex was extracted out of the ion trap with a 7 µs, -80 V extraction pulse and -99 V on the front of the drift cell. These are "heated" injection parameters for our instrument.[42] The mass spectrum collected under gentle injection parameters produced an unresolvable, broad peak ($m/\Delta m$ = ~15, FWHM).

The *E. coli* YbhB collision cross section values increase with increasing charge state (Table 4), as expected.[17-19, 21, 43, 44] The conventional explanation is that protein ions unfold with increasing charge state to reduce Coulomb repulsion energy. The collision cross section for the YbhB dimer 23+, dimer 22+, monomer 11+, and dimer 21+ are plotted on top of each other (Figure 3). The collision cross section decreases as the charge state decreases. Determining the cross section for the odd numbered (e.g. 13+, 15+, etc.) dimer peaks is simple because the nested drift time mobility peak has a unique m/z ratio. For the mass overlapping monomer and dimer, the mobility data usually contains two peaks (Figure 3). In this case, the dimer mobility peak and monomer mobility peaks are not baseline resolved. The interpretation used to determine the mobility peak for the monomer and dimer is as

follows. Counterman et al. in Clemmer's group reported that peptide multimers have a shorter $t_d$ than the monomer.[45] At present, our observations with our mobility instrument and protein multimers follow their observations. The dimer peaks have a higher mobility (i.e. shorter $t_d$) than the monomer peaks, charge normalized. The higher mobility translates into a slightly more compact conformation. For a charge state with overlapping monomer and dimer protein peaks (i.e. *E. coli* YbhB Monomer$^{11+}$ and *E. coli* YbhB Dimer$^{22+}$), the first mobility peak corresponds to the dimer and the next mobility peak is the monomer. The mobility peaks are converted into cross sections. The contribution the monomer and dimer make to the unresolved portion of the mobility peaks are not known. The shape of the low cross section portion (< 2200 Å$^2$) of the *E. coli* YbhB Monomer$^{11+}$ and the high cross section portion of the *E. coli* YbhB Dimer$^{22+}$ (> 5000 Å$^2$) charge states was assumed (Figure 3).

We followed this procedure of assigning the higher mobility peak (i.e. shorter $t_d$) to the dimer ions when calculating the collision cross section for all [monomer $n^+$]$^{n+}$ and [dimer $2n^+$]$^{2n+}$ peaks that overlap in the mass spectrum. For most dimers, the collision cross section is less than twice the collision cross section of the monomer peak. The signal for some dimer mobility peaks are low (less than 100 counts) or the mobility peaks are not resolved at all, making it difficult to definitively assign the dimer mobility and monomer mobility peaks. We assigned an asterisk next to these peaks in our collision cross section tables.

The collision cross section for *E. coli* YbhB monomer is 1220 Å$^2$ at 5+ charge state (Table 4). The dimer 10+ collision cross section is 2080 Å$^2$. This collision cross section is near the value derived from the X-ray crystal structure of the *E. coli* YbhB dimer by Serre [37], the upper limit cross section estimated to be about 2400 Å$^2$. We estimate the collision cross section of the *E. coli* YbhB x-ray crystal (Rutgers Protein Data Bank, 1FJJ) dimer by hand rather than using a computer calculation [46] to perform the exact hard spheres-scattering or projection approximation calculation because the *E. coli* YbhB analyzed in this paper has the additional 28 amino acid HIS tag. The low charge state collision cross section is likely to be a little more compact than the crystal structure, because the interactions that persist in the gas phase are different than solution phase. It is thought that hydrophobic interactions are partially or completely lost in the gas phase, whereas hydrophilic and

electrostatic interactions maintain or increase in strength.[47-49] The protein complex rearranges somewhat to yield conformations with smaller structures in the gas phase than in solution or in a crystal.

The low resolution cross sections for the lowest charge states of the *Arabidopsis* homolog of YbhB and *E. coli* YbhB protein provides parameters to improve structure prediction of protein and non-covalent protein complex in molecular dynamics calculations [50, 51].

**Analysis of the *Arabidopsis* Homolog of the YbhB Protein by nESI – IM – MS Instrument**

The IM-MS of the Arabidopsis YbhB homolog, at a concentration of 100 µM, at pH 7.2, yields molecular mass of 20904 ± 2 Da for the abundant monomer (Figure 4). The dimer peaks are broad; the dimer molecular mass is estimated to be 41800 ± 200 Da (Table 3). The molecular mass includes the 28 amino acid His tag. The non-covalent protein complex was extracted out of the ion trap with either a 7 µs (Figure 4b) or a 12 µs (Figure 4a), -80 V extraction pulse and injection voltage (-99 V), which are "heated" and gentle injection parameters, respectively for our instrument.[42] The charge states adopted by the Arabidopsis YbhB homolog protein are 14+ to 6+ for monomer and 19+ to 12+ for the dimer. The inset shows the peak shape for the monomer 8+ ion. The FWHM is 1.59 and the resolution is 1640 (m/Δm). The dimer is estimated at 18 % and 2% of the total protein detected using the gentle and "heated" injection conditions, respectively. For both conditions, the extent of dimer formation by the *Arabidopsis* YbhB homolog protein is much less than that measured for the *E. coli* YbhB protein under the exact same instrument conditions.

The total counts between Figure 4a and 4b are nearly the same, but the peak intensities are five times greater under the energetic, "heated" ion injection conditions (Figure 4b). All the peaks are sharper because many adducts are knocked off and almost all of the *Arabidopsis* homolog of the YbhB protein dimer has dissociated, due to the higher energy injection into the mobility cell.[42, 45, 52] The dissociation of the *Arabidopsis* homolog of the YbhB protein dimer follows the observations by Counterman and Clemmer,

whereby heating their ion source capillary or increasing the absolute value of the drift tube injection voltage dissociated peptide ion multimers.[45]

All of the collision cross sections (Table 5) are larger under the "heated" injection conditions than those used for the gentle injection conditions (Figure 4). Thus the energetic extraction conditions broke up dimers and slightly unfolded the monomer protein ions. One explanation for the larger cross section is that the "heated" injection conditions disrupted the electrostatic protein interactions by driving off counter ions. As the protein ion no long had some of the constraints provided by the counter ions, it adopted a more open cross section.

For *Arabidopsis* YbhB homolog in low charge states, we expect the collision cross section values to be near the collision cross section derived from the crystal structure. As of yet, no crystallographic data exist for the *Arabidopsis* homolog of the YbhB protein. For many other, well-characterized proteins, the cross sections of the gas-phase cations in medium to low charge states are similar to those expected from the crystal structure. [14, 15, 17-22] The cross section for *Arabidopsis* YbhB homolog $M^{6+}$ is 1360 $Å^2$ and $D^{12+}$ is 2560 $Å^2$. The measured cross section for the *E. coli* YbhB dimer 12+, 2480 $Å^2$, is smaller than the same charged *Arabidopsis* homolog of YbhB protein dimer ion. This likely is the case because the *Arabidopsis* homolog contains eight more amino acids than the *E. coli* YbhB protein dimer.

The 1 mM ammonium acetate was the highest concentration used where distinct protein peaks were seen. The ion source is unheated, so it doesn't drive off adducts nor dissociate multimers as well as using a heated capillary.[45, 53] Unfortunately our instrument also has poor ion transmission due, in part, to the high pressure (0.7 mTorr), measured absolutely with a Baratron capacitance manometer (MKS Instruments, Andover, MA, 690A 01TRC) in the quadrupole immediately preceding the TOF source region.[54, 55] The first *Arabidopsis* homolog of the YbhB protein mass spectra, sprayed out of 10 mM ammonium acetate and 20 mM sodium phosphate, had a very broad peak (data not shown), resolution ~15 ($m/\Delta m$) suggesting that it was complicated by adducts and multimers. This is consistent with other non-covalent protein structures, though at the extreme of having many adducts, in the gas phase [56-59]. We follow the explanation offered by Loo and Robinson here. Water molecules and counter ions critical to the complex are retained when it leaves

the solution phase and enters the gas phase. As stated before, the ion source in our ion mobility instrument is gentle and does not knock off many adducts, operating at about 1.1 mbar and at room temperature. It seems low molecular weight substances, such as water molecules and counter ions, get trapped in the interfacial regions of the protein complex. Fewer adducts are seen on protein monomer peaks because they have less surface area than a dimer.

### *Arabidopsis* Homolog of YbhB, nESI – IM – MS Instrument, Denatured Conditions

The *Arabidopsis* homolog of the YbhB protein (75 µM) was also analyzed in 0.05 % acetic acid solution (10 mM, pH 3.4), on the IM MS via nESI (Figure 5). This mass spectrum needed smoothing by our mobility software (Ionwerks, Houston, TX) to distinguish charge states. Under the acid denaturing conditions, about 60 % of the *Arabidopsis* homolog of the YbhB protein is dimer compared to 18 % *Arabidopsis* YbhB homolog dimer when electrosprayed out of the native buffered pH 7.2, 1 mM ammonium acetate solution (Table 3). This suggests denatured *Arabidopsis* YbhB homolog more readily forms dimer than the native conformations. The monomer and dimer weigh about 20940 ± 60 Da and 41900 ± 500 Da, respectively. The cross sections for the monomer and dimer peaks range from 4360 $Å^2$ for the dimer 25+ ion to 2020 $Å^2$ for the dimer 10+ ion (Table 6). The cross sections from the denatured *Arabidopsis* YbhB homolog protein are the largest for all charge states compared to those from the *Arabidopsis* YbhB homolog protein sprayed via native ESI (Table 6). This confirms that the protein becomes denatured in the acidic solution. Thus, the collision cross section does reflect the size of the molecule in solution, at least when extreme changes are considered.[53]

### *Arabidopsis* Homolog of YbhB and *E. coli* YbhB, MALDI-MS

Three different amounts of *Arabidopsis* homolog of the YbhB protein and *E. coli* YbhB protein, 2.5, 1, and 0.2 µg, were also analyzed by MALDI MS. The one µg of *Arabidopsis* homolog of the YbhB protein and one µg of *E. coli* YbhB protein are shown (Figure 6). The sinapinic acid and trifluoroacetic acid in the matrix is quite acidic, and it is likely that this environment denatures the protein. Conventional MALDI artificially forms protein clusters non-specifically during desorption / ionization process.[59] That said, the

*Arabidopsis* homolog of the YbhB protein forms 24 % dimer and 14 % trimer and *E. coli* YbhB protein forms 26 % dimer and 15 % trimer at 1 µg (Tables 2 and 3). The multimer formation for the *Arabidopsis* homolog of the YbhB protein is consistent with the acid denatured electrospray measurements. The *Arabidopsis* homolog of the YbhB protein forms dimer and trimer at 0.2 µg whereas the *E. coli* YbhB no longer forms dimer nor trimer at 0.2 µg. The dimer and trimer are not too much more abundant at 2.5 µg than at the 1 µg spotted. The MALDI gives an accurate mass of 20963 and 41931 Da for the *Arabidopsis* homolog of the YbhB protein monomer and dimer, respectively. The *E. coli* YbhB weighs 20118 and 40333 Da for the monomer and dimer, respectively. All of the MALDI peaks of the YbhB protein contain adducts.

## CONCLUSION

In summary, the *E. coli* YbhB protein MS result is consistent with Serre [37] in that mostly dimer was formed via native electrospray ionization. The low charge state *E. coli* YbhB dimer 10+ collision cross section (2080Å$^2$) determined by IM is near the cross section (2400Å$^2$) estimated from the x-ray crystal structure.[37] Under native nESI conditions, *E. coli* YbhB protein more readily forms a dimer whereas *Arabidopsis* homolog of the YbhB protein is mostly a monomer. This suggests that solution phase protein-protein interactions in the *E. coli* YbhB dimer are stronger than those in *Arabidopsis* homolog of the YbhB protein dimer. Under acid denatured conditions such as MALDI both *Arabidopsis* homolog of the YbhB protein and *E. coli* YbhB form dimers and trimers. The cross sections of the denatured *Arabidopsis* homolog of the YbhB protein are larger than the ones generated from native ESI conditions. The mass of the *E. coli* YbhB is about 20200 Da and 40400 Da for the monomer and dimer, respectively. The *Arabidopsis* homolog of the YbhB protein weighs about 20900 Da.

## ACKNOWLEDGEMENT

We thank Joel Nott for the MALDI Perseptive Voyager DE Pro MALDI mass spectra. GS acknowledges the GAANN Fellowship (Iowa State University, 2008-2009) for financial support.

**REFERENCES (International Journal of Mass Spectrometry formatting)**

[1] D.L. Smith, Z.Q. Zhang, Probing Noncovalent Structural Features of Proteins by Mass-Spectrometry, Mass Spectrom. Rev., 13 (1994) 411-429.
[2] J.A. Loo, Studying Noncovalent Protein Complexes by Electrospray Ionization Mass Spectrometry, Mass Spectrom. Rev., 16 (1997) 1-23.
[3] J.A. Loo, Electrospray Ionization Mass Spectrometry: A Technology for Studying Noncovalent Macromolecular Complexes, Int. J. Mass Spectrom., 200 (2000) 175-186.
[4] J.M. Daniel, S.D. Friess, S. Rajagopalan, S. Wendt, R. Zenobi, Quantitative Determination of Noncovalent Binding Interactions Using Soft Ionization Mass Spectrometry, Int. J. Mass Spectrom., 216 (2002) 1-27.
[5] K. Breuker, The Study of Protein-Ligand Interactions by Mass Spectrometry - a Personal View, Int. J. Mass Spectrom., 239 (2004) 33-41.
[6] A.J.R. Heck, R.H.H. van den Heuvel, Investigation of Intact Protein Complexes by Mass Spectrometry, Mass Spectrom. Rev., 23 (2004) 368-389.
[7] B.T. Ruotolo, C.V. Robinson, Aspects of Native Proteins Are Retained in Vacuum, Curr. Opin. Chem. Biol., 10 (2006) 402-408.
[8] J.L.P. Benesch, B.T. Ruotolo, D.A. Simmons, C.V. Robinson, Protein Complexes in the Gas Phase: Technology for Structural Genomics and Proteomics, Chem. Rev., 107 (2007) 3544-3567.
[9] T. Wyttenbach, M.T. Bowers, Intermolecular Interactions in Biomolecular Systems Examined by Mass Spectrometry, Annu. Rev. Phys. Chem., 58 (2007) 511-533.
[10] B.T. Ruotolo, J.L.P. Benesch, A.M. Sandercock, S.J. Hyung, C.V. Robinson, Ion Mobility-Mass Spectrometry Analysis of Large Protein Complexes, Nat. Protoc., 3 (2008) 1139-1152.
[11] C. Bich, R. Zenobi, Mass Spectrometry of Large Complexes, Curr. Opin. Struct. Biol., 19 (2009) 632-639.
[12] J.A. Loo, B. Berhane, C.S. Kaddis, K.M. Wooding, Y.M. Xie, S.L. Kaufman, I.V. Chernushevich, Electrospray Ionization Mass Spectrometry and Ion Mobility Analysis of the 20S Proteasome Complex, J. Am. Soc. Mass Spectrom., 16 (2005) 998-1008.
[13] B.C. Bohrer, S.I. Merenbloom, S.L. Koeniger, A.E. Hilderbrand, D.E. Clemmer, Biomolecule Analysis by Ion Mobility Spectrometry, Annu. Rev. Anal. Chem., 1 (2008) 293-327.
[14] C.A. Scarff, K. Thalassinos, G.R. Hilton, J.H. Scrivens, Travelling Wave Ion Mobility Mass Spectrometry Studies of Protein Structure: Biological Significance and Comparison with X-Ray Crystallography and Nuclear Magnetic Resonance Spectroscopy Measurements, Rapid Commun. Mass Spectrom., 22 (2008) 3297-3304.
[15] C.A. Scarff, V.J. Patel, K. Thalassinos, J.H. Scrivens, Probing Hemoglobin Structure by Means of Traveling-Wave Ion Mobility Mass Spectrometry, J. Am. Soc. Mass Spectrom., 20 (2009) 625-631.
[16] L.M.M. Weigang, D. Lanaosch, T. Letzel, Gas-Phase Behavior of Noncovalent Transmembrane Segment Complexes, Rapid Commun. Mass Spectrom., 22 (2008) 4089-4097.
[17] K.B. Shelimov, M.F. Jarrold, Conformations, Unfolding, and Refolding of Apomyoglobin in Vacuum: An Activation Barrier for Gas-Phase Protein Folding, J. Am. Chem. Soc., 119 (1997) 2987-2994.

[18] K.B. Shelimov, D.E. Clemmer, R.R. Hudgins, M.F. Jarrold, Protein Structure in Vacuo: Gas-Phase Confirmations of BPTI and Cytochrome *c*, J. Am. Chem. Soc., 119 (1997) 2240-2248.
[19] S.J. Valentine, J.G. Anderson, A.D. Ellington, D.E. Clemmer, Disulfide-Intact and -Reduced Lysozyme in the Gas Phase: Conformations and Pathways of Folding and Unfolding, J. Phys. Chem. B, 101 (1997) 3891-3900.
[20] A.E. Counterman, D.E. Clemmer, Volumes of Individual Amino Acid Residues in Gas-Phase Peptide Ions, J. Am. Chem. Soc., 121 (1999) 4031-4039.
[21] S. Myung, E.R. Badman, Y.J. Lee, D.E. Clemmer, Structural Transitions of Electrosprayed Ubiquitin Ions Stored in an Ion Trap over Similar to 10 MS to 30 S, J. Phys. Chem. A, 106 (2002) 9976-9982.
[22] B.T. Ruotolo, K. Giles, I. Campuzano, A.M. Sandercock, R.H. Bateman, C.V. Robinson, Evidence for Macromolecular Protein Rings in the Absence of Bulk Water, Science, 310 (2005) 1658-1661.
[23] A. Cavalli, X. Salvatella, C.M. Dobson, M. Vendruscolo, Protein Structure Determination from NMR Chemical Shifts, Proc. Natl. Acad. Sci. U. S. A., 104 (2007) 9615-9620.
[24] A. Bagno, F. Rastrelli, G. Saielli, NMR Techniques for the Investigation of Solvation Phenomena and Non-Covalent Interactions, Prog. Nucl. Magn. Reson. Spectrosc., 47 (2005) 41-93.
[25] S. Grzesiek, H.J. Sass, From Biomolecular Structure to Functional Understanding: New NMR Developments Narrow the Gap, Curr. Opin. Struct. Biol., 19 (2009) 585-595.
[26] S.P. Mielke, V.V. Krishnan, Characterization of Protein Secondary Structure from NMR Chemical Shifts, Prog. Nucl. Magn. Reson. Spectrosc., 54 (2009) 141-165.
[27] F.A.A. Mulder, M. Filatov, NMR Chemical Shift Data and Ab Initio Shielding Calculations: Emerging Tools for Protein Structure Determination, Chem. Soc. Rev., 39 (2010) 578-590.
[28] M. Karplus, J. Kuriyan, Molecular Dynamics and Protein Function, Proc. Natl. Acad. Sci. U. S. A., 102 (2005) 6679-6685.
[29] C.S. Kaddis, S.H. Lomeli, S. Yin, B. Berhane, M.I. Apostol, V.A. Kickhoefer, L.H. Rome, J.A. Loo, Sizing Large Proteins and Protein Complexes by Electrospray Ionization Mass Spectrometry and Ion Mobility, J. Am. Soc. Mass Spectrom., 18 (2007) 1206-1216.
[30] G. Siuzdak, B. Bothner, M. Yeager, C. Brugidou, C.M. Fauquet, K. Hoey, C.M. Chang, Mass Spectrometry and Viral Analysis, Chem. Biol., 3 (1996) 45-48.
[31] M.A. Tito, K. Tars, K. Valegard, J. Hajdu, C.V. Robinson, Electrospray Time-of-Flight Mass Spectrometry of the Intact MS2 Virus Capsid, J. Am. Chem. Soc., 122 (2000) 3550-3551.
[32] Z. Ouyang, Z. Takats, T.A. Blake, B. Gologan, A.J. Guymon, J.M. Wiseman, J.C. Oliver, V.J. Davisson, R.G. Cooks, Preparing Protein Microarrays by Soft-Landing of Mass-Selected Ions, Science, 301 (2003) 1351-1354.
[33] M. Wilm, M. Mann, Analytical Properties of the Nanoelectrospray Ion Source, Anal. Chem., 68 (1996) 1-8.
[34] R. Juraschek, T. Dulcks, M. Karas, Nanoelectrospray - More Than Just a Minimized-Flow Electrospray Ionization Source, J. Am. Soc. Mass Spectrom., 10 (1999) 300-308.

[35] F. Sobott, J.L.P. Benesch, E. Vierling, C.V. Robinson, Subunit Exchange of Multimeric Protein Complexes - Real-Time Monitoring of Subunit Exchange between Small Heat Shock Proteins by Using Electrospray Mass Spectrometry, J. Biol. Chem., 277 (2002) 38921-38929.
[36] F.H. Song, A Study of Noncovalent Protein Complexes by Matrix-Assisted Laser Desorption/Ionization, J. Am. Soc. Mass Spectrom., 18 (2007) 1286-1290.
[37] L. Serre, K.P. de Jesus, C. Zelwer, N. Bureaud, F. Schoentgen, H. Benedetti, Crystal Structures of YbhB and YbcL from *Escherichia coli*, Two Bacterial Homologues to a Raf Kinase Inhibitor Protein, J. Mol. Biol., 310 (2001) 617-634.
[38] Q. Zhao, M.W. Soyk, G.M. Schieffer, K. Fuhrer, M.M. Gonin, R.S. Houk, E.R. Badman, An Ion Trap-Ion Mobility-Time of Flight Mass Spectrometer with Three Ion Sources for Ion/Ion Reactions, J. Am. Soc. Mass Spectrom., 20 (2009) 1549-1561.
[39] Q. Zhao, G.M. Schieffer, M.W. Soyk, T.J. Anderson, R.S. Houk, E.R. Badman, Effects of Ion/Ion Proton Transfer Reactions on Conformation of Gas-Phase Cytochrome *c* Ions, J. Am. Soc. Mass Spectrom., (2010) *in press*.
[40] E.R. Badman, C.S. Hoaglund-Hyzer, D.E. Clemmer, Monitoring Structural Changes of Proteins in an Ion Trap over Similar to 10-200 MS: Unfolding Transitions in Cytochrome *c* Ions, Anal. Chem., 73 (2001) 6000-6007.
[41] E.R. Badman, S. Myung, D.E. Clemmer, Evidence for Unfolding and Refolding of Gas-Phase Cytochrome *c* Ions in a Paul Trap, J. Am. Soc. Mass Spectrom., 16 (2005) 1493-1497.
[42] G.M. Schieffer, D.L. Morast, Q. Zhao, E.R. Badman, R.S. Houk, Time-Resolved Heating and Unfolding of Protein Ions Due to Ion Injection Conditions in an Ion Trap - Ion Mobility - Time-of-Flight Mass Spectrometer, in preparation (2010).
[43] S.J. Valentine, D.E. Clemmer, H/D Exchange Levels of Shape-Resolved Cytochrome *c* Conformers in the Gas Phase, J. Am. Chem. Soc., 119 (1997) 3558-3566.
[44] S.J. Valentine, A.E. Counterman, D.E. Clemmer, Conformer-Dependent Proton-Transfer Reactions of Ubiquitin Ions, J. Am. Soc. Mass Spectrom., 8 (1997) 954-961.
[45] A.E. Counterman, S.J. Valentine, C.A. Srebalus, S.C. Henderson, C.S. Hoaglund, D.E. Clemmer, High-Order Structure and Dissociation of Gaseous Peptide Aggregates That Are Hidden in Mass Spectra, J. Am. Soc. Mass Spectrom., 9 (1998) 743-759.
[46] A.A. Shvartsburg, S.V. Mashkevich, E.S. Baker, R.D. Smith, Optimization of Algorithms for Ion Mobility Calculations, J. Phys. Chem. A, 111 (2007) 2002-2010.
[47] S.N. Jackson, S. Dutta, A.S. Woods, The Use of ECD/ETD to Identify the Site of Electrostatic Interaction in Noncovalent Complexes, J. Am. Soc. Mass Spectrom., 20 (2009) 176-179.
[48] Q.Y. Wu, J.M. Gao, D. JosephMcCarthy, G.B. Sigal, J.E. Bruce, G.M. Whitesides, R.D. Smith, Carbonic Anhydrase-Inhibitor Binding: From Solution to the Gas Phase, J. Am. Chem. Soc., 119 (1997) 1157-1158.
[49] C.V. Robinson, E.W. Chung, B.B. Kragelund, J. Knudsen, R.T. Aplin, F.M. Poulsen, C.M. Dobson, Probing the Nature of Noncovalent Interactions by Mass Spectrometry. A Study of Protein-CoA Ligand Binding and Assembly, J. Am. Chem. Soc., 118 (1996) 8646-8653.
[50] M. D'Abramo, T. Meyer, P. Bernado, C. Pons, J.F. Recio, M. Orozco, On the Use of Low-Resolution Data to Improve Structure Prediction of Proteins and Protein Complexes, J. Chem. Theory Comput., 5 (2009) 3129-3137.

[51] T. Taverner, H. Hernandez, M. Sharon, B.T. Ruotolo, D. Matak-Vinkovic, D. Devos, R.B. Russell, C.V. Robinson, Subunit Architecture of Intact Protein Complexes from Mass Spectrometry and Homology Modeling, Accounts Chem. Res., 41 (2008) 617-627.
[52] C.S. Hoaglund, S.J. Valentine, C.R. Sporleder, J.P. Reilly, D.E. Clemmer, Three-Dimensional Ion Mobility TOFMS Analysis of Electrosprayed Biomolecules, Anal. Chem., 70 (1998) 2236-2242.
[53] J.W. Li, J.A. Taraszka, A.E. Counterman, D.E. Clemmer, Influence of Solvent Composition and Capillary Temperature on the Conformations of Electrosprayed Ions: Unfolding of Compact Ubiquitin Conformers from Pseudonative and Denatured Solutions, Int. J. Mass Spectrom., 187 (1999) 37-47.
[54] C.S. Hoaglund-Hyzer, D.E. Clemmer, Ion Trap/Ion Mobility/Quadrupole/Time of Flight Mass Spectrometry for Peptide Mixture Analysis, Anal. Chem., 73 (2001) 177-184.
[55] I.V. Chernushevich, B.A. Thomson, Collisional Cooling of Large Ions in Electrospray Mass Spectrometry, Anal. Chem., 76 (2004) 1754-1760.
[56] J.A. Loo, Observation of Large Subunit Protein Complexes by Electrospray-Ionization Mass-Spectrometry, J. Mass Spectrom., 30 (1995) 180-183.
[57] E.J. Nettleton, M. Sunde, Z.H. Lai, J.W. Kelly, C.M. Dobson, C.V. Robinson, Protein Subunit Interactions and Structural Integrity of Amyloidogenic Transthyretins: Evidence from Electrospray Mass Spectrometry, J. Mol. Biol., 281 (1998) 553-564.
[58] F. Sobott, M.G. McCammon, C.V. Robinson, Gas-Phase Dissociation Pathways of a Tetrameric Protein Complex, Int. J. Mass Spectrom., 230 (2003) 193-200.
[59] M. Zehl, G. Allmaier, Instrumental Parameters in the MALDI-TOF Mass Spectrometric Analysis of Quaternary Protein Structures, Anal. Chem., 77 (2005) 103-110.

**TABLES**

Table 1) The nESI – IT – IM – TOF MS instrument settings and parameters used to analyze the *Arabidopsis* homolog of YbhB and *E. coli* YbhB protein.

| Instrument settings | |
|---|---|
| nESI | +1.3 to 2.1 kV |
| IT, Fill | 40 to 50 ms |
| IT, cool | 15 to 30 ms |
| IT, extraction voltage | -60 to -80 V |
| IT, extraction pulse | 7 to 12 µs |
| DT Injection | -99 V |
| DT Back | -546 to -597 V |
| Ion funnel | 115 to 150 $V_{pp}$ |
| TOF, mass range | 90 to 120 µs |
| TOF, TDC resolution | 2 to 4 ns |
| Mobility resolution | One point every 100µs to a point every 130 µs |

| DT parameters | |
|---|---|
| Front aperture | 0.5 mm |
| Exit aperture | 1.5 mm |
| Length | 44.45 cm |
| Pressure | 1.45 to 2.0 mbar helium gas |
| Temperature | 23 °C |
| Buffer gas | Helium |

Table 2) *E. coli* YbhB protein results: molecular weights and relative amounts of monomer, dimer, and trimer for YbhB measured by various methods. Experimental conditions for the nESI – IM – MS results are as noted in Table 1. The molecular weights include the 28 amino acid HIS tag.

| | [*E. coli* YbhB protein] | | | | | | |
|---|---|---|---|---|---|---|---|
| | | Relative Amounts | | | Molecular Weights (Da) | | |
| Method | | %M | %D | %T | M | D | T |
| NGE[a] | - | 85 | 15 | - | 20000 | 40000 | |
| nESI native gentle[b] | 100µm | Unable to mass resolve peak | | | | | |
| nESI native heated[c] | 100 µM | 20 | 80 | - | 20200±60 | 40400±400 | |
| MALDI | 1 µg | 59 | 26 | 15 | 20118 | 40333 | 60516 |

[a]NGE = native gel electrophoresis

[b]nESI-IM-MS, native solution conditions (1 mM ammonium acetate, pH ~ 7.2), gentle ion injection conditions

[c]nESI-IM-MS, native solution conditions, energetic ion injection conditions

Table 3) Arabidopsis homolog of YbhB protein results: molecular weights and relative amounts of monomer (M), dimer (D), and trimer (T) for *Arabidopsis* homolog of YbhB measured by various methods. Experimental conditions for the nESI – IM – MS results are as noted in Table 1. The molecular weights include the 28 amino acid His tag.

[*Arabidopsis* homolog of YbhB protein]

| | | Relative Amounts | | | Molecular Weights (Da) | | |
|---|---|---|---|---|---|---|---|
| Method | | %M | %D | %T | M | D | T |
| NGE[a] | - | 85 | 15 | - | 20000 | 40000 | |
| nESI native gentle[b] | 100 μM | 82 | 18 | - | 20904±2 | 41800±200 | |
| nESI native heated[c] | 100 μM | 98 | 2 | - | 20899±4 | - | |
| nESI denatured heated[d] | 75 μM | 40 | 60 | | 20940±60 | 41900±500 | |
| MALDI | 1 μg | 62 | 24 | 14 | 20963 | 41931 | 62985 |

[a]NGE = native gel electrophoresis

[b]nESI-IM-MS, native solution conditions (1 mM ammonium acetate, pH ~ 7.2), gentle ion injection conditions

[c]nESI-IM-MS, native solution conditions, energetic ion injection conditions

[d]nESI-IM-MS, denatured solution conditions (acetic acid, pH ~ 3.4), energetic ion injection conditions

Table 4) Listed are the collision cross sections for *E. coli* YbhB protein monomer (M) and dimer (D) measured by nESI–IM–MS under native solution conditions and with heated ion injection conditions. The cross sections include the 28 amino acid His tag.

| | [*E. coli* YbhB protein] | |
|---|---|---|
| Species & | Measured Cross Sections ($Å^2$) | |
| Charge State | Monomer | Dimer |
| $M^{15+}$ | 3240, 3450 | |
| $M^{14+}$ | 3040 | |
| $M^{13+}$ | 2820 | |
| $D^{25+}$ | | 5540 |
| $M^{12+}/D^{24+}$ | 2670 | 4860 |
| $D^{23+}$ | | 4780 |
| $M^{11+}/D^{22+}$ | 2590 | 4660 |
| $D^{21+}$ | | 3920, 4630 |
| $M^{10+}/D^{20+}$ | 2140 | 3860 |
| $D^{19+}$ | | 3780 |
| $M^{9+}/D^{18+}$ | 1870 | 3700 |
| $D^{17+}$ | | 3630 |
| $M^{8+}/D^{16+}$ | 1750 | 3400 |
| $D^{15+}$ | | 3180 |
| $M^{7+}/D^{14+}$ | 1550 | 3080 |
| $D^{13+}$ | | 2640, 3010 |
| $M^{6+}/D^{12+}$ | 1390 | 2480 |
| $D^{11+}$ | | 2390 |
| $M^{5+}/D^{10+}$ | 1220 | 2080 |

Table 5) Measured collision cross sections for *Arabidopsis* homolog of YbhB protein monomer (M) and dimer (D) measured by nESI–IM–MS under native solution conditions but with different ion injection conditions. The cross sections include the 28 amino acid His tag.

| | [*Arabidopsis* homolog of YbhB protein] | | | |
|---|---|---|---|---|
| | Measured Cross Sections | | Measured Cross Sections | |
| Species & | Monomer ($Å^2$) | | Dimer ($Å^2$) | |
| Charge State | Gentle | Heated | Gentle | Heated |
| $M^{14+}$ | 2630 | 2730 | | |
| $M^{13+}$ | 2410 | 2620 | | |
| $M^{12+}$ | 2320 | 2560 | | |
| $M^{11+}$ | 2130 | 2470 | | |
| $M^{10+}$ | 2000 | 2130 2430 | | |
| $D^{19+}$ | | | 3180 3530 | 3890*, 4360* |
| $M^{9+}/D^{18+}$ | 1570, 1850 | 1560 2000 | 3130 | |
| $D^{17+}$ | | | 3060, 3470 | 3100* |
| $M^{8+}/D^{16+}$ | 1540 | 1540 | 3060 | |
| $D^{15+}$ | | | 2860 | 3020* |
| $M^{7+}/D^{14+}$ | 1490 1550 | 1520 | 2660 | |
| $D^{13+}$ | | | 2630 2930 | 2560* 2950* |
| $M^{6+}/D^{12+}$ | 1360 | | 2560 | |

Table 6) Collision cross sections for *Arabidopsis* homolog of YbhB monomer (M) and dimer (D) measured by nESI-IM-MS, native solution conditions, heated ion injection conditions, native (pH ~ 7) vs. denaturing (pH ~ 3.4) solution conditions. The cross sections include the 28 amino acid His tag.

[*Arabidopsis* homolog of YbhB protein]

| Species & Charge State | Measured Cross Sections Monomer ($Å^2$) native | denatured | Measured Cross Sections Dimer ($Å^2$) native | denatured |
|---|---|---|---|---|
| $M^{18+}$ | 3560 | | | |
| $M^{17+}$ | | 3490 | | |
| $M^{16+}$ | | 3370 | | |
| $M^{15+}$ | | 3280 | | |
| $M^{14+}$ | 2730 | 3090 | | |
| $M^{13+}$ | 2620 | 2950 | | |
| $D^{25+}$ | | | | 4360 |
| $M^{12+}/D^{24+}$ | 2560 | 2830 | | 4260 |
| $D^{23+}$ | | | | 4080 |
| $M^{11+}/D^{22+}$ | 2470 | 2670 | | 3890 |
| $D^{21+}$ | | | | 3660 |
| $M^{10+}/D^{20+}$ | 1560 2430 | 2340 | | 3630 |
| $D^{19+}$ | | | 3840* 4360* | 3520 |
| $M^{9+}/D^{18+}$ | 1560 2000 | 2130 | | 3370 |
| $D^{17+}$ | | | 3100* | 3270 |
| $M^{8+}/D^{16+}$ | 1540 | 1940 | | 3200 |
| $D^{15+}$ | | | 3020* | 3030* 3800* |
| $M^{7+}/D^{14+}$ | 1520 | 1870* | | 2900* |
| $D^{13+}$ | | | 2560* 2950* | 2960* |
| $M^{6+}/D^{12+}$ | | 1450* | | 2600* |
| $D^{11+}$ | | | | 2020* |
| $M^{5+}/D^{10+}$ | | 1430* | | 2020* |

* denotes a broad drift time peak. It is difficult to determine the center of the peak.

**FIGURES**

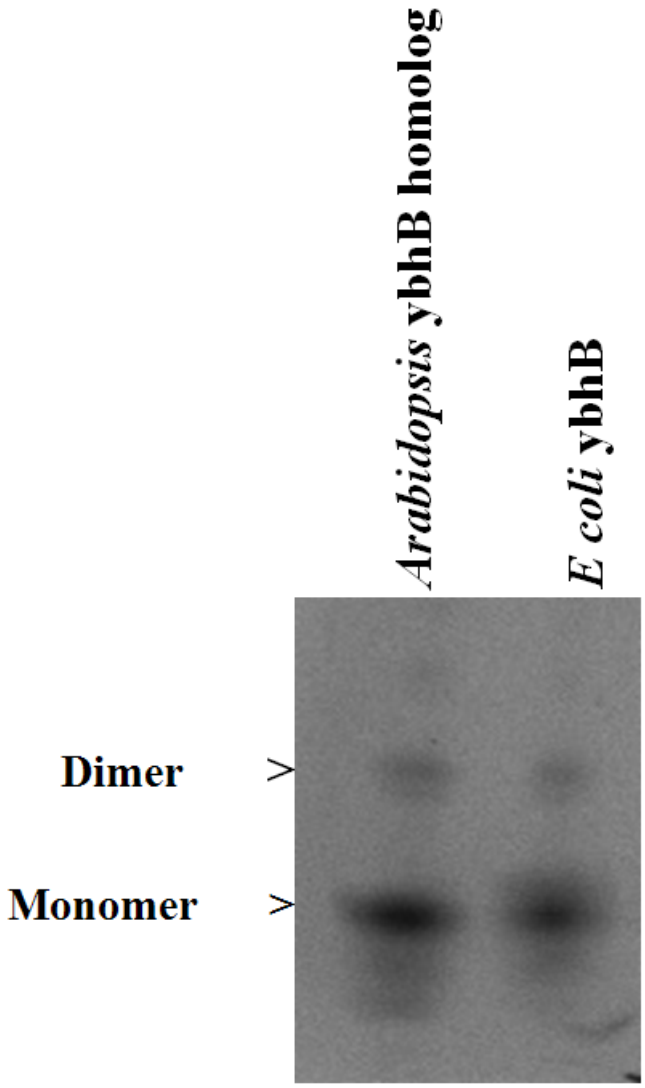


Figure 1) Native gel electrophoresis of the *E. coli* YbhB and the *Arabidopsis* YbhB homolog proteins.

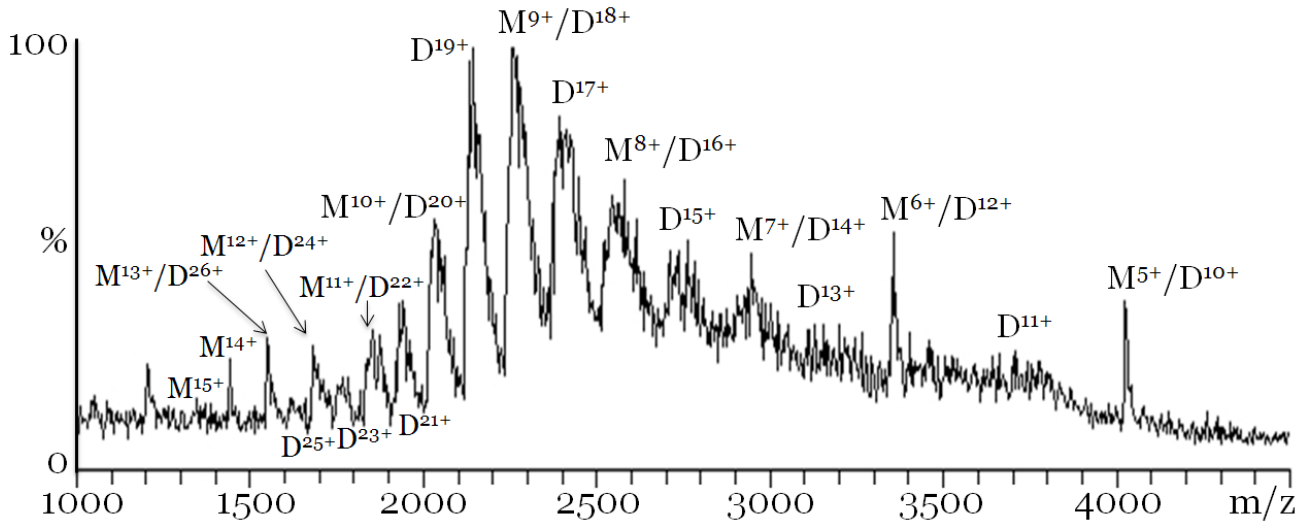


Figure 2) 100µM *E. coli* YbhB protein MS on the nESI-IM-MS instrument. M and D denotes monomer and dimer, respectively. Many adducts remain even though the mass spectrum was taken under "heated" ion trap extraction and drift tube injection instrument conditions. The MS is smoothed to better distinguish the peaks.

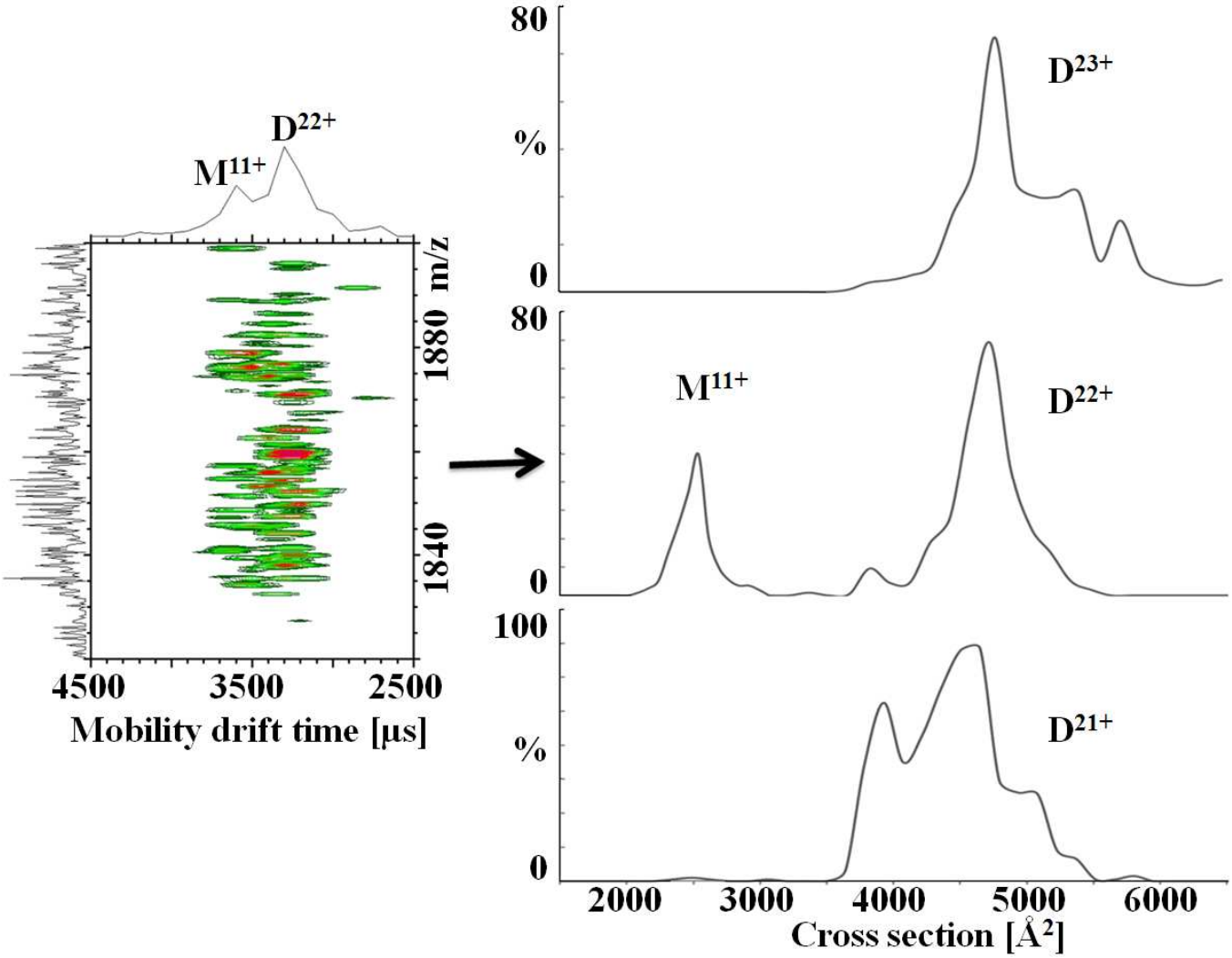


Figure 3) *E. coli* YbhB protein MS cross sections [$Å^2$] for the dimer 23+ (m/z 1757), dimer 22+ (m/z 1837), dimer 21+ (m/z 1924), and the monomer 11+ (m/z 1837) charge states. The mobility for each *E. coli* YbhB charge state was measured by our nESI – IM – MS instrument. The plot on the left shows the raw m/z vs. mobility data. This is an example of mobility peaks corresponding to partially resolved monomer and dimer conformations. The higher mobility peak (i.e. shorter drift time) is assigned as dimer and converted to a cross section, as shown on the right plot.

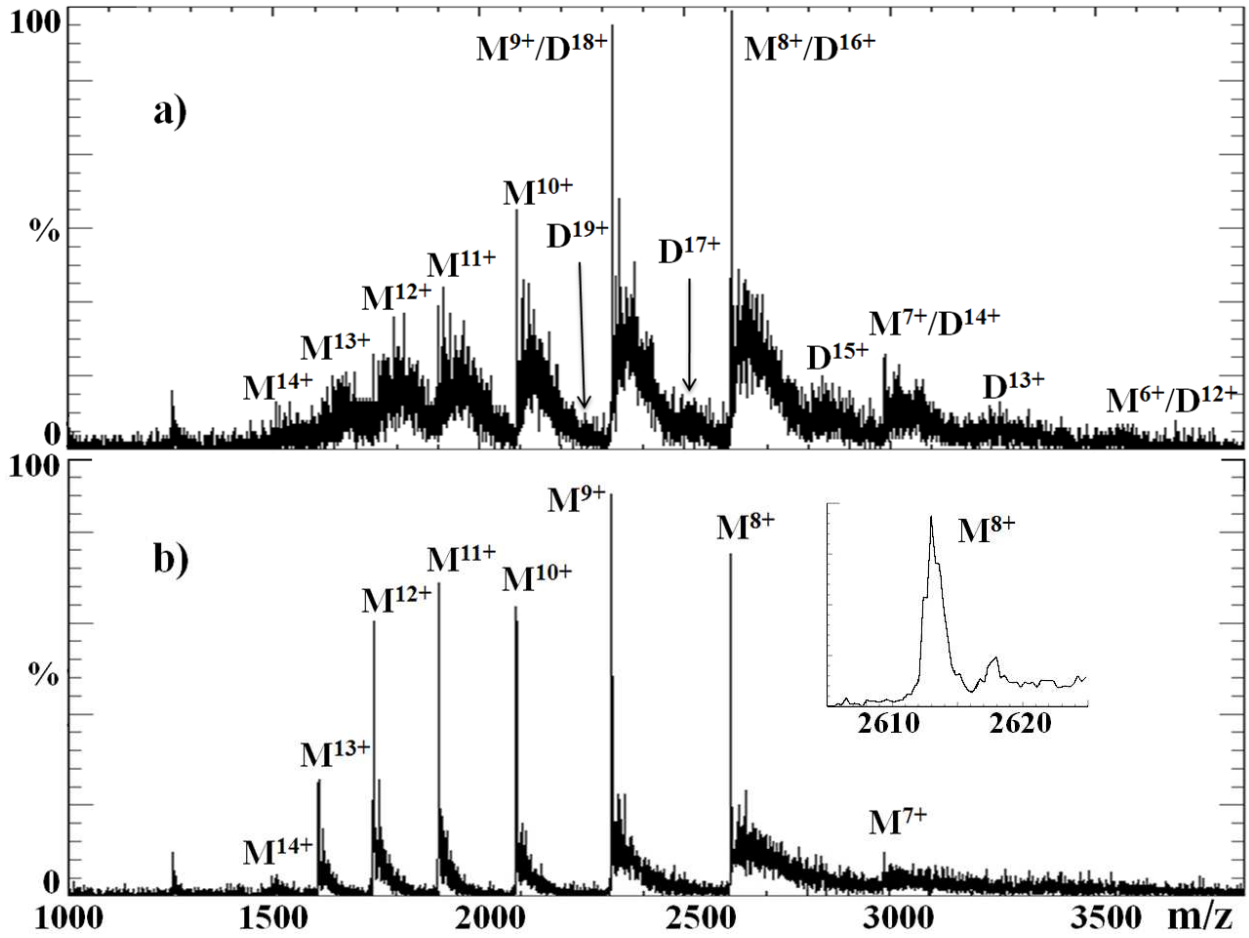


Figure 4) 100µM *Arabidopsis* homolog of YbhB protein mass spectrum, native nESI condition, using the nESI – IM – MS instrument using a) gentle injection conditions and b) heated injection conditions. M and D denotes monomer and dimer, respectively. The total counts are the same in a) and b).
The inset shows the peak shape for the monomer 8+ ion. The FWHM is 1.59 and the resolution is 1640 (m/Δm).
The peaks are not smoothed.

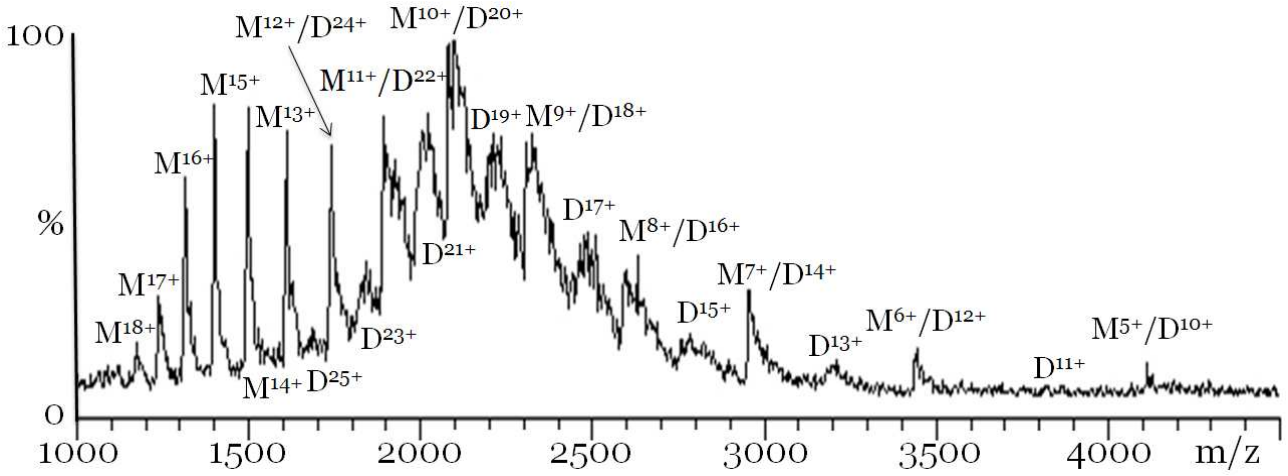


Figure 5) Acidified *Arabidopsis* homolog of YbhB protein mass (75 µM) spectrum analyzed on our nESI – IM – MS instrument. M and D denotes monomer and dimer, respectively. The MS is smoothed. Many adducts ions are still attached, despite taking the mass spectrum under heating ion trap extraction and drift tube injection conditions.

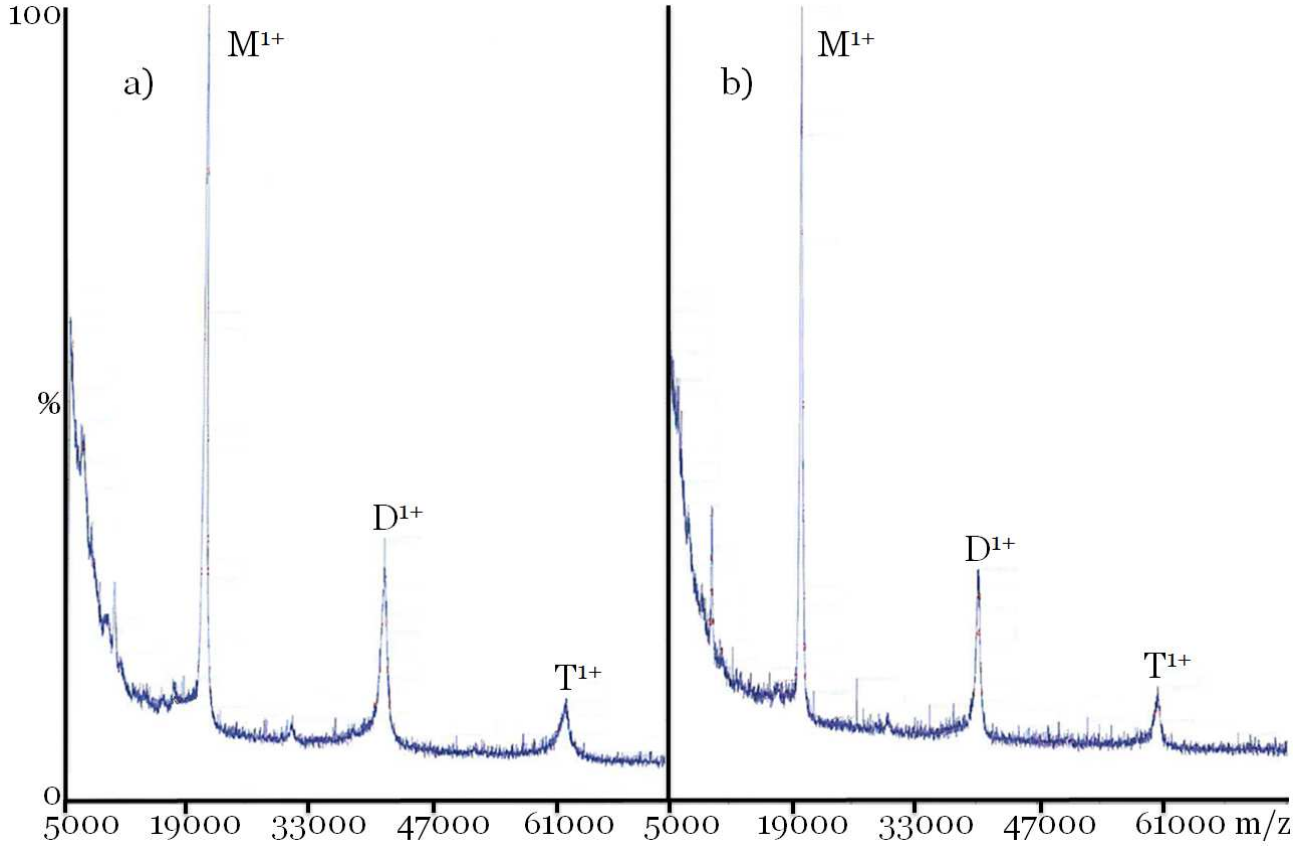


Figure 6) MALDI MS of a) 1 µg *Arabidopsis* homolog of YbhB protein and b) 1µg *E. coli* YbhB protein spotted with Sinapinic acid matrix. The peaks are labeled with charge states of the monomer (M), the dimer, (D), and the trimer (T).

# CHAPTER 4

# TIME-RESOLVED HEATING AND UNFOLDING OF PROTEIN IONS DUE TO ION INJECTION CONDITIONS IN AN ION TRAP – ION MOBILITY – TIME-OF-FLIGHT MASS SPECTROMETER

Gregg M. Schieffer, Derrick L. Morast, Qin Zhao, Ethan R. Badman[b], and R. S. Houk*

Ames Laboratory U. S. Department of Energy
Department of Chemistry
Iowa State University, Ames, IA 50011 USA
*Corresponding Author. Tel (515) 294-9462 Fax-0050 rshouk@iastate.edu

[b]Hoffman-La Roche Inc., Non-Clinical Safety, Nutley, NJ 07110 USA

Submit to: International Journal of Mass Spectrometry

**ABSTRACT**

Our ion trap – ion mobility – TOF MS instrument has exhibited unexpected ion heating. Heating and unfolding of protein ions as they are extracted from a 3D quadrupole ion trap and injected into an ion mobility drift tube are studied. The square wave extraction pulse on the ion trap exit induces extensive unfolding for ions in certain charge states with a range of available conformations. The extent of unfolding differs for even 1 µs differences in extraction pulse duration. This negative square wave on the ion trap exit induces as much unfolding as some 500 electron-volts DC applied to the front of the drift tube. Various proteins unfold to a maximum extent at a common spatial position about 0.9 cm in front of the entrance to the drift tube.

**INTRODUCTION**

Ion mobility spectrometry (IMS) coupled to mass spectrometry, can quickly provide low resolution structural information on gas-phase ions. Low electric field IMS separates ions by shape-to-charge measurement, based on the time they take to drift through an inert gas under a weak electric field in a mobility cell.[1] The drift times from the low-field IMS measurements are readily converted to collision cross sections. The IMS measurement is orthogonal to MS, which measures the mass-to-charge ratio (m/z or Th). The cross-section provides coarse shape and structure information,[1, 2] particularly if it is combined with simulations [3-6] or other experimental data like H/D exchange.

In 2009 we published a paper describing a home-built ion trap – ion mobility – time-of-flight mass spectrometer (IT – IM – TOF MS) with the capability for ion / ion reactions.[7] During experiments to characterize and understand this instrument, we came across the unexpected result that the magnitude of the voltage and duration of the square wave applied to the ion trap exit endcap can greatly affect the measured cross section values and relative abundances of different protein conformers. This effect is particularly noticeable for protein ions in charge states that have several accessible conformations with substantially different cross sections.

This effect, in addition to the injection voltage on the front of the mobility cell, was shown (Figure 5 in [7]) using the ubiquitin 7+ ion (Ubq). A few µs difference in the duration

of the extraction pulse changed the Ubq 7+ ion conformation from compact to elongated. The explanation offered in that paper suggested that ions closer to the entrance of the drift tube experienced more heating from collisions in the gas plume leaving the drift tube entrance when the extraction voltage returned to zero than ions just exiting the trap. As the extraction voltage returned to zero, collisions with the background buffer gas are more energetic. Thus the collisions experienced by the ion packet converted some of the kinetic energy into heat and unfolded the protein ions. Similar effects were reported for cytochrome c.[8, 9]

All ion mobility instruments use an attractive, DC voltage on the entrance of the mobility cell, called the injection voltage, to draw ions into the cell. The magnitude of the injection voltage and ion charge state (electron-Volts) determine the kinetic energy of the collisions that the ions experience with the buffer gas (usually helium or another inert gas) that is leaking out of the drift tube. These collisions occur in a high electric field (E/N) regime where some of the imparted energy activate the ions before being dissipated by subsequent collisions with additional buffer gas. In other words, ions entering the drift tube rapidly heat before their kinetic energies are thermalized by subsequent collisions with the buffer gas.[10, 11] Further collisions within the drift tube cool the ion to the buffer gas temperature; it is estimated that protein ions undergo $10^5$ collisions per centimeter once inside the drift tube filled with helium buffer gas at 1 mbar. Ions can unfold,[7, 10, 12-17] dissociate,[11, 18-23] and have protons stripped by the (helium) buffer gas [12, 20, 24] by manipulating the injection energy.

Our instrument design follows the IM – TOF MS built in Clemmer's group [12, 20, 21, 25], but to our knowledge other groups did not recognize the effect concerning the extraction duration and voltage magnitude. A paper discussing an early design of a IT – IM – MS instrument in Clemmer's group states that varying the extraction pulse duration between 0.2 and 4 µs [18] did not change the quality of the ion signal. The motivation behind lengthening the duration pulse on our instrument beyond 4 µs and using an extraction voltage more negative than the entrance of the drift tube was the need to increase signal for protein ions in low charge states (1+ and 2+) made by proton transfer ion/ion reactions from more highly charged precursors.

Further discussion of this injection heating effect, as well as other examples of intermediate protein charge states prone to this effect, follow in this paper. The unfolding phenomena shown below may have interest in their own right, as protein unfolding sometimes provides clues to protein folding.[26, 27] Furthermore, rapid unfolding events are believed to occur as electrosprayed protein ions are desolvated and extracted into a mass spectrometer.[3, 28] These phenomena are of great interest in the projected use of ESI mass spectrometry to study the three-dimensional structures of biomolecules.

## EXPERIMENTAL

### Protein Samples

The protein samples used are bovine heart cytochrome *c* (Sigma C3131), porcine trypsin (Sigma T0303), bovine ubiquitin (Sigma U6253), lysozyme (Sigma L7651), carbonic anhydrase (Sigma C7025), bovine insulin (Sigma I5500), and bovine pancreatic trypsin inhibitor (BPTI, Sigma T0256 ). The YbhB protein is described here.[29] Each protein was electrosprayed from a 30 μM 1% aqueous acetic acid solution using nanoelectrospray tips (~ 20 μm i.d.). The nanoelectrospray tips were made from capillary tubes (1.5 mm o.d., 0.86 mm i.d.) via a tip puller (P97; Sutter Instruments, Novato, CA).

### Instrumentation

The design and general instrument details for the home built three ion source - ion trap - ion mobility - qTOF mass spectrometer are reported here [7]. Briefly we electrosprayed the protein solution, collected ions in the trap for 20 ms, and cooled them for another 30 ms. Ions were extracted from the trap with an attractive, square wave voltage using a pulse generator (PVX-4150; Directed Energy Corp.; Fort Collins, CO, USA, applied to the exit endcap) and injected into the drift tube mobility cell (Figure 1). The electric field across the drift tube was 11.2 V/cm, which should be in the low-field regime. The TOF mass range was as short as possible (70 – 100 μs) to measure the maximum points across the ion mobility peaks. The ion trap extraction voltage ($V_{ext}$), extraction voltage pulse duration, and drift cell injection voltage ($V_{inj}$) were varied to understand this heating effect. Figure 1 shows a schematic diagram of the ion trap and drift tube entrance. The distance from the trap

center to the trap exit ($z_0$) is 0.707 cm, and the distance from the trap exit to the drift tube entrance ($z_1$) is 1.30 cm, as indicated. Ions are extracted from the trap with a negative voltage pulse of amplitude $V_{ext}$ on the exit end cap. The duration of this pulse varies from 1 µs to as long as 15 µs. The fall and rise times depend on the pulse amplitudes but are less than 40 and 60 ns, respectively, so they do not distort the square wave extraction pulse appreciably. The DC voltage on the drift tube entrance is $V_{inj}$ and is varied from zero to –100 volts; -50 to -100 are typical values.

The drift tube contains He gas at 1.5 to 2.0 mbar. Figure 1 also shows a depiction of a small gas plume flowing out of the drift tube entrance orifice (0.50 mm diam.). Ions from the trap must travel through this plume to get into the drift tube. The dimensions of and conditions in the He plume are not known precisely; the pressure and number density of He are assumed to be intermediate between that in the drift tube (1.5 to 2.0 mbar) and that in the external vacuum chamber (~1 µbar).

The collision cross sections of the protein ions were calculated using:

$$\Omega = \frac{3}{16}\sqrt{\frac{2\pi}{\mu k_B T}}\frac{Q}{n}\frac{t_d U}{L^2} \qquad (1)$$

where Ω = rotationally averaged cross section of the ion of interest, µ = reduced mass, $k_B$ = Boltzmann constant, T = temperature, Q = ion charge, n = number density of buffer gas, calculated using the pressure and temperature in the drift cell. Other parameters are nested drift time, $t_d$, voltage across the drift cell, U, and drift cell length, L. The $t_d$ is corrected for time spent between the drift tube exit and TOF source region, as described.[7]

**Ion Flight Times During Extraction from Ion Trap and Injection into Drift Tube**

Examination of the mobility spectra indicates that the time and amplitude of the extraction voltage pulse ($V_{ext}$, Figure 1) can have a strong effect on the conformer(s) observed and their relative abundances. Analysis of these observations shows that the position of the ion when the negative extraction voltage returns to zero is important. This position is estimated as described below.

Figure 1 shows a schematic diagram of the ion trap and injection region just before the drift tube. Upper case Z is used for position to avoid confusion with ion charge z. Consider an ion at rest in the center of the trap. The potential in the center is ground. A negative voltage (say $V_{ext}$ = -50 volts) is applied to the right endcap electrode to extract the ion. While this voltage is on, the ion travels the distance $Z_0$ = 0.707 cm in a time $t_0$. Here the ion is accelerated through a field gradient region with potential from zero to $V_{ext}$. The time required is $t_0$:

$$t_o^2 = \frac{2mZ_0^2}{Q\,\Delta V} = \frac{2mZ_0^2}{Q\,V_{ext}} \qquad (2)$$

To get into the drift tube, the ion must next travel the distance $Z_1$ = 1.30 cm. Suppose $V_{inj} = V_{ext}$ = -50 volts. In this simple case, the second region is field-free, so the time $t_1$ is given by the familiar time-of-flight equation:

$$t_1^2 = \frac{mZ_1^2}{2QV_{ext}} \qquad (3)$$

For ubiquitin 7+, m = $1.42 \times 10^{-20}$ g, $t_0$ = 5.0 μs, $t_1$ = 4.7 μs
and the total time $t = t_0 + t_1$ = 9.7 μs.

Next consider the more common case when $V_{ext}$ is more negative than $V_{inj}$. Typical values used in this study would be $V_{ext}$ = -100 volts and $V_{inj}$ = -50 volts. The time to the trap exit is still given by Equation 2; in this case $t_0$ = 3.6 μs for ubiquitin 7+. The ion is then decelerated as it continues toward the drift tube. The considerations below are derived from those used to calculate flight times and velocities in a reflectron.[30, 31]

Let $v_{it\ exit}$ and $v_{dt\ ent}$ be the ion velocities at the ion trap exit and drift tube entrance. These values are given by the following equations:

$$v_{it\ exit}^2 = \frac{2QV_{ext}}{m} \qquad v_{dt\ exit}^2 = \frac{2QV_{inj}}{m} \qquad (4)$$

The average velocity $v_{avg}$ in this region is just the mean of these two values, shown with this relationship:

$$v_{avg} = \frac{v_{it\ exit} + v_{dt\ entrance}}{2} \qquad (5)$$

The distance $Z_n$ is then merely:

$$Z_n = (v_{avg}) \text{ x (time between trap and drift tube)} = v_{avg}\,(t_n - t_0) \qquad (6)$$

Thus, using the duration of the ion trap extraction pulse, $t_n$, the approximate position $Z_n$ of the ion, from the endcap electrode, when the pulse returns to zero can be estimated from Equation 6. For the example under consideration (ubiquitin 7+, $V_{ext}$ = -100 volts, $V_{inj}$ = -50 volts), $t_1$ = 3.8 μs and t = 7.4 μs. Thus, ubiquitin 7+ is just leaving the ion trap for an extraction pulse 4 μs long; for a pulse longer than about 8 μs, the ubiquitin 7+ ions are already inside the drift tube when the ion trap extraction voltage returns to zero.

These estimates neglect several factors: a) the ions are not at rest in the trap, b) the ions lose kinetic energy due to collisions (described below), and c) the outside surface of the endcap electrode is curved, which makes the potential not quite linear over the entire distance between the exit and the drift tube entrance. For the present purposes, approximate values of ion velocity and position are adequate.

## RESULTS AND DISCUSSION

### Effect of Extraction Pulse Time

The basic result has been shown for ubiquitin ions in a previous paper [7] and for cytochrome *c* ions in a dissertation.[9] The initial observations are summarized as follows. Ions in high charge states remain unfolded, and ions in low charge states remain folded, regardless of extraction and injection conditions, unless extreme values are employed. For charge states that have a range of accessible conformers of widely different cross sections, e.g., ubiquitin 7+ and cytochrome *c* 8+, the mobility spectra vary substantially with the duration of $V_{ext}$, especially if $V_{ext}$ is more negative than $V_{inj}$ (see Figure 1).

Most other proteins studied here show similar behavior; such charge states are listed in Table 1. A detailed example is shown for carbonic anhydrase 21+ in Figure 2. With the shortest pulse (3 μs) the ions are mostly in compact conformation(s), with some partially unfolded conformers. With the longest pulse (11 μs) the ions are almost all compact. Between these extremes, intermediate behavior is observed. The ions are mostly unfolded

if the extraction pulse lasts for 7 µs. Changing the extraction pulse length by only 1 µs yields a substantially different distribution of conformers in the time regime shown, which indicates that the unfolding events occur on or faster than this time scale.

Extraction conditions used for these and other figures are given for various proteins in Table 2. Note that a variety of conditions were employed. In some experiments, the intent was to reproduce the spatial position of different protein ions, so the extraction and injection conditions were varied as appropriate, based on their mass and charge.

Consider the cross-section distribution shown in Figure 2 for carbonic anhydrase 21+ at extraction time of 6 µs. These ions are mostly unfolded. Use of slightly longer extraction times does not generate much more elongated conformers. The various proteins studied show a similar effect; there is an extraction time value when the extent of unfolding is at or near the maximum. Table 3 lists these experimentally-observed time values. Table 3 also lists the actual distance Z travelled by the protein ions in these extraction times. Although the times vary from protein to protein, the total distances are similar; all are about 1 to 1.2 cm from the ion trap center, or about 0.9 cm in front of the drift tube entrance. This observation shows that this unfolding phenomenon has reached a maximum at a common spatial position for a variety of proteins. It is related to some change that occurs when the ions are between the trap exit and drift tube entrance. Note also that these unfolding effects occur at less negative values of $V_{inj}$ than those described by Jarrold and Clemmer, et al.[10, 12-17, 32]

**Initial Explanation of Unfolding**

The effect shown in Figure 2 and Table 3 is explained with the diagram in Figure 3. The figure assumes the ions are folded and start at rest in the center of the trap. With a short extraction pulse (Figure 3a), the ions are barely outside the trap when the voltage on the exit electrode returns to zero. Unfolding occurs to only a small extent in this case. With a long extraction time (Figure 3c), the ions are already inside the drift tube when the ion trap exit electrode voltage returns to zero. Obviously, the change in $V_{ext}$ can no longer affect these ions. Thus, long extraction times yield spectra with the highest abundances of compact conformers.

The most extensive unfolding is observed when the extraction time is selected such that the ions are between the trap exit and drift tube entrance when $V_{ext}$ returns to zero. Such

a condition exacerbates the amount of unfolding observed. This is illustrated in Figure 3b; the ion has unfolded partially, and then unfolds more extensively in the second part of its travel. Ions that unfold here are then stabilized in open conformations by the many cooling collisions that occur in the higher pressure region just inside the entrance to the drift tube.[10, 32]

Suppose a relatively low value of $V_{inj}$ is used, -50 V. If the ions are between the trap exit (ground) and the drift tube entrance when the extraction pulse returns to zero, the electric field is roughly 50 V/1.3 cm = 30 V/cm. Such a value is well outside the low-field regime for IMS and heating is expected. The time frame of such heating and unfolding events is a few µs, also comparable to the time frame of such processes in high-field asymmetric ion mobility spectrometry (FAIMS).[33, 34]

The time-resolved protein ion heating has no dependence on the shutting down of the RF voltage on the center ring electrode on the ion trap. The $IT_{RF}$ voltage at full amplitude ($V_{0\text{-}p}$ = 5000) shuts off in 15 µs. Ubiquitin 6+ and 7+ ions unfolded under the injection conditions described in this paper 60 µs after turning off the $IT_{RF}$ voltage (data not shown).

**Heating and Unfolding Observations with Ubiquitin 7+**

To further test the above explanation, instrument parameters were varied with ubiquitin as the test protein. Figure 4 shows data for three charge states of ubiquitin measured with the same extraction voltage (-80 volts) and injection energy (260 eV = $zV_{inj}$). The extraction time is varied and selected to put the ions at about the same position when the polarity of $V_{ext}$ changes. We call this position Z in the following discussion.

For Z > 2 cm, the ions are inside the drift tube when the extraction voltage changes, and these ions are mostly folded for all three charge states. Some partially elongated ions are seen from ubiquitin 8+, as expected for a more highly charged species with greater electrostatic repulsion between charged groups.

For short extraction times, Z = 0.5 cm, a distribution of compact, partially elongated and unfolded conformers is seen. Again, the 8+ ion has the highest abundance of unfolded conformers. For intermediate extraction times, selected so that Z = 1.8 cm in each case, all three charge states yield mostly unfolded conformers. In the latter case, the ions are heated enough to entirely remove even the compact forms.

In another experiment, the unfolding and energy transfer caused by the change in extraction voltage are compared to that observed in more conventional experiments, where unfolding is induced by use of a large negative DC voltage on the drift tube entrance.[10, 12-17, 32] Here one set of experiments are done with an extraction pulse duration timed to change when the ions are in the position shown in Figure 3b; these results are termed "heated" conditions. Then "gentle" conditions, (i.e., conditions selected so that the ions are inside the drift tube when the extraction voltage changes, Figure 3c) are used. Vinj is then made more negative to match the extent of unfolding seen under "heated" conditions. In a sense, the mobility spectra observed under "gentle" conditions are titrated to the same values as those seen under "heated" conditions, with the DC injection voltage being the titration variable.

The results are shown for ubiquitin 7+ in Figure 5. Part a shows that the drift tube injection energy has to be as high as 518 eV to match the unfolding induced by the extraction pulse with the drift tube entrance at ground. In Frames b and c, the DC value of the injection energy needed to produce similar unfolding as the extraction pulse are again some 550 eV higher than the trap exit voltage under "gentle" conditions. Something happens to impart a lot of energy to the ions when the injection voltage changes under the "heated" conditions.

Another indication of the energy imparted to the ions by the extraction pulse is depicted in Figure 6. Here the drift tube entrance is kept grounded and a short (1 μs), very negative (-500 V) extraction pulse is used. Ubiquitin 6+ is seen in a range of conformers; ubiquitin7+ and 8+ are unfolded, even though the gentlest injection voltage is used. Comparison with Figure 5 shows that an injection energy of 500 eV or more are need to unfold the ions like this if the effect of the extraction pulse is not used.

**Observations on Trypsin and BPTI**

The importance of the ion's position when the extraction voltage changes was observed for other proteins as well. The relative values of extraction voltage and injection voltage are also important. For example, cross-sections for trypsin 11+ are shown in Figure 7 when the ion extraction voltage and time and injection voltage are selected to reproduce the ion position. In Figure 7a, the ions are at Z = 0.5 cm for all three sets of extraction conditions; the mobility spectra are similar and show all or mostly compact conformers.

In Figure 7c, the ions are inside the drift tube, and all are compact. In Figure 7b, the conditions are such that the ions are at Z = 1.2 cm, a condition where unfolding is expected. For the solid line, the extraction voltage equals the injection voltage, and the ions remain compact. There is less ion heating when there is no voltage gradient between the trap exit electrode and the drift tube entrance during the extraction pulse. In the remaining two plots in Figure 7b, injection voltage is made more negative, to - 75 and -150 volts. This heats the ions and unfolds them more extensively as the extraction voltage is made more negative.

Bovine pancreas trypsin inhibitor (BPTI) is a small, 58 amino acid, protein that is highly constrained by three disulfide bonds. Cross-section results are shown for BPTI in Figure 8 under both gentle and heated injection conditions. Three charge states (4+, 5+, and 6+) are observed. Under gentle conditions, BPTI 4+ is mostly compact conformer(s) with cross-section ~ 620 $Å^2$. Under heated conditions, this ion expands to ~ 800 $Å^2$. BPTI 5+ is almost all in an open conformation, whereas BPTI 6+ has two conformers. The cross sections for the open conformers shown in Figure 8 agree well with those reported by Shelimov with fairly energetic injection conditions.[16] It is likely that the cross sections reported by Shelimov et al. were for ions that were all in the more open state.

**Estimates of Collisions and Kinetic Energy Losses between Ion Trap Exit and Drift Tube Entrance**

Figures 1 and 3 show a plume of helium gas flowing from the drift tube entrance toward the ion trap exit. Presumably, the collisions that excite the ions and unfold them occur in this plume. These collisions will also cause the ions to lose some of their kinetic energy, which could play a role in their unfolding behavior. Thus, an estimate of the number of collisions and the corresponding kinetic energy losses is of interest.

The discussion below is derived from Douglas' paper on kinetic energy losses in a quadrupole collision cell.[35, 36] The entrance aperture diameter is 0.50 mm. Conditions in the He plume are not known exactly; for the present discussion it is assumed to have length L, temperature T = 300 K, average pressure $p_{avg}$, and average number density $n_{avg}$. The drift tube is 1.3 mbar, the vacuum chamber is $1.3 \times 10^{-4}$ mbar,

so $p_{avg}$ is $(1.3 + 1x10^{-4})/2 \sim 0.65$ mbar and $n_{avg}$ is $\sim 1.6 \times 10^{16}$ $cm^{-3}$. The subsequent mobility separation measures the cross section Ω of the protein ion. It is the compact conformers that unfold the most. Ubiquitin ($\Omega \approx 900$ $Å^2 = 9x10^{-14}$ $cm^2$) is taken as the protein of interest. These ions have a mean free path λ given by equation (7).

$$\lambda = {}^{1}/_{n\Omega} \qquad (7)$$

For compact conformers of ubiquitin, $\lambda \sim 7x10^{-4}$ cm. The number of collisions N is just L / λ. If the plume persists back for a distance 10 times the orifice diameter, then L = 0.5 cm and $N = 0.5/7x10^{-4} = 700$ collisions. Thus, hundreds of collisions are expected before the protein ions enter the drift tube. Compact conformers of other protein ions have cross sections of ≈ 1000 $Å^2$, not much larger than that of ubiquitin.

If the ions have initial kinetic energy $E_0$, their energy after one collision is $E_1$:

$$\alpha = \frac{E_1}{E_0} = \frac{m_{protein}^2 + m_{He}^2}{M^2} \qquad (8)$$

where $m_{protein}$ = 8600 Da = $1.43x10^{-20}$ g for ubiquitin, $m_{He}$ = 4 Da = $6.67x10^{-24}$ g, and M = $m_{protein} + m_{He}$.[35] The value of α is 0.9990706 in this case. After N collisions the kinetic energy remaining is approximately $\alpha^N$. For N = 700 collisions, $\alpha^N$ is roughly 0.52. Thus, protein ions in compact conformations are likely to lose roughly half of their initial kinetic energy due to collisions before they enter the drift tube.

This large loss of kinetic energy has several implications. First, much of this initial kinetic energy is converted into internal energy, hence the heating and unfolding. Second, the ions will actually move through the plume more slowly than indicated by the time values discussed above, which do not account for kinetic energy losses. Third, assume $V_{ext}$ is kept more negative than $V_{inj}$ while the ions undergo collisions in the plume, which is the condition that maximizes unfolding. In this case, the positively-charged protein ions will actually see a net electrostatic force back toward the ion trap as they are being slowed down by the collisions, which is an additional effect that would slow them further still. When $V_{ext}$ then changes back to zero, the ions are accelerated into the drift tube, the electric field between trap exit and drift tube entrance is now in the high-field regime (as noted above), and perhaps these “slow” ions are now highly prone to heating and unfolding.

## CONCLUSION

The magnitude and duration of the extraction pulse on the ion trap exit endcap can induce extensive protein ion heating and unfolding for intermediate protein charge states having a wide range of accessible conformations, especially when the extraction voltage is more negative than the voltage on the entrance of the drift tube. Experimental results confirm that simple time-of-flight equations (Eqns. 2 through 6) estimate the time and position of the ion packet when the ion trap exit electrode returns to ground. Generally, protein ions unfold to the maximum extent ~ 0.9 cm in front of the drift tube entrance when the extraction voltage returns to ground. All proteins tested are prone to this effect. BPTI, a protein about the size of ubiquitin, is constrained by three disulfide bonds and does not unfold as extensively as ubiquitin during "heated" injection conditions.

The protein ion heating may be due to the high field-regime formed by the voltage on the entrance to the drift tube when the extraction voltage returns to ground. About half of the ion kinetic energy is lost between the ion trap exit endcap and the drift tube entrance due to collisions in the helium buffer gas plume. Some of this energy converts to internal energy, resulting in heating and unfolding. Also these ions are caught in a high-field regime and unfold, similar to FAIMS experiments. Protein ions already inside the drift tube are not perturbed by the extraction voltage returning to ground. These ion conformers remain the most compact and only the voltage on the drift tube entrance dictates the extent of heating and unfolding.

## ACKNOWLEDGEMENTS

GMS acknowledges funding from the Graduate Assistance in Areas of National Need (GAANN) for the 2008 and 2009 school years.

**REFERENCES (International Journal of Mass Spectrometry formatting)**

[1] B.C. Bohrer, S.I. Merenbloom, S.L. Koeniger, A.E. Hilderbrand, D.E. Clemmer, Biomolecule Analysis by Ion Mobility Spectrometry, Annu. Rev. Anal. Chem., 1 (2008) 293-327.
[2] J.A. McLean, The Mass-Mobility Correlation Redux: The Conformational Landscape of Anhydrous Biomolecules, J. Am. Soc. Mass Spectrom., 20 (2009) 1775-1781.
[3] E. Segev, T. Wyttenbach, M.T. Bowers, R.B. Gerber, Conformational Evolution of Ubiquitin Ions in Electrospray Mass Spectrometry: Molecular Dynamics Simulations at Gradually Increasing Temperatures, Physical Chemistry Chemical Physics, 10 (2008) 3077-3082.
[4] M. D'Abramo, T. Meyer, P. Bernado, C. Pons, J.F. Recio, M. Orozco, On the Use of Low-Resolution Data to Improve Structure Prediction of Proteins and Protein Complexes, J. Chem. Theory Comput., 5 (2009) 3129-3137.
[5] T. Taverner, H. Hernandez, M. Sharon, B.T. Ruotolo, D. Matak-Vinkovic, D. Devos, R.B. Russell, C.V. Robinson, Subunit Architecture of Intact Protein Complexes from Mass Spectrometry and Homology Modeling, Accounts Chem. Res., 41 (2008) 617-627.
[6] T.L. Pukala, B.T. Ruotolo, M. Zhou, A. Politis, R. Stefanescu, J.A. Leary, C.V. Robinson, Subunit Architecture of Multiprotein Assemblies Determined Using Restraints from Gas-Phase Measurements, Structure, 17 (2009) 1235-1243.
[7] Q. Zhao, M.W. Soyk, G.M. Schieffer, K. Fuhrer, M.M. Gonin, R.S. Houk, E.R. Badman, An Ion Trap-Ion Mobility-Time of Flight Mass Spectrometer with Three Ion Sources for Ion/Ion Reactions, J. Am. Soc. Mass Spectrom., 20 (2009) 1549-1561.
[8] Q. Zhao, G.M. Schieffer, M.W. Soyk, T.J. Anderson, R.S. Houk, E.R. Badman, Effects of Ion/Ion Proton Transfer Reactions on Conformation of Gas-Phase Cytochrome *c* Ions, J. Am. Soc. Mass Spectrom., (2010) *in press*.
[9] Q. Zhao, Development of Ion Mobility Mass Spectrometry Coupled with Ion/Ion Reactions: Instrumentation and Applications for Protein Analysis, in: Chemistry, Iowa State University, Ames, IA, 2008, pp. 80-113.
[10] Y.S. Liu, S.J. Valentine, A.E. Counterman, C.S. Hoaglund, D.E. Clemmer, Injected-Ion Mobility Analysis of Biomolecules, Anal. Chem., 69 (1997) A728-A735.
[11] Y.J. Lee, C.S. Hoaglund-Hyzer, J.A. Taraszka, G.A. Zientara, A.E. Counterman, D.E. Clemmer, Collision-Induced Dissociation of Mobility-Separated Ions Using an Orifice-Skimmer Cone at the Back of a Drift Tube, Anal. Chem., 73 (2001) 3549-3555.
[12] C.S. Hoaglund, S.J. Valentine, C.R. Sporleder, J.P. Reilly, D.E. Clemmer, Three-Dimensional Ion Mobility TOFMS Analysis of Electrosprayed Biomolecules, Anal. Chem., 70 (1998) 2236-2242.
[13] S.J. Valentine, J.G. Anderson, A.D. Ellington, D.E. Clemmer, Disulfide-Intact and -Reduced Lysozyme in the Gas Phase: Conformations and Pathways of Folding and Unfolding, J. Phys. Chem. B, 101 (1997) 3891-3900.
[14] S.J. Valentine, D.E. Clemmer, H/D Exchange Levels of Shape-Resolved Cytochrome *c* Conformers in the Gas Phase, J. Am. Chem. Soc., 119 (1997) 3558-3566.
[15] S.J. Valentine, A.E. Counterman, D.E. Clemmer, Conformer-Dependent Proton-Transfer Reactions of Ubiquitin Ions, J. Am. Soc. Mass Spectrom., 8 (1997) 954-961.

[16] K.B. Shelimov, D.E. Clemmer, R.R. Hudgins, M.F. Jarrold, Protein Structure in Vacuo: Gas-Phase Confirmations of Bpti and Cytochrome C, J. Am. Chem. Soc., 119 (1997) 2240-2248.
[17] K.B. Shelimov, M.F. Jarrold, Conformations, Unfolding, and Refolding of Apomyoglobin in Vacuum: An Activation Barrier for Gas-Phase Protein Folding, J. Am. Chem. Soc., 119 (1997) 2987-2994.
[18] C.S. Hoaglund, S.J. Valentine, D.E. Clemmer, An Ion Trap Interface for ESI-Ion Mobility Experiments, Anal. Chem., 69 (1997) 4156-4161.
[19] Y.S. Liu, D.E. Clemmer, Characterizing Oligosaccharides Using Injected-Ion Mobility Mass Spectrometry, Anal. Chem., 69 (1997) 2504-2509.
[20] S.C. Henderson, S.J. Valentine, A.E. Counterman, D.E. Clemmer, Esi/Ion Trap/Ion Mobility/Time-of-Flight Mass Spectrometry for Rapid and Sensitive Analysis of Biomolecular Mixtures, Anal. Chem., 71 (1999) 291-301.
[21] C.S. Hoaglund-Hyzer, D.E. Clemmer, Ion Trap/Ion Mobility/Quadrupole/Time of Flight Mass Spectrometry for Peptide Mixture Analysis, Anal. Chem., 73 (2001) 177-184.
[22] C.S. Hoadlund-Hyzer, J.W. Li, D.E. Clemmer, Mobility Labeling for Parallel CID of Ion Mixtures, Anal. Chem., 72 (2000) 2737-2740.
[23] C.S. Hoaglund-Hyzer, Y.J. Lee, A.E. Counterman, D.E. Clemmer, Coupling Ion Mobility Separations, Collisional Activation Techniques, and Multiple Stages of MS for Analysis of Complex Peptide Mixtures, Anal. Chem., 74 (2002) 992-1006.
[24] S.G. Lias, J.F. Liebman, R.D. Levin, Evaluated Gas-Phase Basicities and Proton Affinities of Molecules - Heats of Formation of Protonated Molecules, J. Phys. Chem. Ref. Data, 13 (1984) 695-808.
[25] E.R. Badman, S. Myung, D.E. Clemmer, Gas-Phase Separations of Protein and Peptide Ion Fragments Generated by Collision-Induced Dissociation in an Ion Trap, Anal. Chem., 74 (2002) 4889-4894.
[26] A.V. Finkelstein, Can Protein Unfolding Simulate Protein Folding?, Protein Eng., 10 (1997) 843-845.
[27] A.V. Finkelstein, O.V. Galzitskaya, Physics of Protein Folding, Phys. Life Rev., 1 (2004) 23-56.
[28] K. Breuker, F.W. McLafferty, Stepwise Evolution of Protein Native Structure with Electrospray into the Gas Phase, $10^{(-12)}$ to $10^{(2)}$ S, Proc. Natl. Acad. Sci. U. S. A., 105 (2008) 18145-18152.
[29] G.M. Schieffer, L. Brachova, B.J. Nikolau, E.R. Badman, R.S. Houk, The YbhB Protein from *Escherichia coli* and *Arabidopsis thaliana* Homolog of YbhB Characterized by Mass Spectrometry and Ion Mobility Mass Spectrometry, in preparation, (2010).
[30] R.J. Cotter, Time-of-Flight Mass Spectrometry: Instrumentation and Applications in Biological Research, American Chemical Society, Washington, DC, 1997.
[31] E. deHoffmann, V. Stroobant, Mass Spectrometry: Principles and Applications, Second ed., John Wiley & Sons Ltd, Chichester; New York, 2001.
[32] D.E. Clemmer, M.F. Jarrold, Ion Mobility Measurements and Their Applications to Clusters and Biomolecules, J. Mass Spectrom., 32 (1997) 577-592.
[33] A.A. Shvartsburg, F.M. Li, K.Q. Tang, R.D. Smith, Distortion of Ion Structures by Field Asymmetric Waveform Ion Mobility Spectrometry, Anal. Chem., 79 (2007) 1523-1528.

[34] S.J. Valentine, S.L. Koeniger, D.E. Clemmer, A Split-Field Drift Tube for Separation and Efficient Fragmentation of Biomolecular Ions, Anal. Chem., 75 (2003) 6202-6208.
[35] T. Covey, D.J. Douglas, Collision Cross-Sections for Protein Ions, J. Am. Soc. Mass Spectrom., 4 (1993) 616-623.
[36] B.A. Collings, D.J. Douglas, Conformation of Gas-Phase Myoglobin Ions, J. Am. Chem. Soc., 118 (1996) 4488-4489.

Table 1) The protein ion charge states listed below are prone to the ion heating effect described in this paper and analyzed on the IT-IM-TOF MS instrument. This list is not exhaustive.

| | |
|---|---|
| Ubiquitin | 8+, 7+, 6+, 5+ |
| Trypsin | 11+, 10+ |
| Cytochrome *c* | 9+, 8+, 7+ |
| Carbonic anhydrase | 21+ |
| Lysozyme | 10+, 9+ |
| Insulin | 3+, 4+ |
| YbhB | 10+, 9+ |
| BPTI | 6+, 4+ |

Table 2) Listed are the ion extraction conditions used for various figures. A position ≥ 2.1 cm means the ion packet is fully inside the drift tube when the extraction voltage returns to 0 V.

| Figure | Extraction [V] | Extraction time [us] | Injection [V] | KE [eV] | position [cm] |
|---|---|---|---|---|---|
| 2, CA 21+ | -80 | 3-11 | -33 | 693 | variable, 0.5 to 2.6 |
| 4a, Ubiquitin 6+ | -80 | 3, 8, 12 | -44 | 260 | 0.5, 1.8, 2.9 |
| 4b, Ubiquitin 7+ | -80 | 3, 8, 12 | -37 | 260 | 0.5, 1.9, 3.1 |
| 4c, Ubiquitin 8+ | -80 | 3, 7, 12 | -32 | 260 | 0.5, 1.7, 3.1 |
| 5a, Ubiquitin 7+ | -80 | 6, 12 | 0, -74 | 0, 518 | 1.1, 3.5 |
| 5b, Ubiquitin 7+ | -80 | 6, 12 | -7, -85 | 49, 595 | 1.2, 3.6 |
| 5c, Ubiquitin 7+ | -80 | 6, 12 | -19, -97 | 133, 679 | 1.2, 3.7 |
| 6, Ubq 6, 7, 8+ | -500 | 1 | 0 | 0 | 0.4 |
| 7a, Trypsin 11+ | -50, -75, -150 | 5, 4, 3 | -49 | 540 | 0.5 |
| 7b, Trypsin 11+ | -50, -75, -150 | 9, 8, 6 | -49 | 540 | 1.2 – 1.3 |
| 7c, Trypsin 11+ | -50, -75, -150 | 14, 13, 11 | -49 | 540 | 2.3 |
| 8a, BPTI 4+ | -80 | 6, 12 | -49 | 200 | 1.1, 2.7 |
| 8b, BPTI 5+ | -80 | 6, 12 | -49 | 250 | 1.3, 3.1 |
| 8c, BPTI 6+ | -80 | 6, 12 | -49 | 300 | 1.5, 3.5 |

Table 3) Axial position of maximum unfolding and corresponding extraction conditions for several proteins. The position, Z, includes the ion trap, $Z_0$, 0.707 cm distance. $Z = Z_0 + Z_n$

| | | | Experimental Conditions | | |
|---|---|---|---|---|---|
| Protein & chg state | (m/z) | Position of max unfolding (Z, cm) | Extraction Time (µs) | $V_{ext}$ (Volts) | $V_{inj}$ |
| Ubiquitin 7+ | 1225 | 1.1 | 6 | -100 | -26 |
| Cytochrome c 8+ | 1530 | 1.0 | 6 | -100 | -26 |
| BPTI 4+ | 1630 | 1.1 | 6 | -80 | -49 |
| Carbonic anhydrase 21+ | 1383 | 1.2 | 6 | -80 | -33 |
| Trypsin 11+ | 2133 | 1.3 | 8 | -75 | -49 |
| Trypsin 11+ | 2133 | 1.0 | 5 | -150 | -49 |

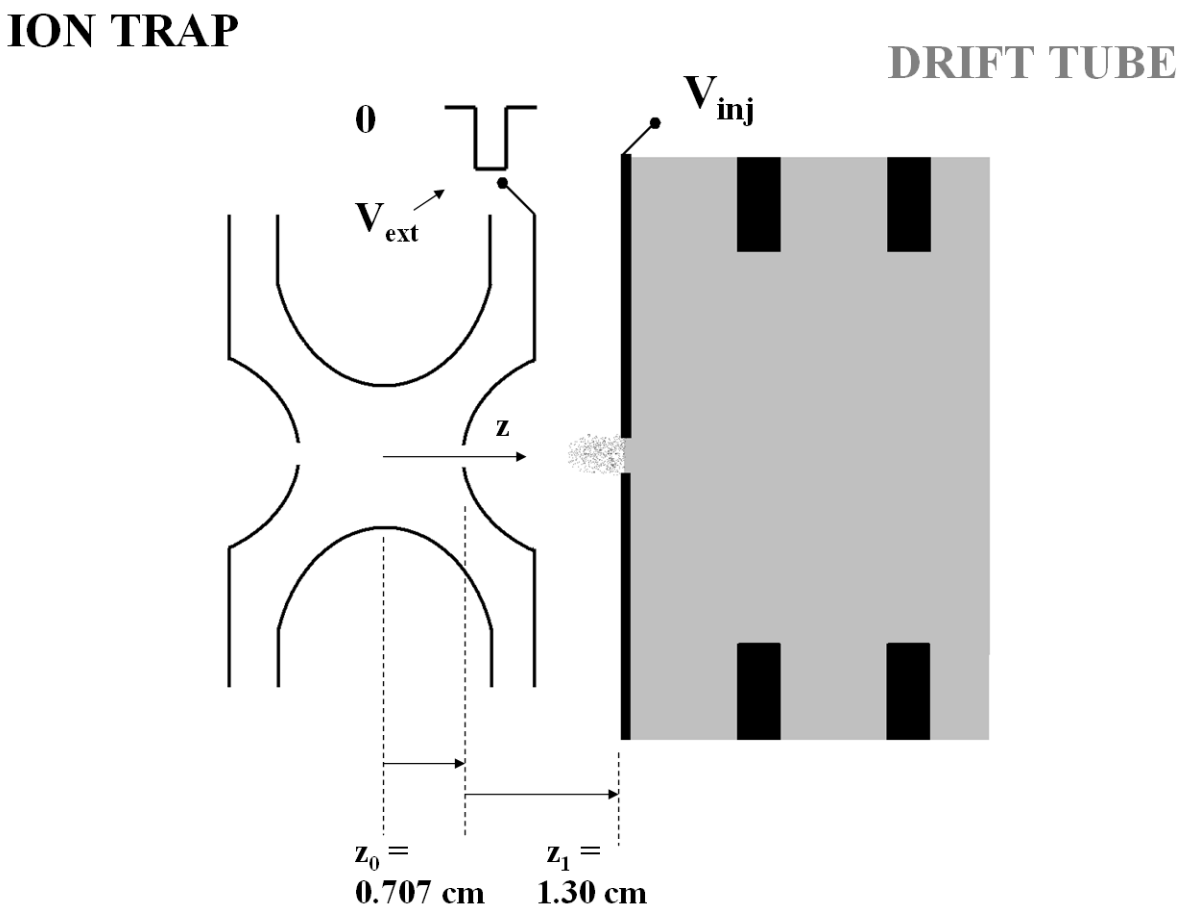


Figure 1) Schematic diagram showing the ion trap, entrance of drift tube, applied voltages, and the distances pertinent to the injection of molecules into the drift tube. The total distance, $Z = Z_0 + Z_1$ from the center of the ion trap to the entrance of the drift tube is 2.01 cm. A square wave ($V_{ext}$, typically ~ -80 V) applied to the exit endcap of the ion trap draws ions out of the trap. The voltage on the entrance of the drift tube ($V_{inj}$, typically -50 V) helps entrain ions into the tube. In the data shown below, unfolding is most extensive when $V_{ext}$ is more negative than $V_{inj}$.

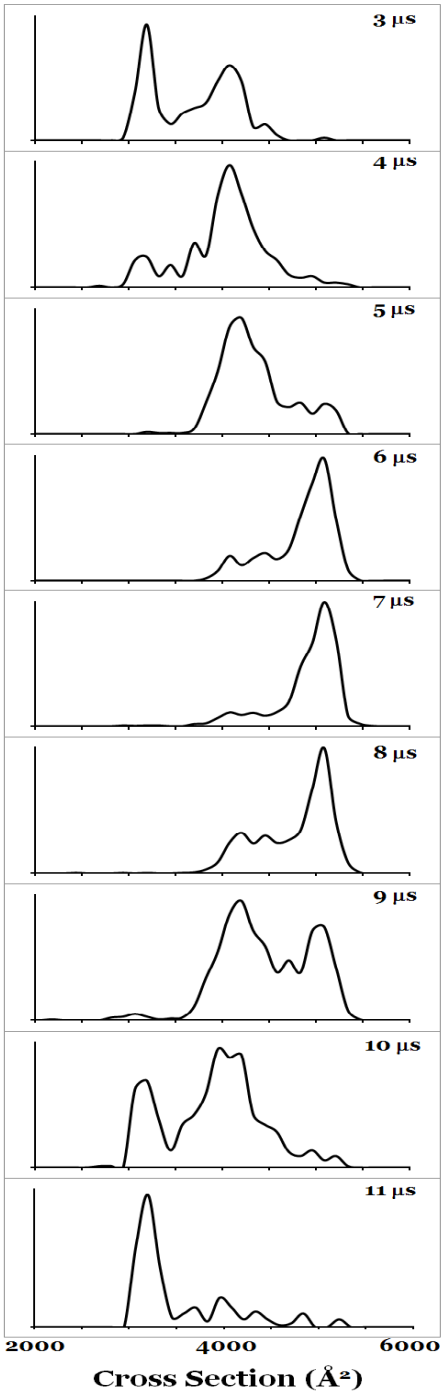


Figure 2) Collision cross-sections for carbonic anhydrase 21+ (m/z 1383) at indicated extraction times. See Table 2 for other experimental details.

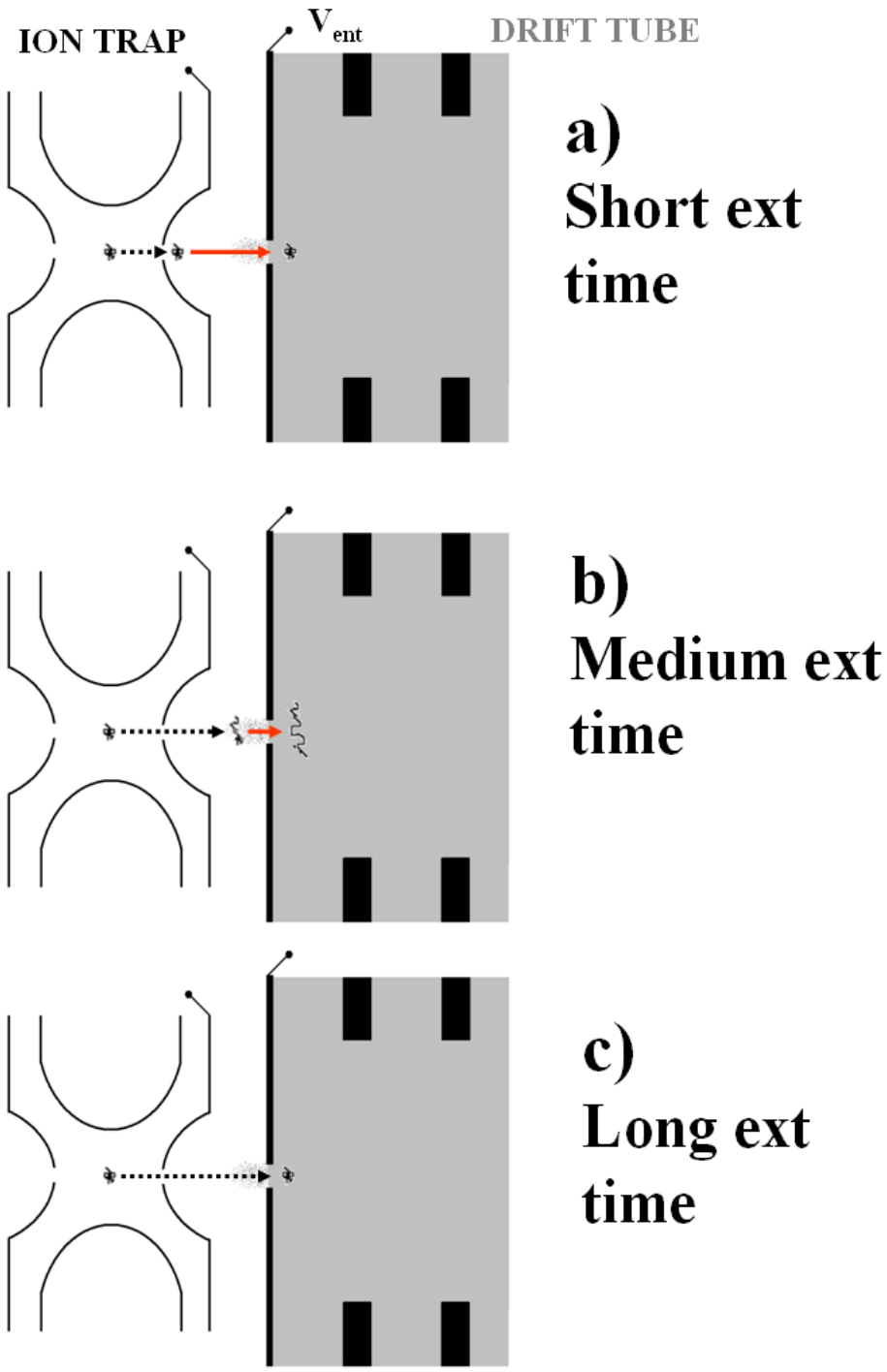


Figure 3) Depiction of mechanism for observed variation of protein unfolding with duration of extraction pulse. See text for discussion.

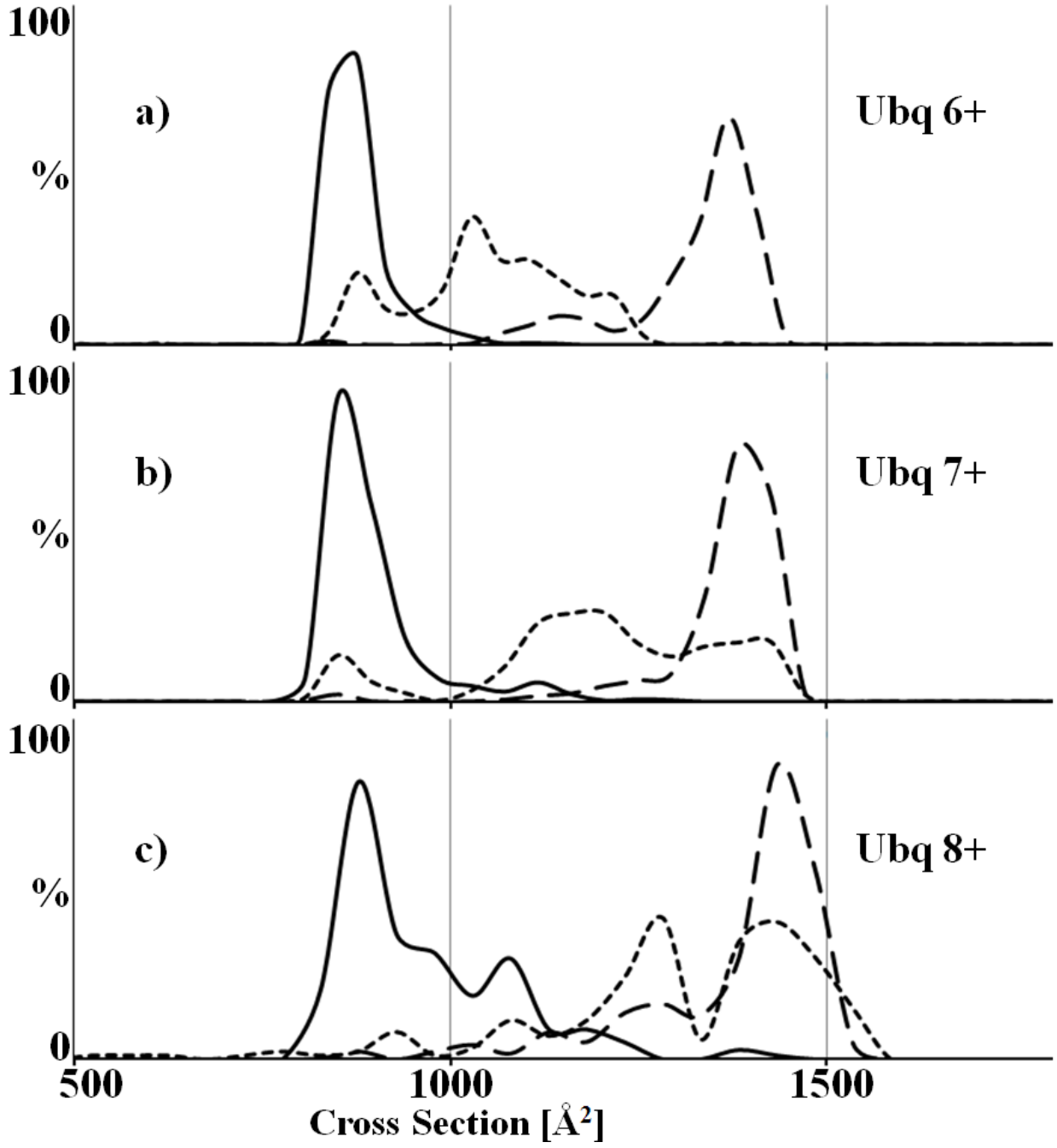


Figure 4) Cross-sections for ubiquitin ions in charge states a) 6+ (m/z 1429), b) 7+ (m/z 1225), and c) 8+ (m/z 1072) at three positions along their path into the DT when the extraction voltage returns to 0 V. The solid line denotes the CCS when the ion packet is fully inside the DT, the short dashed line denotes the CCS when the ion packet is 0.5 cm (inside IT), and the long dashed line denotes the CCS when the ion packet is 1.8 cm (in between the IT and DT) from the center of the ion trap. The ions were injected into the DT at -260 eV. The CCS counts are normalized to each other. Instrument conditions pertinent to this experiment are listed in Table 2.

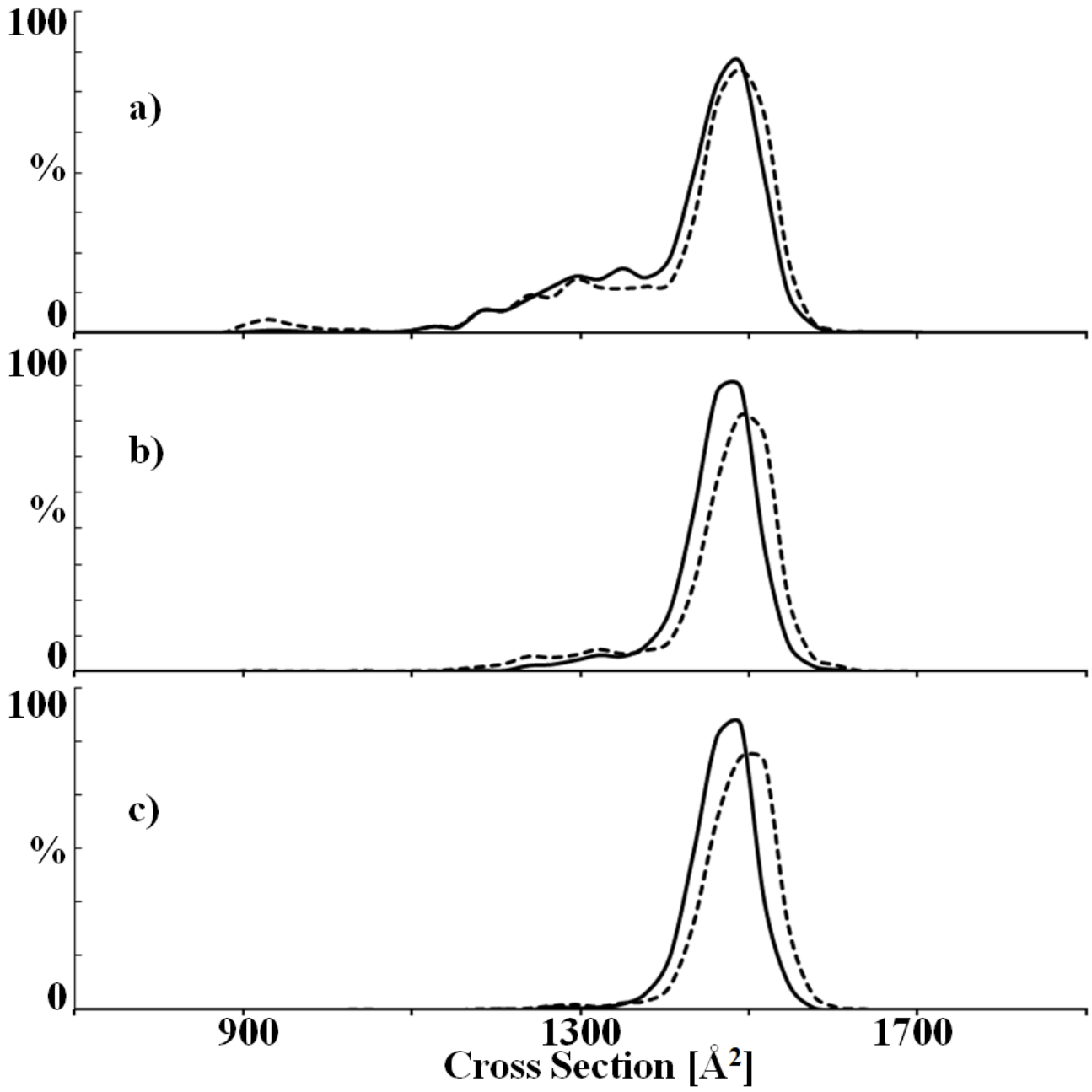


Figure 5) The cross sections for ubiquitin 7+ (m/z 1225) ion analyzed under gentle (solid line) and heating (dashed line) injection conditions. Similar Ubq 7+ cross sections are compared in a), b), and c). The injection voltage is a) 0 eV, heated; 518 eV, gentle, b) 49 eV, heated; 595 eV gentle and c) 133 eV, heated; 679 eV gentle. The eV difference for a) 518 eV, b) 546 eV, and c) 546 eV is the energy imparted to the Ubq 7+ under the heating injection conditions. Instrument conditions pertinent to this figure are listed in Table 2.

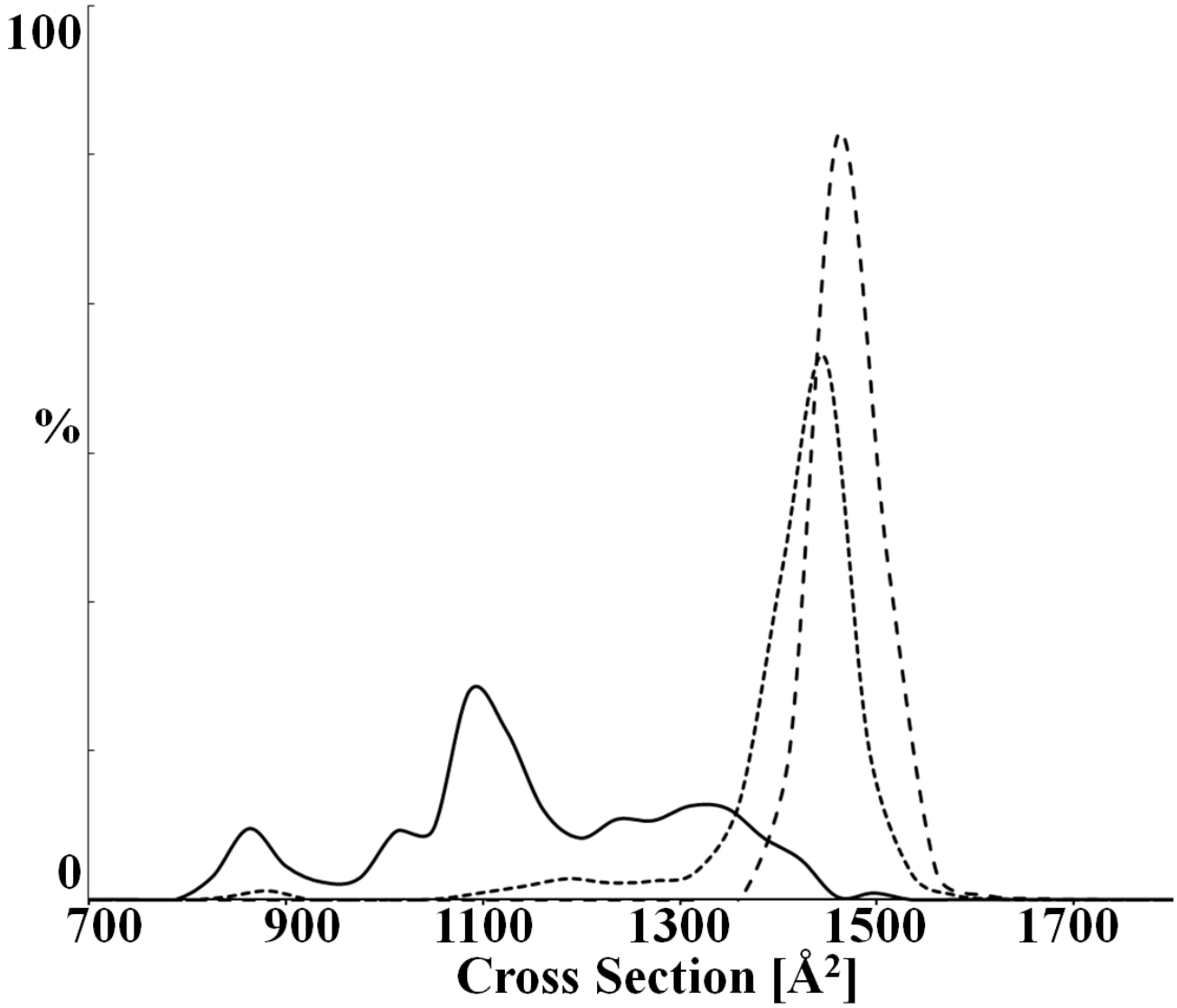


Figure 6) The cross section of ubiquitin ions injected using 0 V (grounded) on the drift tube entrance. The extraction pulse is -500 V for 1 µs. The solid line is Ubq 6+, the short dashed line is Ubq 7+, and the long dashed line is Ubq 8+. Instrument conditions pertinent to this figure are listed in Table 2.

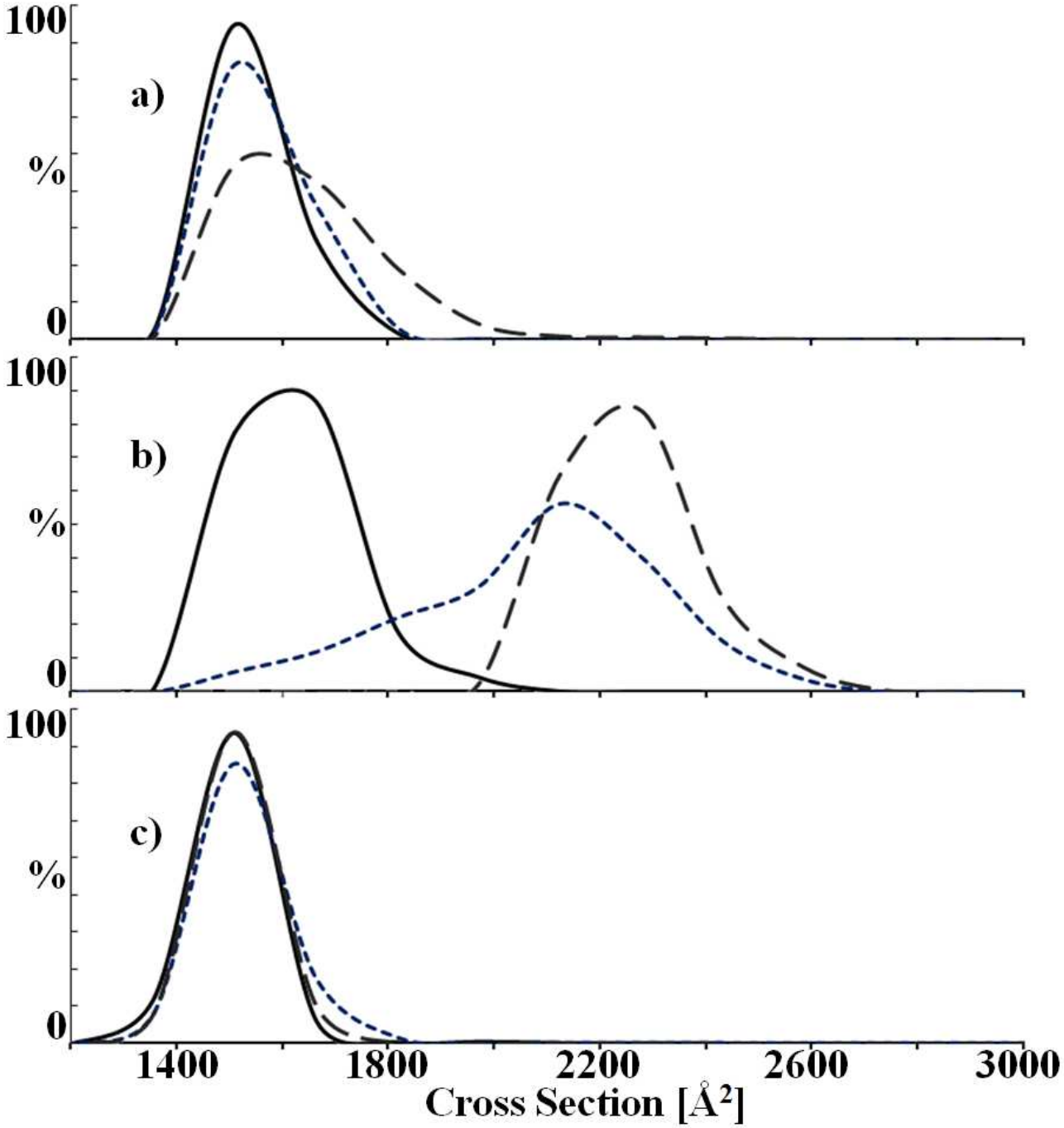


Figure 7) The cross section of trypsin 11+ (m/z 2133) when the ion packet is a) 0.5 cm (inside IT), b) 1.3 cm (between IT and DT), and c) 2.3 cm (inside DT) from the center of the IT when the extraction voltage returns to zero. The solid line used -50 V, the short dashed line used -75 V, and the long dashed line use -150 V as the extraction voltage on the exit endplate of the IT. The CCS counts are normalized to each other. Instrument conditions pertinent to this figure are listed in Table 2.

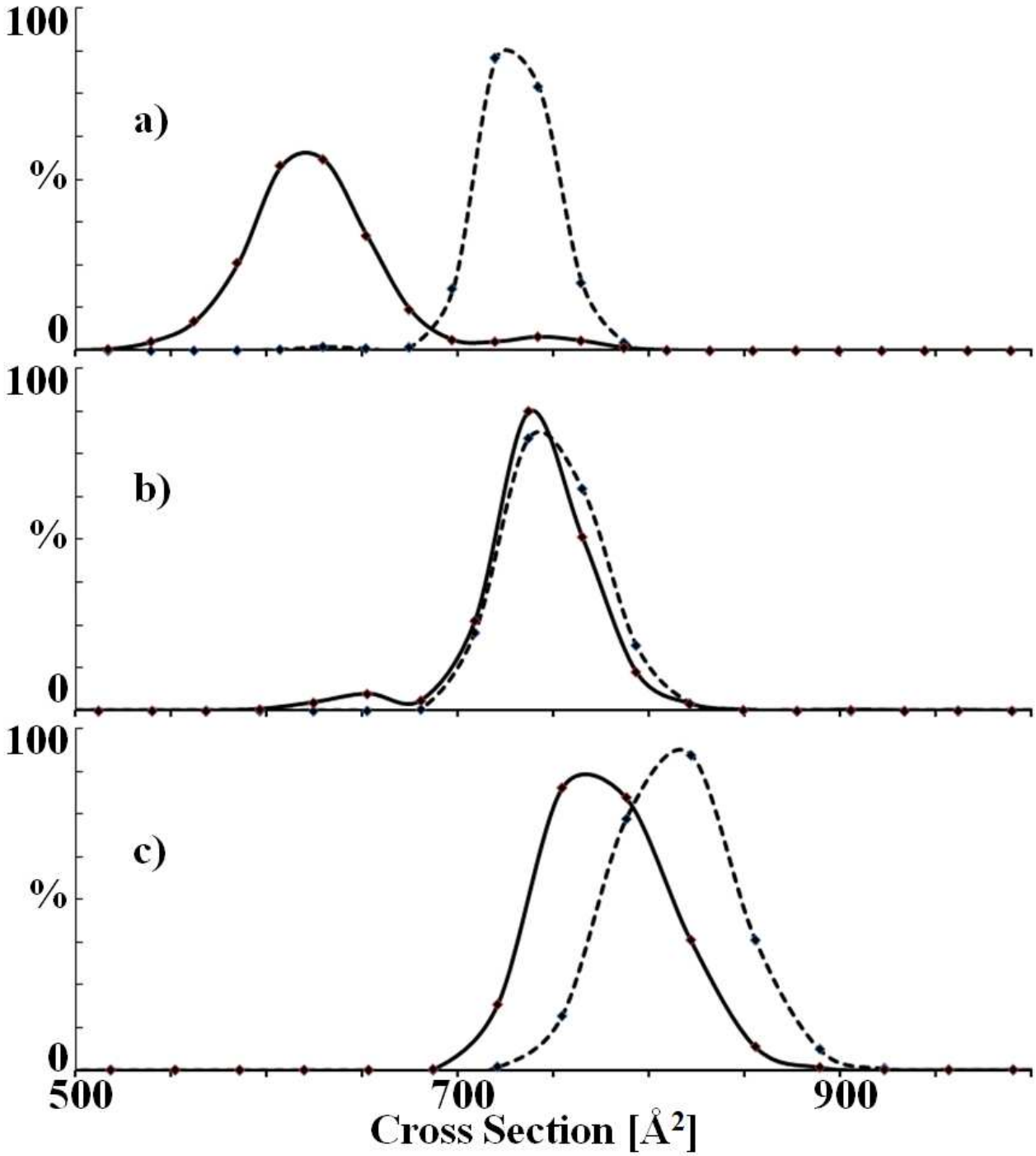


Figure 8) Cross-sections for BPTI a) 4+ (m/z 1631), b) 5+ (m/z 1304), and c) 6+ (m/z 1087) under gentle (solid line) and heated (dashed line) injection conditions. Instrument conditions pertinent to this figure are listed in Table 2.

# CHAPTER 5
# GENERAL CONCLUSION AND OVERVIEW OF FUTURE DIRECTIONS

The projects discussed in this dissertation are tied together using mass spectrometry. One project focused on extending the mass spectrometric methods to quickly ascertain coal degradation products using DART (Chapter 2). The high mass accuracy coupled with the elemental composition software enables tentative elemental composition assignments for the coal product ions. The pyrocatechol reaction at 83 bar solubilized the coal the best and released the largest water soluble ions. Another project involved imaging plant metabolites by laser desorption ionization at atmospheric pressure. The basic technique was proven using colloidal graphite to analyze metabolites (Appendix III). That paper discusses the findings by analyzing standard metabolites and plant tissue. Implementing the plant metabolite imaging with a commercial AP – LDI source is in the works.

The IT – IM – TOF MS instrument allows for the manipulation and measurement of the shape of biomolecules (Chapters 3 & 4 and Appendix I & II). Characterizing the instrument using well known proteins, ubiquitin (Appendix I; Zhao and Soyk, JASMS 2009) and cytochrome *c* (Appendix II, Zhao JASMS 2010), resulted in two papers. Briefly, the specific gas phase protein shape for each charge state adopted after proton transfer ion / ion reactions is not dependent on the original protein charge states nor the solution conditions, with some mild exceptions (Figure 6, Cytochrome *c*, Appendix II). The analysis of the YbhB proteins expanded the use of the instrument to study protein complexes under native solution nanoelectrospray ionization (native ESI). The *E. coli* YbhB protein was found to have stronger gas phase protein-protein interactions than the *Arabidopsis* homolog of the YbhB protein. *E. coli* YbhB, it primarily exists as dimer in an ammonium acetate buffer solution. The *Arabidopsis* homolog of the YbhB protein was primarily monomer under native ESI conditions, but was 60 % dimer in an acid denatured solution. Finally, the time resolved protein ion heating paper (Chapter 4) addressed and explained the phenomenon involving the duration and magnitude of the extraction pulse unfolding protein ions. The number of instruments utilizing the ion mobility and mass spectrometry interface will rapidly grow next twenty years, especially for the separation and measurement of the shape of biomolecules.

Most of the chapters in this dissertation are devoted to the implementation and use of the IT – IM – TOF MS instrument. In turn, in order of importance and ease of implementation, I have suggestions for future design modifications for the instrument:

1) Fix the switch that sets which voltages are applied so that ion / ion reactions can resume.

2) More points are needed across the mobility peak via interleaving! Interleaving is a specific time delay developed by Ionwerks to get more data points across a mobility peak. The Argos is the master instrument controller. It sends an external trigger to start the mobility and TOF flight-time measurements by Ionwerks' TDC. Unfortunately this arrangement prevents interleaving. To perform interleaving, the TDC needs to trigger the Argos when to start its scan function. This works well, except that the Argo has a "walking" incremental step that is invisible to the scan function but is present *between* each scan. Thus the mobility peak "walks" in discrete steps as measured by the Ionwerks mobility software. There must be a way to stop or disconnect the "walking" step from the Argos box, and thus allow interleaving.

Talk with Griffin Technologies (part of ICx Technologies) to remove and / or account for this "walking", incremental step. In Woods' lab, the Ionwerks TDC trigger communicates to an external laser to fire. The TDC trigger has enough power to trigger the Argos, too. The laser does not have the capability to run an additional scan step. Tom Egan (Ionwerks) recommends using an interleaving step between two and five. If the interleaving increments are too high, then the amplitude of the mobility peak signal is spread too thin and shot noise takes over, reducing the smoothness of the mobility peak.

3) Place a functioning 2D, linear ion trap in place of the 3D ion trap. Young Jin Lee, circa 2003, was the first to implement this to an IM – MS instrument. Matt Soyk's and Qin Zhao's dissertations thoroughly discuss this proposition.

4) Valentine and Clemmer published a split drift tube design in 2003. A skimmer cone and three vacuum connections are placed at the back of the drift tube. The ions are directed through the skimmer cone and the vacuum connections are plumbed to their own vacuum pump. This design reduces the gas flow through the exit aperture into the main vacuum chamber. All of Clemmer's current instruments and the T-wave use this design.

5) If the pressure in the chamber is still too high, try decreasing the size of the drift tube exit aperture from 1.5 mm to 1.0 mm. Ideally a higher drift tube pressure,
3 to >6.6 mbar, would be accessible.
6) Add another, small vacuum chamber, with additional pumping, between the quadrupole and TOF MS region.
7) Future mobility cell designs will incorporate radial focusing along the length of the cell to focus ions in the xy direction. An RF voltage, such as that used with the ion funnel, will probably work best for radial focusing.

Last a list of future experiments for Bender is found here. It is not exhaustive.
1) Electron transfer dissociation (ETD) – IM of peptides and proteins. Some of instruments built by Thermo and modifications to ABI Sciex allow ETD reactions. ETD combined with traditional CID enables top-down protein analysis. In short, top-down proteomics bypasses solution phase digestion. Proteins can be broken apart, mass analyzed, and characterized in the gas phase, speeding up analysis. IM is another phase of separation and low-field IM measurements give low resolution collision cross section (CCS) measurements. Thus, the sequence information of the protein fragments are combined with details about their shapes.
2) Catalog the shape of well characterized proteins to the 1+ charge state. Compare the low charge state CCS to x-ray crystallography and NMR measurements. Note the charge state the protein will likely be in solution. This paper can be submitted to the Journal of Physical and Chemical Reference data.
3) Measure the temporal development of the folding of a protein after a proton transfer reaction. Time resolution of 1 μs should be possible.
4) Measure the shape of amyloids free of metal ions and with metal ions attached. This research would be a continuation of work started by Lentz.
5) Protein ion heating due to injection conditions using “temperature” peptides characterized by Remes and Glish. The fragmentation patterns of these peptides will give some insight into the energy imparted during the injection process. Perhaps the “temperature” peptides can be internal calibrants with protein exposed to the same instrument conditions.

**ACKNOWLEDGMENTS**

Funding for some of this work came from Iowa State University: College of Liberal Arts and Sciences, Office of Biotechnology, Plant Sciences Institute, the Carver Trust and the Iowa State University Vice Provost for research. These sources generously provided for the construction and use of the three ion source – ion trap – ion mobility – qTOF MS instrument, affectionately called Bender. Working with this instrument produced the instrumentation skills and helped shape patience and perseverance into my character. The AP-LDI work (Appendix III) work was supported by the Ames Laboratory U. S. Department of Energy, Office of Basic Energy Sciences. The Ames Laboratory is operated by Iowa State University of Science and Technology under DOE Contract #DE-AC02-07CH11358. Ciris Energy through John Verkade dutifully supported the coal project. Libuse and Basil Nikolau generously worked with Dr. Houk and me to characterize the *E. coli* YbhB and *Arabidopsis* homolog of YbhB proteins. The GAANN fellowship generously supported the last two years of research. Thanks to Proctor and Gamble for a travel grant that helped send me to the 57th ASMS Conference in Philadelphia, PA. Last, I thank Iowa State and the ISU Chemistry department (led by Keith Woo) for providing good, stable facilities in which to work.

Some at my undergrad, University of St. Thomas in St. Paul, MN, told me choosing a major adviser is more important than choosing your spouse. While I think those counselors exaggerate, my graduate school experience places some weight to the maxim. I thank Melva Cain, the University of St. Thomas Stockroom manager, for helping instill and encourage discipline and a love for chemistry. I thank Dr. Tony Borgerding at the University of St. Thomas for introducing and teaching me how to do chemical instrumentation research. I thank Dr. Ethan Badman for taking me into his group and teaching me much about mass spectrometry and instrumentation. I hope the best for him and his family. We didn't get to work much together before he left ISU in 2006 to pursue a good career in the pharmaceutical industry. Professor Sam Houk graciously accepted Matt, Qin, and I into his research group. Wow. Matt, Qin, and I owe our careers to Dr. Houk for helping us finish our education. I heartily thank him for his efforts. Qin and Matt are excellent coworkers. I'm happy to know a hard worker and good friend in Qin. I thank Derrick Morast for working with me for the past couple years (2008 – 2010). He's a good, persistent worker, and I look forward to his

promising future. Last, thanks to all the Houk Group members. DC and I slogged through the plant metabolite project. Travis, first of all, Sally, and Chris listened and supported me in my studies. Thanks to Megan Mekoli and Toni Smith for good support, too.

The song, “My Will Be a Dead Man”, by Project 86 seems to capture well the pruning and growth I’ve encountered since submitting to the Gospel in 2000. I need to lay down my life and pick up my cross (Lk 9:23) and love God with my entire person (Lk 10:27-28). Life contains so many things to learn, process, and discern. I hope that all this gives Him glory. Two people who’ve helped develop my understanding of the world are the writings of Rev. Martin Luther King, Jr. and the writings and sermons of Dr. Greg Boyd. The Perspectives course shaped my worldview, too. In keeping with the Christian tradition, I remember the past, live in the present (Love and Faith), and look forward to the future (Hope).

Saving the best for last (Jn 2), my wife and closest friend, Tiffany, deserves first accolades. Tiffany understands life and the Gospel, which keeps me centered. I look forward to many, many more years of G & T. My parents, Paul and Ruth, encourage my seeking of truth and supporting me wherever my heart leads me. And my siblings are great. I’m happy to be part of this large family. Cheers to my extended family as well. I feel supported and accepted by them all.

# APPENDIX I

## AN ION TRAP – ION MOBILITY – TIME OF FLIGHT MASS SPECTROMETER WITH THREE ION SOURCES FOR ION/ION REACTIONS

Qin Zhao,* Matthew W. Soyk,* Gregg M. Schieffer, R.S. Houk,[†]

Ethan R. Badman[‡]

Iowa State University, Department of Chemistry, Ames, IA, 50011 USA

Katrin Fuhrer, Marc Gonin

Tofwerk AG, Uttigenstrasse 22, CH-3600 Thun, Switzerland

*These authors contributed equally to this work

[†]Ames Laboratory U. S. Dept. of Energy, Iowa State University, Ames IA 50011 USA

[‡] Hoffmann-La Roche Inc., Non-Clinical Safety, 340 Kingsland St., Nutley, NJ, 07110 USA

A paper published in the *Journal of the American Society for Mass Spectrometry*, 2009, 20, 1549-1561.

**ABSTRACT**

This instrument combines the capabilities of ion/ion reactions with ion mobility (IM) and time-of-flight (TOF) measurements for conformation studies and top-down analysis of large biomolecules. Ubiquitin ions from either of two electrospray ionization (ESI) sources are stored in a 3D ion trap (IT) and reacted with negative ions from atmospheric sampling glow discharge ionization (ASGDI). The proton transfer reaction products are then separated by IM and analyzed via a TOF mass analyzer. In this way, ubiquitin +7 ions are converted to lower charge states down to +1; the ions in lower charge states tend to be in compact conformations with cross sections down to ~ 880 $Å^2$. The duration and magnitude of the ion ejection pulse on the IT exit and the entrance voltage on the IM drift tube can affect the measured distribution of conformers for ubiquitin +7 and +6. Alternatively, protein ions are fragmented by collision-induced dissociation (CID) in the IT, followed by ion/ion reactions to reduce the charge states of the CID product ions, thus simplifying assignment of charge states and fragments using the mobility-resolved tandem mass spectrum. Instrument characteristics and the use of a new ion trap controller and software modifications to control the entire instrument are described.

Keywords: ion trap, ion mobility, time-of-flight mass spectrometry, protein conformation, ubiquitin

**INTRODUCTION**

Despite the widespread use of mass spectrometry (MS) for biological analyses, further improvements in MS instrumentation are desirable, particularly in areas like proteomics [1] and characterization of large macromolecular complexes [2, 3] . These instrumentation improvements provide analytical capabilities that enable new biological studies not envisioned previously.

Ion mobility (IM) [4, 5] has become a very useful technique for analysis of biological ions in the gas phase [6]. IM provides information about ion size and structure [7], as it rapidly separates ions based on collision cross-section, rather than just m/z ratio. The use of IM to disperse a mixture of ions in time prior to analysis via a time-of-flight (TOF) MS, i.e, nested drift (flight) time measurements, is an important recent advance. These experiments were pioneered by Clemmer and coworkers in the mid-1990's [8] and have now been used by several other groups [9-13]. The recent Synapt ESI-IMS-MS by Waters Corp. provides a commercially available instrument for gas-phase ion conformation study by IM using a novel travelling wave approach [9].

In a series of instrumental designs, the Clemmer group has made various modifications to the initial ESI-IM-TOF, including the insertion of a collision cell between the IM drift tube and the TOF for mobility labeling experiments [14, 15], and the addition of an IT prior to the mobility drift tube to improve the duty cycle from the continuous ESI source [16, 17]. One publication demonstrated MS/MS capabilities with an ion trap prior to IM-TOF [18], but the entire instrument was not under computer control. Therefore, only relatively simple experiments were possible.

IM has been used to analyze the products of ion-molecule reactions [19] including proton transfer [20, 21], H/D exchange [22], and solvation [23-26]. In these studies the desired reactions take place either in the atmospheric pressure ion source interface region or in the drift tube itself. Thus, only short reaction times and certain reagent ions can be used. In addition, performing reactions in the IM cell can make spectral interpretation difficult because the analysis and chemistry occur at the same time. In the current experiments, the ion/ion reaction is decoupled from the subsequent mobility and mass analysis. Therefore, the reaction time and chemistry of reagent ions are controlled more effectively, including a wider selection of reagent ions from independent ion sources.

Gas-phase ion/ion reactions provide another dimension for bioanalysis. Pioneering work by Smith and coworkers [27, 28] was followed by a continuing series of experiments by McLuckey's group [29]. Ion/ion reactions are rapid, versatile, and can be controlled via various ion manipulation schemes. The most common type of reaction has been proton

transfer to manipulate the charge states of multiply-charged ions [30] and simplify complex MS/MS spectra [31, 32]. Use of product ions in low charge states can improve mass accuracy and resolution, especially with low resolution mass analyzers. Various instruments specifically for ion/ion reactions include ones with two [33-36], three [37], or four [38] independent ion sources arranged around an IT, although use of pulsed sources and a single ion extraction system is also possible [39, 40]. Electron transfer is another useful process, especially electron transfer dissociation (ETD) [33, 41, 42]. ETD is now becoming widely used in proteomics and for determination of post translational modifications. Several instruments combine an IT for ETD reactions with a high resolution mass analyzer, for example, the modified QSTAR/TOF MS spectrometer in McLuckey's group [43, 44] and the hybrid linear IT/Orbitrap MS by Coon's group [45, 46].

Here we describe the first instrument to include capabilities for both ion/ion reactions and IM-TOF-MS measurements. Initial experiments and instrument characteristics are described, including use of a new ion trap controller and software to control the entire instrument. Ubiquitin is used as a test compound to compare the new results with the extensive previous studies of this protein [21, 47-52].

## EXPERIMENTAL

Bovine ubiquitin (Sigma-Aldrich, St. Louis, MO) was used without further purification. Protein concentrations were 20 to 30 μM in 1% aqueous acetic acid for positive ion mode. Nano-ESI emitters were pulled from glass capillaries (1.5 mm o.d., 0.86 mm i.d.) by a micropipette puller (P-97, Sutter Instruments, Novato, CA). Nano-ESI was performed by applying +1 kV to +1.2 kV to the protein solution via a stainless steel wire through the back of the sample capillary. Negative ions from perfluoro-1,3-dimethylcyclohexane (PDCH, Sigma-Aldrich , St. Louis, MO) were used as the proton acceptor reagent.

**Instrumentation**

***General.*** The instrument is shown to scale in Figure 1. It contains three independent ion sources: two for ESI and one for ASGDI [53]. Ions from these sources are stored in the 3D quadrupole IT for reaction. The products are separated by the IM drift tube, followed by a quadrupole-time-of-flight mass spectrometer (q-TOF).

The vacuum chamber consists of an 8" Conflat cube, which houses the three ion sources, ion optics, and turning quadrupole deflector (TQ, Extrel, Pittsburgh, PA). The cube is evacuated by a turbomolecular pump (Turbo-V550 MacroTorr, 550 L/s $N_2$, Varian Inc., Palo Alto, CA) backed by a mechanical pump (SD-30, Varian, Palo Alto, CA) and is attached to a custom built rectangular chamber (304 stainless steel, 35.6 cm wide × 76.2 cm long × 33.0 cm high) that also houses the IT, IM drift tube, and quadrupole collision cell. The TOF is in an aluminum housing (8.90 cm × 25.4 cm × 66.7 cm) attached to the back of the chamber; the TOF tube is oriented vertically. The main vacuum chamber (i.e., the chamber that houses the drift cell and quadrupole collision cell) is evacuated by two diffusion pumps (Diffstak 250/2000M and 160/700M, BOC Edwards) backed by mechanical pumps (E2M40 and RV12, respectively, BOC Edwards, Wilmington, MA). The TOF is pumped by a turbomolecular pump (Turbovac 361, 400 L/s $N_2$, Leybold Inc., Woodbridge, Ont.), backed by a mechanical pump (RV12, BOC Edwards). Convectron and ion gauges (Series 375 and 358, Helix Technology Corporation, Mansfield, MA) measure the ion source and chamber pressures (all are uncorrected). The base pressures are $7.5\times10^{-8}$ mbar in the main chamber and $3.3\times10^{-7}$ mbar in the TOF when the sources are closed. In normal operation, one ESI source and the ASGDI source are open, and helium is added to the drift tube (~1.3 to 2.0 mbar) through a precision leak valve (Model 203, Granville Phillips, Boulder, CO). The main chamber pressure is then $\sim1\times10^{-4}$ mbar and the pressure in the TOF region is $9\times10^{-7}$ mbar.

***Ion Sources.*** The basic design for a three ion source interface (Figure 1) has been described previously [38]. The three sources are arranged around three faces of the 8"

Conflat cube. One source is on the ion optical axis of the IT and IM drift tube and the other two are orthogonal to it. The two ESI sources are identical. The interface region, which is 5.08 cm in diameter and 1.59 cm deep, is machined out of an 8" ConFlat flange. A 254 μm diameter aperture separates the interface region from atmosphere, and a 381 μm diameter aperture separates the interface region from the high vacuum region. Two lenses between the apertures focus ions through the interface region. Each ESI interface region operates at ~1 mbar during the experiment and is pumped by a mechanical pump (E2M40, BOC Edwards). The nano-ESI voltages are provided by 5 kV power supplies (ORTEC 659, Oak Ridge, TN).

The ASGDI source interface region has the same design and dimensions as the ESI sources but without the interface lenses. It is pumped by a mechanical pump (E2M40, BOC Edwards). PDCH headspace vapors are sampled via a 0.64 cm diameter Nylon tube connecting the sample container and the outer aperture plate. The source pressure (~0.79 mbar) is regulated by a bellows valve (SS-4BMW, Swagelok) inserted in the tubing between the compound headspace and the source region. The ASGDI source uses a 3 kV power supply (ORTEC 556, Oak Ridge, TN) and a high voltage pulser (PVX-4150, Directed Energy Corp., Fort Collins, CO) that is trigged by a TTL pulse from the Argos IT controller (Griffin Analytical Technologies, West Lafayette, IN), to apply a ~ -420 V pulse between the outer and inner (grounded) aperture plates. This ASGDI pulse lasts for the time required to add reagent anions to the IT, typically 5 to 20 ms.

Each ion source has three cylindrical lenses attached to the vacuum side of the flange to focus the ions from the exit aperture of the source into the TQ. The second lens is split in half with distinct voltages applied to each half and serves as a deflector for direction focusing. The TQ was modified by severing the electrical connection between diagonally opposing rods and by applying four independent DC potentials to the four TQ rods. This allows ions to either be deflected $90^{o}$ onto the axis of the instrument or to be passed straight through.

After the TQ, three lenses focus the ions into the IT. Two home-built high-voltage switches, controlled by TTL signals from the Argos IT controller, switch the voltages applied to the TQ and three subsequent lenses to allow ions from the desired ion source into the IT.

Six nine-channel DC power supplies (±500 V, TD9500, Spectrum Solutions, Russellton, PA) generate the potentials for the ion optics from the sources to the ion trap.

***Ion Trap.*** The 3D quadrupole IT (ideal geometry, $r_0$ = 1.0 cm, $z_0$ = 0.707 cm, RM Jordan, Grass Valley, CA) is attached to the drift tube; the exit aperture is 1.3 cm from the front plate of the drift tube. During ion trapping the end caps are at ground, except during resonance excitation and mass selection, and the DC potential on the ring electrode is zero to prevent any asymmetric fields. The 665 kHz ion trapping voltage is generated by a home-built LC circuit that provides up to 5000 $V_{0p}$. The maximum low mass cutoff value is ~m/z 1220 (calculated assuming an ideal ion trap geometry). For the work presented here, the low mass cutoff is typically ~m/z 200 to allow for confinement of the $PDCH^-$ reagent anions from the ASGDI.

A 0 to 10 V dc control signal from the Argos IT controller determines the rf trapping voltage. A custom control generates the initial low-level RF voltage, measures feedback to stabilize the RF voltage, and contains calibration data. The initial RF voltage is first amplified to 0 to 200 $V_{0p}$ by a 50 W commercial amplifier (AG1020, T&C Power Conversion Inc., Rochester, NY) and finally by the custom LC circuit to the full 0 to 5000 $V_{0p}$. Measured stabilities of the full RF voltage are better than 1%. A TTL input allows the RF wave to be shut off in ~15 µs at any RF amplitude. The shutoff is not locked to the RF phase.

The ion trap timing and voltages are controlled by an Argos IT controller and software (see block diagram in Supplementary Information). The Argos provides the master clock for the entire instrument, as well as two independent arbitrary waveform outputs, digital TTL triggers, and analog control outputs (0 to 4 V). One arbitrary waveform output provides the 0 to 10 V dc control signal for the ion trap RF; the other is applied to the front endcap electrode (after being amplified by x17 to 85 $V_{p-p}$) to perform mass selection and resonance excitation. The TTL triggers are used to start the ASGDI source, control the high voltage switches for the ion sources, and start the ion injection pulse for the mobility

experiment. A custom 8-channel driver is used to increase the power of the TTL signals to enable them to trigger 50 Ω loads. The ion injection TTL pulse enables the high voltage pulser (PVX-4150, Directed Energy Corp., Fort Collins, CO, applied to the exit endcap) to eject ions from the ion trap. Typically the ejection pulse for positive ions is -100 to -150 V applied for 3 to 5 μs to the trap end cap closest to the drift tube (Figure 1). Two analog signals are used to control the quadrupole collision cell, described below.

***Drift Tube.*** The drift tube (modified from a design provided by Valentine et al. [54, 55]) consists of alternating 12.7 cm diameter 304 stainless steel lenses (0.16 cm thick, 12.7 cm o.d. 4.40 cm i.d.) and Delrin insulating rings (1.27 cm thick, 12.7 cm o.d., 8.26 cm i.d.). The drift tube is 44.45 cm long (together with the ion funnel) with a 0.5 mm diameter entrance aperture. A chain of 2 MΩ resistors connects the lenses, creating an electric field (typically 12.4 V/cm) down the drift tube. Unless stated otherwise, the voltage applied to the front of the drift tube is typically -30 to -100 V, i.e., more negative than the grounded IT. Thus, the injection voltage into the drift tube is the voltage on the entrance, and the injection energy in the lab frame is charge x injection voltage. A capacitance manometer (690A13TRC, MKS Instrument, Methuen, MA) measures the He pressure inside the drift tube, which is typically 1.33 to 2.00 mbar, controlled via another precision leak valve.

***Ion Funnel.*** To improve ion transmission efficiency, an ion funnel [54, 56] is integrated into the back of the drift tube (Figure 1). The funnel is based on the device described by the Smith [56] and Jarrold groups [57]. After the last ring of the drift tube, a series of 25 stainless steel electrodes (0.079 cm thick, 12.7 cm o.d.) with circular apertures whose inner diameters decrease linearly from 4.293 to 0.483 cm is attached. The ion funnel electrodes are sealed together using 0.318 cm thick Delrin spacers and Viton o-rings giving a funnel length of 11.11 cm. Thus, the helium pressure in the drift tube and ion funnel are the same. The electrodes are connected to each other with a series of resistors (Vishay, 500 k **Ω,** 0.6 W, ±1%). One voltage is applied to the entrance of the drift tube, and a second voltage is

applied to the exit of the ion funnel to set the axial electric field down the drift tube-ion funnel assembly. The electrode spacing and resistor voltages in the ion funnel are selected so that the axial electric field is the same as that in the rest of the drift tube [57].

In the ion funnel, alternate lenses are capacitively coupled (Vishay, 1000 pF, 1.5 $kV_{rms}$, ±20%) to form two lens chains. RF voltages (Ardara RF power supply, # PSRF-100, Ardara Technologies, North Huntingdon, PA) that are 180° degrees out of phase from each other are applied to each chain with amplitudes ~90 $V_{pp}$ at 360 kHz. A capacitor to ground decouples the RF voltage from the drift tube lenses. There is one DC only electrode after the exit of the ion funnel with a pressure-limiting aperture (1.0 mm diam).

In this instrument, the ion funnel increases the overall total ion signal by a factor of ~7. Here, the basis of comparison is to a drift tube with the same overall length (44.45 cm) and exit aperture, but all electrodes have the same ID (4.40 cm), spacing (1.27 cm), and DC electric field (typically 12 V/cm) with no RF voltage. In this experiment, total ion signal is measured by extracting ions from the TOF extractor at high repetition rates into the flight tube and reflecting them to the TOF microchannel plate (MCP) detectors. The measured cross sections are the same whether the ion funnel is inserted or not.

Another set of three lenses behind the drift tube-ion funnel focuses ions into the quadrupole collision cell (Figure 1). The voltages supplied to the ion funnel dc lens, the lenses before the collision cell, the entrance and exit lenses of the collision cell, and the lenses between the collision cell and the TOF are floated on the drift tube exit voltage using a nine-output floating power supply (TD9500HV, Spectrum Solutions Inc., Russellton, PA).

***Quadrupole-TOF.*** The quadrupole collision cell (Figure 1) transmits ions from the ion funnel to the TOF. It also provides for CID of ions labeled by mobility (i.e., a pseudo MS/MS step) [14, 15], although this capability is not shown in this paper. The quadrupole ($d_0$ = 9.5 mm, 880 kHz, 3600 $V_{0p}$ per pole, Extrel, Pittsburgh, PA) is followed by an orthogonal W-reflectron TOF (Tofwerk, Thun, Switzerland). The collision cell and its electronics are floated using an isolation transformer (SIT 30-1000, Stangenes Industries Inc.,

Palo Alto, CA). The collision cell is mounted on the vacuum side of an 8" Conflat flange that is attached to the back of the main vacuum chamber. A capacitance manometer (Model 690A01TRC, MKS Instrument, Methuen, MA) measures the pressure inside the collision cell, which is typically ~$8\times10^{-4}$ mbar of He from the drift tube. Additional collision gas can be added via another precision leak valve. The Argos IT controller (Figure 2) supplies two 0 to 4 V analog signals that are amplified to 0 to 10 V and -200 to 200 V, respectively, and then used by the quadrupole power supply to control the rf amplitude and to supply the dc bias to the collision cell rods to set the collision energy.

After the ions exit the collision cell, they are focused into the source region of the TOF by a series of 10 lenses mounted in the hole machined out of the 8" Conflat flange between the collision cell and the TOF, which is mounted vertically on the air side of the flange. One lens is split into half-plates for vertical direction focusing. The ions are extracted upwards into the TOF drift region by a 2 μs pulse and are then accelerated into the drift region by ~5800 V. The voltages on the TOF electrodes and detector are controlled by the TOF software, which communicates directly with the TOF power supply. The TOF has a W-reflectron and can be operated in V-mode or in W-mode. Only the V-mode is used in this paper; the effective flight path is ~1.5 m.

The ion detector is an eight-anode MCP (Ionwerks, Houston, TX) that has post acceleration voltage of ~6000 V. The signal is amplified ×100 by two four-channel preamplifiers (XCD quad amplifier/discriminator, Ionwerks, Houston, TX) and then sent to an 8 channel time-to-digital converter (TDC×8, Ionwerks, Houston, TX). The TOF software reads the data from the TDC to create 2D data that contain both drift time and mass spectral information.

The timing of the TOF data acquisition (Figure 3) is similar to methods described previously [8, 16]. As shown by the bottom three traces in Figure 3, the TOF timing controller gets signals from the software and an external trigger and sends TTL triggers to the TDC×8 and to the TOF extraction pulser. The mobility acquisition is started by the ion injection pulse (a trigger from the Argos), after which the TOF timing controller starts sending TTL triggers—at specific intervals depending on the mass range being acquired—

simultaneously to the TDC×8 and the TOF extraction. In a typical experiment 100 TOF extractions are taken within each 10 ms mobility spectrum, up to a maximum m/z value of 2400. Mass spectra could be measured to higher m/z values, but there would be fewer such mass spectra over the duration of the IM peaks. Alternatively, interleaving [58] could be used to improve the number of points in the IM spectra, although this makes the data files larger.

***Measurement of Cross Sections.*** Ion cross-sections can be determined from the IM drift times [59]:

(1)

$$\Omega = \frac{(18\pi)^{1/2}}{16}\frac{ze}{(k_b T)^{1/2}}\left[\frac{1}{m_i}+\frac{1}{m_b}\right]^{1/2}\frac{1}{N(0)}\frac{t_D E}{L}\frac{760}{P}\frac{T}{273.2}$$

where z = ion charge (+1, +2, …), e = charge on electron, $m_i$ = ion mass, $m_b$ = mass of the buffer gas particle, E = electric field through drift, L = length of the drift tube, $t_D$ = flight time through the drift tube, N(0) = gas number density at STP, P, T = pressure and temperature of the buffer gas.

The instrument provides the time between the ejection pulse from the IT and the start pulse of the TOF. For Eqn. 1, the measured time $t_D$ should be only the time spent inside the drift tube. Therefore, the ion flight times between the drift tube and TOF source region (i.e., through the quadrupole and the ion lenses just to the left of it in Figure 1) are calculated from the lens dimensions and applied voltages and subtracted from the total time between IT and TOF extractor. The calculated times through the lenses and quadrupole range from 127 μs for ubiquitin +8 to 360 μs for ubiquitin +1, i.e., the ions with the shortest and longest drift times. About 70% of this time is spent inside the quadrupole collision cell.

Many experimental parameters pertaining to the drift tube and ion funnel (e.g., axial electric field, injection pulser voltage, rf voltage on the ion funnel, etc.) were varied. Under the experimental conditions used in this work, none affected the numerical values of the measured cross sections, confirming that the ion mobility measurement is in the low field regime. Four parameters did influence the number of mobility peaks observed and their relative abundances: the voltage on the first electrode of the drift cell, the pressure in the drift cell, and the duration and magnitude of the voltage pulse used to eject ions from the IT. These effects are described below.

## RESULTS AND DISCUSSION

***IM-TOFMS after Ion/Ion Reactions.*** In early research on proton transfer reactions with IM, a basic neutral gas was introduced into the source region to create lower charge state ions through an in-source proton transfer reaction [21, 60]. In the present instrument, the total reaction time and reagent ion identity can be controlled. The experimental timing diagram (Figure 3) is similar to those previously shown for ion/ion reactions [38], except the usual IT mass analysis step is replaced by injection of product ions into the IM drift tube. The experiment scan function shown in Figure 3 includes acquisition of nested drift (flight) time mobility data.

These capabilities are illustrated using charge reduction reactions of multiply charged ubiquitin ions with PDCH anions. The reagent anions are mainly $[M\text{-}F]^{-\cdot}$ and $[M\text{-}CF_3]^{-\cdot}$ ions, as seen from a similar ASGDI source in another paper recently published from our group [61]. The signal ratio $[M\text{-}F]^{-}/ [M\text{-}CF_3]^{-}$ is approximately 1.5 in the present device.

For a typical ion/ion reaction-IM experiment, ubiquitin ions are injected for 50 to 100 ms, $PDCH^{-}$ ions are injected for 5 to 50 ms, and both polarity ions are trapped in the IT to react for 20 to 150 ms, depending on the product ion charge states desired. An extraction pulse (-100 V for 3 to 10 µs) is then applied to the back end cap of the ion trap to inject ions into the drift tube. For the IM separation the He pressure in the drift tube is 1.4 mbar, and the electric field applied is 12.4 V/cm across the drift cell, with various injection voltages.

Figure 3a shows a 3D mobility-m/z spectrum of ubiquitin before proton transfer reactions. The main charge state observed for ubiquitin under these solution and source conditions is +7 with a small but measurable amount of +8. The mass resolution shown is $m/\Delta m = 1000$ at m/z 1224.6. Mass accuracies are within 28 ppm, using cytochrome *c* +8 and +9 ions as external calibrants.

Figure 3b, c and d show spectra after ion/ion charge reduction reaction of ubiquitin with $PDCH^-$. Ubiquitin +8 and +7 ions are converted to lower charge states than those produced directly by ESI, using longer fill and reaction times. The ions in lower charge states are better resolved in the IM dimension, probably because a) fewer conformations are available at lower charge state, and/or b) at lower charge states the conformations are more folded and have more uniform cross sections.

Previous attempts at analysis of protein mixtures by CID after IM separation suffered because protein ions in high charge states were not resolved in the mobility separation [62]. Thus, mobility labeling for proteins is not as useful as for peptides. Ion/ion reaction combined with IM separations provides a new technique to improve the performance of mobility labeling (for on-the-fly MS/MS) for top-down analysis of intact proteins.

The various drift time vs m/z plots in Figure 3 show dense "bunches" of ions at the expected m/z values and diffuse "streaks" at all m/z values. These streaks have the same drift time as the expected ions; this is especially evident in Figures 3c and 3d for the ions in low charge states. Thus, it is believed that this background is caused by protein ions that get into the TOF region at times other than the TOF extraction pulse.

***Cross-Section Measurements.*** Observed values for ubiquitin ions using three injection voltages are depicted in Figure 4. Numerical cross section values from the plots in Figure 4 are listed in Table 1, and conditions and scale values are given in Table 2. IM spectra and the resulting cross sections obtained at higher injection voltages do not differ appreciably from those measured at -50 V and are not shown.

First, consider the +8 and +7 ions, which come directly from the ESI source. The +8 ions are unfolded at all injection voltages, while the +7 ions are observed in up to three IM

peaks, as noted above. The +6 to +1 ions come from proton transfer reaction, mainly with the +7 ubiquitin ions originally present. Reducing the charge state converts the ubiquitin ions to more compact conformers. For ions in the lower charge states, the single IM peak gets narrower as charge state is reduced. For ubiquitin +1, the FWHM of the ion mobility peak (~500 µs) is still a factor of three wider than the FWHM of the diffusion limited peak (~175 µs, calculated as described in the literature) [63-65]. Thus, we suggest that the single IM peaks for ubiquitin in low charge states are comprised of contributions from several unresolved conformers [49], and fewer such conformers are present at lower charge states.

Numerical data for cross sections are given in Table 1. Multiple entries indicate values from several discernable peaks in the IM spectra (Figure 5). The ions in low charge states have essentially a single value of cross section corresponding to folded conformer(s) of ubiquitin, even though the original ubiquitin +7 ions have a variety of conformations before the ion/ion reaction. In general, the measured cross-sections of +8 to +4 ubiquitin ions are in the range of the literature values [21]. This is the first report of cross-sections for ubiquitin +3, +2 and +1 ions.

Most of the numerical cross section values in Table 1 do not vary much with injection voltage. For the 5+ ions, the cross section shown in the table does appear to change, but examination of Figure 4 shows that this is mainly due to changes in peak structure and width from various conformers induced by the changes in injection voltage.

This device also provides reasonable IM spectra for ions injected at very low kinetic energy, although the transmission and sensitivity are naturally lower at very low injection voltage. Apparently, some ions in the trap are moving toward the drift tube before the negative injection pulse is applied to the endcap. Otherwise ions could not enter the higher-pressure drift tube (~1 mbar) at a nominal injection voltage of zero.

***Effects of Drift Tube Injection Conditions on Folding of Ubiquitin Ions.*** Clemmer's group [21] studied how injection energy influences mobility spectra of ubiquitin ions and the apparent number and relative abundance of protein conformers. At low injection

energy (385 eV, or 55 V for ubiquitin +7), different conformers were observed and the distributions were expected to reflect the distribution of conformers from the ion source [21].

Similar effects were seen in the present work for ubiquitin ions in certain charge states, as shown in Figure 4, which includes results at lower injection voltages (i.e., 0 volts) than those reported by Clemmer. The relative abundances of various peaks in the IM spectra do not change further as injection voltage is raised above 50 V (data from -60 V to -150 V are not shown). Briefly, Figure 4 shows that +8 ions remain unfolded, and +5 to +1 ions remain folded, regardless of injection voltage. For the intermediate charge states +6 and +7, lower injection voltage generally favors formation of more folded conformers. More open conformers for the +6 and +7 ions are also less abundant at lower pressure inside the drift tube (data not shown).

In general, these observations are consistent with ions being heated and unfolded initially by collisions in the short space (1.3 cm) between the trap exit and drift tube. Ions in intermediate charge states have various folded states accessible and may refold when further collisions cool the ions, either during extraction or inside the drift tube. Differential scattering of larger ions outside the acceptance of the small entrance aperture (0.5 mm diam.) of the drift tube may also contribute to these observations.

The duration and magnitude of the negative voltage pulse applied to eject ions from the IT can also affect the number of peaks in the IM spectra for the +7 ions, i.e., those ions that are prone to folding changes. Such effects are most pronounced if the ejection pulse is more negative than the voltage on the entrance to the drift tube. Figure 5 depicts an extreme example; the ejection pulse amplitude is -100 V, and the drift tube entrance is at -30 V. Ubiquitin +7 ions are mostly folded using the shortest ejection pulse (1 µs). A variety of conformers are seen at 3 µs, while the ions are unfolded when the ejection pulse lasts for 5 or 7 µs. Curiously, the ions are folded if the ejection pulse is extended further to 9 or 10 µs. The drift time changes corresponding to the various cross sections shown in Figure 5 are substantial (~ 100 µs), much longer than even the longest injection times, so the observed cross section changes are attributed to real changes in protein conformation, not just differences in injection time.

We have not found descriptions of effects quite like those shown in Figure 5 in previous literature involving injection of ions into IM drift tubes. A long ion ejection pulse is of use mainly because it improves signals for ions in low charge states, as if ~ 10 µs are required to draw the less highly charged ions out of the trap. Fortunately, the ions in low charge states remain folded anyway, and a long extraction pulse is generally not needed to obtain adequate sensitivity for the ions in the intermediate charge states that are more susceptible to folding changes. Use of an extraction pulse that is less negative than the entrance to the drift tube also reduces the magnitude of these folding changes.

Varying the injection voltage and duration of the ion ejection pulse also induces similar changes in conformations of cytochrome c, especially the +7 and +8 ions. [66] We offer the following tentative, qualitative explanation for these observations. It seems like the location of the ions when the pulse polarity changes is important. Consider the plots in Figure 5 with an ejection pulse amplitude of -100 V for various times. A ubiquitin 7+ ion at rest in the center of the trap would take 3.6 µs to travel the 0.707 cm to the trap exit. Some ions are moving toward the trap exit and get there sooner, others take longer. For short ejection pulses (1 µs), the ejected ions have not gone far past the trap when the ejection pulse goes back to zero. If the trap exit remains at -100 V long enough, the ions go through this 1.3 cm long region and are all inside the drift tube before the trap exit voltage changes. At -100 V this transit is estimated to take 4.2 µs, for a total time of ~ 8 µs. The longest ejection pulse used (10 µs) exceeds this transit time, so the trap exit remains at a constant voltage (-100 V) until all the ions are inside the drift tube. Thus at either short (1 µs) or long (10 µs) ejection times, most of the ions remain folded, and the mobility spectra in these two cases are similar.

With -100 V ejection pulses for times between 3 µs and 9 µs, many of the ions are between the trap exit and the drift tube entrance when the voltage on the trap exit returns to zero. As the ejection pulse duration increases from 3 to 5 to 7 µs, the ions are expected to be closer to the drift tube entrance, where the density of He gas escaping from the drift tube is higher than it is closer to the trap exit. This voltage change and the accompanying collisions with gas induce the observed folding changes. For 5 µs and 7 µs, the ions are mostly

unfolded. The unfolding effects are more extensive at times where the bulk of the ions are still between the ion trap exit and drift tube entrance when the voltage on the trap exit returns to zero.

At an ejection time of 9 µs, some of the ejected ions are already inside the drift tube when the voltage on the trap exit changes, so some ions are not affected by the voltage change. The resulting mobility spectrum shows ions in a range of conformations, like that observed at 3 µs. There are still collisions with gas for either short or long ejection pulses; apparently these collisions are most effective at changing the conformations of the ions if the ions are closer to, but not inside the drift tube when the trap exit voltage changes.

Badman et al. [67] and Myung et al. [48] observed that the folding and unfolding of cytochrome c and ubiquitin ions in intermediate charge states occurred while ions were stored for ~ 100 ms in a 3-D ion trap. In the present work, changing the duration of the extraction pulse from 1 µs to 10 µs can also affect the observed conformations, so some folding and unfolding events apparently can occur on the microsecond time scale.

The underlying causes of the changes reported here could be related to recent work by Shvartsburg et al. [52], who studied conformation changes in ubiquitin ions during field asymmetric waveform ion mobility spectrometry (FAIMS). They attribute such conformation changes to heating induced repetitively during the high voltage segments of the FAIMS waveform. Each high voltage segment lasts ~ 0.1 µs; during many FAIMS cycles, the cumulative conformation changes induced on ubiquitin ions in intermediate charge states (especially +7) as a result of many such excitation/heating events are substantial.

The charge states where folding changes are expected probably vary between proteins, so these effects should be evaluated on a case-by case basis. So far, ions in the higher and lower charge states are less prone to these folding changes. Even for these charge states, there may still be subtle changes in the distributions of closely-related conformers hidden by the relatively low IM resolution in our experiments, compared to the much narrower peaks seen in Clemmer's tandem IM work [68, 69].

***CID on Intact Proteins followed by Charge Reduction.*** This instrument also has potential value for top-down proteomics measurements, as indicated by the following example. Figure 6a shows a spectrum obtained after isolating only the +7 charge state of ubiquitin in the ion trap. Mass selection was performed by applying first a 30 kHz 12 $V_{p-p}$ AC waveform to the entrance endcap of the ion trap to resonantly eject lower mass ions during an RF ramp. Then a 20 kHz 10 $V_{p-p}$ AC waveform ejected higher mass ions during another RF ramp [38]. The IM peak in Figure 6a is narrower than that in Figure 3 because a higher injection voltage (-150 V) was used for Figure 6a.

In a subsequent experiment, ubiquitin +7 ions were stored in the ion trap for 20 ms and activated for 100 ms at 50 kHz, 23 $V_{p-p}$. The fragment spectrum (Figure 6b) shows CID product ions in a variety of relatively high charge states that are only moderately resolved in the IM dimension. Thus, it is not easy to assign them at first.

Figure 6c shows the spectrum resulting from charge reduction of the fragment ions in the ion trap with PDCH anions (injection for 20 ms, reaction for 100 ms). The spectrum shifts to higher m/z, and the dispersion in the IM dimension is greatly improved. Many of the charge-reduced CID fragments can now be assigned by comparing the observed m/z values with those of fragments generated from the known sequence of ubiquitin. The mass tolerance for these assignments is 0.6 Th. The assumption that the fragment ions in Figure 6c are in low charge states greatly simplifies these assignments. Most of the fragments observed here are b and y ions; $b_{18}$ and $y_{58}$ are abundant fragments, in agreement with other studies [38, 70].

The IM plot for the charge-reduced fragments (Figure 6c) shows distinct groups that fall along slanted lines of different slopes for peptide fragment ions in +1, +2 and +3 charge states, as noted by Clemmer and co-workers. This phenomenon provides additional evidence to help assign charge states. These groups merge closer together at higher charge states [17], which is one reason they are poorly resolved in Figure 7b.

Armed with the identities of the charge-reduced fragments (Figure 6), many of the original, more highly charged fragments in Figure 6 can now be assigned. For example, $y_{58}^{2+}$ is in the charge-reduced spectrum. Thus, a more highly charged version ($y_{58}^{5+}$ in this case)

should appear in the original CID spectrum (Figure 6), along with the complementary $b_{18}^{2+}$ ions. Note that the charge states of these two fragments add up to the original +7, as expected. Here we assume that the peptide fragment ions do not dissociate further during the charge reduction reactions, as shown by McLuckey [31]. A number of other, similar cases are identified in Figure 6.

## CONCLUSION

This is the first instrument that combines ion/ion reactions and IM separations with full computer control of all functions. It should prove useful for study of the effects of protein charge state on conformation, which is key to the general question of the relation between gas-phase conformation and that in solution [71-73]. Protein ions in solution generally have lower net charges than those observed in the gas phase after ESI; this methodology provides a way to access ions in these physiologically relevant charge states. Other types of ion/ion reactions, such as ETD, formation of protein-metal, protein-ligand and protein-protein complexes, should also be possible, with the added benefit of the ability to also manipulate charge state. Finally, manipulation of charge state of CID products facilitates high throughput top-down protein analysis. A number of improvements in the instrumentation, such as use of a linear ion trap instead of the 3D ion trap, CID at higher energy, CID of mobility-selected ions using the quadrupole collision cell, and multiple reflections in the TOFMS for higher resolution, are under investigation in our laboratory. Also, a more detailed study of conformation changes in the μs time scale between the ion trap and the drift tube may prove interesting in its own right.

## ACKNOWLEDGEMENTS

The authors acknowledge helpful discussions with Steve Valentine (Indiana Univ.); Scott McLuckey for the design of high-voltage switches; Brent Knecht, Garth Patterson, Brent Rardin, and Mitch Wells (Griffin Analytical) for assistance with the Argos and software; David Prior (Pacific Northwest National Lab) for design of the IT RF amplifier; and Randy Pedder (Ardara Technologies, North Huntingdon, PA) for advice on use of the RF

supply for the ion funnel. Other custom electronics were designed and constructed by Lee Harker (Ames Lab Engineering Services Group); vacuum welding by Charlie Burg (Ames Lab); precision machining by Richard Egger, the late Steve Lee, and Terry Soseman (ISU Chemistry Machine Shop). Derrick Morast analyzed the ubiquitin sample with another ESI instrument to evaluate its purity. ERB acknowledges funding from Waters Corp. via an ASMS Research Award. Funding from Iowa State University: College of Liberal Arts and Sciences, Office of Biotechnology, Plant Sciences Institute, and the Carver Trust are gratefully acknowledged.

Supplementary Information: block diagram of hardware for instrument control and data acquisition.

**REFERENCES**

1. Pandey, A.; Mann, M. Proteomics to Study Genes and Genomes *Nature* **2000**, *405*, 837-846.
2. Sobott, F.; McCammon, M. G.; Hernandez, H.; Robinson, C. V. The Flight of Macromolecular Complexes in a Mass Spectrometer *Philos. Trans. R. Soc. Lond. Ser. A-Math. Phys. Eng. Sci.* **2005**, *363*, 379-389.
3. Loo, J. A.; Berhane, B.; Kaddis, C. S.; Wooding, K. M.; Xie, Y. M.; Kaufman, S. L.; Chernushevich, I. V. Electrospray Ionization Mass Spectrometry and Ion Mobility Analysis of the 20s Proteasome Complex *J. Am. Soc. Mass Spectrom.* **2005**, *16*, 998-1008.
4. St. Louis, R. H.; Hill, H. H. Ion Mobility Spectrometry in Analytical Chemistry *Crit. Rev. Anal. Chem.* **1990**, *21*, 321-355.
5. Collins, D. C.; Lee, M. L. Developments in Ion Mobility Spectrometry-Mass Spectrometry *Anal. Bioanal. Chem.* **2002**, *372*, 66-73.
6. Bohrer, B. C.; Merenbloom, S. I.; Koeniger, S. L.; Hilderbrand, A. E.; Clemmer, D. E. Biomolecule Analysis by Ion Mobility Spectrometry *Annu. Rev. Anal. Chem.* **2008**, *Vol. 1*, 293-327.
7. Jarrold, M. F. Peptides and Proteins in the Vapor Phase *Annu. Rev. Phys. Chem.* **2000**, *51*, 179-207.
8. Hoaglund, C. S.; Valentine, S. J.; Sporleder, C. R.; Reilly, J. P.; Clemmer, D. E. Three-Dimensional Ion Mobility Tofms Analysis of Electrosprayed Biomolecules *Anal. Chem.* **1998**, *70*, 2236-2242.
9. Smith, D. P.; Giles, K.; Bateman, R. H.; Radford, S. E.; Ashcroft, A. E. Monitoring Copopulated Conformational States During Protein Folding Events Using Electrospray Ionization-Ion Mobility Spectrometry-Mass Spectrometry *J. Am. Soc. Mass Spectrom.* **2007**, *18*, 2180-2190.
10. Steiner, W. E.; Clowers, B. H.; English, W. A.; Hill, H. H. Atmospheric Pressure Matrix-Assisted Laser Desorption/Ionization with Analysis by Ion Mobility Time-of-Flight Mass Spectrometry *Rapid Commun. Mass Spectrom.* **2004**, *18*, 882-888.
11. Steiner, W. E.; Clowers, B. H.; Fuhrer, K.; Gonin, M.; Matz, L. M.; Siems, W. F.; Schultz, A. J.; Hill, H. H. Electrospray Ionization with Ambient Pressure Ion Mobility Separation and Mass Analysis by Orthogonal Time-of-Flight Mass Spectrometry *Rapid Commun. Mass Spectrom.* **2001**, *15*, 2221-2226.
12. Stone, E.; Gillig, K. J.; Ruotolo, B.; Fuhrer, K.; Gonin, M.; Schultz, A.; Russell, D. H. Surface-Induced Dissociation on a MALDI -Ion Mobility-Orthogonal Time-of-Flight Mass Spectrometer: Sequencing Peptides from an "in-Solution" Protein Digest *Anal. Chem.* **2001**, *73*, 2233-2238.
13. Stone, E. G.; Gillig, K. J.; Ruotolo, B. T.; Russell, D. H. Optimization of a Matrix-Assisted Laser Desorption Ionization-Ion Mobility-Surface-Induced Dissociation-Orthogonal-Time-of-Flight Mass Spectrometer: Simultaneous Acquisition of Multiple Correlated MS1 and MS2 Spectra *Int. J. Mass Spectrom.* **2001**, *212*, 519-533.
14. Hoaglund-Hyzer, C. S.; Li, J. W.; Clemmer, D. E. Mobility Labeling for Parallel CID of Ion Mixtures *Anal. Chem.* **2000**, *72*, 2737-2740.
15. Hoaglund-Hyzer, C. S.; Clemmer, D. E. Ion Trap/Ion Mobility/Quadrupole/Time of Flight Mass Spectrometry for Peptide Mixture Analysis *Anal. Chem.* **2001**, *73*, 177-184.

16. Henderson, S. C.; Valentine, S. J.; Counterman, A. E.; Clemmer, D. E. ESI/Ion Trap/Ion Mobility/Time-of-Flight Mass Spectrometry for Rapid and Sensitive Analysis of Biomolecular Mixtures *Anal. Chem.* **1999**, *71*, 291-301.
17. Myung, S.; Lee, Y. J.; Moon, M. H.; Taraszka, J.; Sowell, R.; Koeniger, S.; Hilderbrand, A. E.; Valentine, S. J.; Cherbas, L.; Cherbas, P.; Kaufmann, T. C.; Miller, D. F.; Mechref, Y.; Novotny, M. V.; Ewing, M. A.; Sporleder, C. R.; Clemmer, D. E. Development of High-Sensitivity Ion Trap Ion Mobility Spectrometry Time-of-Flight Techniques: A High-Throughput Nano-LC-IMS-TOF Separation of Peptides Arising from a Drosophila Protein Extract *Anal. Chem.* **2003**, *75*, 5137-5145.
18. Badman, E. R.; Myung, S.; Clemmer, D. E. Gas-Phase Separations of Protein and Peptide Ion Fragments Generated by Collision-Induced Dissociation in an Ion Trap *Anal. Chem.* **2002**, *74*, 4889-4894.
19. Green, M. K.; Lebrilla, C. B. Ion-Molecule Reactions as Probes of Gas-Phase Structures of Peptides and Proteins *Mass Spectrom. Rev.* **1997**, *16*, 53-71.
20. Valentine, S. J.; Anderson, J. G.; Ellington, A. D.; Clemmer, D. E. Disulfide-Intact and -Reduced Lysozyme in the Gas Phase: Conformations and Pathways of Folding and Unfolding *J. Phys. Chem. B* **1997**, *101*, 3891-3900.
21. Valentine, S. J.; Counterman, A. E.; Clemmer, D. E. Conformer-Dependent Proton-Transfer Reactions of Ubiquitin Ions *J. Am. Soc. Mass Spectrom.* **1997**, *8*, 954-961.
22. Valentine, S. J.; Clemmer, D. E. H/D Exchange Levels of Shape-Resolved Cytochrome *c* Conformers in the Gas Phase *J. Am. Chem. Soc.* **1997**, *119*, 3558-3566.
23. Woenckhaus, J. Drift Time Mass Spectrometric Protein Hydration Experiments *Int. J. Mass Spectrom.* **2002**, *213*, 9-24.
24. Woenckhaus, J.; Mao, Y.; Jarrold, M. F. Hydration of Gas Phase Proteins: Folded +5 and Unfolded +7 Charge States of Cytochrome *c J. Phys. Chem. B* **1997**, *101*, 847-851.
25. Fye, J. L.; Woenckhaus, J.; Jarrold, M. F. Hydration of Folded and Unfolded Gas-Phase Proteins: Saturation of Cytochrome *c* and Apomyoglobin *J. Am. Chem. Soc.* **1998**, *120*, 1327-1328.
26. Wyttenbach, T.; Liu, D. F.; Bowers, M. T. Hydration of Small Peptides *Int. J. Mass Spectrom.* **2005**, *240*, 221-232.
27. Loo, R. R. O.; Udseth, H. R.; Smith, R. D. A New Approach for the Study of Gas-Phase Ion-Ion Reactions Using Electrospray Ionization *J. Am. Soc. Mass Spectrom.* **1992**, *3*, 695-705.
28. Loo, R. R. O.; Udseth, H. R.; Smith, R. D. Evidence of Charge Inversion in the Reaction of Singly Charged Anions with Multiply Charged Macroions *J. Phys. Chem.* **1991**, *95*, 6412-6415.
29. Pitteri, S. J.; McLuckey, S. A. Recent Developments in the Ion/Ion Chemistry of High-Mass Multiply Charged Ions *Mass Spectrom. Rev.* **2005**, *24*, 931-958.
30. Stephenson, J. L.; McLuckey, S. A. Ion/Ion Proton Transfer Reactions for Protein Mixture Analysis *Anal. Chem.* **1996**, *68*, 4026-4032.
31. Stephenson, J. L.; McLuckey, S. A. Simplification of Product Ion Spectra Derived from Multiply Charged Parent Ions Via Ion/Ion Chemistry *Anal. Chem.* **1998**, *70*, 3533-3544.
32. McLuckey, S. A.; Reid, G. E.; Wells, J. M. Ion Parking During Ion/Ion Reactions in Electrodynamic Ion Traps *Anal. Chem.* **2002**, *74*, 336-346.

33. Syka, J. E. P.; Coon, J. J.; Schroeder, M. J.; Shabanowitz, J.; Hunt, D. F. Peptide and Protein Sequence Analysis by Electron Transfer Dissociation Mass Spectrometry *Proc. Natl. Acad. Sci. U. S. A.* **2004**, *101*, 9528-9533.
34. Stephenson, J. L.; McLuckey, S. A. Adaptation of the Paul Trap for Study of the Reaction of Multiply Charged Cations with Singly Charged Anions *Int. J. Mass Spectrom. Ion Process.* **1997**, *162*, 89-106.
35. Reid, G. E.; Wells, J. M.; Badman, E. R.; McLuckey, S. A. Performance of a Quadrupole Ion Trap Mass Spectrometer Adapted for Ion/Ion Reaction Studies *Int. J. Mass Spectrom.* **2003**, *222*, 243-258.
36. Wu, J.; Hager, J. W.; Xia, Y.; Londry, F. A.; McLuckey, S. A. Positive Ion Transmission Mode Ion/Ion Reactions in a Hybrid Linear Ion Trap *Anal. Chem.* **2004**, *76*, 5006-5015.
37. Xia, Y.; Liang, X. R.; McLuckey, S. A. Pulsed Dual Electrospray Ionization for Ion/Ion Reactions *J. Am. Soc. Mass Spectrom.* **2005**, *16*, 1750-1756.
38. Badman, E. R.; Chrisman, P. A.; McLuckey, S. A. A Quadrupole Ion Trap Mass Spectrometer with Three Independent Ion Sources for the Study of Gas-Phase Ion/Ion Reactions *Anal. Chem.* **2002**, *74*, 6237-6243.
39. Liang, X. R., Xia, Y., McLuckey, S. A. Alternately Pulsed Nanoelectrospray Ionization/Atmospheric Pressure Chemical Ionization for Ion/Ion Reactions in an Electrodynamic Ion Trap *Analytical Chemistry* **2006**, *78*, 3208-3212.
40. Liang, X. R.; Han, H. L.; Xia, Y.; McLuckey, S. A. A Pulsed Triple Ionization Source for Sequential Ion/Ion Reactions in an Electrodynamic Ion Trap *J. Am. Soc. Mass Spectrom.* **2007**, *18*, 369-376.
41. Pitteri, S. J.; Chrisman, P. A.; Hogan, J. M.; McLuckey, S. A. Electron Transfer Ion/Ion Reactions in a Three-Dimensional Quadrupole Ion Trap: Reactions of Doubly and Triply Protonated Peptides with $SO2^{\cdot -}$ *Anal. Chem.* **2005**, *77*, 1831-1839.
42. Chrisman, P. A.; Pitteri, S. J.; Hogan, J. M.; McLuckey, S. A. $SO2^{\cdot -}$ Electron Transfer Ion/Ion Reactions with Disulfide Linked Polypeptide Ions *J. Am. Soc. Mass Spectrom.* **2005**, *16*, 1020-1030.
43. Han, H.; Xia, Y.; Yang, M.; McLuckey, S. A. Rapidly Alternating Transmission Mode Electron-Transfer Dissociation and Collisional Activation for the Characterization of Polypeptide Ions *Anal. Chem.* **2008**, *80*, 3492-3497.
44. Xia, Y.; Han, H.; McLuckey, S. A. Activation of Intact Electron-Transfer Products of Polypeptides and Proteins in Cation Transmission Mode Ion/Ion Reactions *Anal. Chem.* **2008**, *80*, 1111-1117.
45. Phanstiel, D.; Zhang, Y.; Marto, J. A.; Coon, J. J. Peptide and Protein Quantification Using Itraq with Electron Transfer Dissociation *J. Am. Soc. Mass Spectrom.* **2008**, *19*, 1255-1262.
46. McAlister, G. C.; Berggren, W. T.; Griep-Raming, J.; Horning, S.; Makarov, A.; Phanstiel, D.; Stafford, G.; Swaney, D. L.; Syka, J. E. P.; Zabrouskov, V.; Coon, J. J. A Proteomics Grade Electron Transfer Dissociation-Enabled Hybrid Linear Ion Trap-Orbitrap Mass Spectrometer *J. Proteome Res.* **2008**, *7*, 3127-3136.
47. Li, J. W.; Taraszka, J. A.; Counterman, A. E.; Clemmer, D. E. Influence of Solvent Composition and Capillary Temperature on the Conformations of Electrosprayed Ions:

Unfolding of Compact Ubiquitin Conformers from Pseudonative and Denatured Solutions *Int. J. Mass Spectrom.* **1999**, *187*, 37-47.
48. Myung, S.; Badman, E. R.; Lee, Y. J.; Clemmer, D. E. Structural Transitions of Electrosprayed Ubiquitin Ions Stored in an Ion Trap over Similar to 10 ms to 30 s *J. Phys. Chem. A* **2002**, *106*, 9976-9982.
49. Koeniger, S. L.; Merenbloom, S. I.; Sevugarajan, S.; Clemmer, D. E. Transfer of Structural Elements from Compact to Extended States in Unsolvated Ubiquitin *J. Am. Chem. Soc.* **2006**, *128*, 11713-11719.
50. Koeniger, S. L.; Clemmer, D. E. Resolution and Structural Transitions of Elongated States of Ubiquitin *J. Am. Soc. Mass Spectrom.* **2007**, *18*, 322-331.
51. Segev, E.; Wyttenbach, T.; Bowers, M. T.; Gerber, R. B. Conformational Evolution of Ubiquitin Ions in Electrospray Mass Spectrometry: Molecular Dynamics Simulations at Gradually Increasing Temperatures *Phys. Chem. Chem. Phys.* **2008**, *10*, 3077-3082.
52. Shvartsburg, A. A.; Li, F. M.; Tang, K. Q.; Smith, R. D. Distortion of Ion Structures by Field Asymmetric Waveform Ion Mobility Spectrometry *Anal. Chem.* **2007**, *79*, 1523-1528.
53. McLuckey, S. A.; Glish, G. L.; Asano, K. G.; Grant, B. C. Atmospheric Sampling Glow-Discharge Ionization Source for the Determination of Trace Organic-Compounds in Ambient Air *Anal. Chem.* **1988**, *60*, 2220-2227.
54. Him, T.; Tolmachev, A. V.; Harkewicz, R.; Prior, D. C.; Anderson, G.; Udseth, H. R.; Smith, R. D.; Bailey, T. H.; Rakov, S.; Futrell, J. H. Design and Implementation of a New Electrodynamic Ion Funnel *Anal. Chem.* **2000**, *72*, 2247-2255.
55. Valentine, S. J.; Koeniger, S. L.; Clemmer, D. E. A Split-Field Drift Tube for Separation and Efficient Fragmentation of Biomolecular Ions *Anal. Chem.* **2003**, *75*, 6202-6208.
56. Tang, K.; Shvartsburg, A. A.; Lee, H. N.; Prior, D. C.; Buschbach, M. A.; Li, F. M.; Tolmachev, A. V.; Anderson, G. A.; Smith, R. D. High-Sensitivity Ion Mobility Spectrometry/Mass Spectrometry Using Electrodynamic Ion Funnel Interfaces *Anal. Chem.* **2005**, *77*, 3330-3339.
57. Julian, R. R.; Mabbett, S. R.; Jarrold, M. F. Ion Funnels for the Masses: Experiments and Simulations with a Simplified Ion Funnel *J. Am. Soc. Mass Spectrom.* **2005**, *16*, 1708-1712.
58. Fuhrer, K.; Gonin, M.; McCully, M. I.; Egan, T. F.; Ulrich, S. R.; Vaughn, V. W.; Burton Jr, W. D.; Schultz, J. A.; Gillig, K. J.; Russell, D. H. Monitoring of Fast Processes by TOFMS,*49th ASMS Conference on Mass Spectrometry and Allied Topics* Chicago, Illinois May 27-31, 2001.
59. Clemmer, D. E.; Jarrold, M. F. Ion Mobility Measurements and Their Applications to Clusters and Biomolecules *J. Mass Spectrom.* **1997**, *32*, 577-592.
60. Loo, R. R. O.; Winger, B. E.; Smith, R. D. Proton Transfer Reaction Studies of Multiply Charged Proteins in a High Mass-to-Charge Ratio Quadrupole Mass Spectrometer *J. Am. Soc. Mass Spectrom.* **1994**, *5*, 1064-1071.
61. Soyk, M. W.; Zhao, Q.; Houk, R. S.; Badman, E. R. A Linear Ion Trap Mass Spectrometer with Versatile Control and Data Acquisition for Ion/Ion Reactions *J. Am. Soc. Mass Spectrom.* **2008**, *19*, 1821-1831.

62. Badman, E. R.; Hoaglund-Hyzer, C. S.; Clemmer, D. E. Dissociation of Different Conformations of Ubiquitin Ions *J. Am. Soc. Mass Spectrom.* **2002**, *13*, 719-723.
63. Mason, E. A.; McDaniel, E. W. In *Transport Properties of Ions in Gases*; John Wiley & Sons: New York, 1988, pp 86-91.
64. Badman, E. R.; Myung, S.; Clemmer, D. E. Evidence for Unfolding and Refolding of Gas-Phase Cytochrome *c* Ions in a Paul Trap *J. Am. Soc. Mass Spectrom.* **2005**, *16*, 1493-1497.
65. Koeniger, S. L.; Merenbloom, S. I.; Clemmer, D. E. Evidence for Many Resolvable Structures within Conformation Types of Electrosprayed Ubiquitin Ions *J. Phys. Chem. B* **2006**, *110*, 7017-7021.
66. Zhao, Q.; Soyk, M. W.; Houk, R. S.; Badman, E. R. Effects of Ion/Ion Reactions on Conformation of Gas-Phase Cytochrome *c* Ions *J. Am. Soc. Mass Spectrom.* **2009**, *to be submitted*
67. Badman, E. R.; Hoaglund-Hyzer, C. S.; Clemmer, D. E. Monitoring Structural Changes of Proteins in an Ion Trap over ~10 to 200 ms: Unfolding Transitions in Cytochrome *c* Ions *Anal. Chem.* **2001**, *73*, 6000-6007.
68. Koeniger, S. L.; Merenbloom, S. I.; Valentine, S. J.; Jarrold, M. F.; Udseth, H. R.; Smith, R. D.; Clemmer, D. E. An IMS-IMS Analogue of MS-MS *Anal. Chem.* **2006**, *78*, 4161-4174.
69. Merenbloom, S. I.; Koeniger, S. L.; Valentine, S. J.; Plasencia, M. D.; Clemmer, D. E. IMS-IMS and IMS-IMS-IMS/MS for Separating Peptide and Protein Fragment Ions *Anal. Chem.* **2006**, *78*, 2802-2809.
70. Xia, Y.; Liang, X. R.; McLuckey, S. A. Ion Trap Versus Low-Energy Beam-Type Collision-Induced Dissociation of Protonated Ubiquitin Ions *Anal. Chem.* **2006**, *78*, 1218-1227.
71. Breuker, K.; McLafferty, F. W. Native Electron Capture Dissociation for the Structural Characterization of Noncovalent Interactions in Native Cytochrome *c Angew. Chem.-Int. Edit.* **2003**, *42*, 4900-4904.
72. Breuker, K.; McLafferty, F. W. The Thermal Unfolding of Native Cytochrome *c* in the Transition from Solution to Gas Phase Probed by Native Electron Capture Dissociation *Angew. Chem.-Int. Edit.* **2005**, *44*, 4911-4914.
73. Breuker, K.; McLafferty, F. W. Stepwise Evolution of Protein Native Structure with Electrospray into the Gas Phase, 10(-12) to 10(2) s *Proc. Natl. Acad. Sci. U. S. A.* **2008**, *105*, 18145-18152.

**TABLES**

Table 1**)** Measured cross-sections for ubiquitin ions in different charge states. +7 and +8 ions are from the ESI source, ions with charge states +6 to +1 are made from mostly +7 ions by ion/ion reaction. See text for conditions. The cross-sections are determined from the apex of the various mobility peaks (Figure 5) according to Equation 1. Uncertainties are estimated to be approximately 50 $Å^2$ based on many repeated measurements over several months.

| Charge state | Cross-Section ($Å^2$) at Indicated Injection Voltage | | | |
|---|---|---|---|---|
| | 0 V | -30 V | -50 V | -100 V |
| +8 | 1428 | 1430 | 1430 | 1428 |
| +7 | 1393 | 1394 | 1394 | 1393 |
| +6 | 863,1056,1314 | 863,1056, 1314 | 1314 | 1312 |
| +5 | 872, 979 | 979 | 1033 | 1031 |
| +4 | 904 | 861 | 904 | 902 |
| +3 | 855 | 813 | 814 | 814 |
| +2 | 854 | 856 | 857 | 857 |
| +1 | 882 | 861 | 882 | 861 |

Table 2) Reaction conditions and vertical scale values for cross-section plots in Figure 5. Other conditions: ubiquitin fill time 50 ms, extraction pulse from ion trap -100 V for 5 μs except for +1 ions, which were pulsed out for 10 μs at -150 V.

| | Time Values (ms) | | Full-Scale Signal (counts/s) | | |
|---|---|---|---|---|---|
| Charge | PDCH | | At Indicated Injection Voltage | | |
| State | Fill | Reaction | 0 V | -30 V | -50 V |
| +8* | | 60* | 38 | 137 | 83 |
| +7* | | 60* | 189 | 546 | 380 |
| +6 | 20 | 60 | 33 | 154 | 116 |
| +5 | 20 | 60 | 136 | 522 | 373 |
| +4 | 20 | 60 | 26 | 191 | 81 |
| +3 | 45 | 150 | 258 | 642 | 873 |
| +2 | 45 | 150 | 350 | 182 | 114 |
| +1 | 50 | 180 | 18 | 320 | 159 |

*These ions were observed directly from the ESI source without ion/ion reaction.

To keep the total trapping time constant without inducing ion/ion reactions, the

ASGDI source was turned off while these ions were measured.

**FIGURES**

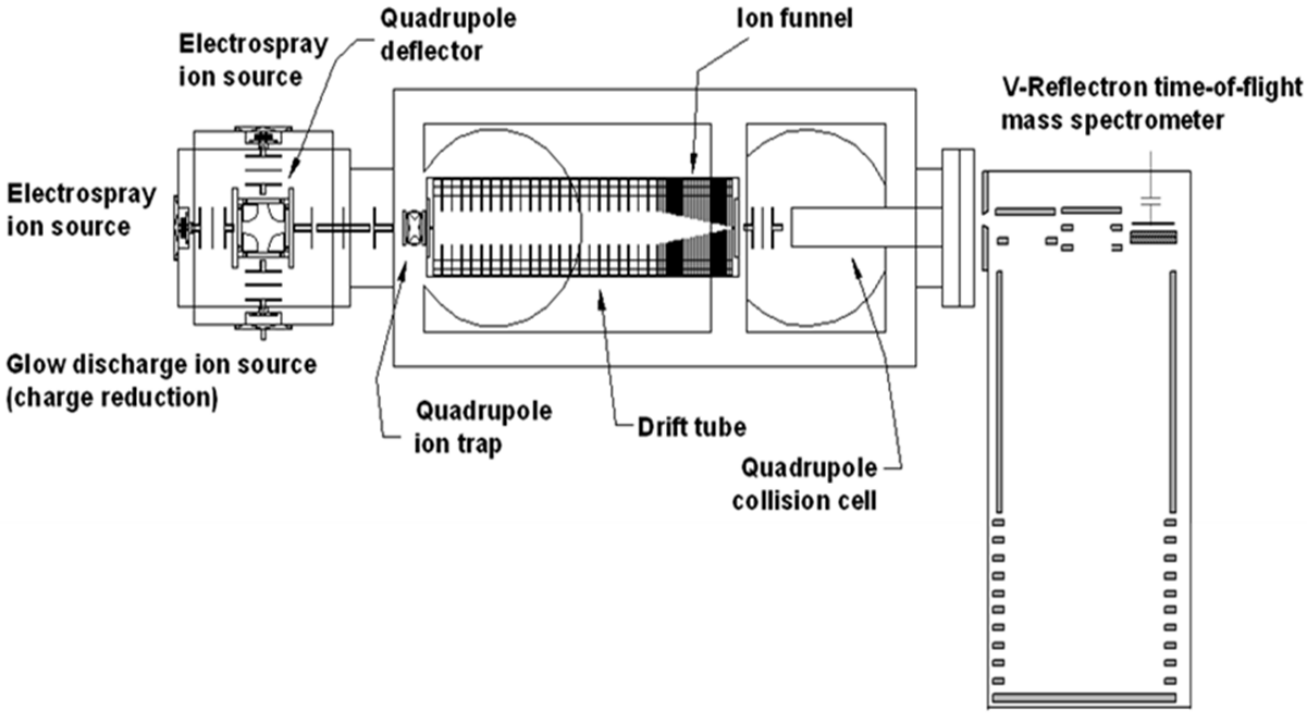


Figure 1) Scale diagram showing overall instrument, including two ESI and one ASGDI sources, ion optics, quadrupole deflector, IT, IM drift tube with ion funnel and q-TOF. The ion source cube is 20 cm wide.

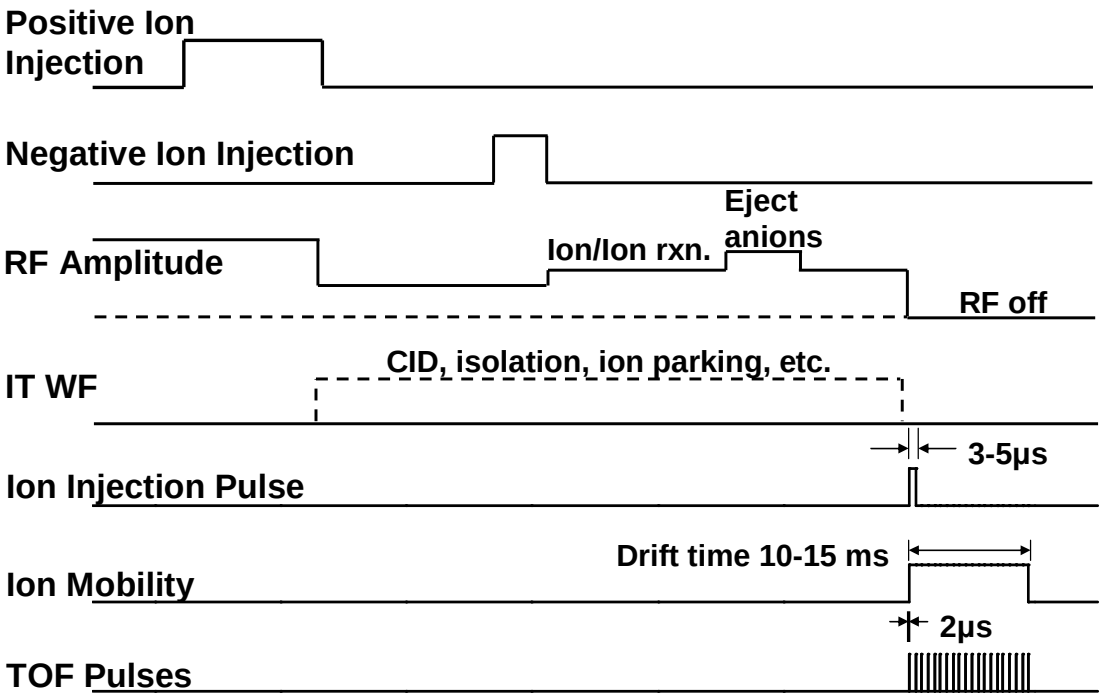


Figure 2) A generic scan function for an ion/ion reaction followed by nested flight time/ion mobility experiment. The top and second plots show the time during which positive and negative ions are injected. The third plot shows the amplitude of the RF trapping voltage applied to the ring electrode of the ion trap. The lower three plots show the times when ions after ion/ion reaction are injected into the drift tube, ion mobility data acquisition and TOF extraction pulses.

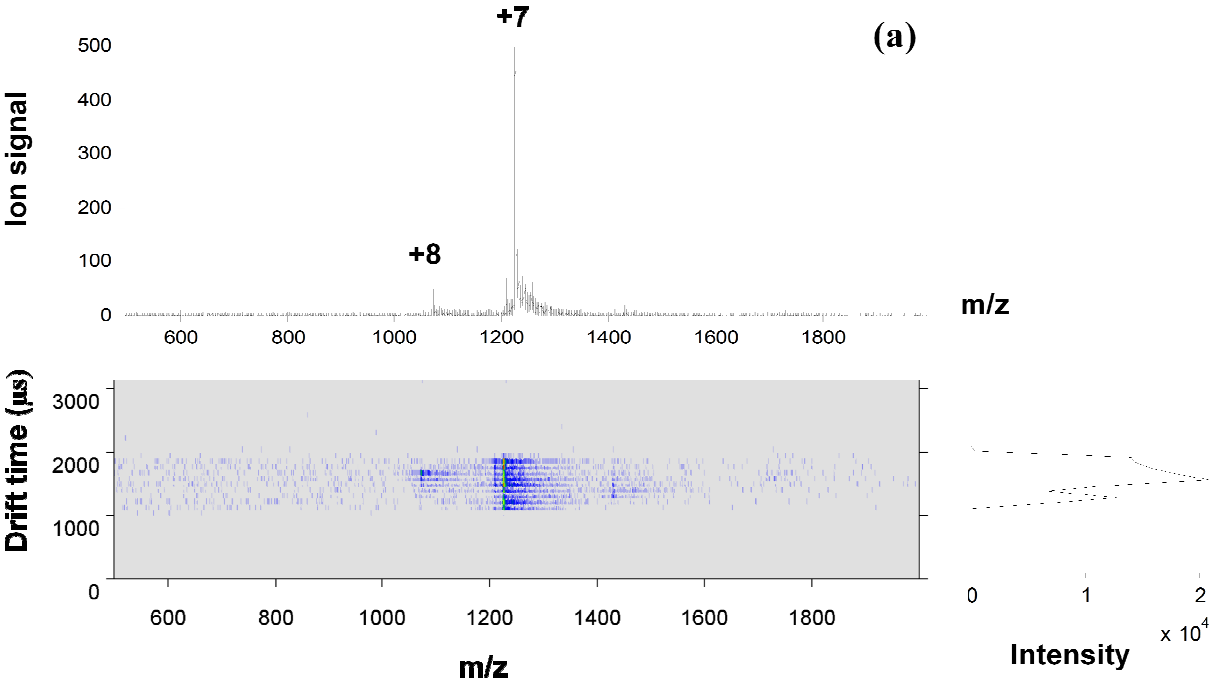
(a)
+7
+8
Ion signal
m/z
Drift time (µs)
m/z
Intensity
x 10^4

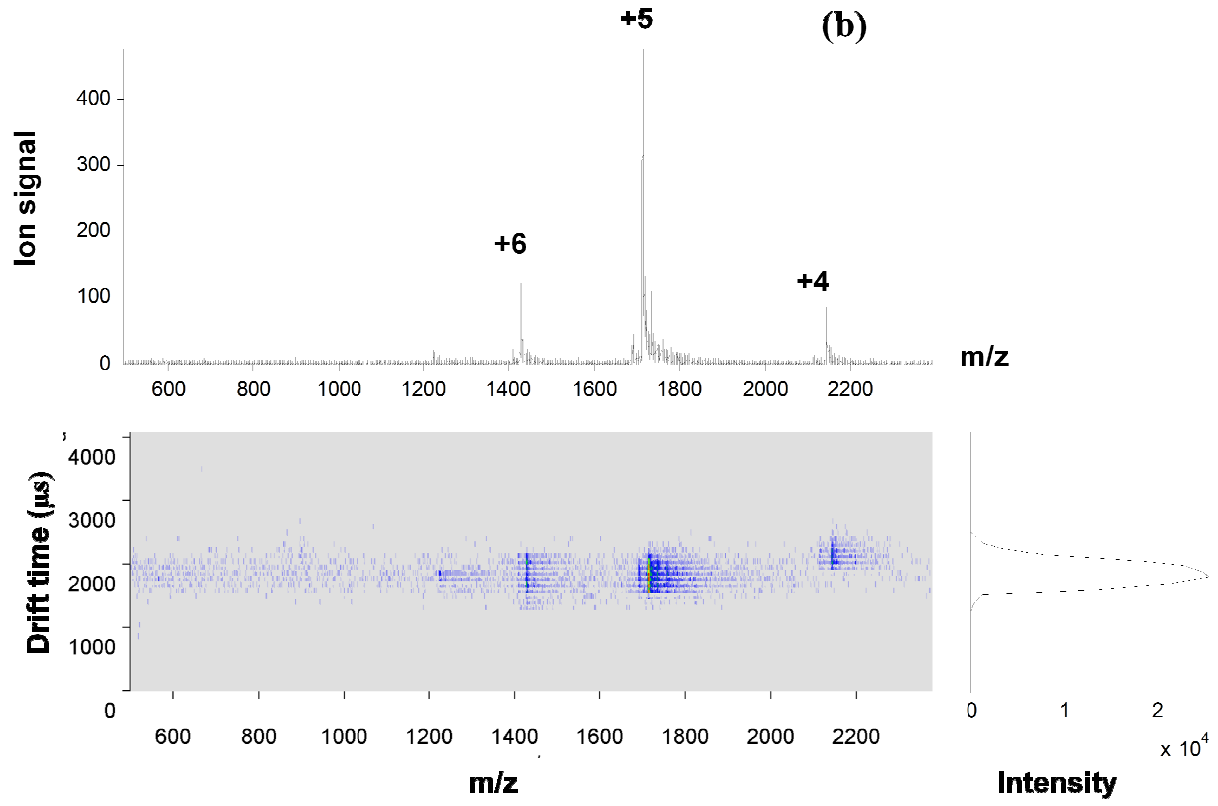
(b)
+5
+6
+4
Ion signal
m/z
Drift time (µs)
m/z
Intensity
x 10^4

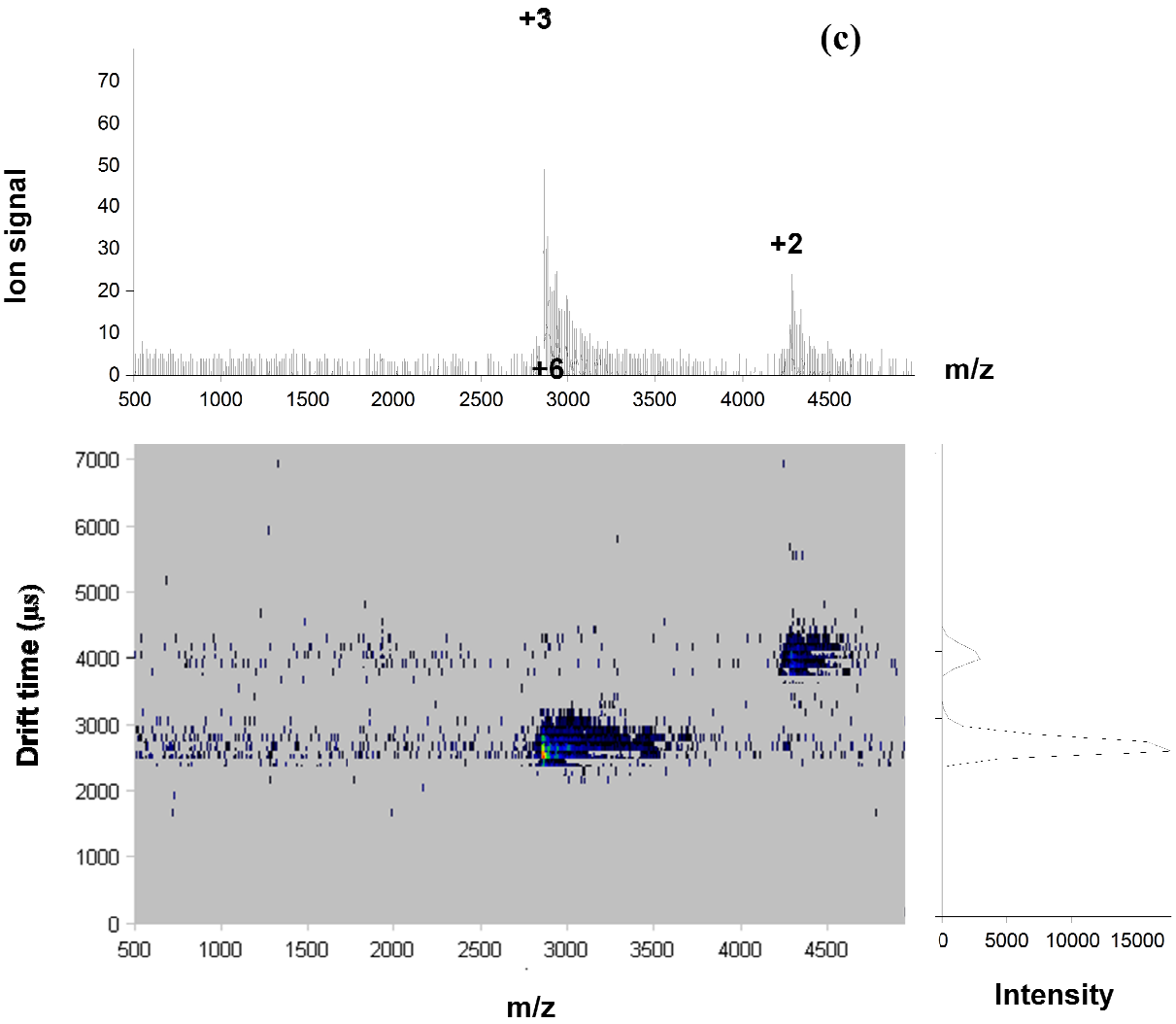
(c)
+3
+2
+6
Ion signal
m/z
Drift time (µs)
m/z
Intensity

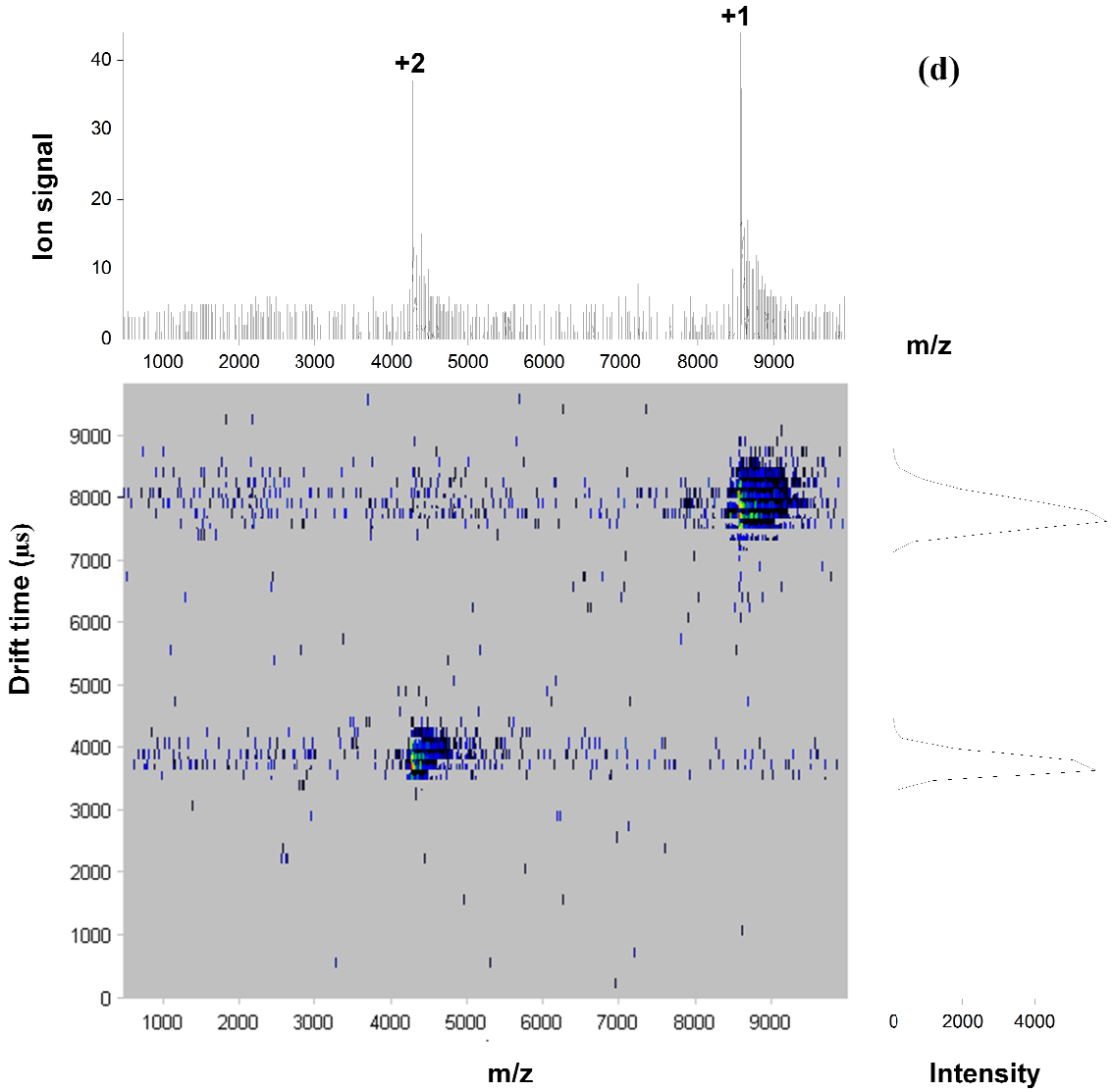


Figure 3a) 3D mobility mass spectrum of ubiquitin; 3D mobility mass spectrum of ubiquitin after reaction with PDCH negative ions: b) PDCH fill time 20 ms, ion/ion reaction time 60 ms; c) PDCH fill time 45 ms, ion/ion reaction time 150 ms; d) PDCH fill time 50 ms, reaction time 180 ms. The ions in lower charge states are more readily resolved by IM. Conditions: 0.30 mg/ml ubiquitin aqueous solution with 1% acetic acid, drift voltage -30 V to -580 V, drift pressure 1.39 mbar, IT fill time for ubiquitin 50 ms, data acquisition time: 10 s for (a), (b), (c), and 20 s for (d).

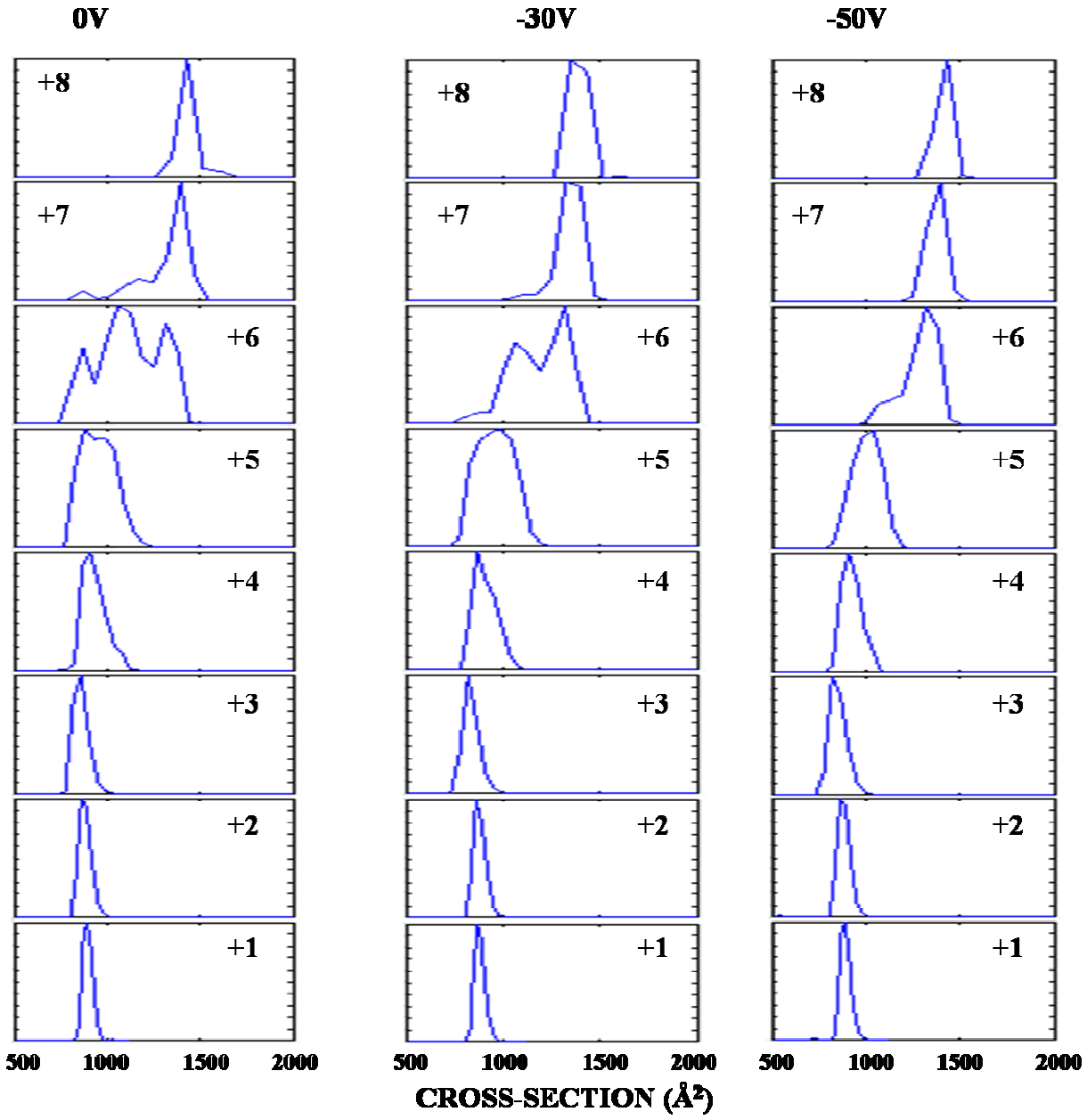


Figure 4) Cross section distributions for ubiquitin ions in various charge states. +8 and +7 ions are made from nano-ESI of 0.30 mg/ml ubiquitin aqueous solution with 1% acetic acid. The other ions are made by ion/ion reaction with PDCH anions under the conditions described in Table 2. Vertical scale values are also given in Table 2. Numerical values for cross section are listed in Table 1. The injection voltages are 0, -30 V, or -50 V, as indicated. The IT ejection pulse is –100 V for 5 μs, and the axial electric field through the drift tube is 12.4 V/cm.

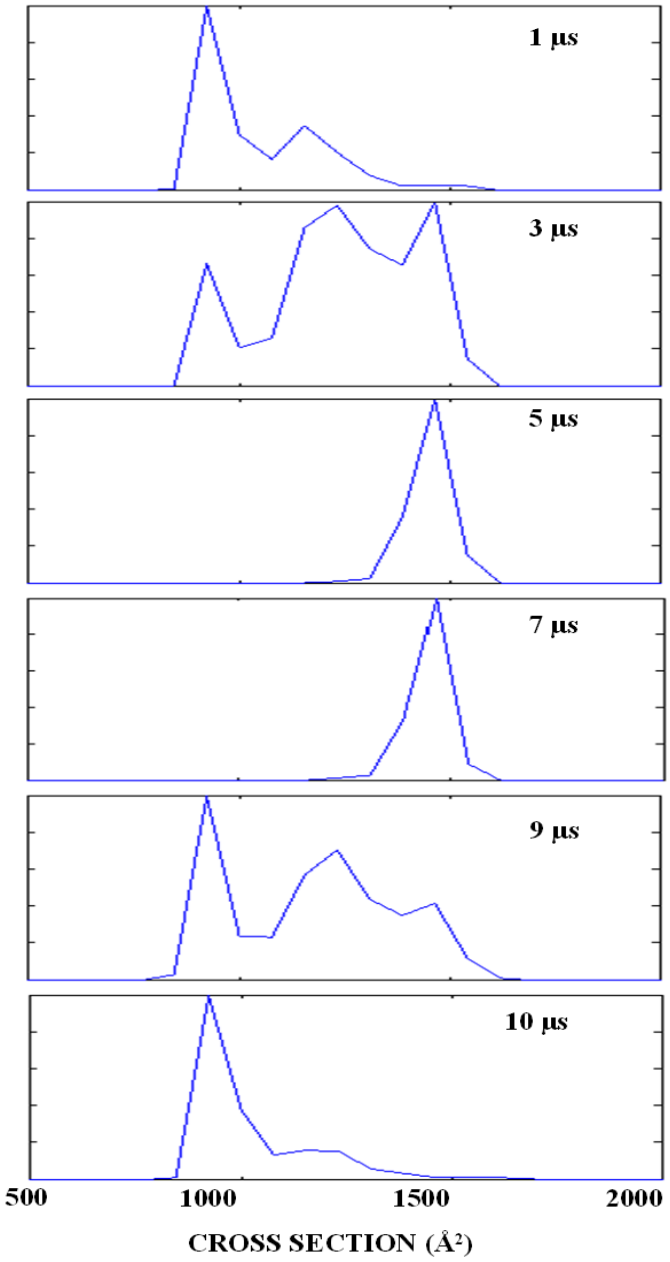


Figure 5) Effect of duration of IT ejection pulse on conformations of ubiquitin +7 ions directly from ESI source, without ion/ion reaction. IT ejection voltage = -100 V, IM injection voltage = -30 V.

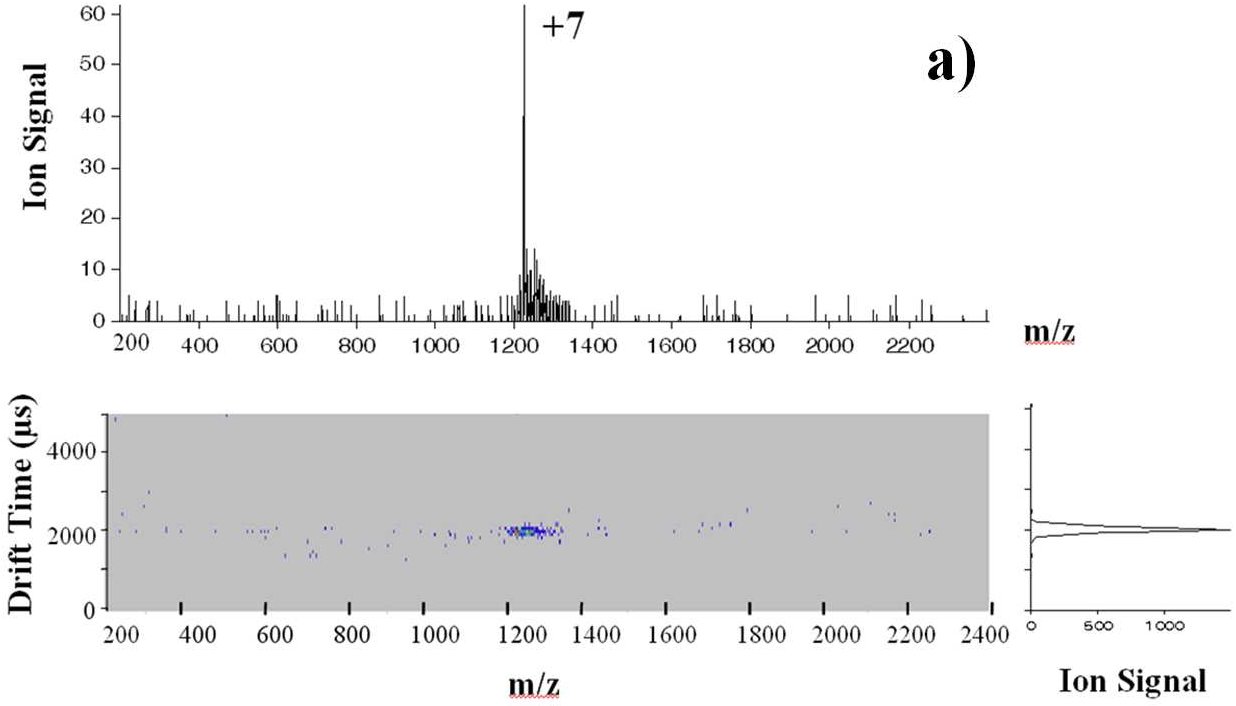
a)
+7
Ion Signal
m/z
Drift Time (µs)
m/z
Ion Signal

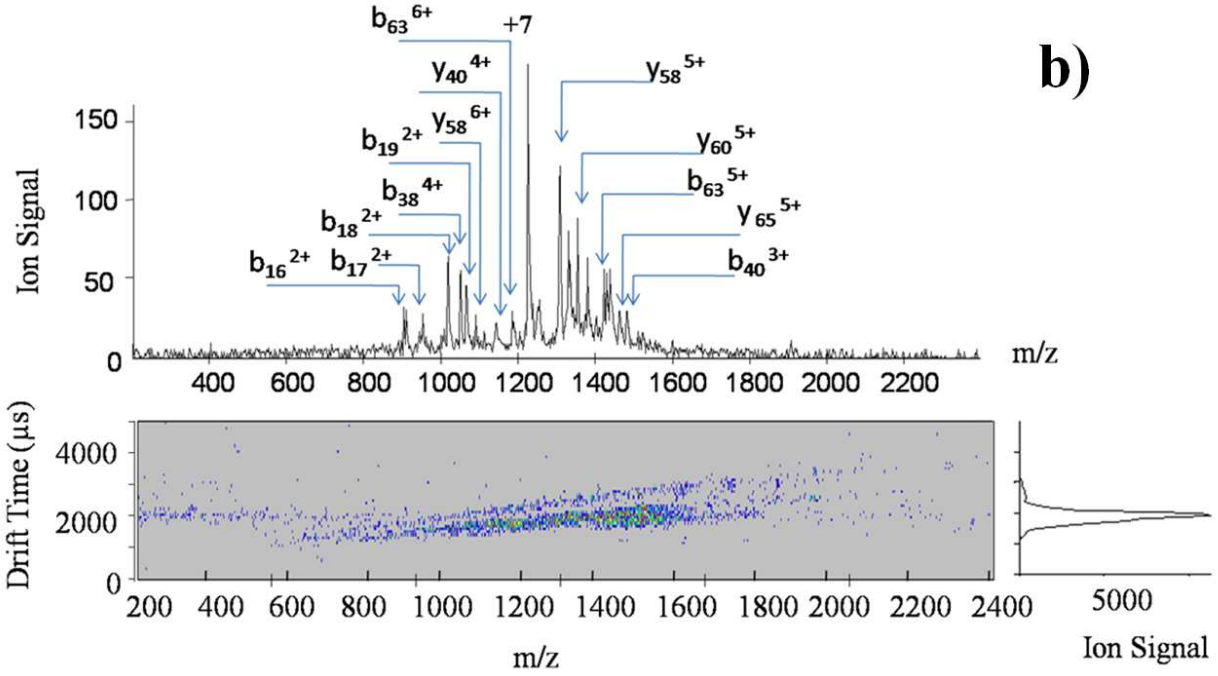
b)
b63 6+
+7
y40 4+
y58 5+
y58 6+
b19 2+
y60 5+
b38 4+
b63 5+
b18 2+
y65 5+
b16 2+
b17 2+
b40 3+
Ion Signal
m/z
Drift Time (µs)
m/z
5000
Ion Signal

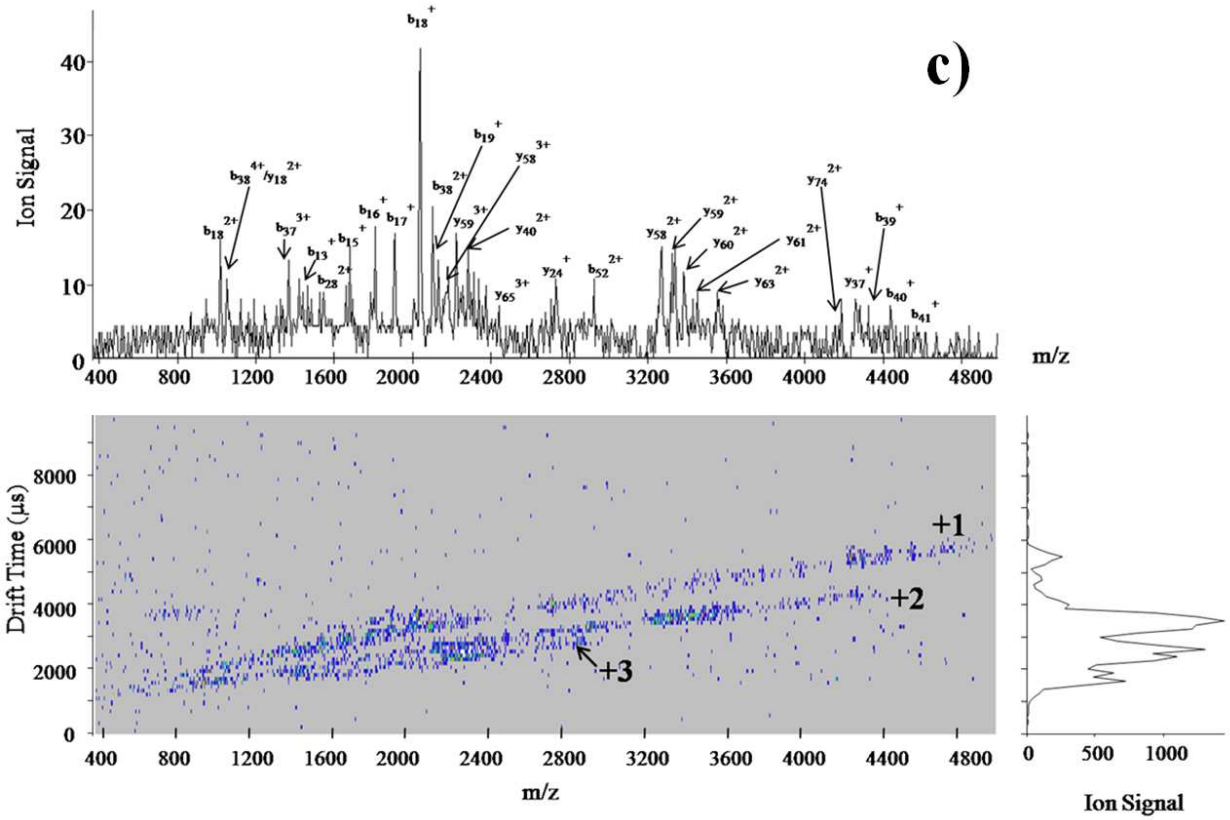


Figure 6) CID results**:** a) 3-D ion mobility spectrum of ubiquitin +7 ions isolated in 3-D IT; b) fragments directly from CID of ubiquitin +7 ions in IT; c) charge reduced CID fragments from ubiquitin +7 ions after reaction with PDCH anions for 100 ms.

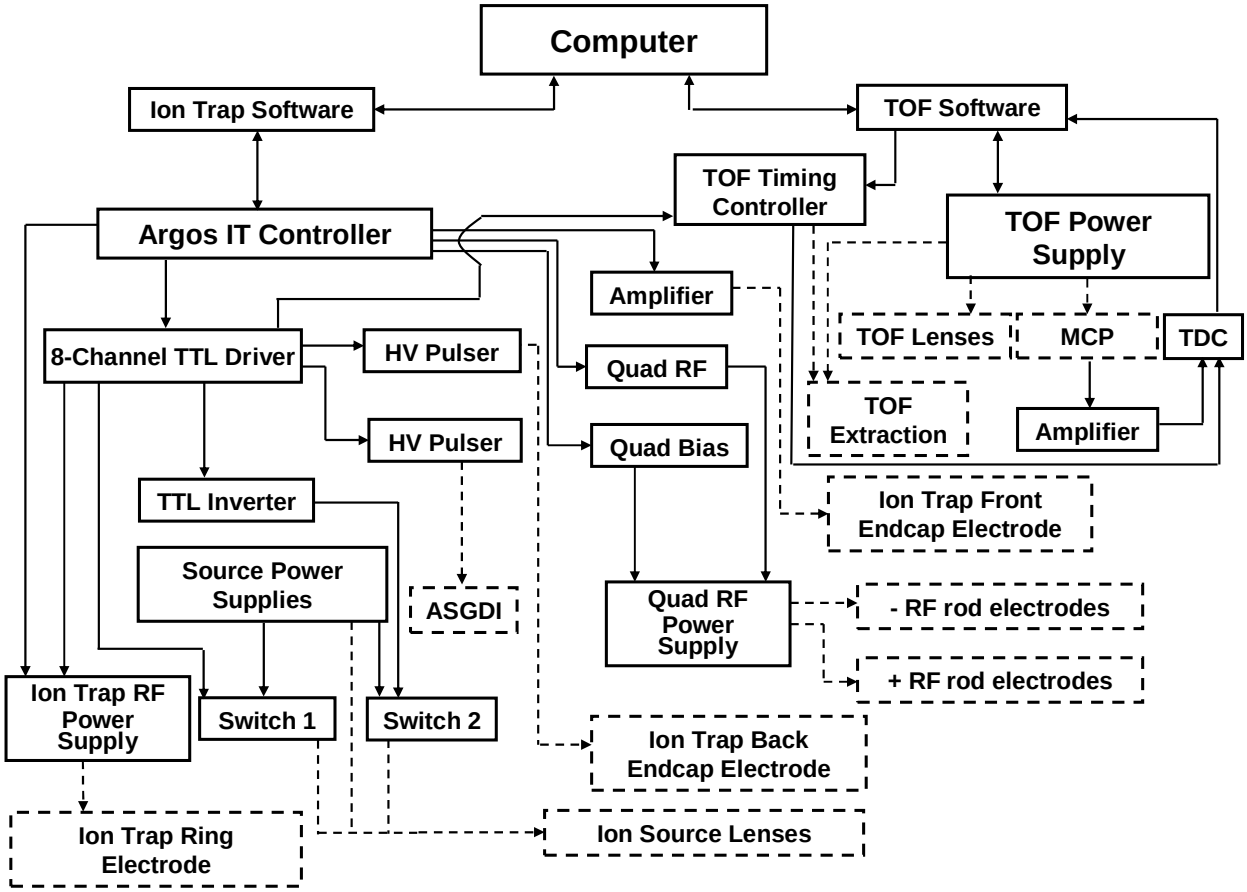


Caption for Supplemental Figure: Electronics block diagram (see text for details). The solid lines indicate instrument control electronics, and the dashed lines indicate hardware in the vacuum chamber.

# APPENDIX II

## EFFECTS OF ION/ION PROTON TRANSFER REACTIONS ON CONFORMATION OF GAS-PHASE CYTOCHROME *C* IONS

Qin Zhao, Gregg M. Schieffer, Matthew W. Soyk,[a] Timothy J. Anderson, R. S. Houk* and Ethan R. Badman[‡]

Department of Chemistry, Iowa State University, Ames, IA, 50011 USA

*Ames Laboratory U. S. Dept. of Energy, Iowa State University, Ames IA 50011 USA

[‡] Author for correspondence

Current Address: Hoffman-La Roche Inc., Non-Clinical Safety,

Nutley, NJ 07110 USA

[a]Current Address: LECO, 3000 Lakeview Ave., St. Joseph MI 49085 USA

A manuscript accepted with revisions by the *Journal of the American Society for Mass Spectrometry*, 2010, *in press*.

**ABSTRACT**

Positive ions from cytochrome *c* are studied in a 3-D ion trap/ion mobility (IM)/quadrupole-time-of-flight (TOF) instrument with three independent ion sources. The IM separation allows measurement of the cross section of the ions. Ion/ion reactions in the 3-D ion trap that remove protons cause the cytochrome c ions to refold gently without other degradation of protein structure, i.e., fragmentation or loss of heme group or metal ion. The conformation(s) of the product ions generated by ion/ion reactions in a given charge state are similar regardless of whether the cytochrome c ions are originally in +8 or +9 charge states. In the lower charge states (+1 to +5) cytochrome *c* ions made by the ion/ion reaction yield a single IM peak with cross section of ~ 1110 to 1180 $Å^2$, even if the original +8 ion started with multiple conformations. The conformation expands slightly when the charge state is reduced from +5 to +1. For product ions in the +6 to +8 charge states, ions created from higher charge states (+9 to +16) by ion/ion reaction produce more compact conformation(s) in somewhat higher abundances, compared to those produced directly by the electrospray ionization (ESI) source. For ions in intermediate charge states that have a variety of resolvable conformers, the voltage used to inject the ions into the drift tube, and the voltage and duration of the pulse that extracts ions from the ion trap, can affect the observed abundances of various conformers.

## INTRODUCTION

The determination of protein conformation is important in many biological applications. Of the various methods for these measurements, mass spectrometry (MS) has certain advantages such as speed and the need for only small amounts of sample. The variations of MS for study of protein conformation include ion mobility (IM) [1-4], H/D exchange [5-9], and native electron capture dissociation (NECD)[10, 11]. Of these methods, IM provides a direct way to examine the gas-phase conformation of the ions by probing the average cross-section of the protein ions via collisions with buffer gas [3, 4]. Early IM research on protein folding and unfolding was done with an IM-quadrupole instrument [1]. To study ions in lower charge states than those made directly from the electrospray ionization (ESI) source, a basic collision gas (e.g., acetophenone or 7-methyl-1, 3, 5-triazabicyclo [4,4,0] dec-5-ene, MTBD) [12] was introduced into the source region. The neutral gas extracted protons from the protein ion and created lower charge state ions through proton transfer reactions in the source. In these studies, the reactions took place only in the atmospheric pressure ion source interface region. Thus, control and variation of the reaction time and extent of reaction were difficult, and only certain reagent species were available.

Gas-phase ion/ion reactions provide another dimension for gas-phase bioanalysis by MS. To date, these reactions have been mainly used to simplify complex MS/MS spectra [13, 14] or generate fragments for structural assignment [15, 16] by methods like electron transfer dissociation (ETD) [17-19].

Recent instrumentation improvements have greatly extended the type of structural information and number of possible experiments available in this area. The development of a 3-D trap-IM-time of flight (TOF) instrument allows time dependent studies of gas-phase protein ions, including folding, unfolding and structural transitions [20-23]. A multi-stage IMS-MS instrument [24, 25] provides two important new functions. First, a protein ion with a specific structure can be selected by IMS, then activated and separated in the next drift region. Second, “state-to-state” structural transitions can be studied by structure selection-activation cycles.

A three-source-ion trap-drift tube-q-TOF instrument was recently developed by our group to combine ion/ion reactions with IM-TOF measurements [26, 27]. The present paper describes how proton transfer ion/ion reactions can be used to manipulate charge state and study the effect of ion/ion reactions on the conformations of cytochrome *c* ions. This protein is chosen so the present results can be compared to those from extensive previous studies [10, 22, 23, 28-36].

## EXPERIMENTAL

The design and general operating conditions for the home-built three source instrument are described in another paper [26]. Bovine heart cytochrome *c* (Sigma-Aldrich, St. Louis, MO) was used without further purification in all experiments. Usually this protein was dissolved at 20 to 30 µM in water with 1% aqueous acetic acid. Water alone was used as solvent with 15 µM protein for one set of results; this lower protein concentration suppressed cytochrome c dimer ions, which were otherwise abundant from unbuffered water solutions. Another study used 50% methanol/water with 1% acetic acid. These samples were introduced through one nano-ESI source in positive mode.

Positive cytochrome *c* ions were stored in the trap first, then negative ions were added by switching the voltages on the ion optics. Negative ions from perfluoro-1,3-dimethylcyclohexane (PDCH, $C_8F_{16}$, Sigma-Aldrich, St. Louis MO) were used as the proton transfer reagent. Negative PDCH ions were created by atmospheric sampling glow discharge ionization (ASGDI) in a second source [37, 38]. These PDCH negative ions were roughly 60% $[M\text{-}F]^-$ (i.e., $C_8F_{15}^-$) and the rest $[M\text{-}CF_3]^-$ [38, 39].

Both positive cytochrome c ions and negative PDCH ions were trapped together in the 3-D trap and allowed to react for times between 50 ms to 200 ms, with the reaction time selected to optimize the yield of product ion in the desired charge states. Thus, the cytochrome *c* ions spent ~ 100 to 300 ms in the trap. In this time regime, the mobility spectra and relative abundances of various cytochrome c conformers were not strongly dependent on trapping time, as seen by Badman et al. [22, 23] and verified by us [27]. These

time-dependent folding-unfolding effects were seen mainly for 9+ ions; most of the present work deals with lower charge states.

The product ions were then injected into the drift tube for IM separation, followed by m/z analysis and detection by TOF-MS. The drift tube was 44.45 cm long and contained helium at 1.3 to 2 mbar. The default operating conditions for ion mobility measurement were as follows. The ion trap ejection pulse was zero to -100 V for 3 µs, and the injection voltage on the drift tube entrance was -150 V. These conditions provided the best signal and minimized variation of IM spectra with duration of the injection pulse [26]. The injection voltage was varied for Figure 1, and -50 V was used for Figure 6, for reasons discussed below.

The axial electric field in the drift tube was 12 to 13 V/cm. Cross sections were calculated from the mass resolved mobility spectra as described previously [3, 26]. In particular, the drift time is calculated by measuring the total time between the ion trap exit pulse and the observation of ions at the TOF detector. The flight time between the exit of the drift tube and the TOF source region is calculated from the instrument dimensions, applied voltages and m/z ratio and subtracted from the total time to give the actual time spent in the drift tube [26].

The number of measured points in the mobility spectra are determined by the time for the slowest ion to reach the TOF detector, which can be as long as 100 µs for ions in low charge states. This limits the ability to resolve fine structure in the mobility spectra. The actual number of points in the mobility spectra are plotted in representative examples shown below. For charge states that yield single mobility peaks, cross section values are reproducible to approximately 50 $Å^2$ from day to day; this uncertainty value is also affected by the number of points across the mobility peaks.

## RESULTS AND DISCUSSION

**Effect of Injection Voltage and Ion Trap Ejection Conditions on Conformations of Cytochrome c +8 Ions.** In this device, there is a plume of gas leaving the drift tube (~1 mbar) and moving toward the exit of the ion trap. Ions from the trap pass through this plume as they enter the drift tube. Clemmer's group [12] found that collisions with helium in this plume can heat and unfold protein ions, especially for proteins in intermediate charge states that have various conformations available. Their results mainly deal with the effect of the injection energy as controlled by the charge state and the voltage on the entrance to the drift tube. The effects observed are generally attributed to heating and unfolding in the initial collisions. The resulting mobility spectra can then be affected by cooling induced by subsequent collisions later in the drift tube.

Clemmer's group mainly reports results at moderate to high injection energy, i.e., lab energy of 385 eV or 64 V for ubiquitin +6 to 38 V for ubiquitin +10 ions [12]. Our initial paper [26] reports similar effects for ubiquitin, including results at injection energies as low as 0 eV, i.e., both ion trap and drift tube entrance at ground. As shown in Figure 1, at extremely low injection voltage, the cytochrome c 8+ ions are all in compact conformation(s), i.e., relatively low cross sections. As the injection voltage increases to -30 V (240 eV lab energy), some of the compact conformers start to unfold. As injection voltage increases above -40 V (320 eV) to -70 V (560 eV), the ions progress through partially folded to elongated structures, as described in the literature [22]. Roughly 30% of the 8+ ions do not unfold completely even at the highest injection voltage used, -150 V, for a lab kinetic energy of 1200 eV. This is the value used for most of the results presented below.

In our previous work [26], conformation changes in ubiquitin 7+ are described as the ejection pulse duration changes. Similar effects are observed with cytochrome c 8+ and 7+. As with injection energy effects, these conformation changes are most extensive for those ions in intermediate charge states with various accessible conformations. If ions in these "intermediate" charge states are close to, but not inside, the entrance to the drift tube when the ion trap ejection pulse goes to zero, the ions can unfold. Such changes are also most extensive if the ion trap exit voltage is more negative than the drift tube entrance voltage. Ions in low or high charge states show less extensive folding changes with ejection pulse

duration. Experimentally, longer ejection pulses improve the abundance of ions in low charge states, which is how the effect of ejection pulse duration was first found. The precise causes of this effect are being further studied.

For the results presented above, experimental conditions were used that minimize variations in conformation with injection pulse duration. In particular, changes in folding and conformation that depend on ejection pulse duration are minimal if the drift tube entrance voltage (usually -150 V) is kept more negative than the ion trap ejection pulse (-100 V).

**Effect of Charge Reduction Reaction on the Conformation of Cytochrome *c* Ions.** In 1% acetic acid/water solution, ESI produces cytochrome *c* ions in two main charge states, 8+ and 9+ (Figure 2) [1]. Although their IM drift times overlap, resolved mobility peaks for the +8 and +9 ions can be extracted by selecting the desired m/z window in the 3D mass-mobility spectrum. Note that the 8+ ion has two resolvable mobility peaks, which are generally attributed to different gas-phase conformations. The cross sections for these two peaks are ~ 1710 and 1900 $Å^2$ (Table 1); this difference represents the minimum resolvable difference in cross section seen so far with this particular device.

In the mass spectrum the main peaks from cytochrome *c* are accompanied by less abundant satellite peaks at higher m/z values. These latter peaks were originally thought to be adduct ions made inside the device, perhaps by addition of diffusion pump oil molecules to the protein ions while they traverse the drift tube [40]. However, these satellite peaks are also observed when the same solutions are analyzed with other mass spectrometers that do not have diffusion pumps, so they are attributed mainly to impurities in the cytochrome *c* samples [41].

To study how ion/ion reactions affect the conformation of protein ions, either +8 or +9 ions are isolated in the 3-D ion trap first. The cross section plots are similar to those obtained when both +8 and +9 ions are stored and ejected into the drift tube together without m/z isolation inside the ion trap (data not shown) [42]. If the storage time in the trap is

increased to at least 200 ms, the mobility spectrum remains the same, so the ions do not heat and unfold appreciably in the trap (data not shown) [42].

PDCH negative ions are then injected into the ion trap from the ASGDI source and react with cytochrome c ions to remove protons for the desired time. A typical spectrum after ion/ion reaction is shown in Figure 3. The resulting cross sections (Table 1) agree well with those reported in the literature [23]. The proton transfer reactions leave the protein ions in a range of charge states, which can be as low as 1+ [26]. As expected, these reactions do not displace the covalently-bound heme group; proton transfer is gentle enough that the noncovalently-bound heme group in myoglobin remains after multiple proton transfer reactions [43, 44].

Cross-section values for cytochrome *c* ions in each charge state, produced by reaction of isolated 8+ or 9+ ions with PDCH negative ions in the trap, are summarized in Table 1. The distributions of cross section observed for each charge state are indicated in Figure 4. These distribution plots indicate the relative abundances of the various conformers of cytochrome *c* ions in the various charge states.

In general, the distributions of conformations for ions in a given charge state are similar whether the reactions started with either 8+ or 9+ ions. The wider mobility peaks seen for 7+ and 6+ ions after ion/ion reaction suggest that there may be several additional conformations that are not fully resolved. The ions in lower charge states (5+ to 1+) have only one mobility peak, even when the reactant ion was the 8+ form with two mobility peaks originally.

Comparison of our cross section values with literature values (Table 1) can be summarized as follows:

a) Our value for cytochrome c 9+ (1975 $Å^2$) is close to the lowest literature value (1964 $Å^2$) ; we did not observe a conformer with cross section 2215 $Å^2$ for cytochrome c 9+.

b) For charge states 5+ and lower, our values are similar to but a bit smaller than those from the literature;

c) For charge states 6+ to 8+, we see fewer resolvable conformers, mainly because of our limited mobility resolution, see Experimental section. For 8+ and 7+, we do not see the more folded conformers with cross sections ~ 1250 $Å^2$.

The literature values noted in Table 1 from the work of Shelimov et al. [45] were measured for ions in lower and intermediate charge states that were made by proton transfer reaction with neutral gas during ion extraction. The other literature values listed from Badman et al. [23] were measured with an earlier IMS-TOF-MS device similar to that used in the present work. More work is needed to determine if the observed differences are just instrumental effects or represent real differences in conformation(s) of ions depending on their origin.

It is tempting to assert that observation of just one mobility peak means the ions have only one conformation. The narrowest mobility peak seen for the 9+ ion of cytochrome *c* has a full width at half maximum (fwhm) of ~180 µs (Figure 2). Calculations indicate the contribution to the fwhm of this peak from diffusion to be only ~ 16 µs, much less than the peak width observed [46]. Under these experimental conditions, $Cs_7I_6^+$ ions or protonated reserpine ions (from ESI of CsI or reserpine in water) yield single mobility peaks ~80 µs fwhm, roughly half the width of the narrowest protein peaks. Thus, the "single" mobility peaks seen for cytochrome *c* probably correspond to the juxtaposition of unresolved peaks from ions in several conformations of similar size, as shown by Clemmer et al. for ubiquitin [24]. For brevity, we use phrases like "one conformation" or "a single conformation" in the discussion below, with this caveat in mind.

These results show that the protein ions can fold to one or more compact conformations during the charge reduction reaction. This observation is explained as follows. When the protein ions pass into the vacuum system, the solvent molecules evaporate, counter ions are also lost, and the attraction between hydrophobic portions of the molecules diminishes. Thus, the highly charged protein ion opens rapidly to "partially unfolded" or "unfolded" conformations [11, 12, 23, 31, 32]. The ion/ion reaction in the ion trap then removes protons, whose charges keep the protein unfolded. Intramolecular charge repulsion becomes weaker as protons are removed, so the protein ions fold to more compact conformations, at least until very low charge states are achieved, as discussed below.

For cytochrome *c* ions in the gas phase, ions with cross-sections ~ 1050 $Å^2$ to 1350 $Å^2$ are generally assigned to "most compact" conformation(s) [2, 23]. Thus, Figure 4 shows that the proton transfer reactions in the 3-D ion trap allow the original "unfolded" protein to

pass gradually through several partially folded conformations and eventually assume compact conformations.

Close examination of Table 1 and the mobility plots in Figure 4 shows that the 5+ ion has the smallest cross section, and cross sections for those ions in the "most compact" conformation increase slightly as charge state is reduced from 5+ to 1+. Apparently, as more protons are removed from the 5+ ion, the cytochrome c molecule expands by a small but measurable amount. This effect is also observed for ubiquitin in low charge states [26], but the size increase is not as extensive as for cytochrome *c*.

Possible reasons for this observed expansion at very low charge state are as follows. In low charge states, stabilization from ionic hydrogen bonds helps keep the protein ion folded. As the last few $H^+$ ions are removed, this stabilization is lost, and the protein ion expands somewhat [10, 11, 47]. A similar explanation is as follows. Starting with ions in high charge states, suppose the proton transfer reaction initially removes protons with the lowest gas-phase basicity, such as protons on lysine residues that are not shielded by other residues of the protein structure. After the ion has been converted to a low charge state, further reactions remove protons from the most basic residues (e.g., arginines) that are partially stabilized by non-covalent interactions with other residues. Thus, when these last protons are removed, some weak interactions on the protein surface are lost, the structure is then more flexible and less compact.

**Conformation of Ions Made by Ion/Ion Reaction Compared to Those Produced Directly by ESI.** To generate ions in lower original charge states, cytochrome *c* is sprayed from either of two solvents: a) water without acetic acid or buffer, or b) water buffered with ammonium acetate (2 mM, pH ~ 7). These cytochrome *c* ions are then measured without ion/ion reaction, and the results are compared to those obtained by charge reduction reactions of more highly charged ions from water/acetic acid solutions.

Figure 5 compares cross section distributions for ions in various charge states, prepared either by ion/ion reaction or by ESI directly. First, consider the results for the 7+ and 6+ charge states. For 7+ ions made by ion/ion reaction, two broad mobility peaks are seen with about the same average cross section and relative abundances, regardless of

whether the ions started as 9+ or 8+. For the 7+ ions made directly by ESI, two mobility peaks are also seen, but the cross sections are different; the ions from water are more elongated, the ions from ammonium acetate buffer are more compact, compared to the 7+ ions made by ion/ion reaction. A similar trend is seen for the 6+ ions; here the elongated conformers are more abundant when the 6+ ions are made by ion/ion reaction than directly by ESI.

For cytochrome *c* 5+, the ions made by ion/ion reaction have a single mobility peak at lower cross section than the ions from water directly but a little higher cross section than the 5+ ions from ammonium acetate buffer. This single mobility peak gets narrower for the 4+ ions and approaches values ~ 900 $Å^2$ for the ions from ammonium acetate, a value generally considered to be typical of compact forms. For the 5+ and 4+ ions made from water, the cross section of the main mobility peak is larger, ~ 1100 $Å^2$.

There is also some interesting information from low-abundance mobility peaks. For the 4+ ions made directly by ESI, from either water or ammonium acetate, small but measurable amounts of conformers at even smaller cross section are observed, in broad agreement with some previous measurements on cytochrome *c*, e. g., Figure 6 of reference [45] The 5+ ions from water also have a small but measurable amount of larger conformer(s) at ~1400 $Å^2$; these conformer(s) are not seen when the 5+ ions are made either by ion/ion reaction of from ammonium acetate.

Thus, the mobility spectra can differ depending on the origin of the ions, particularly for intermediate charge states like those studied here that have various accessible conformers. This observation is relevant to several important issues. How much of the original solution structure is retained in the gas-phase ions observed in these and other ESI experiments? [10, 11, 47] If ions made by ESI in moderate or high charge states are trapped and reacted down to lower charge states, do they go back into conformations like those in the original solution? The apparatus and methodology described here could be used to help address these matters.

**"Stepwise" Proton Transfer Reactions.** For the ion/ion reactions described above, a single instrument step is used, and the fill and reaction times are varied to produce ions in particular charge states. For example, a reaction time of ~50 ms converts the 8+ ions mainly to 6+ and 5+, while making 2+ and 1+ ions requires reaction for ~100 ms.

These reactions can also be done in successive instrumental steps. The reaction can be stopped at a desired pair of charge states and then continued as desired. For example, positive ions in the 8+ and 9+ charge states are stored in the ion trap, and much smaller amounts of negative PDCH ions are injected, i. e., PDCH ions are added for fill times of only ~10 ms. The ion/ion reaction is allowed to proceed for ~60 ms; cytochrome c 7+ and 8+ ions result. Another 10 ms batch of PDCH ions are added, the reaction is continued for another 50 ms, and the cytochrome *c* ions 7+ and 8+ ions are converted to 6+ and 7+.

These sequential reactions can be continued to make ions in any pair of adjacent charge states down to 3+ and 2+.[38] For each instrumental step, careful control of the reaction time and reagent amount in the trap results in removal of only one charge. This method is an alternative to ion parking [48] to enhance the yield of ions in a particular charge state. The advantage is that it can avoid the collisional heating that could accompany the excitation step in ion parking, which may induce conformation changes in the protein ions. The mobility spectra of these ions made by this "stepwise" scheme are similar to those obtained from ions made "all at once". [39]

**Effect of Methanol on Charge State and Conformation of Ions Made by Ion/Ion Reaction.** Even if the ions generated by ESI are solvent-free, they may still retain some aspects of their conformation(s) in the original solution. For example, Breuker and co-workers [31, 32] report simulations that indicate that cytochrome *c* unfolds partially soon after the solvent is removed, but that the gas-phase ions still have some of the structural components of the original folded protein. The final charge states of the ions, and presumably their eventual gas-phase conformations, can be manipulated to some extent by changing solvent conditions. For ubiquitin from water with 1% acetic acid, the more compact conformations observed are more abundant than for ubiquitin ions formed from 50/50 water/methanol solution with 1% acetic acid [49].

To study the effect of initial solution conditions on the folding process induced by ion/ion reaction, cytochrome *c* in 50/50 water/methanol solution with 1% acetic acid is sprayed. This solvent produces ions in higher initial charge states (16+ to 9+), as expected (Figure 6a) [39]. These highly charged ions yield single mobility peaks, again as expected if electrostatic repulsion keeps the ions unfolded. Ion/ion reaction with PDCH negative ions

for various times converts these ions to charge states 8+ to 2+, with cross section distributions shown in Figure 6b. The same trend as in Figure 4 is found; the cytochrome *c* ions fold to more compact conformations as charges are removed.

For these results, a lower injection voltage (-50 V) was used on the entrance to the drift tube to prevent fragmentation of the cytochrome c ions in high charge states. Therefore, cross section plots for the 9+ to 2+ charge states obtained at -50 V from $H_2O$/acetic acid are also shown (Figure 6c). Comparison of Figures 6b and 6c shows that, as charge state is reduced, the ions generally fold to similar conformations even when they start in very high charge states. For example, the 4+ ions in Figure 6b began as 9+ to 16+ but have a similar distribution of cross section as the 4+ ions in Figure 6c, which began as 8+ and 9+. Open conformers are moderately more abundant for the 7+, 8+ and 9+ ions made from the more highly charged reactants (compare Figures 6b and 6c). Also, the cross section distribution plots obtained for 8+, 9+ ions and their products at an injection voltage of -50 V (Figure 6c) are not greatly different from those obtained at -150 V (Figure 4).

**Folding Transitions of Cytochrome *c* Ions Induced by Gas-Phase Ion/Ion Reaction.** From all the results discussed above, some general conclusions are:

a) reduction of the charge state via ion/ion reaction can induce folding of the ions, b) changes in folding of the elongated ions follow a similar pathway as that of the ions with partially folded structures,

c) ions in low charge states made by ion/ion reactions fold to similar conformations independent of their initial charge state,

d) for product ions in intermediate charge states (5+ to 8+), the distribution of conformers observed after ion/ion reaction depends somewhat on the charge state of the reactant cytochrome c ions.

e) the ions expand slightly as charge state is reduced from 5+ to 1+, and

f) some partially unfolded conformers survive even when the ions are injected into the drift tube with high kinetic energies.

Starting with ions in high charge states that are unfolded in the trap, then reducing charge state via ion/ion reaction, is one way to induce and study folding changes in the ions.

The observation that folding in the gas phase yields conformers of similar abundance and cross section regardless of the initial conformation and charge state of the ions indicates these various ions fold via similar pathways. Dill [50] describes protein folding mechanisms pictorially by "folding funnels" of several possible shapes; different conformers funnel into the native state finally. Our observations fit his "rugged energy landscape" model [50], which is a bumpy funnel with kinetic traps, energy barriers, and some narrow pathways through to the native state. Our research [26] and also that from Clemmer's lab [12] shows that the observed abundances of some conformers can be changed easily by increasing the injection energy, but some conformations remain very stable despite this heating process. The stable conformations represent the valleys in the bumpy folding funnel.

Our observations are also consistent with other depictions of protein folding, i.e., Englander's mechanism of folding through predetermined pathways with optional folding errors [34]. Specifically, Englander [51] finds a "misfolded" intermediate state in H/D exchange studies of cytochrome c that could be analogous to a "bump" in the funnel in the viewpoint described by Dill [50].

## CONCLUSION

Gas-phase ion-ion reactions combined with IM measurements provide a new way to study conformation changes in protein ions. Exothermic processes like these multiple proton transfer reactions might be expected to simply heat the ions and unfold them [52]. However the collisions with the bath gas in the 3-D trap cool the ions, [53] so folded protein ions stay folded after proton transfer reaction. Thus, ion/ion reactions can be performed while the ions remain in, or perhaps re-fold into, biologically-interesting conformations.

The ion conformations formed via charge reduction reactions at relatively low pressure inside the ion trap could also be compared to those formed from ion/molecule reactions with neutral base gases in the ESI ion source, using reactions described by Zenobi [54, 55]. This experiment could probe the time frame over which ions liberated by ESI assume their final conformations, which is important to the key issue of whether the conformations of the ions produced by ESI resemble those in the solution [10, 31, 32, 47].

In addition to the charge reduction reactions described here, this three source-ion trap-IM-TOFMS should facilitate other ion/ion reaction studies pertinent to bioanalysis. The identity and amount of reagent ion and the reaction time can be controlled over wide ranges. Other reactions such as ETD [17, 18], metal addition [56] , and some sequential reactions (e.g., ETD followed by charge reduction to simplify assignment of the ETD fragments) should be possible.

The time progression of kinetic processes that change either the m/z value or the conformation of the ions should be measurable, at least for processes that occur on time scales long compared to the duration of the measurement (~ 1 s). The possibility of deliberately inducing unfolding and measuring its time duration with resolution of a few μs [26] is intriguing. It should also be possible to induce folding processes with some time resolution by starting with unfolded ions in a high charge state and reducing the charge, then terminating the ion/ion reaction quickly, with subsequent measurement of conformation by IMS. These and other studies are underway in our laboratory.

## ACKNOLEDGEMENTS

This work was funded by a grant from the Vice Provost for Research, Iowa State University. QZ and MS acknowledge the Conoco-Phillips Fellowship (Iowa State University, 2006-2007 and 2007-2008) for financial support. MS also acknowledges the GAANN Fellowship (Iowa State University, 2008) and the Velmer A. and Mary K. Fassel Fellowship (Iowa State University, 2006-2007). We thank Kathrin Breuker for suggesting one mechanism to explain the observed expansion of the ions at very low charge states. We also thank the three reviewers for helpful comments.

**REFERENCES**

1. Hoaglund, C. S.; Valentine, S. J.; Sporleder, C. R.; Reilly, J. P.; Clemmer, D. E. Three-Dimensional Ion Mobility TOFMS Analysis of Electrosprayed Biomolecules. *Anal. Chem.* **1998,** *70,* 2236-2242.

2. Clemmer, D. E.; Hudgins, R. R.; Jarrold, M. F. Naked Protein Conformations - Cytochrome *c* in the Gas-Phase. *J. Am. Chem. Soc.* **1995,** *117,* 10141-10142.

3. Clemmer, D. E.; Jarrold, M. F. Ion Mobility Measurements and Their Applications to Clusters and Biomolecules. *J. Mass Spectrom.* **1997,** *32,* 577-592.

4. Bohrer, B. C.; Merenbloom, S. I.; Koeniger, S. L.; Hilderbrand, A. E.; Clemmer, D. E. Biomolecule Analysis by Ion Mobility Spectrometry. *Annu. Rev. Anal. Chem.* **2008,** *Vol. 1,* 293-327.

5. Robinson, E. W.; Williams, E. R. Multidimensional Separations of Ubiquitin Conformers in the Gas Phase: Relating Ion Cross Sections to H/D Exchange Measurements. *J. Am. Soc. Mass Spectrom.* **2005,** *16,* 1427-1437.

6. Wood, T. D.; Chorush, R. A.; Wampler, F. M.; Little, D. P.; O'Connor, P. B.; McLafferty, F. W. Gas-Phase Folding and Unfolding of Cytochrome *c* Cations. *Proc. Natl. Acad. Sci. U.S.A.* **1995,** *92,* 2451-2454.

7. Freitas, M. A.; Hendrickson, C. L.; Emmett, M. R.; Marshall, A. G. Gas-Phase Bovine Ubiquitin Cation Conformations Resolved by Gas-Phase Hydrogen/Deuterium Exchange Rate and Extent. *Int. J. Mass Spectrom.* **1999,** *187,* 565-575.

8. Cassady, C. J.; Carr, S. R. Elucidation of Isomeric Structures for Ubiquitin [M+12H] (12+) Ions Produced by Electrospray Ionization Mass Spectrometry. *J. Mass Spectrom.* **1996,** *31,* 247-254.

9. Freitas, M. A.; Hendrickson, C. L.; Marshall, A. G. Correlation between Solution and Gas-Phase Protein Conformation: H/D Exchange, IRMPD, and ESI FT-ICR MS. *Proc. SPIE-Int. Soc. Opt. Eng.* **2000,** *3926,* 61-68.

10. Breuker, K.; McLafferty, F. W. The Thermal Unfolding of Native Cytochrome *c* in the Transition from Solution to Gas Phase Probed by Native Electron Capture Dissociation. *Angew. Chem. Int. Edit.* **2005,** *44,* 4911-4914.

11. Breuker, K.; McLafferty, F. W. Native Electron Capture Dissociation for the Structural Characterization of Noncovalent Interactions in Native Cytochrome *c*. *Angew. Chem. Int. Edit.* **2003,** *42,* 4900-4904.

12. Valentine, S. J.; Counterman, A. E.; Clemmer, D. E. Conformer-Dependent Proton-Transfer Reactions of Ubiquitin Ions. *J. Am. Soc. Mass Spectrom.* **1997,** *8,* 954-961.

13. Stephenson, J. L.; McLuckey, S. A.; Reid, G. E.; Wells, J. M.; Bundy, J. L. Ion/Ion Chemistry as a Top-Down Approach for Protein Analysis. *Curr. Opin. Biotechnol.* **2002,** *13,* 57-64.

14. Stephenson, J. L.; McLuckey, S. A. Simplification of Product Ion Spectra Derived from Multiply Charged Parent Ions Via Ion/Ion Chemistry. *Anal. Chem.* **1998,** *70,* 3533-3544.

15. Breuker, K.; Oh, H. B.; Lin, C.; Carpenter, B. K.; McLafferty, F. W. Nonergodic and Conformational Control of the Electron Capture Dissociation of Protein Cations. *Proc. Natl. Acad. Sci. U.S.A.* **2004,** *101,* 14011-14016.

16. Ge, Y.; Lawhorn, B. G.; ElNaggar, M.; Strauss, E.; Park, J. H.; Begley, T. P.; McLafferty, F. W. Top Down Characterization of Larger Proteins (45 KDa) by Electron Capture Dissociation Mass Spectrometry. *J. Am. Chem. Soc.* **2002,** *124,* 672-678.
17. Syka, J. E. P.; Coon, J. J.; Schroeder, M. J.; Shabanowitz, J.; Hunt, D. F. Peptide and Protein Sequence Analysis by Electron Transfer Dissociation Mass Spectrometry. *Proc. Natl. Acad. Sci. U.S.A.* **2004,** *101,* 9528-9533.
18. Pitteri, S. J.; Chrisman, P. A.; Hogan, J. M.; McLuckey, S. A. Electron Transfer Ion/Ion Reactions in a Three-Dimensional Quadrupole Ion Trap: Reactions of Doubly and Triply Protonated Peptides with $SO2^{\cdot-}$. *Anal. Chem.* **2005,** *77,* 1831-1839.
19. Chrisman, P. A.; Pitteri, S. J.; Hogan, J. M.; McLuckey, S. A. SO2- Electron Transfer Ion/Ion Reactions with Disulfide Linked Polypeptide Ions. *J. Am. Soc. Mass Spectrom.* **2005,** *16,* 1020-1030.
20. Badman, E. R.; Hoaglund-Hyzer, C. S.; Clemmer, D. E. Dissociation of Different Conformations of Ubiquitin Ions. *J. Am. Soc. Mass Spectrom.* **2002,** *13,* 719-723.
21. Myung, S.; Badman, E. R.; Lee, Y. J.; Clemmer, D. E. Structural Transitions of Electrosprayed Ubiquitin Ions Stored in an Ion Trap over Similar to 10 ms to 30 s. *J. Phys. Chem. A* **2002,** *106,* 9976-9982.
22. Badman, E. R.; Myung, S.; Clemmer, D. E. Evidence for Unfolding and Refolding of Gas-Phase Cytochrome *c* Ions in a Paul Trap. *J. Am. Soc. Mass Spectrom.* **2005,** *16,* 1493-1497.
23. Badman, E. R.; Hoaglund-Hyzer, C. S.; Clemmer, D. E. Monitoring Structural Changes of Proteins in an Ion Trap over ~10 to 200 ms: Unfolding Transitions in Cytochrome *c* Ions. *Anal. Chem.* **2001,** *73,* 6000-6007.
24. Koeniger, S. L.; Merenbloom, S. I.; Clemmer, D. E. Evidence for Many Resolvable Structures within Conformation Types of Electrosprayed Ubiquitin Ions. *J. Phys. Chem. B* **2006,** *110,* 7017-7021.
25. Koeniger, S. L.; Merenbloom, S. I.; Sevugarajan, S.; Clemmer, D. E. Transfer of Structural Elements from Compact to Extended States in Unsolvated Ubiquitin. *J. Am. Chem. Soc.* **2006,** *128,* 11713-11719.
26. Zhao, Q.; Soyk, M. W.; Schieffer, G. M.; Fuhrer, K.; Gonin, M.; Houk, R. S.; Badman, E. R. An Ion Trap-Ion Mobility-Time of Flight Mass Spectrometer with Three Ion Sources for Ion/Ion Reactions. *J. Am. Soc. Mass Spectrom.* **2009,** *20,* 1549-1561.
27. Badman, E. R.; Schieffer, G. M.; Soyk, M.; Zhao, Q.; Anderson, T. J. An ESI-Ion Trap-Ion Mobility-q-TOF to Study Ion-Ion Reactions of Intact Biopolymers. Proceedings of the 53rd ASMS Conference on Mass Spectrometry and Allied Topics; San Antonio, TX June 6-9, 2005.
28. Valentine, S. J.; Clemmer, D. E. H/D Exchange Levels of Shape-Resolved Cytochrome *c* Conformers in the Gas Phase. *J. Am. Chem. Soc.* **1997,** *119,* 3558-3566.
29. Englander, S. W.; Sosnick, T. R.; Mayne, L. C.; Shtilerman, M.; Qi, P. X.; Bai, Y. W. Fast and Slow Folding in Cytochrome *c*. *Accounts Chem. Res.* **1998,** *31,* 737-744.
30. McLafferty, F. W.; Guan, Z. Q.; Haupts, U.; Wood, T. D.; Kelleher, N. L. Gaseous Conformational Structures of Cytochrome *c*. *J. Am. Chem. Soc.* **1998,** *120,* 4732-4740.
31. Steinberg, M. Z.; Breuker, K.; Elber, R.; Gerber, R. B. The Dynamics of Water Evaporation from Partially Solvated Cytochrome *c* in the Gas Phase. *Phys. Chem. Chem. Phys.* **2007,** *9,* 4690-4697.

32. Steinberg, M. Z.; Elber, R.; McLafferty, F. W.; Gerber, R. B.; Breuker, K. Early Structural Evolution of Native Cytochrome *c* after Solvent Removal. *ChemBioChem* **2008,** *9*, 2417-2423.
33. Hoang, L.; Maity, H.; Krishna, M. M. G.; Lin, Y.; Englander, S. W. Folding Units Govern the Cytochrome *c* Alkaline Transition. *J. Mol. Biol.* **2003,** *331*, 37-43.
34. Krishna, M. M. G.; Englander, S. W. A Unified Mechanism for Protein Folding: Predetermined Pathways with Optional Errors. *Protein Sci.* **2007,** *16*, 449-464.
35. Krishna, M. M. G.; Lin, Y.; Rumbley, J. N.; Englander, S. W. Cooperative Omega Loops in Cytochrome *c*: Role in Folding and Function. *J. Mol. Biol.* **2003,** *331*, 29-36.
36. Maity, H.; Rumbley, J. N.; Englander, S. W. Functional Role of a Protein Foldon - an Omega-Loop Foldon Controls the Alkaline Transition in Ferricytochrome *c*. *Proteins Struc. Func. Bioinform.* **2006,** *63*, 349-355.
37. McLuckey, S. A.; Glish, G. L.; Asano, K. G.; Grant, B. C. Atmospheric Sampling Glow-Discharge Ionization Source for the Determination of Trace Organic-Compounds in Ambient Air. *Anal. Chem.* **1988,** *60*, 2220-2227.
38. Soyk, M. W.; Zhao, Q.; Houk, R. S.; Badman, E. R. A Linear Ion Trap Mass Spectrometer with Versatile Control and Data Acquisition for Ion/Ion Reactions. *J. Am. Soc. Mass Spectrom.* **2008,** *19*, 1821-1831.
39. Zhao, Q. Development of Ion Mobility Mass Spectrometry Coupled with Ion/Ion Reactions: Instrumentation and Applications for Protein Analysis. Iowa State University Chapter 2 & 3.
40. Dugourd, P.; Hudgins, R. R.; Clemmer, D. E.; Jarrold, M. F. High-Resolution Ion Mobility Measurements. *Rev. Sci. Instrum.* **1997,** *68*, 1122-1129.
41. McLuckey, S. A. Recent Developments in Ion/Ion Chemistry for Bioanalysis. Federation of Analytical Chemistry and Spectroscopy Societies Conference; Memphis, TN 2007,
42. Zhao, Q. Development of Ion Mobility Mass Spectrometry Coupled with Ion/Ion Reactions: Instrumentation and Applications for Protein Analysis. Iowa State University Chapter 3.
43. Stephenson, J. L.; VanBerkel, G. J.; McLuckey, S. A. Ion-Ion Proton Transfer Reactions of Bio-Ions Involving Noncovalent Interactions: Holomyoglobin. *J. Am. Soc. Mass Spectrom.* **1997,** *8*, 637-644.
44. Chrisman, P. A.; Newton, K. A.; Reid, G. E.; Wells, J. M.; McLuckey, S. A. Loss of Charged Versus Neutral Heme from Gaseous Holomyoglobin Ions. *Rapid Commun. Mass Spectrom.* **2001,** *15*, 2334-2340.
45. Shelimov, K. B.; Clemmer, D. E.; Hudgins, R. R.; Jarrold, M. F. Protein Structure in Vacuo: Gas-Phase Conformations of BPTI and Cytochrome *c*. *J. Am. Chem. Soc.* **1997,** *119*, 2240-2248.
46. Mason, E. A.; McDaniel, E. W. In *Transport Properties of Ions in Gases*; John Wiley & Sons: New York, 1988, pp 86-91.
47. Breuker, K.; McLafferty, F. W. Stepwise Evolution of Protein Native Structure with Electrospray into the Gas Phase, $10^{(-12)}$ to $10^{(2)}$ s. *Proc. Natl. Acad. Sci. U.S.A.* **2008,** *105*, 18145-18152.
48. McLuckey, S. A.; Reid, G. E.; Wells, J. M. Ion Parking During Ion/Ion Reactions in Electrodynamic Ion Traps. *Anal. Chem.* **2002,** *74*, 336-346.

49. Li, J. W.; Taraszka, J. A.; Counterman, A. E.; Clemmer, D. E. Influence of Solvent Composition and Capillary Temperature on the Conformations of Electrosprayed Ions: Unfolding of Compact Ubiquitin Conformers from Pseudonative and Denatured Solutions. *Int. J. Mass Spectrom.* **1999,** *187,* 37-47.
50. Dill, K. A.; Chan, H. S. From Levinthal to Pathways to Funnels. *Nature Struc. Biol.* **1997,** *4,* 10-19.
51. Maity, H.; Maity, M.; Englander, S. W. How Cytochrome *c* Folds, and Why: Submolecular Foldon Units and Their Stepwise Sequential Stabilization. *J. Mol. Biol.* **2004,** *343,* 223-233.
52. Stephenson, J. L.; McLuckey, S. A. Ion/Ion Reactions in the Gas Phase: Proton Transfer Reactions Involving Multiply-Charged Proteins. *J. Am. Chem. Soc.* **1996,** *118,* 7390-7397.
53. Wells, J. M.; Chrisman, P. A.; McLuckey, S. A. Formation and Characterization of Protein-Protein Complexes in Vacuo. *J. Am. Chem. Soc.* **2003,** *125,* 7238-7249.
54. Touboul, D.; Jecklin, M. C.; Zenobi, R. Rapid and Precise Measurements of Gas-Phase Basicity of Peptides and Proteins at Atmospheric Pressure by Electrosonic Spray Ionization-Mass Spectrometry. *J. Phys. Chem. B* **2007,** *111,* 11629-11631.
55. Touboul, D.; Jecklin, M. C.; Zenobi, R. Investigation of Deprotonation Reactions on Globular and Denatured Proteins at Atmospheric Pressure by ESSI-MS. *J. Am. Soc. Mass Spectrom.* **2008,** *19,* 455-466.
56. Newton, K. A.; McLuckey, S. A. Gas-Phase Peptide/Protein Cationizing Agent Switching Via Ion/Ion Reactions. *J. Am. Chem. Soc.* **2003,** *125,* 12404-12405.

**TABLE**

Table 1) Average cross-sections for cytochrome *c* ions in different charge states

| | Cross Sections ($Å^2$) | | | |
|---|---|---|---|---|
| Charge | Measured in Present Work | | Literature Values | |
| State | From 9+ | From 8+ | Shelimov [45] | Badman [23] |
| 9+ | 1975 | | 1964 | |
| | | | 2215 | |
| 8+ | 1468 | 1709 | 1250 | 1260 |
| | 1715 | 1900 | 1702, 1845 | 1477, 1709 |
| | | | 2061 | 1854, 2071 |
| 7+ | 1493 | 1488 | 1247, 1620, | 1257, 1426, 1629 |
| | 1708 | 1704 | 1785, 2007 | 1792, 2018 |
| 6+ | 1179 | 1085 | 1244, | 1254 |
| | 1364 | 1359 | 1393, 1602 | 1400, 1611 |
| 5+ | 974 | 970 | 1196, | 1205 |
| | | | 1340 | 1352 |
| 4+ | 1015 | 1069 | 1153 | 1160 |
| 3+ | 1073 | 1071 | 1139 | 1150 |
| 2+ | 1055 | 1134 | | |
| 1+ | 1138 | 1135 | | |

## FIGURES

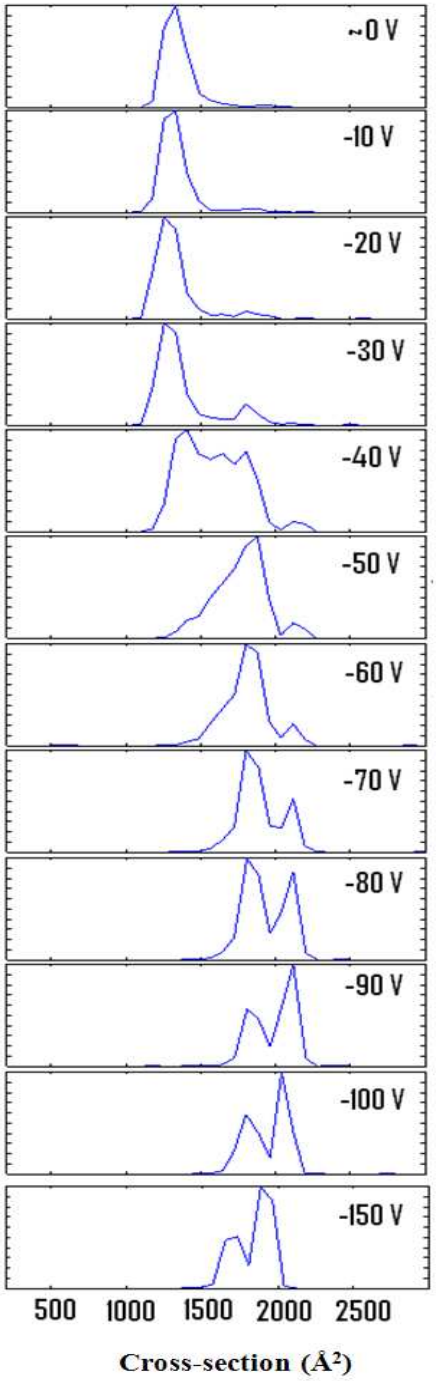


Figure 1) Cross-section distributions for cytochrome *c* 8+ ions at different injection voltage into the drift tube.

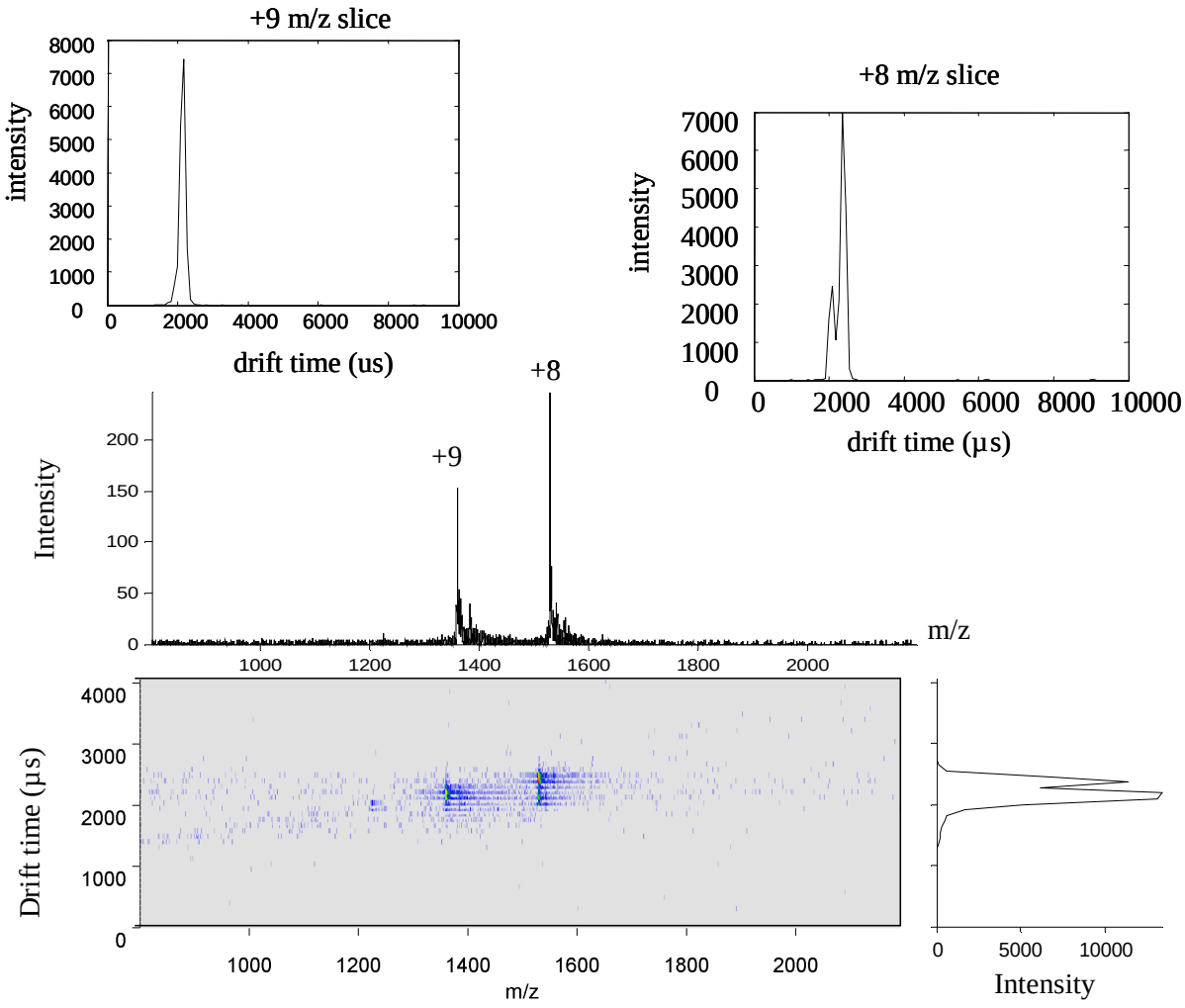


Figure 2) Nested 3-D IM-TOF mass spectrum of 30 µM cytochrome *c* in water with 1% acetic acid. The summed mass and ion mobility spectra are in the middle and at the lower right, respectively. The extracted IM spectra for cytochrome *c* 8+ and 9+ ions are displayed at the top.

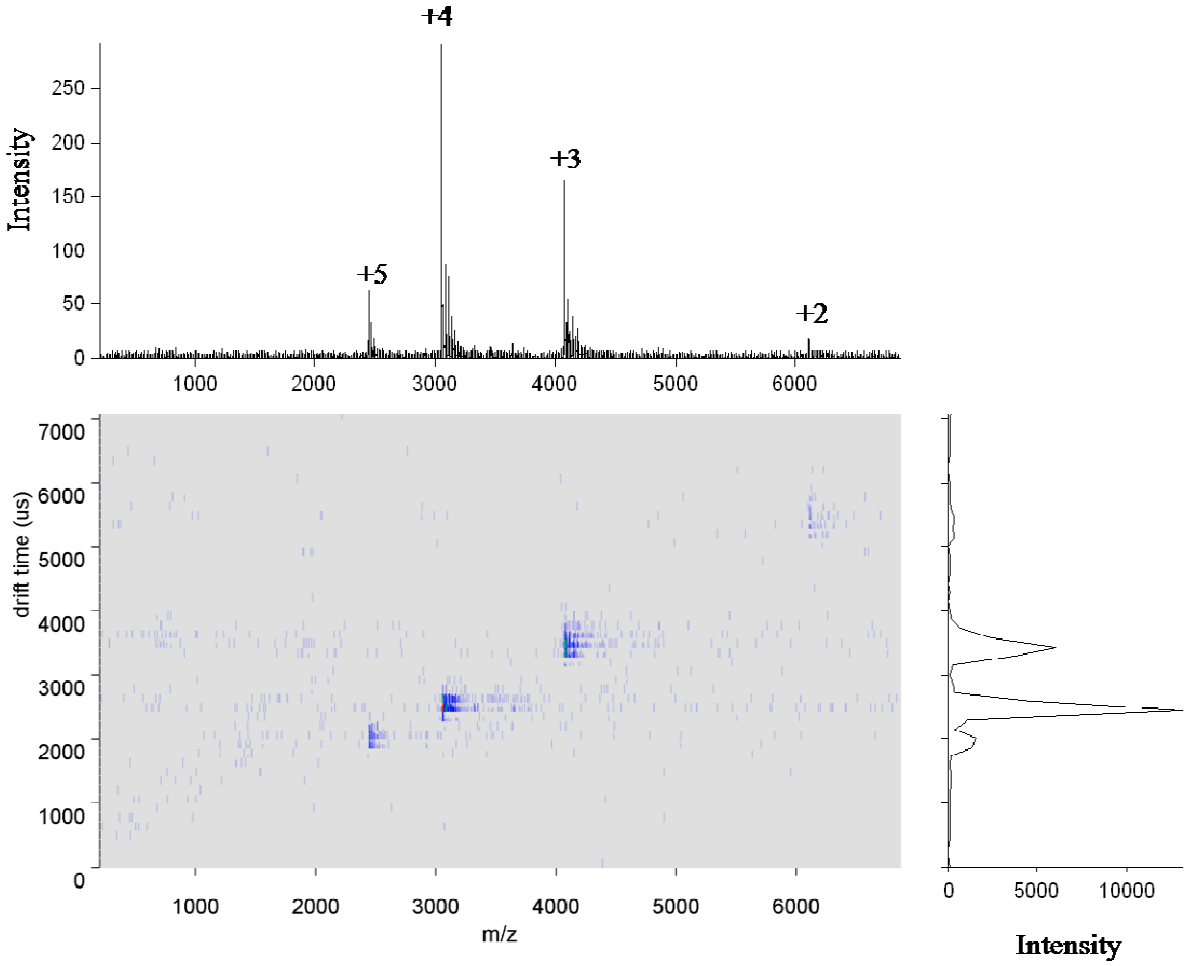


Figure 3) 3-D spectrum after isolated 8+ cytochrome *c* ions react with PDCH negative in the ion trap for 100 ms.

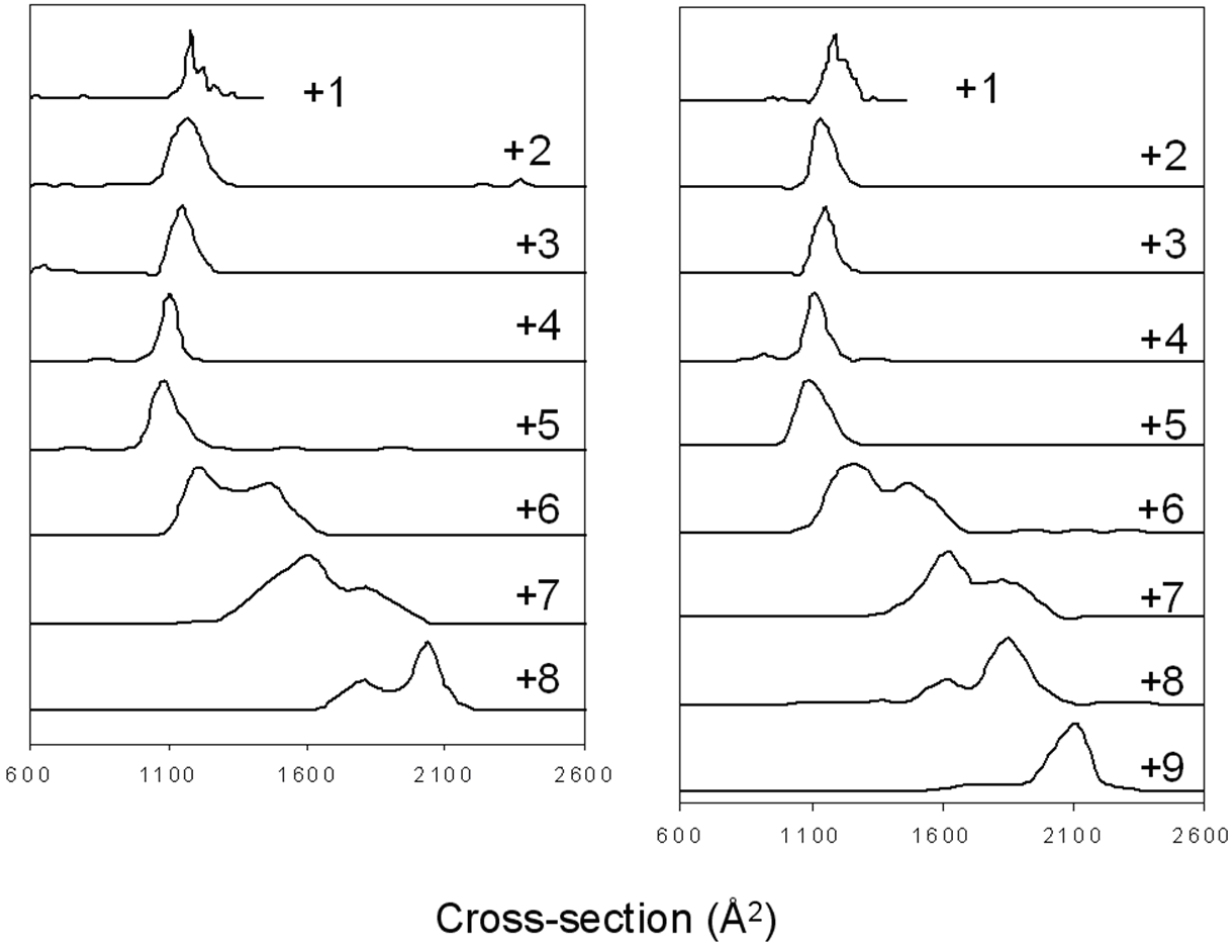


Figure 4) Distribution of cross sections for cytochrome *c* ions in each charge state. For the plots at the left, the cytochrome *c* ions were initially in the 8+ state; ion/ion reaction time was 50 ms to go to 4+ and 110 ms to go to 1+. The right plots are for charge reduction of 9+ cytochrome c ions for 40 ms to go to 4+ and 80 ms to go to 1+.

Figure 5) Distribution of cross sections for cytochrome *c* ions in charge states 7+ to 4+. The ions are either made by ion/ion reaction from the 9+ or 8+ species in the ion trap, or observed directly by ESI from either water or aqueous ammonium acetate buffer. For the 5+ ions, the asterisks denote an unusual "open" conformer seen only when these ions are made directly by ESI, not by ion/ion reaction. (see next page)

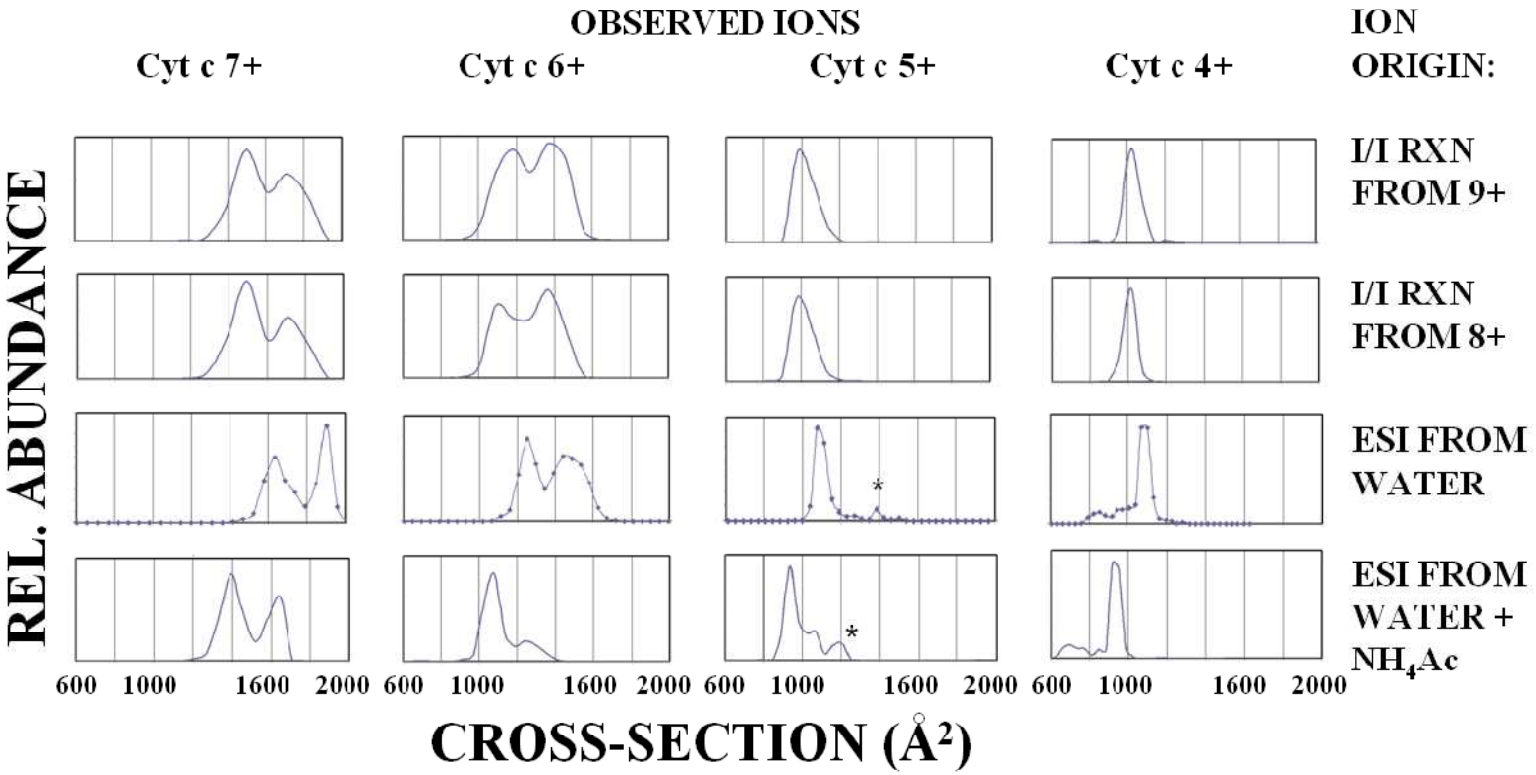
OBSERVED IONS
Cyt c 7+
Cyt c 6+
Cyt c 5+
Cyt c 4+
ION ORIGIN:
I/I RXN FROM 9+
I/I RXN FROM 8+
ESI FROM WATER
ESI FROM WATER + NH4Ac
REL. ABUNDANCE
600 1000 1600 2000
CROSS-SECTION (Å²)

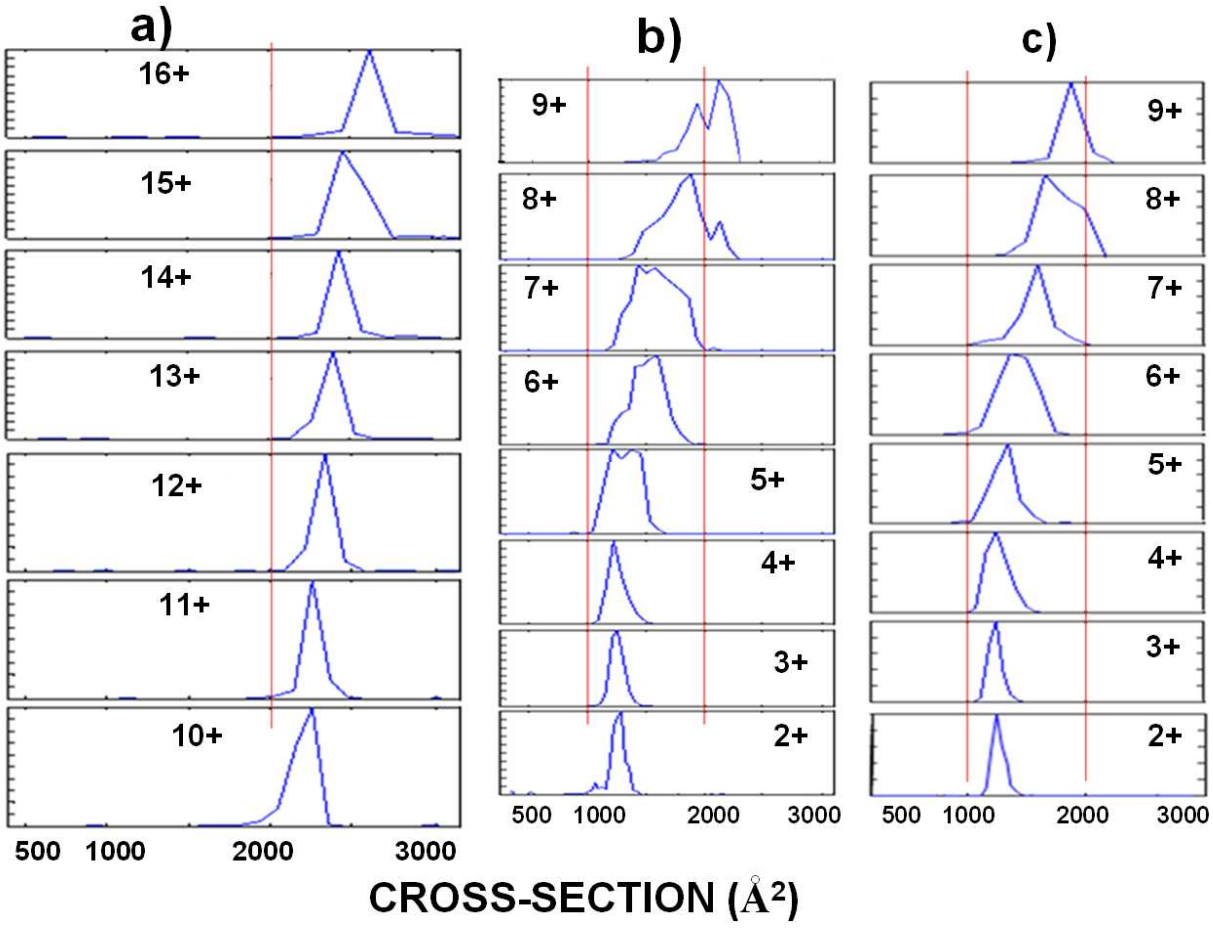


Figure 6) Distribution of cross section for cytochrome *c* ions obtained with -50 V on drift tube entrance. Red or gray lines have been added at 1000 and 2000 $Å^2$ for comparison.:

a) cross sections of ions produced directly by ESI from 50% MeOH/$H_2O$ with 1% acetic acid.

b) cross sections of ions produced by ion/ion reaction of cytochrome *c* +9 to +16 from 50% MeOH/$H_2O$ with 1% acetic acid.

c) cross sections of cytochrome c +8 and +9 ions from $H_2O$ with 1% acetic acid and ion/ion reaction products for comparison.

# APPENDIX III

## ATMOSPHERIC PRESSURE LASER DESORPTION/IONIZATION OF PLANT METABOLITES AND PLANT TISSUE USING COLLOIDAL GRAPHITE

D. C. Perdian, Gregg M. Schieffer, and R. S. Houk*

Ames Laboratory U. S. Department of Energy

Department of Chemistry

Iowa State University, Ames IA 50011 USA

A paper published in *Rapid Communications in Mass Spectrometry*, 2010, 24, 397-402.

## ABSTRACT

Colloidal graphite is a promising matrix for atmospheric pressure laser desorption/ionization mass spectrometry. Intact $[M+H]^+$ and $[M-H]^-$ ions are readily produced from a wide range of small molecule plant metabolites particularly anthocyanins, fatty acids, lipids, glycerides, and ceramides. Compared to a more traditional organic acid matrix, colloidal graphite provides more efficient ionization for small hydrophobic molecules and has a much cleaner background spectrum, especially in negative ion mode. Some important metabolites, e.g., fatty acids and glycosylated flavonoids, can be observed from *Arabidopsis thaliana* leaf and flower petal tissues *in situ*.


## INTRODUCTION

Since its development,[1, 2] matrix-assisted laser desorption/ionization (MALDI) has become an invaluable tool for the analysis of a large number of biological molecules including proteins,[3-5] peptides,[4, 6] oligonucleotides[7] and oligosaccharides.[8, 9] MALDI-MS techniques have been applied to study numerous biological functions including protein-protein interactions,[10] and bio-marker discovery.[11] MALDI has also become a popular method for imaging mass spectrometry (IMS)[12-14] of biological tissues. For spatial imaging analysis a MALDI matrix can be sprayed onto the tissue, a series of micro-droplets can be applied to the sample, or both methods can be employed on the same sample.[15]

The most popular matrices for MALDI experiments have been organic acid compounds, such as α-cyano-4-hydroxycinnamic acid, 2,5-dihydroxybenzoic acid (DHB), as well as other organic acids.[16, 17] Organic acid matrices readily generate intact, singly-charged protein and peptide ions, but like any analytical technique have some limitations for other analytes. Generally, ionization of the analyte in MALDI is best if the analyte and matrix co-crystallize. The amount of co-crystallization varies with the hydrophobicity of the analyte molecules; more hydrophilic analyte molecules usually co-crystallize better. A variety of sample preparation methods have been developed to increase the successfulness of MALDI methods for hydrophobic proteins, such as varying temperature during the co-crystallization

step[18] and using organic solvent mixtures to facilitate the analyte/matrix co-crystallization.[19, 20] The crystalline structure of the organic acids sometimes causes spatial inhomogeneities in the resulting layer of solid matrix.[21] For imaging experiments, spatial homogeneity is extremely important for quality mass spectral images. The use of organic acids as matrices also generates many background ions at low *m/z* values, which often overlap with analyte ions from small analyte molecules.[22]

A variety of methods have been developed to overcome these limitations. Room temperature molten salts, or ionic liquids, have been used as matrices and provide more homogeneous signal compared to traditional MALDI matrices.[23] Ionic liquids have also been used to improve the ionization efficiencies of some molecules, such as glycosaminoglycan disaccharides.[24] Atmospheric pressure infrared MALDI using concomitant water as a matrix has been used to image plant metabolites.[25, 26] The native water matrix produces a cleaner background spectrum, as no additional matrix is required. Using this technique, Vertes and coworkers were able to image sucrose, glucose, fructose, and citric acid from strawberry skin samples.[26] They were also able to identify over 50 plant metabolites from a variety of plant tissues, including potato tubers, onion storage leaf, white lily flower petal, and a section of an almond kernel. Several metabolites in a white lily (*Lilium candidum*) flower petal were also imaged spatially.[25]

Various nanomaterials have been used as alternate methods for MALDI experiments. Silver nanoparticles were used as a matrix in a surface-assisted laser desorption/ionization experiments to ionize estrogen molecules.[27] Colloidal Ag was used as a matrix for LDI-IMS experiments which monitored the spatial distribution of metabolites in *Arabidopsis thaliana* plant tissue.[28] Gold nanoparticles have been used to analyze small biomolecules using visible lasers.[29]

Graphite has been used in various forms as a matrix for LDI-MS experiments.[30-35] Sunner et al. used graphite for surface-assisted laser desorption ionization of peptides and proteins from liquid solutions.[30] Zenobi et al. used graphite/liquid mixtures to successfully ionize several types of molecules including proteins, peptides, polysaccharides, and polymers.[31] Graphite was incorporated into a thin layer chromatography (TLC) plate and

used as matrix for LDI.[32] Graphite-assisted laser desorption/ionization (GALDI) was also used to study light-induced aging in tri-terpene dammar and mastic varnishes.[33] Low molecular weight polymers were analyzed on a graphite plate by LDI-MS without an additional matrix.[34] GALDI also effectively ionized fatty acid molecules from triglycerides, food, and phospholipid samples.[35]

Most of the above experiments with graphite were done with the sample stage at high vacuum, $10^{-4}$ torr or less. Recently, Yeung and co-workers used colloidal graphite to ionize and image small molecules with the sample at intermediate pressures (100 to 200 mTorr).[36, 37] With colloidal graphite, small hydrophobic analytes were analyzed with a greater efficiency than traditional organic acid MALDI matrices. It was shown previously that polar phospatidyl choline and sphingomyelins suppressed the signal from other less-polar lipids within a sample using MALDI-MS.[38] This was not the case using colloidal graphite LDI-MS.[36] Colloidal graphite also provides a simple sample preparation procedure that provides very homogeneous sample coverage. This GALDI method was able to successfully ionize a variety of compounds, including phospholipids, cerebrosides, phospatidylcholines, and sulfatides,[36] fatty acids, organic acids, flavonoids, and oligosaccharides.[37] Cha et al. also used colloidal graphite to image plant metabolites *in situ* from the tissue of various parts of the *Arabidopsis thaliana* plant.[39]

This paper describes initial experiments showing the effectiveness of colloidal graphite LDI-MS at atmospheric pressure. The advantages and figures of merit of this technique described above are maintained at the elevated pressure. Compared to reduced pressure LDI, atmospheric pressure LDI-MS and IMS experiments using colloidal graphite should offer higher sample throughput and could perhaps be developed to allow molecular imaging on living tissues.

## EXPERIMENTAL

**Samples** – Standards, MALDI matrices, and solvents used were purchased from Fisher Scientific (Fairlawn, NJ). Total brain lipid extract was purchased by Avanti Polar Lipids Inc. (Alabaster, AL) The colloidal graphite in 2-propanol (IPA) and heptane aerosol spray (Aerodag G®) was purchased from Acheson Colloids (Port Huron, MI). The *Arabidopsis thaliana* wild type plant samples were provided by Basil Nikolau, Iowa State University.

**Sample Preparation** – For the analysis of standards, 2 or 3 µL of standard solutions were pipetted onto the stainless steel sample plate and allowed to air dry. All sample loadings were 20 to 50 ng, except stearic acid in which 20 µg of the sample was deposited. Anthocyanin standards were dissolved in methanol; all other standards and extracts were dissolved in chloroform. Spotting of 3 µL (methanol) and 2 µL(chloroform) was more than enough to cause the sample to spread out to cover the entire sampling area (circular, ~3 mm diameter) before drying. Taking into account the spreading of the sample and the laser spot size (200 µm), the actual amount of analyte that is sampled by the laser is much less than the sample loading values. Colloidal graphite was then sprayed onto the sample plates over the dried residues in three 5 second bursts from a distance of approximately 20 cm. The sprayed samples were air dried for 5 minutes.

Plant tissue samples were attached to the stainless steel sample plates via conducting double sided tape. Colloidal graphite in IPA was sprayed in the same manner as the standard samples.

For comparison and setup purposes, a few conventional MALDI samples were prepared by making a 1:1 by volume analyte-to-matrix solution, pipetting 3 µL of the 1:1 mixture onto the sample plate, followed by air-drying for 30 minutes. The matrix solution was a saturated solution of DHB in 50/50% (% v/v) $H_2O$/acetonitrile with 0.1 % trifluoroacetic acid.

**Laser –** A solid state Nd:YAG laser (LSX-100, Cetac Technologies, Omaha, NE) quadrupled to a wavelength of 266 nm was used for these experiments. This laser was originally designed for the high pulse energies normally used for laser ablation - inductively coupled plasma - mass spectrometry. Operating conditions of the laser were: repetition rate 20 Hz, initial pulse energy 800 µJ, spot size 200 µm diameter. The pulse energy was attenuated to approximately 200 µJ by placing neutral density filters (ThorLabs, Newton, NJ) in the path of the beam. The incident angle of the laser beam onto the sample was approximately 25º from the sample surface.

**Mass Spectrometer** - An LCQ Advantage 3D ion trap mass spectrometer (Thermo Finnigan, Bremen, Germany) was used for these experiments. The atmospheric pressure chemical ionization (APCI) source designed for use on the LCQ advantage was modified to hold a stainless steel sample plate. The sample plate was placed orthogonal to the MS heated capillary inlet at a distance of 4 mm. For positive ions the sample plate voltage was +250 to +1000 volts for colloidal graphite or +2000 to +300 volts for MALDI with DHB matrix. These values were chosen to maximize signal; the ranges cited represent the day-to-day variation of the optimum values. Similar voltages of opposite polarity were used for negative ions. The automatic gain control of the mass spectrometer was turned off; instead injection times of 100 to 250 ms were used. The figures for standards and extracts represent one mass spectrum (one microscan) and are not averaged. Using a laser repetition rate of 20 Hz, the spectra are produced from a maximum of 2-5 laser shots. The mass spectra for the plant tissue samples are the average of 10 mass spectra (10 microscans) with injection times of 250 ms (maximum 50 laser shots). The ion trap functions were not synchronized to the laser pulses.

## RESULTS AND DISCUSSION

**Analysis of Standards** – Standards were analyzed for the initial determination of the effectiveness of colloidal graphite for desorption and ionization of typical plant metabolite molecules at atmospheric pressure. The same colloidal graphite coating can be used in either positive or negative ion modes. The mass spectra for particular compounds from the general classes ceramides (Fig 1a), phospatidylcholines (Fig 1b), and glycerols (Fig 1c) show mainly intact protonated ions in positive mode. The origin of the $[M+H]^+$ ions is interesting. There is no proton donor added to the graphite, as in conventional MALDI. Perhaps there are such impurities in the graphite, or proton donating reagent ions like $H(H_2O)_n^+$ clusters in the air through which the ions pass. The mass spectra for compounds from the anthocyanin (Fig. 2a and 2b) and fatty acid (Fig. 2c) classes show mainly deprotonated $[M-H]^-$ ions in negative mode.

The background spectra for colloidal graphite experiments are relatively clean when an appropriate laser energy is used. If the laser energy is too high, a variety of background ions can be seen which are most likely carbon cluster ions created from the graphite itself.[36] The peaks at *m/z* 675 (Fig. 1b) and *m/z* 373 (Fig. 1c) are attributed to unknown contaminants in the standard samples.

$[M-H]^-$ ions from the anthocyanin isomers morin (Fig. 2a) and quercetin (Fig. 2b) are isobaric but can be distinguished using tandem mass spectrometric techniques (Fig. 3). The diagnostic fragment ion for flavonoid molecules[40] is observed at *m/z* 151 in both spectra. The diagnostic fragment for morin[40], *m/z* 149, and the diagnostic fragment ion for quercetin[40], *m/z* 179, are both observed from the respective $[M+H]^+$ or $[M-H]^-$ ions.[39] All spectra show reasonable signal to noise ratios.

The most prominent peaks in all mass spectra are the intact $[M+H]^+$ or $[M-H]^-$ ions, providing evidence that the use of colloidal graphite for AP-LDI-MS experiments is a soft ionization technique. The mass spectrum of 24:0 ceramide (Fig. 1a) does show a peak at *m/z* 633, which corresponds to the loss of $H_2O$ fragment from $[M+H]^+$. Other LDI-MS spectra of 24:0 ceramide taken with the source at intermediate pressure (170 mtorr) show mainly

$[M+Na-H_2O]^+$ and $[M+Na]^+$, with little or no $[M+H]^+$ ion.[41] Others have observed less fragmentation for LDI at atmospheric pressure compared to reduced pressure sources.[42]

The advantages of using colloidal graphite over traditional MALDI matrices can be seen by comparing the LDI mass spectra for a total brain lipid extract coated with colloidal graphite (Fig. 4a) or DHB (Fig. 4b). All of the peaks from this mixture are less abundant, and some are barely seen, using DHB as a matrix. This is especially apparent in the *m/z* range 400 to 550, where most of the ions detected by colloidal graphite LDI-MS are not observed in the MALDI mass spectrum. The specified concentrations in the total brain lipid extract are 16.7% phosphatidylethanolamine, 10.6% phosphatidylserine, 9.6% phosphatidylcholine, 2.8% phosphatidic acid, 1.6% phosphatidylinositol, and 58.7% other compounds.

Possible classes of compounds detected in Figure 4 include phosphatidylethanolamines (*m/z* ~400 to 900), phosphatidylserines (*m/z* ~450 to 900), phosphatidylcholines (*m/z* ~ 460 to 900), and phosphatidylinositols (*m/z* ~ 500 to 900). These all contain non-polar fatty-acid chains whose varying length and degrees of unsaturation cause the wide range in molecular weights and subsequent *m/z* values. These hydrophobic molecules do not co-crystallize with the DHB matrix and therefore do not desorb and/or ionize as efficiently as the molecules do when analyzed with colloidal graphite. A similar effect was seen when using α-cyano-4-hydroxycinnamic acid as the MALDI matrix. It has been shown that a greater number of lipids from extracts could be identified using colloidal graphite as a matrix rather than DHB at intermediate pressure MALDI.[36]

**Analysis of Plant Tissue** – Two different types of plant tissue were analyzed to determine if using colloidal graphite for LDI-MS experiments is sensitive enough for measurement of plant metabolites at atmospheric pressure. A leaf from an *Arabidopsis thaliana* wild type sample was analyzed and several peaks from fatty acid molecules in the cuticular wax are observed (Fig. 5). The analysis of a flower petal from the same *Arabidopsis thaliana* wild type sample displays several peaks that could correspond to mono-

glycoside flavonoid molecules (Fig. 6a) as well as several diglycoside flavonoid molecules (Fig. 6b). The compounds shown in the figures are identified based on matches to mass spectra from metabolites identified in this plant sample by MS/MS methods in previous work.[28, 39]

## CONCLUSIONS

This paper shows that colloidal graphite is an effective matrix for LDI-MS at atmospheric pressure. The method is sensitive enough to identify at least some plant metabolites *in situ* and raises the possibility of performing molecular imaging mass spectral analysis of plant tissues *in vivo*. Better sensitivity would be welcome; possible improvements include pulsed dynamic focusing for ion extraction,[43] a counter-current $N_2$ flow,[44] and/or addition of supplemental ionization techniques like electrospray. Sensitivity improvements would extend the range of compounds that can be measured and would facilitate use of smaller laser spots to improve spatial resolution. A software controlled translational stage to move the sample stage during mass analysis will provide the means for molecular imaging.

## ACKNOWLEDGEMENTS

We would like to thank Basil Nikolau and Zhihong Song from the Department of Biochemistry, Biophysics and Molecular Biology, Iowa State University of Science and Technology for providing the *Arabidopsis thaliana* plant samples. We would also like to thank Sangwon Cha for advice on the use of colloidal graphite as a matrix. This work is supported by the Ames Laboratory U. S. Department of Energy, Office of Basic Energy Sciences. The Ames Laboratory is operated by Iowa State University of Science and Technology under DOE Contract #DE-AC02-07CH11358.

**REFERENCES**


1. Karas M, Bachmann D, Hillenkamp F. *Anal. Chem.* 1985; **57:** 2935.
2. Tanaka K, Waki H, Satoshi YI, Yoshikazu A, Tamio Y, Matsuo YT, *Rapid Commun. Mass Spectrom.* 1988; **2:** 151.
3. Jungblut P, Thiede B. *Mass Spectrom. Reviews* 1997; **16:** 145.
4. Dai Y, Whittal RM, Li L. *Anal. Chem.* 1999; **71:** 1087.
5. Chaurand P, Stoeckli M, Caprioli RM. *Anal. Chem.* 1999; **71:** 5263..
6. Kaufmann R, Kirsch D, Spengler B. *Intern. J. Mass Spectrom. Ion Proc.* 1994; **131:** 355.
7. Lecchi P, Pannell LK. *J. Am. Soc. Mass Spectrom.* 1995; **6**: 972.
8. Finke B, Stahl B, Pfenninger A, Karas M, Daniel H, Sawatzki G. *Anal. Chem.* 1999; **71:** 3755.
9. Joseph Z. *Mass Spectrom. Rev.* 2004; **23**: 161.
10. Farmer TB, Caprioli RM, *J. Mass Spectrom.* 1998; **33**: 697.
11. Pevsner PH, Melamed J, Remsen T, Kogos A, Francois F, Kessler P, Stern A, Anand S. *Biomarkers Med.* 2009; **3**: 55.
12. Cornett DS, Reyzer ML, Chaurand P, Caprioli RM. *Nat. Meth.* 2007; **4:** 828.
13. Burnum KE, Frappier SL, Caprioli RM, *Ann. Rev. Anal. Chem.* 2008; **1:** 689.
14. Hsieh Y, Chen J, Korfmacher WA. *J. Pharm. Tox Meth.* 2007; **55:** 193.
15. Sugiura Y, Shimma S, Setou M. *Anal. Chem.* 2006; **78:** 8227.
16. Beavis RC, Chaudhary T, Chait BT. *Org. Mass Spectrom.* 1992; **27:** 156.
17. Kampmeier J, Dreisewerd K, Schürenberg M, Strupat K. *Intern. J. .Mass Spectrom. Ion Process.* 1997; **169:** 31..
18. Bird GH, Lajmi AR, Shin JA. *Anal. Chem.* 2002; **74:** 219.
19. Green-Church KB, Limbach PA. *Anal. Chem.* 1998; **70:** 5322.
20. Kim YJ, Freas A, Fenselau C. *Anal. Chem.* 2001; **73:** 1544.
21. Luxembourg SL, McDonnell LA, Duursma MC, Guo X, Heeren RMA. *Anal. Chem.* 2003; **75:** 2333.
22. Cohen L, Gusev A. *Anal. Bioanal.Chem.* 2002; **373:** 571.
23. Armstrong DW, Zhang LK, He L, Gross ML. *Anal. Chem.* 2001; **73:** 3679.
24. Laremore TN, Linhardt RJ. *Rapid Comm. Mass Spectrom.* 2007; **21:** 1315.
25. Li Y, B. Shrestha B, Vertes A. *Anal. Chem.* 2008; **80:** 407.
26. Li Y, B. Shrestha B, Vertes A. *Anal. Chem.* 2007; **79:** 523.
27. Chiu TC, Chang LC, Chiang CK, Chang HT. *J. Am. Soc. Mass Spectrom.* 2008; **19**: 1343.
28. Cha S, Song Z, Nikolau BJ, Yeung ES. *Anal. Chem.* 2009; **81:** 2991.
29. Spencer MT, Furutani H, Oldenburg SJ, Darlington TK, Prather KA. *J. Phys. Chem. C*, 2008; **112**: 4083.
30. Sunner J, Dratz E, Chen YC. *Anal. Chem.* 1995; **67:** 4335.
31. Dale MJ, Knochenmuss R, Zenobi R. *Anal. Chem.* 1996; **68:** 3321.
32. Peng S, Edler M, Ahlmann N, Hoffmann T, Franzke J. *Rapid Comm. Mass Spectrom.* 2005; **19:** 2789.

33. Zumbuhl S, Knochenmuss R, Wulfert S, F. Dubois F, M. J. Dale MJ, Zenobi R. *Anal. Chem.* 1998; **70:** 707.
34. Kim HJ, Lee JK, Park SJ, Ro HW, Yoo DY, Yoon DY. *Anal. Chem.* 2000; **72:** 5673.
35. Park KH, Kim HJ. *Rapid Comm. Mass Spectrom.* 2001; **15:** 1494.
36. Cha S, Yeung ES. *Anal. Chem.* 2007; **79:** 2373.
37. Zhang H, Cha S, Yeung ES. *Anal. Chem.*, 2007; **79**: 6575.
38. Petkovic M, Schiller J, Müller M, Benard S, Reichl S, Arnold K, Arnhold J. *Anal. Biochem.* 2001; **289:** 202.
39. Cha S, Zhang H, Ilarslan HI, Syrkin E, Brachova WL, Nikolau BJ, Yeung ES. *Plant J.* 2008; **55:** 348.
40. Buchner N, Krumbein A, Rohn S, Kroh LW. *Rapid Comm. Mass Spectrom.* 2006; **20:**, 3229.
41. Cha S, Yeung ES. Personal Communication
42. Moyer SC, Cotter RJ. *Anal. Chem.* 2002; **74**: 468A.
43. Tan PV, Laiko VV, Doroshenko VM. *Anal. Chem.* 2004; **76:** 2462.
44. Miller CA, Yi D, Perkins PD. *Rap. Comm. Mass Spectrom.* 2003; **17:** 860.

## FIGURES

*Figure 1*

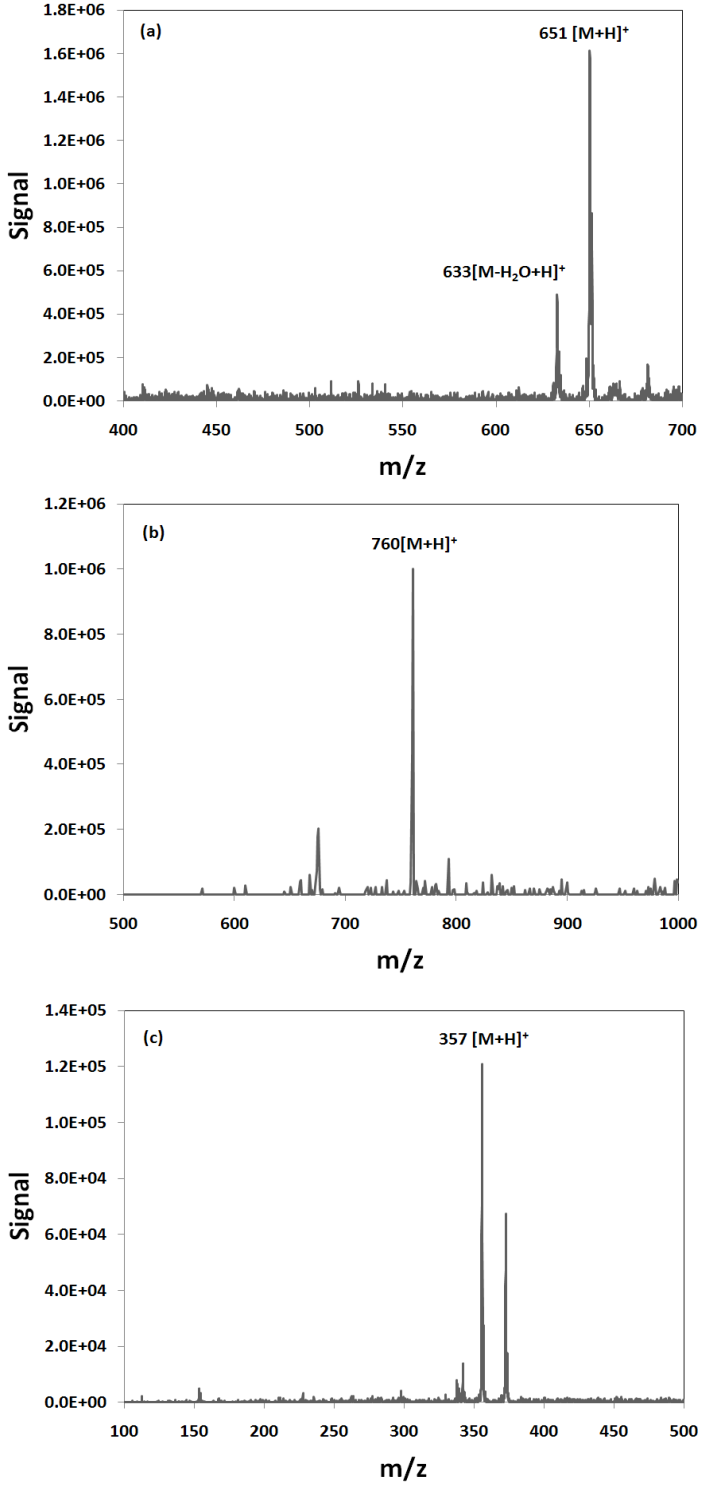


Figure 1) Positive ion mass spectra of standards: a) 24:0 ceramide, 50 ng, b) 1,2-diacyl-sn-glycerol-3-phosphocholine, 20 ng, and c) 1-oleoylglycerol, 20 ng.

*Figure 2*

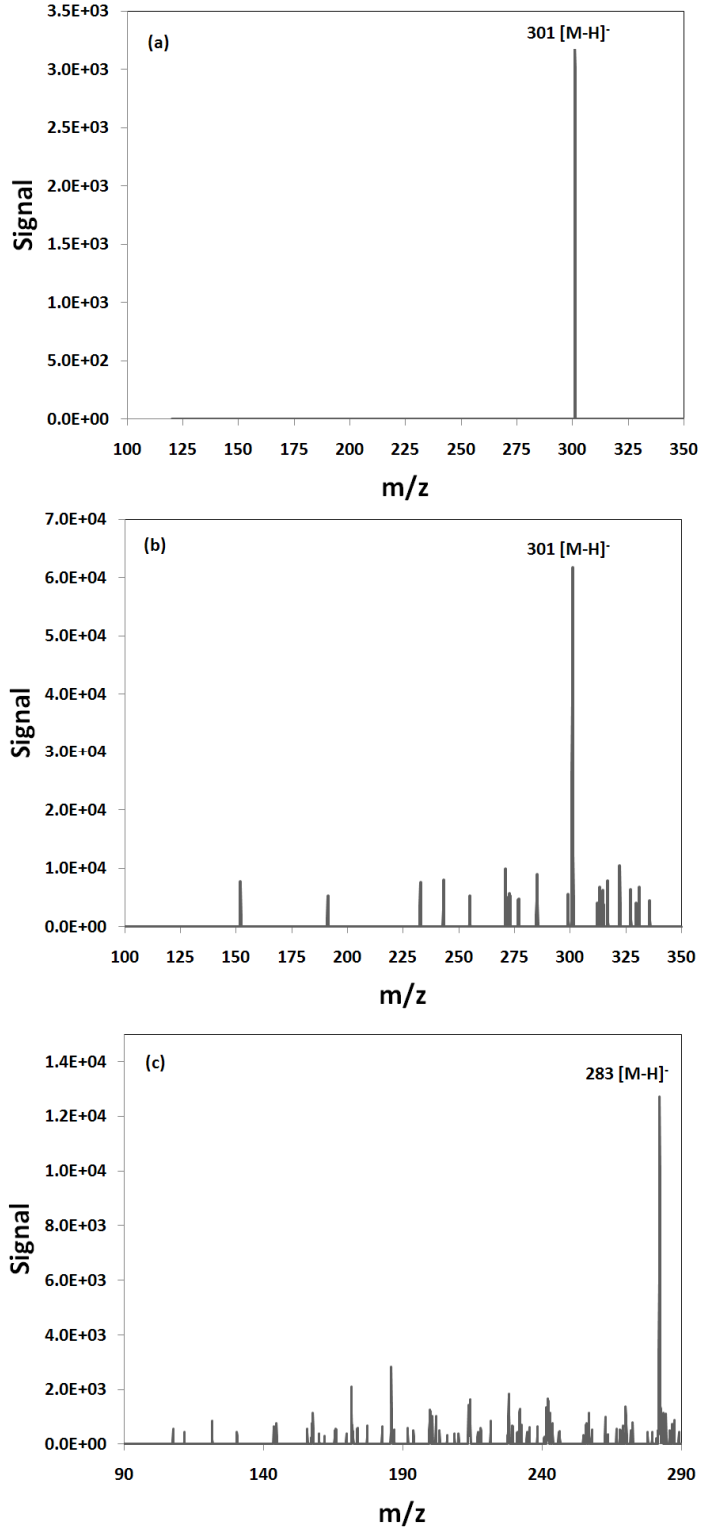


Figure 2) Negative ion mass spectra of standards: a) morin, 20 ng, b) quercetin, 20 ng, and c) stearic acid, 18 µg.

*Figure 3*

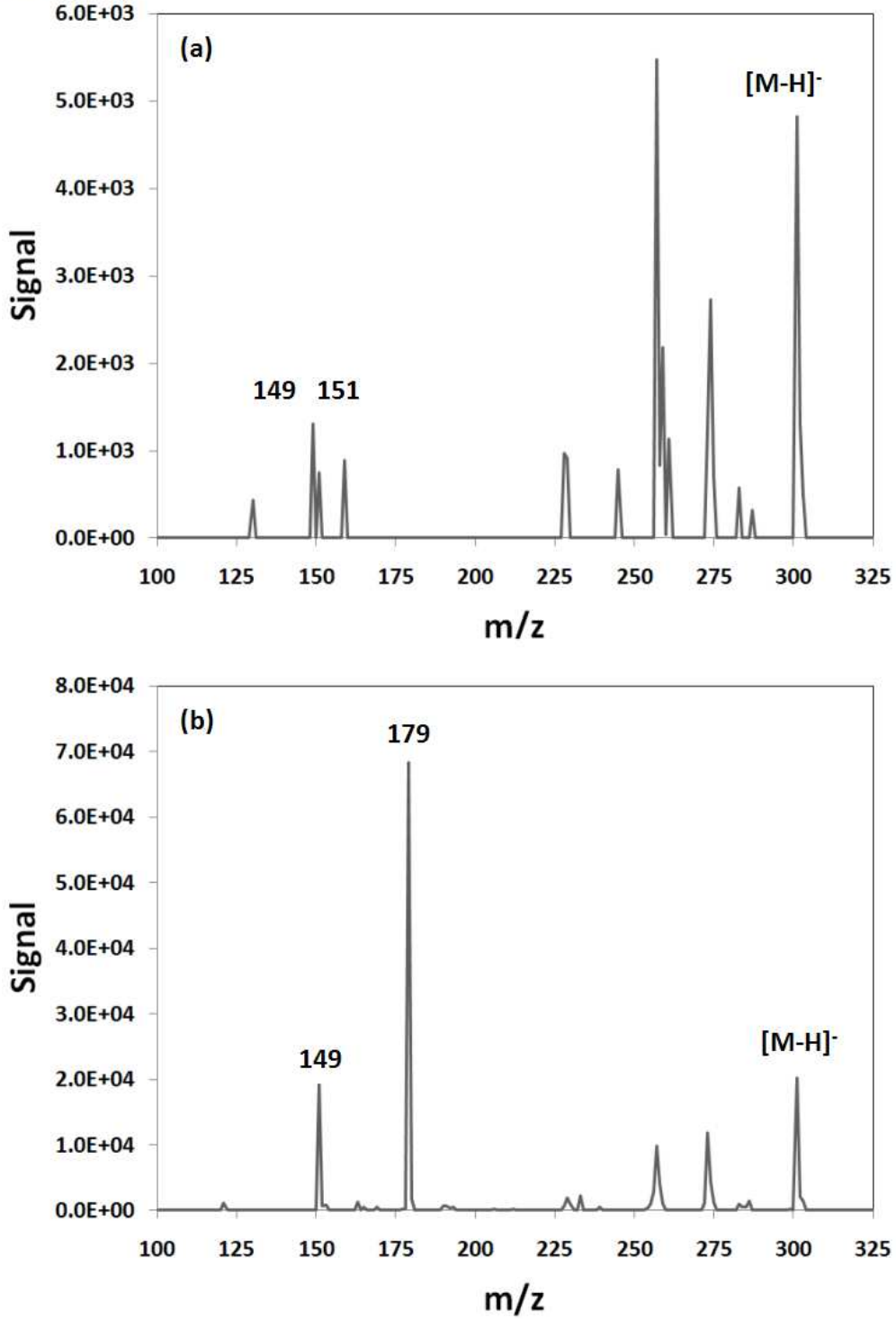


Figure 3) MS/MS spectra from $[M-H]^-$ ions from standards of anthocyanin isomers a) morin, 100 ng, and b) quercetin, 100 ng. The diagnostic product ion for anthocyanin molecules is *m/z* 151. See ref. 40 for structure of product ions.

*Figure 4*

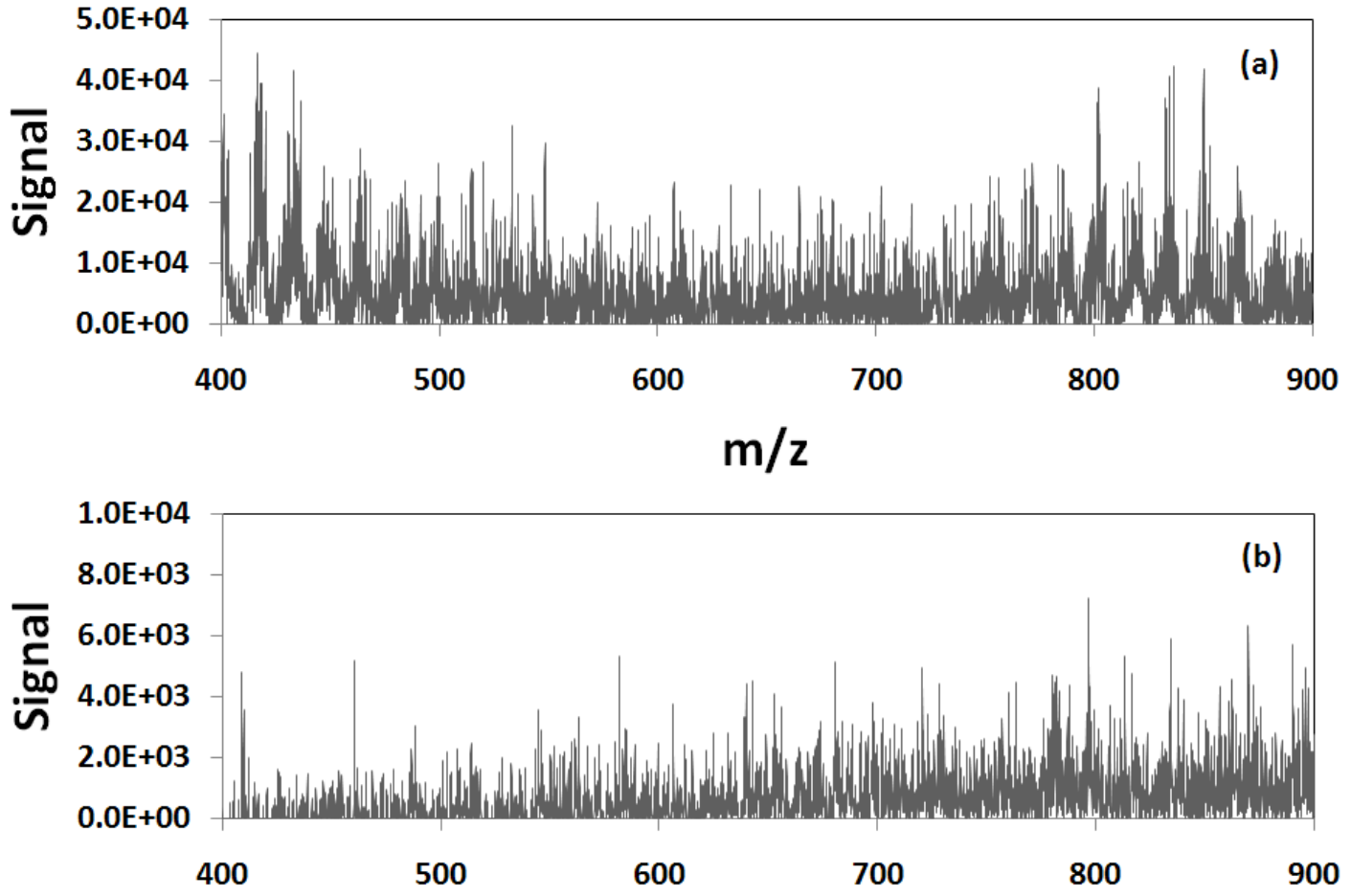


Figure 4) Mass spectra of total brain lipid extract (50 ng) using (a) colloidal graphite LDI and (b) DHB MALDI analysis. Note the difference in the vertical scales of the two spectra.

*Figure 5*

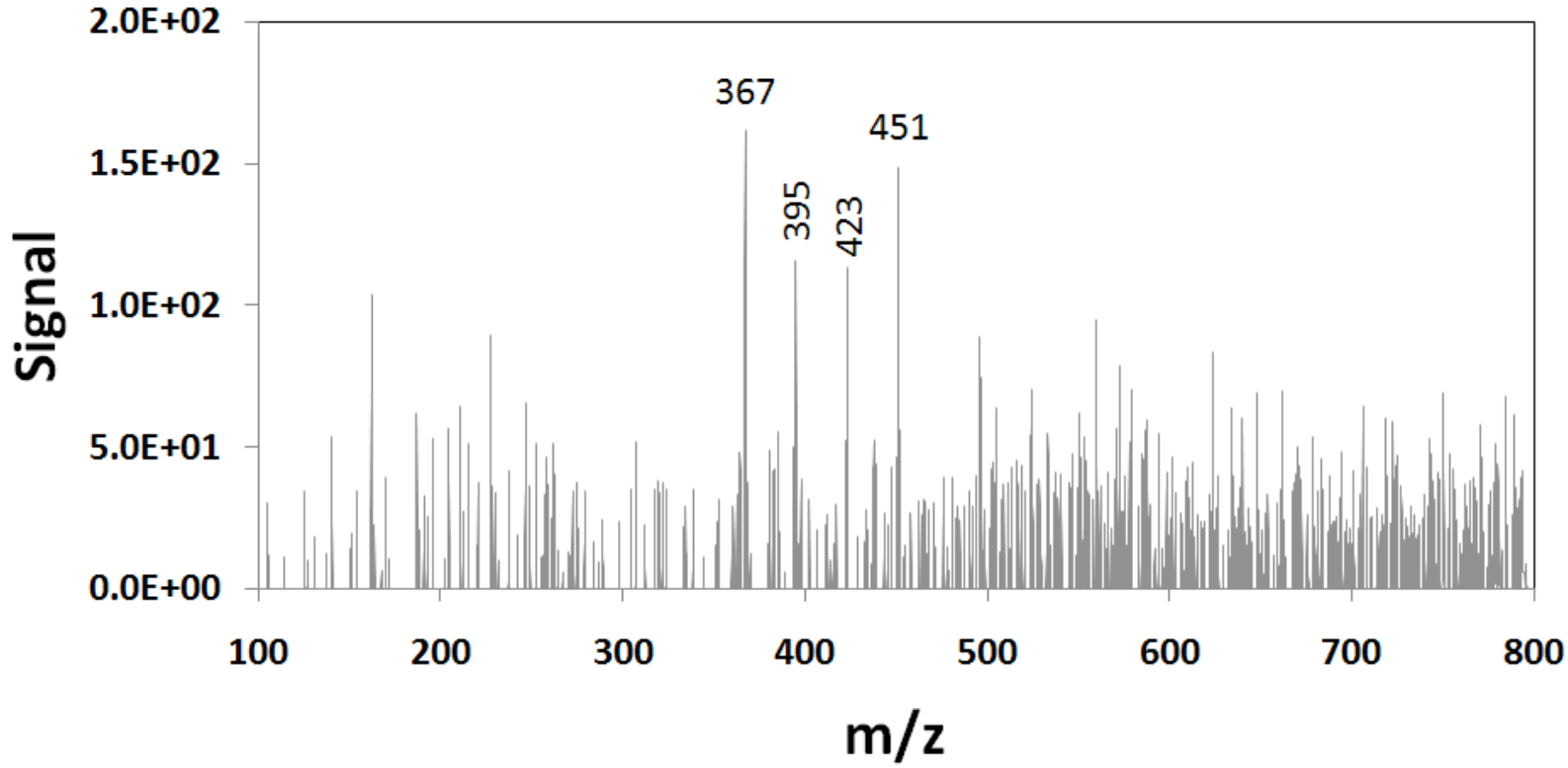


Figure 5) Mass spectrum of *Arabidopsis thaliana* leaf using colloidal graphite LDI-MS in negative ion mode. Possible molecular identifications for peaks are *m/z* 367 $[M-H]^-$ C24 fatty acid - tetracosanoic acid, *m/z* 395 $[M-H]^-$C26 fatty acid - octacosanoic acid, *m/z* 423 $[M-H]^-$C28 fatty acid - hexacosanoic acid, and *m/z* 451 $[M-H]^-$ C30 fatty acid tricosanoic acid.

*Figure 6*

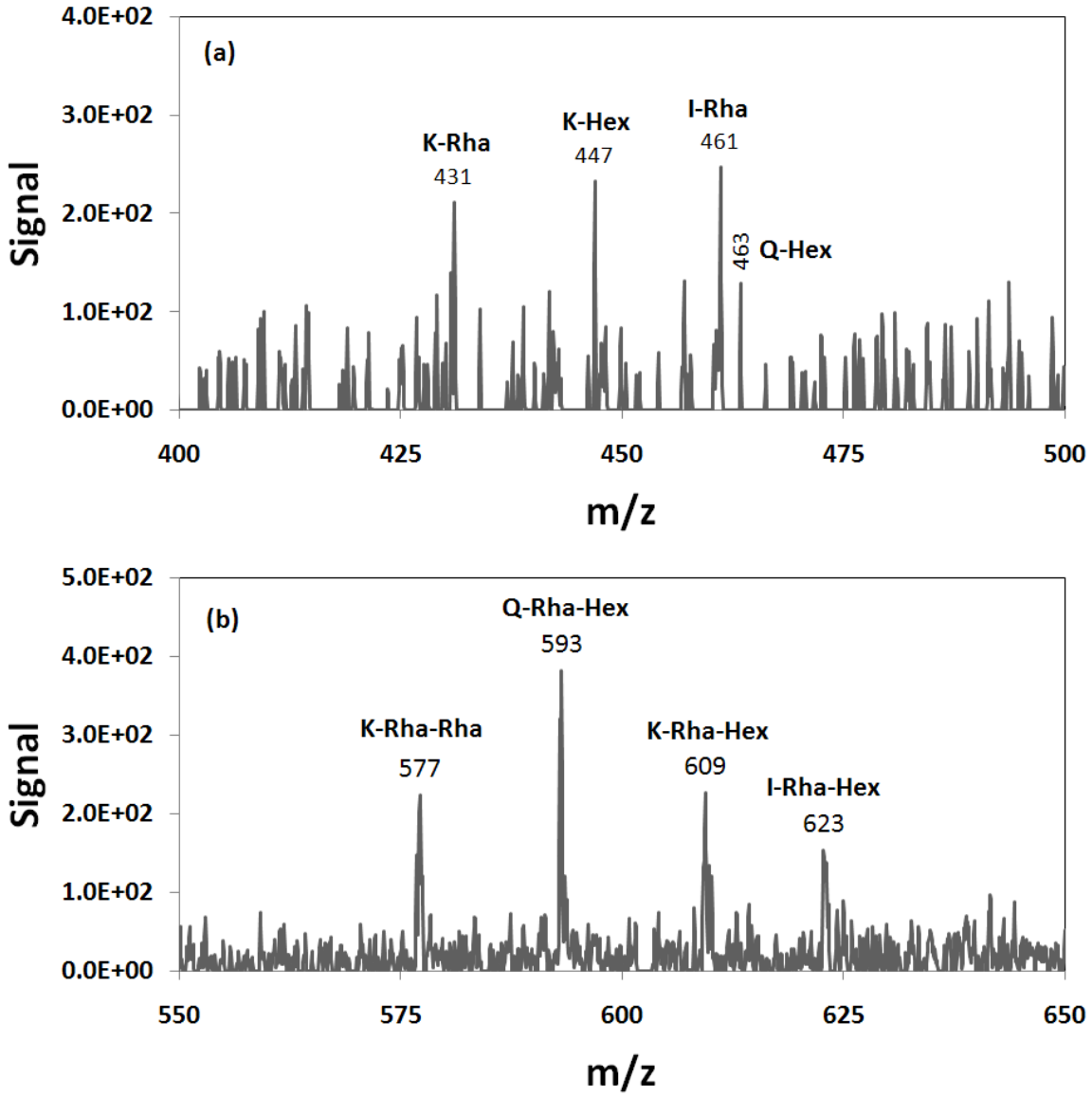


Figure 6) Mass spectra of *Arabidopsis thaliana* flower petal using colloidal graphite in negative ion mode. Possible molecular identifications for assigned peaks for (a) are *m/z* 431 $[M-H]^-$ Kaempferol-Rhamnoside, *m/z* 461 $[M-H]^-$ Isorhamnnetin-Rhamnoside *m/z* 447 $[M-H]^-$ Kaempferol-Hexoside, and *m/z* 463 $[M-H]^-$ Quercertin-Hexoside. Possible molecular identifications for assigned peaks for (b) are *m/z* 577 $[M-H]^-$Kaempferol-Rhamnoside-Rhamnoside, *m/z* 593 $[M-H]^-$Kaempferol-Rhamnoside-Hexoside, *m/z* 609 $[M-H]^-$ Quercetin-Rhamnoside-Hexoside, and *m/z* 623 $[M-H]^-$ Isorhamnetin-Rhamnoside-Hexoside.